The effect of anaerobic biodegradation on the phase partitioning of a multicomponent dense non-aqueous phase liquid

Alexandra Hockin

A thesis submitted in partial fulfillment
of the requirements for the degree of
Masters of Science

March 2018

Supervisors:
Dr. Ir. S.M. Hassanizadeh, Utrecht University
J.A. van Leeuwen, Deltares
Dr. J. Gerritse, Deltares

Universiteit Utrecht

Faculty of Geoscience
Earth Surface and Water
Utrecht University
The Netherlands

Deltares
Enabling Delta Life

Abstract

Many former petrochemical sites are contaminated with highly toxic benzene, toluene, ethylbenzene, xylenes (BTEX) and polycyclic aromatic hydrocarbons (PAHs). Through batch experiments, the potential for anaerobic natural attenuation and source zone biostimulation was evaluated for a former manufactured gas plant in Amersfoort (The Netherlands). Previous research found indications for increased degradation in batches with pure phase tar stimulated with additional electron acceptors. However, these same batches had the highest aqueous phase benzene concentrations. Our research suggests that tar in the batches acts as a hydrophobic matrix, initially adsorbing component from the aqueous phase. However, as the matrix is degraded by anaerobic biodegradation it releases components back to the aqueous phase. To prove this hypothesis, hydrocarbons were spiked to batches with and without a non-aqueous phase liquid (NAPL). The results of these experiments found that NAPLs sorb aqueous phase hydrocarbons and the effects are most pronounced for components with a $\log K_{ow} > 3.5$. In the biologically stimulated batches, we propose a critical mass of tar is degraded and a new equilibrium state is established with higher-than-sterile aqueous benzene concentrations. This is a result of the selective degradation of tar components and the loss of storage capacity within the remaining tar. To evaluate the relative effectiveness of different electron acceptors on tar degradation, a method was developed to conduct a mass balance of tar components in each of the gas, aqueous and tar phases. Ten mobile aromatic and nineteen PAHs ranging from two to six rings were quantified in the aqueous phase in an initial test of the method. Degradation in batches results in substantially higher-than-sterile aqueous concentrations of benzene and PAHs larger than fluorene. This research highlights a potential risk of source zone enhanced bioremediation. Stimulating batches results in an overall mass loss of tar but a substantial release of tar components to the aqueous phase, which could result in increasing the size of contaminant plume zones in-situ.

Acknowledgements

I am grateful to my supervisors Dr. Ir. S. M. Hassanizadeh (Utrecht University), Johan van Leeuwen (Deltares) and Dr. Jan Gerritse (Deltares) for giving me the opportunity to work on this challenging and rewarding project. Their trust, guidance and enthusiastic support throughout this research was greatly appreciated.

This research would not have been possible without the technical support and guidance from many people at Deltares, Utrecht University and TNO. From Deltares, I am indebted to Daniel Giesen who first proposed the idea of the tar as a 'passive sampler'; to Marcelle van der Waals who was always willing to help both in the lab or in the field; Andre Cinje, Fredericke Hannes and Erik van Vilsteren for their help in sample collection and analysis; Dominika Kanjaniuk from Utrecht University was endlessly helpful in developing the methods for the GC's, the small column chromatography and was a great friend during this project; and to Alex van Renesse van Duivenbode, TNO, for his help with sample analysis.

I would like to thank my family and friends who have always supported me, listened patiently to all of the frustrations and excitements that come with research and for having encouraged me to pursue my goals, no matter if they took me across the ocean and far away. Finally, thank you to my best friend and partner Cjestmir, who has heard more about this project than anyone else and was an unending source of inspiration and encouragement throughout this research.

Statement of Originality of the MSc Thesis

I declare that:

1. this is an original report, which is entirely my own work,

2. where I have made use of the ideas of other writers, I have acknowledged the source in all instances,

3. where I have used any diagram or visuals I have acknowledged the source in all instances,

4. this report has not and will not be submitted elsewhere for academic assessment in any other academic course.

Student data:

Name: Alexandra Hockin

Registration number: 5950287

Date: March 19, 2018

Signature: Alex Hockin

Contents

List of Figures

List of Tables

Chapter 1

Introduction

1.1 Introduction

Many former industrial sites are contaminated with petroleum hydrocarbons. Common sources of contamination include leaking underground storage tanks, pipelines and waste pits as well as accidental spills during transportation (Alvarez & Illman, 2006). Petroleum hydrocarbons consist of several hundred compounds and two groups of particular concern are BTEX (benzene, toluene, ethylbenzene and xylenes) and PAHs (polycyclic aromatic hydrocarbons) due to their risk to public health and persistence in the environment.

BTEX components are monoaromatic hydrocarbons which are relatively soluble and tend to travel long distances in groundwater (Alvarez & Illman, 2006). Benzene in particular is a known human carcinogen. The EPA drinking water limit for benzene is 0.005 mg/L, orders of magnitude lower than other BTEX components (toluene 1 mg/L, ethylbenzene 0.7 mg/L and xylenes 10 mg/L, EPA 2009). As a result benzene is often the limiting chemical at contaminated sites determining remediation goals.

PAHs consist of multiple fused aromatic rings and are formed during the incomplete combustion of organic matter at high temperatures (Haritash & Kaushik, 2009). The stability of the aromatic rings make these components difficult to degrade. Moreover, as their molecular weight increases, the solubility in water decreases, increasing the persistence of PAHs in the environments (Haritash & Kaushik, 2009).

When hydrocarbons are spilled on site they may exist as a separate, non-aqueous phase liquid (NAPL). The fate and transport of NAPLs in the subsurface depend on their distinct physical and chemical properties. NAPL may be grouped into two classes based on their comparative density to water. LNAPL refers to lighter-than-water NAPLs, which float on top of the water table, while DNAPLs are denser-than-water and tend to sink through the water table and come to rest on aquitards or other low permeability zones (Mayer & Hassanizadeh, 2005). When DNAPLs sink through the unsaturated and saturated zones some liquid is retained within the pores as residual saturation, known as trailing. Furthermore, due to the heterogeneous nature of the subsurface, when DNAPLs encounter areas of lower permeability the flow of NAPL may be diverted. This diversion leads to spreading of the contamination within the subsurface. DNAPL can therefore exist within the subsurface as multiple pools of pure phase liquid, that may or may not be interconnected.

NAPLs may be composed of a single chemical, such as perchloroethylene (PCE), or a complex mixture of many chemicals, such as gasoline or tar. Within the subsurface, NAPLs undergo phase partitioning between the solid, aqueous and gas phases. NAPLs constituents tend to adsorb to sediment grains, dissolve into passing groundwater or if present in the unsaturated zone volatilize into gas present in the pores. Within the saturated zone, NAPLs are particularly per-

sistent pollutants due to the slow dissolution of components into groundwater, creating long-term contamination which can last for decades or longer after the initial spill. Furthermore, the high toxicity of petroleum products such as benzene make even low concentrations in groundwater a threat to drinking water supplies.

The large number of contaminated sites and relatively high cost of engineered remediation systems has resulted in a paradigm shift towards risk-based approaches, which consider the level of contamination and risk posed to public health of individual sites weighed against clean-up costs. Monitored natural attenuation (MNA) is a remediation strategy which emerged as a result. MNA is a passive remediation option which relies on natural processes (physical, chemical and biological) occurring on site to control the concentration, distribution and transportation of contaminants in soil and groundwater (Bekins *et al.*, 2001). MNA requires continuous monitoring and evaluation at sites to ensure contaminants are not spreading or threatening drinking water supplies for example.

More traditional site remediation techniques include physical, chemical and biological treatments. Physical treatments include the extraction or excavation of soil and ex-situ treatment or disposal (eg. dig-and-dump and pump-and-treat). Chemical treatments include the addition of strong oxidizing or reducing agents which often irreversibly transform contaminants into different chemicals by means of electron transfer (Alvarez & Illman, 2006). Finally, biological treatment (bioremediation) enhances natural microbiological processes which break down contaminants into less complex and often less harmful, components.

Bioremediation is a cost-effective and non-destructive means to remediate contaminated sites. Bioremediation can take above ground or off site (ex-situ) or on site within the subsurface (in-situ). In-situ bioremediation alters the natural environment to overcome specific site limitations to degradation, for example a lack of electron acceptors, nutrients or suitable carbon substrate. Not all contaminants and site are amenable to in-situ treatment, for example heavy metal contamination or highly stratified soils (Alvarez & Illman, 2006). However, in-situ bioremediation minimizes land disturbance, hazardous waste transport and disposal and long term treatment costs.

In-situ bioremediation can occur under aerobic or anaerobic conditions. Whether a contaminant will degrade preferentially under aerobic or anaerobic conditions depends on the oxidation state of the target contaminant. Aerobic rates of degradation are generally higher, however, due to the limited availability and solubility of oxygen it is quickly depleted in groundwater at contaminated sites. Anaerobic degradation is of particular interest due to the lower implementation cost (Langenhoff *et al.*, 2009). In anaerobic conditions biodegradation can occur under nitrate-, sulfate- or iron-reducing and methanogenic conditions (Langenhoff *et al.*, 2009).

Bioremediation can be approached through either biostimulation or bioaugmentation. Biostimulation supplies rate limiting nutrients, electron acceptors/donors and in some cases carbon substrates. Biostimulation enhances the activity of the indigenous microbial community. Bioaugmentation on the other hand, involves the addition of bacteria with specialized abilities to degrade target contaminants in-situ. Bioaugmentation is preferred for sites with particularly persistent contaminants (eg. MTBE, PCE) which cannot be degraded by bacteria commonly found in the subsurface (Alvarez & Illman, 2006). Biostimulation is suitable for sites where target contaminants are degraded by bacteria found ubiquitously in the environment, such as hydrocarbons. In the past, bioremediation has been applied in relatively low concentration plume zones, however there has been growing interest in recent years to apply bioremediation techniques to the high concentration source zones (Langenhoff *et al.*, 2009).

Biostimulation in plume zones may temporarily reduce concentrations of contaminants in the groundwater. However, without source zone treatment contaminants will rebound once treatment is stopped (EPA, 2013; Ponsin *et al.*, 2014). Enhanced bioremediation of NAPL source zones has been effective in some cases, though data are limited on the long term effects (Müller *et al.*, 2017; Ponsin *et al.*, 2014). Source zone remediation technologies have traditionally focused on the

solubilization of NAPL source zones, by flushing with surfactants and cosolvents, the mobilization by reducing the interfacial tension or density or by air sparging, which is only suitable for removing volatile components (McCray *et al.*, 2011).

Some research on the combined effects of biodegradation and NAPL component partitioning have been done (Carr *et al.*, 2000; Garcia-Junco *et al.*, 2003; Pfeiffer *et al.*, 2005; Ramsburg *et al.*, 2010, 2011). Garcia-Junco *et al.* (2003) found that partitioning of PAHs was enhanced by microbial degradation in batch experiments. The authors found that bacteria adhered to the NAPL-water interface and increased the transfer of PAHs from the NAPL through their cells. Increased concentrations of PAHs however were not observed in the aqueous phase. The mineralization rate was measured by stable isotope analysis and was found to exceed the abiotic partitioning rate of PAHs in experiments lacking bacteria.

Studies by Ramsburg *et al.* (2010) found that cis-dichloroethene (cis-DCE) and vinyl chloride (VC), daughter products of microbial degradation of PCE, had a strong thermodynamic driving force to partition into the remaining PCE DNAPL. In their study, 60-70% of the cis-DCE and VC produced was sequestered in the PCE DNAPL. The implication therefore was that degradation rates may be underestimated due to the low concentration of degradation products if partitioning effects are not considered.

Other studies, such as Pfeiffer *et al.* (2005), examined how degradation was overestimated at a PCE contaminated site which was amended with vegetable oil as a substrate for microbial degradation. The authors found that chlorinated ethenes partitioned from the groundwater to the vegetable oil, decreasing groundwater concentrations around the injection well. The decreased concentrations were initially thought to indicate increased microbial degradation, while the authors found that partitioning could partially account for the changes observed. Furthermore, as the vegetable oil sorbed more chlorinated ethenes, the affinity of the oil changed, favoring higher chlorinated ethenes over time.

Carr *et al.* (2000) studied how the terminal degradation products affected the source zone longevity by examining the partitioning coefficients of different degradation products of PCE. The authors found that if the terminal chlorinated ethene was VC that source zone longeviity was reduced as VC partitions more strongly to the aqueous phase where it is available for further degradation. If the terminal chlorinated ethene was trichloroethene (TCE), however, source zone longevity was not decreased to the same extent as TCE partitions more strongly to the remaining PCE.

Therefore, the partitioning of not only tar components but their degradation products are an important factor in the study of source zone remediation schemes. Furthermore, the preferential degradation of tar components by bacteria will affect equilibrium concentrations between the groundwater and NAPL. Degradation within the source zone has the potential to enhance dissolution into the aqueous phase, however, if the bacteria present are not able to degrade the components released then source zone remediation has the potential to increase the extent of plume zone contamination.

To the best of our knowledge no studies have extensively studied how biodegradation impacts the differential partitioning of tar components in the presence of a petroleum hydrocarbon NAPL source. In this study the effect of biodegradation on the phase partitioning of tar components was examined in microcosms which simulated source zone conditions. Different electron acceptors and substrate were added to batches and the effects on the sorbtion and release of tar components as a result of differential degradation of tar components was observed. Additional batch experiments were performed to demonstrate the partitioning behavior of tar components in the presence of a pure phase NAPL. Finally, a method to extract and quantify the concentration of tar components in each of the gas, aqueous and non-aqueous phases was developed.

1.2 Motivation

A case study is currently underway at a former pintsch gas factory in Amersfoort. At this site unlined waste lagoons were used to dispose of the DNAPL tar waste by-product of the pintsch gas manufacturing process (Gkekas, 2014; van Leeuwen & Gerritse, 2016). Over time the tar flowed by gravity through the subsurface creating three contamination zones; a pool of mobile pure phase DNAPL, an area of immobile residual DNAPL above the pure phase pool and a plume of contaminated groundwater (Wagner, 2015). Qualitative analysis of tar from site by gas chromatography with time of flight mass spectrometry and gas chromatrography mass spectrometry (GCxGC TOFMS and GC-MS) revealed the Amersfoort tar to be composed of over 980 compounds (van Leeuwen, 2018)

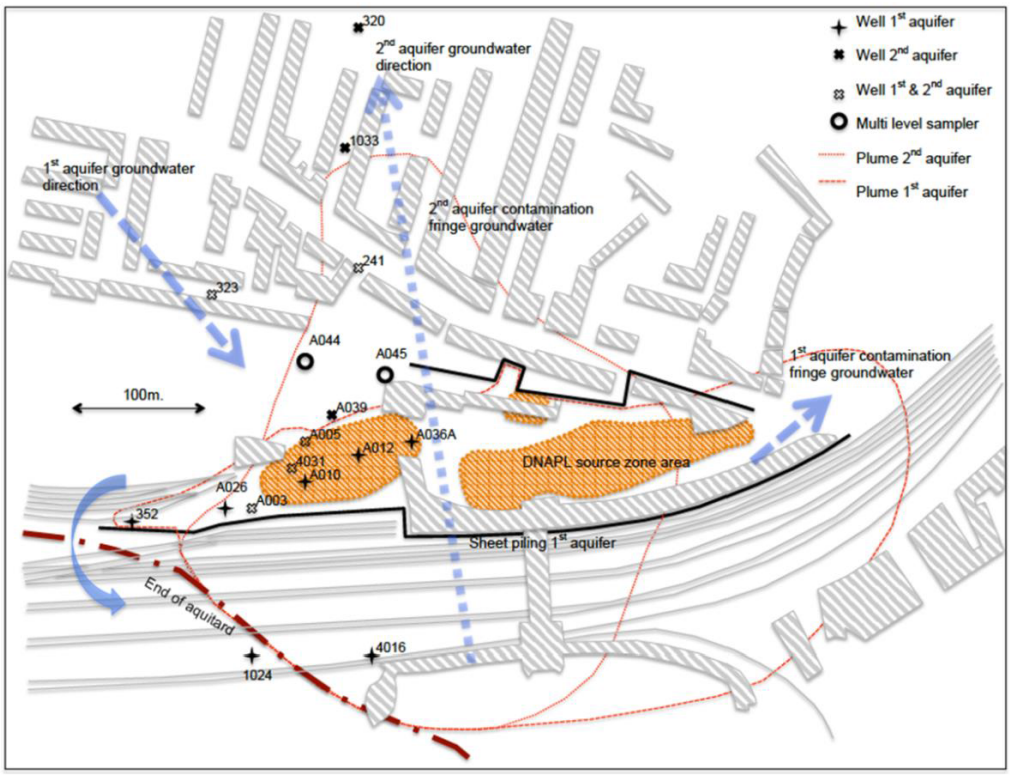

Figure 1.1: *Overview of contamination at Amersfoort Central Station. DNAPL source zone shaded in orange, direction of groundwater flow in blue arrows, plume contamination zones in the first and second aquifers outlines in red dashed lines (Gerritse* et al.*, 2017)*

In May 2014 batch experiments were created to compare the bioremediation potential of different redox conditions by stimulating anaerobic batches with different electron acceptors and substrates. One series of batches simulated the source zone with contaminated groundwater and source zone sediment from Amersfoort (Figure 1.2). Batch experiments were created in triplicate (A, B, C) and carried out with three different electron acceptors (nitrate, chlorate and sulfate) and two substrates (acetate and succinate) to compare the bioremediation potential of different redox conditions.

Brock (2016), van Logtestijn (2017) and Wagner (2015) examined the geochemical and microbial conditions within the batches. Wagner (2015) found denitrifying organisms present in the stimulation batch series, indicating the source zone conditions in the high series batches was not toxic to the microorganisms. The addition of nitrate and succinate appeared to increase the degradation rate as there was visually less tar in stimulated batches after 3 months (Wagner, 2015).

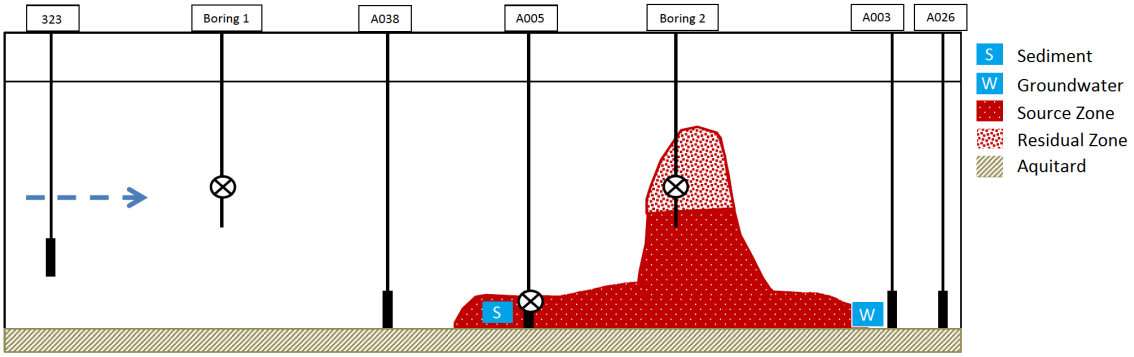

Figure 1.2: *Sources of sediment and groundwater used in the batch experiments. The blue arrow indicates the direction of groundwater flow, well locations indicated by black vertical lines (van Leeuwen, 2018).*

Figure 1.3: *Appearance of stimulation batches at the time of creation in May 2014 (van Leeuwen, 2018).*

Brock (2016) and van Logtestijn (2017) performed liquid chromatography mass spectroscopy (LC-QTOF-MS) to identify and quantify signature metabolites of mobile tar components in one replicate of each batch treatments. The no addition batch (9A) had higher metabolite concentrations than the sterile batch (8A). The authors suggested, therefore, that degradation took place in the no addition batches, but only until the depletion of electron acceptors Brock (2016); van Logtestijn (2017). The sum of signature metabolites was lowest in the treatment batches, which suggested continued degradation of metabolites due to the additional electron acceptors.

DNA analysis was also performed van Logtestijn (2017). The stimulated batches (10-14) had much higher gene counts than the no addition and sterile batches, suggesting the addition of electron acceptors stimulated bacterial growth. Specifically, nitrate reducing bacteria genes were high in the nitrate batches (batches 10-12). The gene for naphthalene degradation, nmsA was

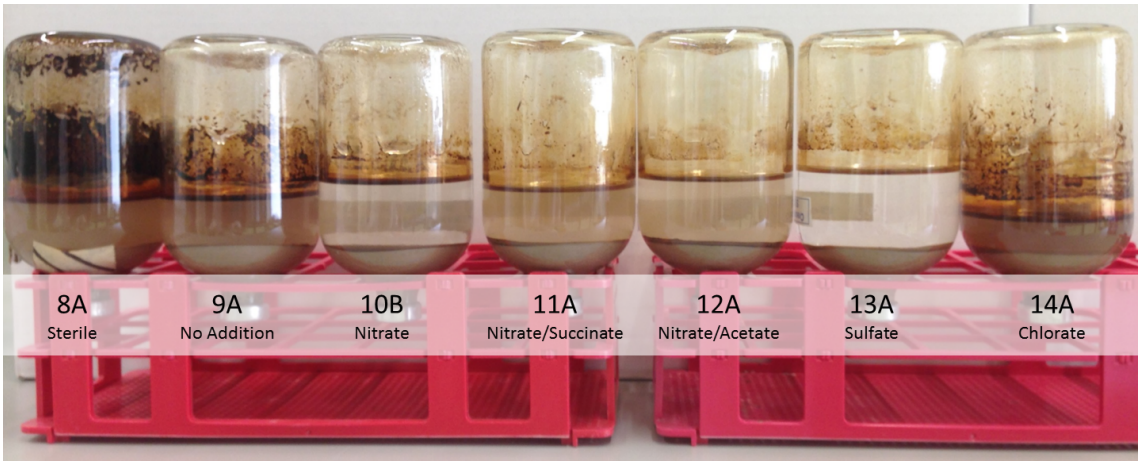

Figure 1.4: *Appearance of stimulation batches after 3 years, photo from August 2017. The batches show distinct differences between the sterile, no addition and stimulated batches. Stimulated batches (10-14) show distinctly less tar than sterile and the no addition batches*

similar for batches 8-12, suggesting stimulation had little or no effect on naphthalene degradation.

Finally, analysis by gas chromatography with a flame ionized detector (GC-FID) found methane peaks in all but the sterile batches, indicating methanogenic biodegradation. Therefore, prior to this research there was ample indication that biodegradation was taking place in treatment batches, and initially in the no addition batches, based on the apparent visual loss of tar, the low metabolite concentrations, the high bacteria and gene count data and the presence of methane.

However, despite all the evidence that biodegradation was taking place preliminary measurements of the concentration of volatile aromatics in batches found the concentration of benzene to be substantially *higher* in the stimulated batches than in the sterile and no addition batches (Figure 1.5). In fact, the sterile batches has the lowest concentration of benzene of any of the batch treatments.

We propose a new conceptual model to explain the changes in tar concentration between the batch treatments. Within treatment batches two main processes control the concentration of hydrocarbons in the aqueous phases: (1) physio-chemical processes, namely partitioning and solubility, and (2) metabolic processes degrading the hydrocarbons by bacteria. These processes interact and create new equilibrium conditions within the stimulated and no addition batches that differ from the sterile batch, where bacteria were sterilized. Prior to the measurement of the batches, it was assumed that degradation would result in lower aqueous phase hydrocarbon concentrations.

However, as bacteria degraded tar components in the aqueous phase there was dissolution of tar components from the tar into the water to maintain equilibrium. The tar can be seen in this respect as a hydrophobic matrix, releasing components to the aqueous phase at a rate proportional to that which they are degraded by bacteria. This phenomena can be compared conceptually to two-phase partitioning bioreactors which use synthetic organic phases to dose substrates (xenobiotic chemicals) at sub-inhibitory concentrations to reactors with bacteria to remediate contaminated waste waters (Daugulis, 2001). However, in the case of the present batch experiments, the organic phase (tar) was also the substrate (hydrocarbons). As the bacteria degraded hydrocarbons, more were released from the tar phase, resulting in an overall mass loss of the tar. Furthermore, bacteria degrade certain components more readily than others, resulting in a shift in the tar composition to a NAPL composed of more and more difficult to degrade compounds (Peters *et al.*, 2000). This shift in composition results in a new equilibrium between the tar and the aqueous phases and possibly different tar-water partitioning coefficients between batch treatments.

We proposed that in the batches with additional electron acceptors and/or substrate that the

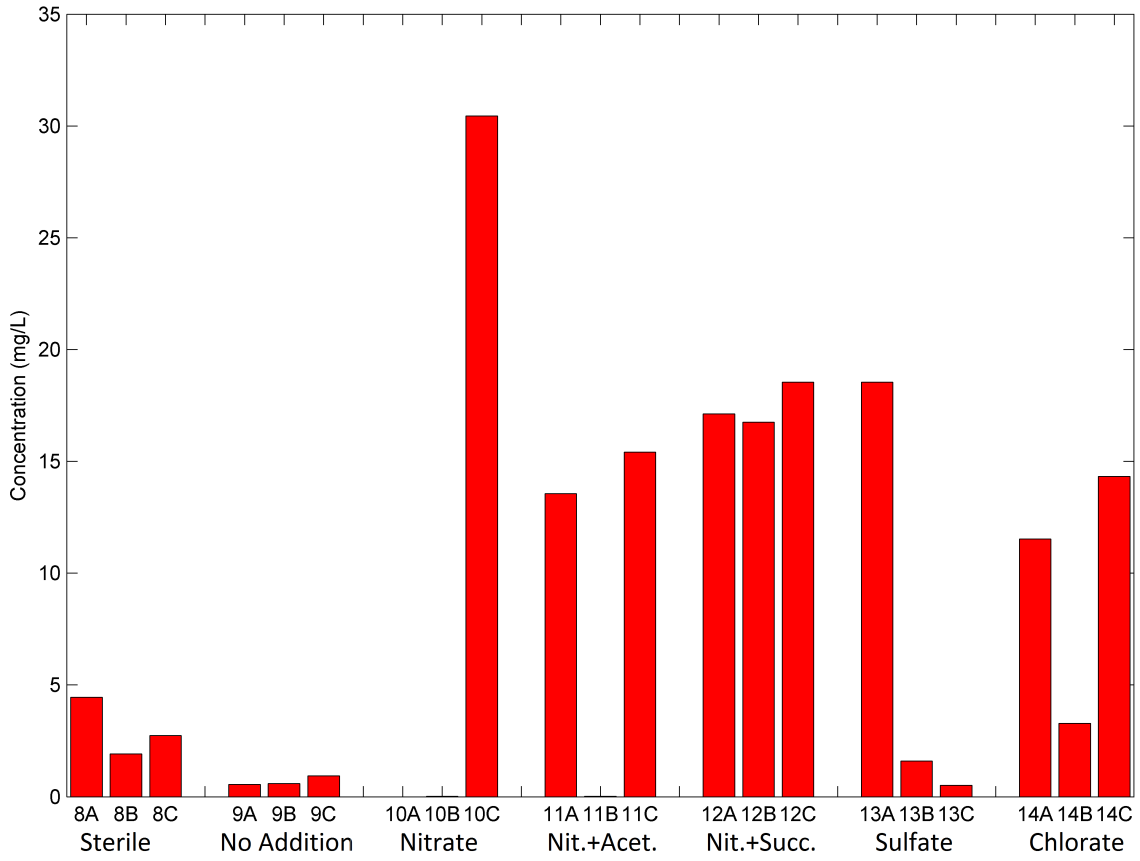

Figure 1.5: *Preliminary measuremnts of the concentration of benzene in the batch experiments, measured by headspace analysis on GC-FID and the concentration in the aqueous phase calculated from Henry's coefficicent.*

bacteria were able to degrade the tar below a critical mass. At this point the storage capacity of the tar was too small and components were released to the aqueous phase resulting in higher concentrations in stimulated batches than in the sterile batch. To confirm this hypothesis a method to quantify the concentration of an additional twelve volatile aromatics in the gas and aqueous phase of the batches was developed. Moreover, a series of batch experiments were created to determine if the tar was indeed acting as a hydrophobic matrix and sorbing hydrocarbons from the aqueous phase to the tar phase, thereby decreasing the measured aqueous concentrations.

To fully understand the dissolution behavior in the batch experiments, however, it is necessary to know both the mole fraction and solubility of each component in the tar. To calculate the mole fractions the tar itself must be quantitatively analyzed, requiring a representative sample from each batch bottle. However, this sample would be difficult, if not impossible, to obtain as batch bottles are not well mixed reactors. Bottles were shaken gently on orbital shakers resulting in the development of microcosms within bottles. These microcosm may have discrete redox conditions and phase partitioning (Figure 1.6). The tar, which began as a single homogeneous medium has separated into multiple phases with potentially different partitioning behavior, concentration and mass. Therefore, it would not be possible to take a single, small representative sample of tar from bottles for quantification.

The only method going forward would be a total extraction of the bottles to conduct a thorough mass balance of the chemicals in each phase within the bottle. However, extraction of tar components and mass balance of each microcosm in the bottle would be prohibitively complicated. Therefore the tar must be considered as a single medium again and the extraction of tar concentra-

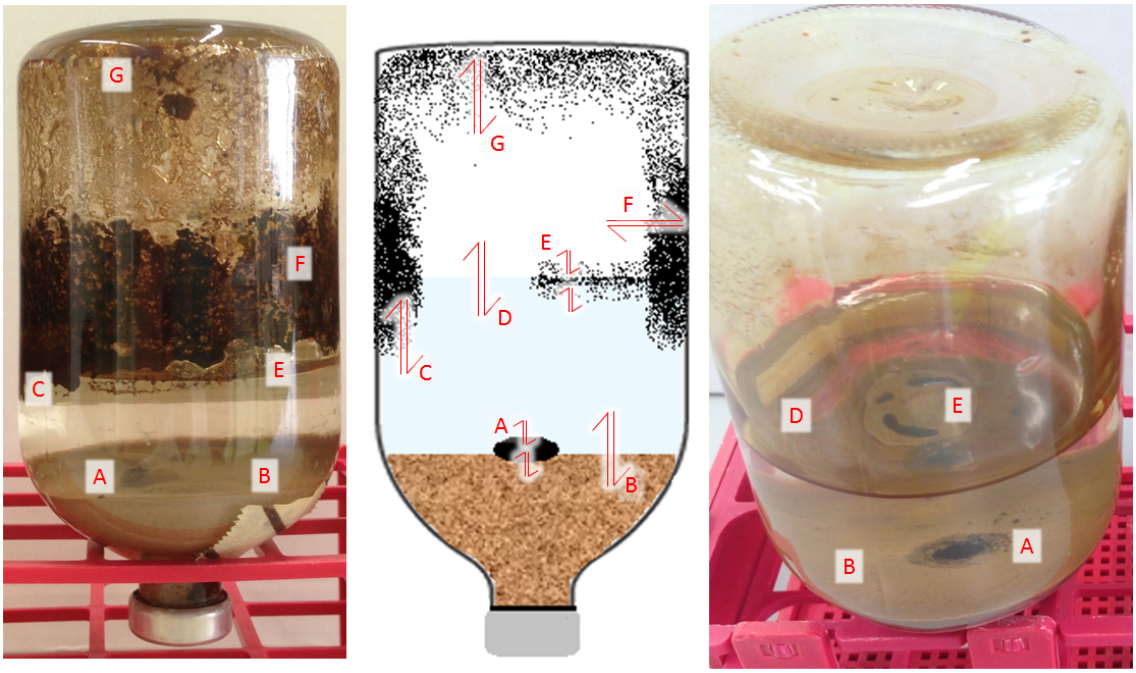

Figure 1.6: *Microcosm environments within batch bottles. Red arrows indicate exchange between phases in the bottle. Tar has developed in different niches within the bottles, where potentially different redox conditions have developed. Tar may have a unique composition within each niche with unique partitioning coefficients, concentration of tar components and total mass. Phase exchange summary: (A) tar-sediment/tar-aqueous, (B) sediment-aqueous, (C) tar-aqueous, (D) aqueous-gas, (E) tar-aqueous/aqueous-gas, (F), (G) tar-gas exchange in different location within the batch. Batch bottle on the left is sterile batch 8B, batch bottle on the right is nitrate-succinate batch 11A.*

tions performed on the bottle as a whole. Naturally this is a simplification but was the only feasible option within the time constraints of this project. Only after evaluation of the total mass balance can the differences between the batch treatments (electron acceptor/substrates) be compared for their relative effectiveness on stimulating degradation.

1.3 Research Questions

1. Does the concentration of volatile aromatic hydrocarbons in the aqueous phase differ between batch treatments?
2. Does biodegradation cause the tar to release less degradable, high solubility components resulting in higher aqueous concentrations of tar components?
3. Does the tar act as a hydrophobic matrix initially adsorbing aqueous phase concentrations of aromatic hydrocarbons?
4. What is the mass balance of volatile and non-volatile tar components in the gas and aqueous phases within stimulation batch treatments?

1.4 Research Objectives

1. Develop a GC-FID method to quantify the concentration of 13 volatile aromatic hydrocarbons in the batch treatments.

2. Design a series of batch experiments to determine if tar from Amersfoort sorbs and/or releases aqueous phase volatile aromatic hydrocarbons, lowering the aqueous phase concentrations.

3. Develop a method to perform a mass balance of tar components in each of the gas, aqueous and non-aqueous phases.

Chapter 2

Background and Literature Review

2.1 NAPL in the Environment

Contaminants may be present in the environment in one or more of the following phases: solid, gas, aqueous and non-aqueous phases. NAPLs may be composed of a single single (pure) component or be present as complex multicomponent mixtures. Driven by the chemical potential between the different phases, NAPL components will transfer between the different phases (Mayer & Hassanizadeh, 2005). Equilibrium is established when the chemical potential is equal between the different phases. Figure 2.1 summarizes the different phases and the laws governing partitioning between them.

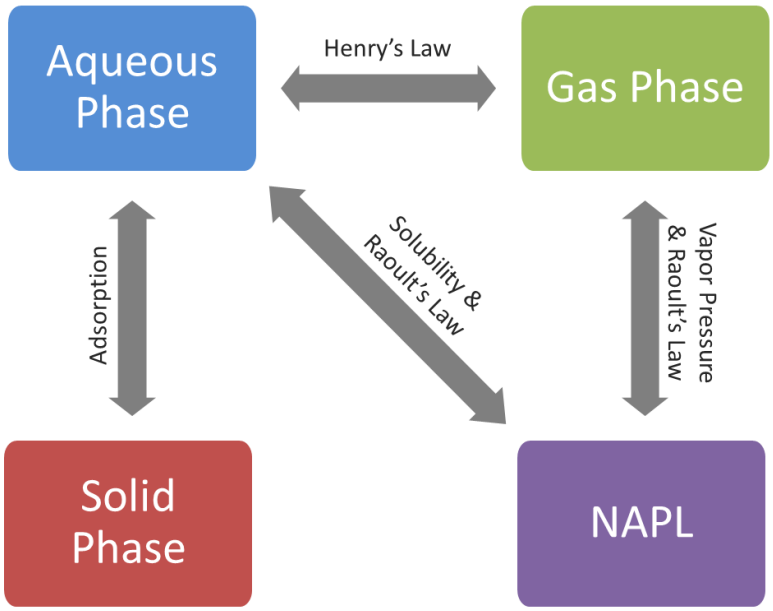

Figure 2.1: *Equilibrium partitioning between phases is governed by the chemical potential of different phases, recreated from Mayer & Hassanizadeh (2005)*

Phase partitioning is governed by NAPL component solubility, vapor pressure, mole fraction and phase density (Mayer & Hassanizadeh, 2005). Dissolution is the mass transfer from the NAPL to the aqueous phase and is governed by the solubility and mole fraction of NAPL components.

Raoult's law dictates that;

$$C^i_{sol} = \chi^i_n C^i_{pure} \tag{2.1}$$

Where C^i_{sol} is the solubility concentration, χ^i_n is the mole fraction in the NAPL and C^i_{pure} is the solubility if the component were present in pure form. In all cases the superscript denotes component i of a multicomponent mixture. This form of Raoult's law assumes activity coefficients of unity.

Equilibrium between the NAPL and gas phase is governed by the vapor pressure. The vapor pressure of a component is the partial pressure of a component in equilibrium with its pure form (Mayer & Hassanizadeh, 2005);

$$P^i_p = \chi^i_n P^i_{vap} \tag{2.2}$$

Where P^i_p is the equilibrium partial pressure, χ^i_n is the mole fraction in the NAPL and P^i_{vap} is the vapor pressure.

Equilibrium between the aqueous and gas phase is governed by Henry's Law (Mayer & Hassanizadeh, 2005). Henry's law can have many forms, one example is;

$$H^i_m = \frac{P^i_p}{c^i_{aq}} \tag{2.3}$$

where c^i_{aq} is the molar concentration in the aqueous phase and H^i_m is the Henry's constant with units of pressure $\times$ volume/mole. The dimensionless Henry's constant K^i_h was used in our calculations which gives the ratio between the gas and aqueous concentrations:

$$K^i_h = \frac{C^i_g}{C^i_{aq}} \tag{2.4}$$

Where K^i_h is dimensionless Henry's constant, C^i_g is the concentration in the gas phase and C^i_{aq} is the aqueous concentration.

For single component NAPLs the gas and aqueous concentrations are governed by the vapor pressure and solubility limits. However for multicomponent NAPLs, where a chemical is only a dilute component of the whole, the partitioning coefficient is defined by the ratio between the NAPL concentration and the aqueous concentration;

$$K^i_n = \frac{C^i_n}{C^i_{aq}} \tag{2.5}$$

Where K^i_n is the partitioning coefficient between the NAPL and aqueous phase, C^i_n is the concentration in the NAPL and C^i_{aq} is the aqueous concentration of component i.

2.2 Spatial Distribution and Dissolution Behavior of NAPL

Simple models of flow assume full contact between groundwater flowing through NAPLs and instantaneous equilibrium at the NAPL-water interface. However, often concentrations of NAPL components in groundwater are lower than solubility because of mass transfer limitations, heterogeneities in the subsurface, multicomponent effects, dilution and spatial and temporal variation due to biodegradation and sorption (Mayer & Hassanizadeh, 2005).

Consider a parcel of water flowing through the subsurface (Figure 2.2). Beginning upstream from the source zone, the initial concentration of tar components is zero. The parcel then encounters the NAPL pool and there is equilibrium at the NAPL-water interface, causing dissolution of tar components to the aqueous phase (zone (1) in Figure 2.2, Mayer & Hassanizadeh 2005). Due to dispersion, components dissolved in the groundwater then spread away from the interface parallel to the length of the pool (zone (2) in Figure 2.2). Finally, advection along the length of the pool spreads the dissolved components further, increasing the concentration in the passing groundwater (zone (3) in Figure 2.2). This creates concentration profiles along and transverse to the pool.

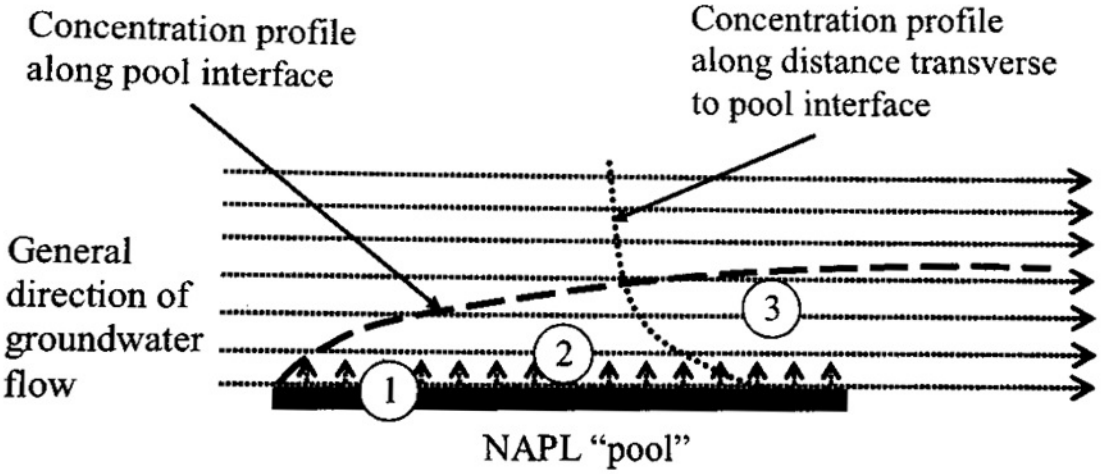

Figure 2.2: *Model of NAPL pool dissolution from Mayer & Hassanizadeh 2005. (1) Equilibrium at the interface between NAPL pool and passing groundwater resulting in maximum solubility concentrations at the NAPL-water interface, (2) Dispersion of dissolved NAPL components away from the NAPL-water interface, (3) Advection of dissolved NAPL components with groundwater flow. The dashed line shows the horizontal groundwater concentration gradient along the NAPL pool, increasing from zero upstream of the pool. The dotted line shows the vertical groundwater concentration gradient, decreasing from component solubility at the NAPL-water interface to zero away from the interface due to dilution effects*

The composition of the NAPL also has influence on the dissolution and concentrations in passing groundwater. For single component NAPLs, the maximum groundwater concentration is equal to the solubility limit of the pure component. For multicomponent NAPLs, as given in equation 2.1, the maximum groundwater concentration is dependent on both the solubility and mole fraction in the NAPL. Furthermore, the concentration in the NAPL will vary spatially and temporarily as a result of the preferential dissolution of different tar components (Fraser *et al.*, 2008; Peters *et al.*, 1997).

Therefore, components with the highest solubility are leached from the NAPL to the groundwater first, giving initially higher concentrations in the groundwater which then decrease over time as the NAPL is depleted. As a result, lower solubility components begin to leach from the pool to the groundwater only later (Fraser *et al.*, 2008). Relatively simple Raoult's law models of mass discharge from NAPL source zones can give insight into the changing source zone composition (Fraser *et al.*, 2008). These changes in the NAPL composition can effect the partitioning coefficient and therefore the equilibrium between NAPL and groundwater. Finally, there is emerging evidence that some components of tar change spatially as NAPL migrates through the subsurface, resulting in composition changes at the leading edge of source zones (Birak & Miller, 2009).

In addition to changing source zone conditions, dilution also impacts the down gradient concen-

tration of NAPL components, as a result of dispersion and mixing within the plume (Figure 2.2). Therefore concentrations downgradient of the source zone may be substantially less than solubility limits would predict. Recharge and infiltration to groundwater can result in seasonal variation of groundwater concentrations as well.

2.3 Biodegradation Principles

In addition to physical effects, the fate and transport of NAPL components is also controlled by biological processes. Microbes within the subsurface can transform or eliminate harmful components from groundwater. In-situ bioremediation can occur under aerobic or anaerobic conditions. Whether a contaminant will degrade preferentially under aerobic or anaerobic conditions depends on the oxidation state of the target contaminant. Aerobic rates of degradation are generally higher, due to the high oxidation–reduction (redox) potential of oxygen, however, it quickly depletes in contaminated sites, creating anaerobic conditions. Without oxygen, bacteria use nitrate, iron, manganese, sulfate and carbonate as the terminal electron acceptor (Figure 2.3).

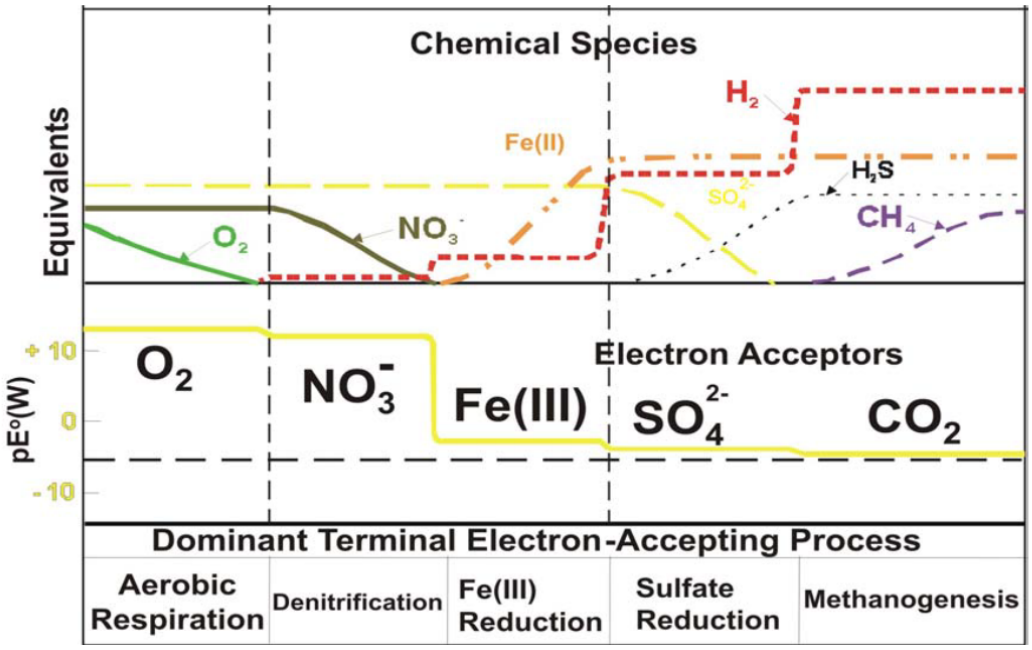

Figure 2.3: *Terminal electrons acceptors listed in order of decreasing energy yield for bacterial metabolism (EPA, 2013).*

Two forms of bioremediation include biostimulation and bioaugmentation. Bioaugmentation is often employed at contaminated sites in combination with biostimulation, where the degrader bacteria are not found or particularly specialized. For example the species *Dehalococcoides* is the only known species which can completely dechlorinate PCE to ethene (Da Silva *et al.*, 2006). Most studies deal with plume zone biodegradation, not source zone, however recent insights suggest that source zone degradation has previously been underestimated (Meckenstock *et al.*, 2014).

2.3.1 Requirements for Biodegradation

The following are general requirements for biodegradation;

Presence of microorganisms on site able to degrade the contaminant of interest. BTEX degraders for example are ubiquitous as the bacteria have evolved to feed on hydrocarbons

(Alvarez & Illman, 2006).

Accessibility of contaminants to bacteria dissolved in the aqueous phase. It is more difficult to degrade components strongly sorbed to sediment or in the NAPL. However, (Meckenstock *et al.*, 2014) has shown that micro-droplets of water in NAPL contain microbes capable of degradation within the source zone.

Activation of degradation enzymes due to the presence of contaminant at high enough concentrations. The activation concentration can be relatively low, for example toluene's degradation activation concentration is only 50 μg/L (Alvarez & Illman, 2006).

Absence of inhibitory substances The presence of more easily degradable substrates can inhibit degradation. For example m-xylene is considered the most degradable xylene and has been shown to inhibit the degradation of o- and p-xylene (Meckenstock *et al.*, 2004). The accumulation of toxic by-products can also inhibit degradation. The creation of H_2S during anaerobic degradation under sulfate reducing conditions can be toxic at 200 mg/L (Beller & Reinhard, 1995). The concentration of the contaminant itself can also inhibit degradation if present in high enough concentrations (Alvarez *et al.*, 1991).

Availability of electron acceptors and electron donors The stoichiometry of degradation reactions needs to be considered during remediation design. For example, toluene requires different concentrations depending on the different electron acceptors - 1 mg/L of toluene requires 3.13 mg/L of O_2, 4.85 mg/L of NO_3, 4.70 mg/L of SO_4^{2-} or 21.85 mg/L of Fe^{3+} (Alvarez & Illman, 2006).

Availability of nutrients Organisms require nutrients (eg. nitrogen, phosphorous) to synthesize amino acids, enzymes, and for a host of other cellular activities (Alvarez & Illman, 2006). Microbes also require trace metals (eg. iron, magnesium, nickle, cobalt, zinc), however high concentrations can also be toxic.

Geochemical conditions conducive to growth Every strain of microorganisms have their optimal range of pH and temperature at which they mineralize contaminants. Temperatures in the subsoil however are not usually in the optimal range of 20-30°C at many contaminated sites, however the temperature is also not so low it inhibits microbial growth (EPA, 2013)

2.4 Hydrocarbon Degradation

Benzene has been shown to degrade under nitrate, sulfate and iron reducing conditions (Meckenstock *et al.*, 2016) and under stimulated methanogenic conditions. Wilson *et al.* (1986) showed the first example of methanogenic benzene degradation. The process was slow, however, and took 120 weeks and had a lag time of 40 weeks. In methanogenic conditions benzene is degraded via phenol to methane and CO_2. Benzene degradation was first reported under sulfate reducing conditions by Edwards & Grbic-Galic (1992) and under nitrate reducing conditions first by Majora *et al.* (1988). Benzene degradation can proceed by carboxylation to benzoate (Abu Laban *et al.*, 2009; Kunapuli *et al.*, 2007) and hydroxylation to phenol (Caldwell & Suflita, 2000). Pure isolates of benzene degrading cultures are rare and generally a consortia of bacteria are present in benzene degrading cultures (Foght, 2008).

Toluene is the most readily degraded of the BTEX components under all reducing conditions (Foght, 2008). In sediment columns toluene was readily degraded in 1-2 months, while benzene was recalcitrant over 500 days (Langenhoff *et al.*, 1996). Toluene is degraded by fumarate addition through the enzyme benzylsuccinate synthase (bssA). Several pure strain cultures of toluene degrading bacteria have been isolated (Foght, 2008).

Like toluene, xylenes are degraded by fumarate addition, though they differ in their degradation susceptibility. Generally m-xylene is considered the most readily degradable xylene, while o- and p-xylene are less readily degraded, though complete degradation has been shown in some cultures (Edwards *et al.*, 1992)

Ehtylbenzene degradation rates differ between bacterial cultures. Sulfate (Elshahed *et al.*, 2001) and nitrate (Reinhard *et al.*, 1997) reducing cultures have been reported. Pathways for ethylbenzene degradation include fumarate addition or hydroxylating to form 1-phenlethanol (Ball *et al.*, 1996)

PAHs have also been shown to degrade in anaerobic conditions (Meckenstock *et al.*, 2016). Studies have focused mainly on naphthalene and methylnaphthalene degradation, which are activated by methylation and addition of fumarate via carboxylation (Callaghan, 2013). Chang *et al.* (2002) were able to degrade 80-100% of phenanthrene, acenaphtene, anthracene, fluorene and pyrene in soils with PAH-adapted anaerobic cultures. In their study Chang *et al.* (2002) found that degradation was affected by the pH, temperature and carbon source. Degradation of greater than 4 ring PAHs has been shown, though it is not clear in studies if they are used as substrates or are co-metabolized (Meckenstock *et al.*, 2004). Naphthalene and methylnaphtalene have been degraded under sulfate reducing conditions (Coates *et al.*, 1996; Meckenstock *et al.*, 2016) and under methanogenic conditions (Berdugo-Clavijo *et al.*, 2012), however, only a few studies have demonstrated degradation under iron reducing conditions (Kleemann & Meckenstock, 2011) or nitrate reducing conditions (Eriksson *et al.*, 2003; Rockne *et al.*, 2000).

Component must be in the aqueous phase in order to be available to bacteria for biodegradation. Therefore the rate of dissolution from the NAPL to the aqueous phase can be limiting if the degradation rate exceeds the dissolution rate. Furthermore, source zones are assumed to have uniform NAPL component distributions (Geller & Hunt, 1993). However, internal concentration gradients of NAPL components are likely, where the concentration at the NAPL-water interface is lower than the concentration away from the interface (Conrad *et al.*, 1992; Mackay *et al.*, 1991). The diffusion of tar components within the NAPL therefore may limit the equilibrium concentration at the NAPL-water interface, limiting source zone depletion of tar components. Recent work by Meckenstock *et al.* (2014) however, found that tiny droplets (1-3 μL) of water within pure phase tar samples were habitats microorganisms which were anaerobically degrading the tar.

2.5 Monitoring Degradation

Monitoring biodegradation must consider three lines of evidence: (1) geochemical conditions, (2) the concentration of mobile tar components, intermediates and metabolites in groundwater and (3) microbial conditions (Figure 2.4).

2.5.1 Geochemical Conditions

Changes in pH, redox, anion and cation concentrations can indicate degradation is taking place in-situ (Alvarez & Illman, 2006). These parameters are also important to monitor as remediation interventions can have unexpected or undesirable consequences. For example changes in pH can lead to the mobilization of heavy metals in the soil (EPA, 2013).

2.5.2 Mobile Tar Components and Metabolites

The presence of metabolites can indicate the occurrence of anaerobic degradation. Signature metabolites are particularly useful, as they are specific to the parent compound and indicate

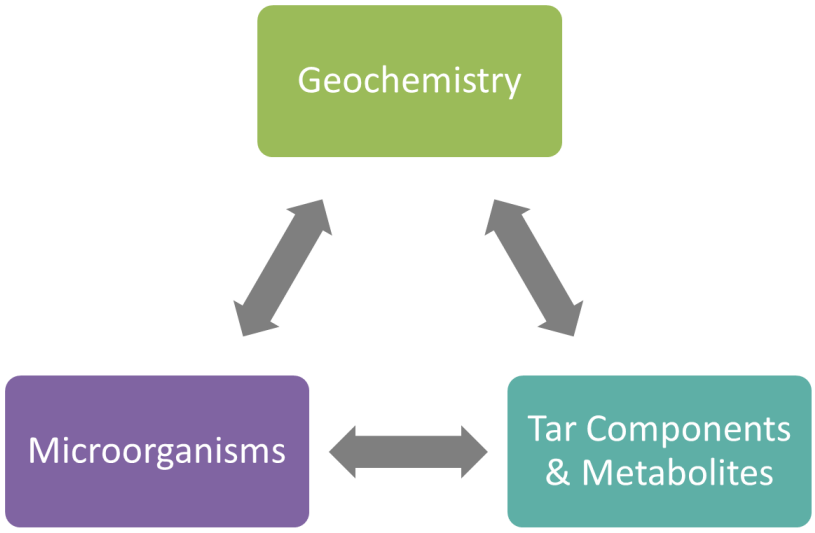

Figure 2.4: *Three lines of evidence necessary for monitoring biodegradation, recreated from van Leeuwen & Gerritse (2016)*

degradation by a particular reaction is occurring (Callaghan, 2013). Table B.1 summarizes the important metabolite and degradation pathways relevant to this study.

2.5.3 Microbial Conditions

Coupled to the detection of signature metabolites is the screening for specific enzymes and genes in microbes(See Table B.1). For example, the detection for the genes benzylsuccinate synthase or naphthyl-2-methylsuccinate sunthase characterize the fumarate addition degradation pathway for aromatic hydrocarbons (Callaghan, 2013). Specific bacteria can also be monitored, for example bacteria belonging to the *Peptococcacaea* have been identified as benzene and naphthalene degraders and therefore their presence is indicative of benzene and/or naphthalene degradation (van der Zaan *et al.*, 2012).

2.6 Site Description: Amersfoort

Located at the Amersfoort Central Station a former manufactured gas plant (FMGP) was in operation from 1910 - 1957 that produced Pintsch gas for lighting railway cars. Typical coal tar waste from FMGP are complex mixtures of 200-350 components (Birak & Miller, 2009). However, previous research on Amersfoort by GCxGC TOFMS and GC-MS analysis found 980 components, including aliphatics, aromatic, PAH, heterocyclic and oxygenated compounds (ALcontrol Laboratories, 2011; van Leeuwen, 2018). Significantly, no published data were available about Pintsch gas tars prior to the analysis of the Amersfoort oil. From GC-MS analysis and partitioning tests 24 components of interest were identified as soluble in water (van Leeuwen, 2018).

Historical aerial photos and recent site investigation found that the bulk of the contamination is located below the original disposal lagoons (Figure 1.1, van Leeuwen & Gerritse 2016). The tar is a multicomponent DNAPL, 3-5% denser than water. As the waste lagoons were unlined, the tar sunk by gravity through the subsurface, coming to rest on an aquitard (Eem layer) located between 10-12 meters below ground surface (mbgs) (van Leeuwen & Gerritse, 2016).

Previous interventions on site include the installation in 1999 of 1200 m^2 of sheet pilling to isolate the contaminated zone (van Leeuwen & Gerritse, 2016). The 'funnel & gate' system directed groundwater towards an aerobic bio-screen to treat the groundwater and prevent the spread of

further contamination (van Leeuwen & Gerritse, 2016). However, after the installation of the sheet pilling it was found that groundwater was being diverted and flowing around the southern end of the sheets (Figure 1.1, van Leeuwen & Gerritse 2016).

The site has a two aquifer system, with the first aquifer being a fine silt-coarse sand layer from the Twente formation, which extends down to 11 mbgs (Palm *et al.*, 2010). The aquifer is partially confined by the clay/peat Eem layer. The Eem layer is not considered a completely confining layer as it thins from 2 m in the northeast to less than 1 m in the southwest and disappears completely 100 m southwest of the edge of the sheet pilling (van Leeuwen & Gerritse, 2016).

Groundwater flow differs between the two aquifers. In the first aquifer groundwater flows from northwest to southeast, where it is diverted by the sheet pilling, flowing around the south-west edge of the pilling and through the 'funnel' to the east (Figure 1.1). At the west edge of the sheet pilling the Eem layer thins and groundwater flows down around the edge of the layer, from the first aquifer to the second (Figure 2.5). Generally, within the second aquifer the groundwater flow direction is from south to north-northwest (Gerritse *et al.*, 2017).

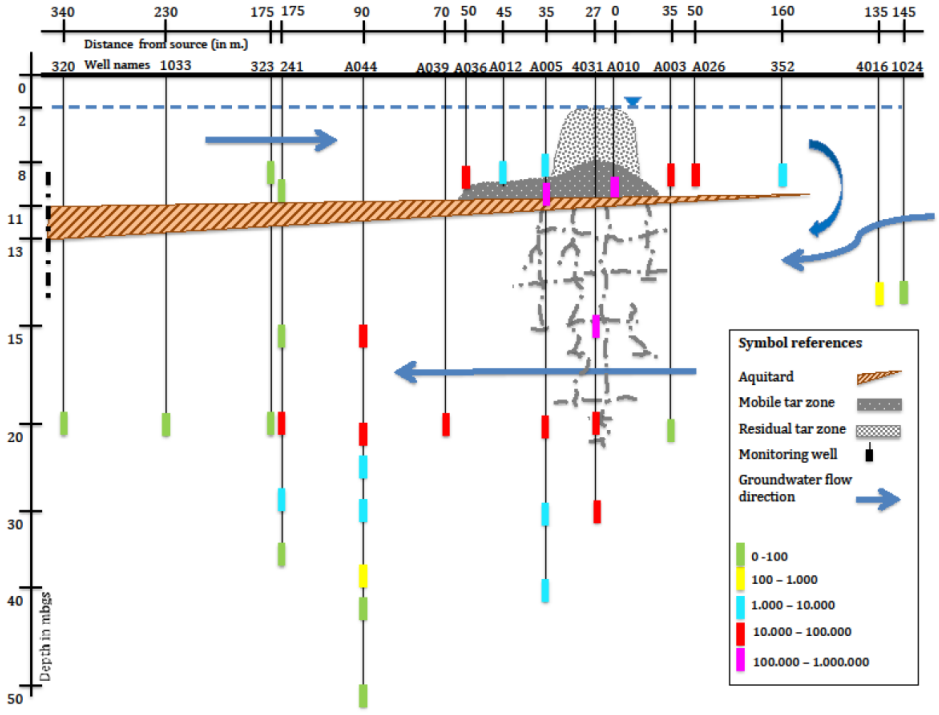

Figure 2.5: *Profile view of site layout showing the thinning Eem layer, BTEX concentrations in wells and general groundwater flow patterns (Gerritse* et al.*, 2017)*

The hydraulic conductivity varies on site, from 1.73 - 5.14 m/day depending on the depth within the first aquifer (Palm *et al.*, 2010). Groundwater flow velocities in the first aquifer were calculated from the measured groundwater level in the field (van Leeuwen & Gerritse, 2016). The groundwater velocity varies from 3 m/yr to 15 m/yr between the sheet pilling, increasing toward to the edge of the eastern gate to a maximum of 25 m/yr just outside the gate (van Leeuwen & Gerritse, 2016). To the north-west of the sheet pilling, the groundwater flow is 23 m/yr, to the north of the sheet pilling 23 m/yr and to the south 12 m/yr (van Leeuwen & Gerritse, 2016).

The redox conditions of groundwater in the first aquifer are nitrate reducing upstream of the source zone and iron and sulfate reducing downstream (Wagner, 2015). In the second aquifer the redox conditions are primarily iron-reducing and methanogenic (Wagner, 2015). The soil has low organic carbon content, limiting adsorption (Goossen & Booms, A, 2013). The bulk density of the

soil is approximately 1700 kg/m^3 with average porosity of 0.32 (van Leeuwen & Gerritse, 2016).

Three distinct zones of contamination have been identified;

Mobile Source Zone The source zone contains an estimated 2 - 6 million kg of tar and extends between 6-12 mbgs in the first aquifer (Figure 2.6). Furthermore, the Eem layer is considered a poor confining layer and pure phase DNAPL has been pumped from as deep as 25 mbgs (van Leeuwen & Gerritse, 2016). The main DNAPL pool covers an estimated 11 hectares (van Leeuwen & Gerritse, 2016).

Immobile Residual Zone The residual zone is located above the mobile pool of DNAPL, extending between 3-6 mbgs. The residual zone is highly variable with discontinuous blobs and ganglia of varying degrees of saturation (Figure 2.7). Even within the residual zone small pools of pure NAPL are found on the order of cm to tens of cm in scale (van Leeuwen & Gerritse, 2016). The residual zone is approximately 16.7 hectares in size (van Leeuwen & Gerritse, 2016).

Plume Zone Two contamination plumes exist at Amersfoort within the first and second aquifers. Due to the complex groundwater flow patters the direction and extent of the plumes differ between the aquifers (Figure 1.1). Within the first aquifer the plume zone covers an area of 11.5 hectares and in the second aquifer an area of 7.6 hectares, respectively (Wagner, 2015). The plumes delimited by the benzene and naphthalene intervention concentrations of 30 and 70 μg/L, respectively (Wagner, 2015). Within the second aquifer contamination as deep as 40 mbgs has been detected (van Leeuwen & Gerritse, 2016)

(a) *Pure phase tar (A033son2, 10.5 mbgs)* (b) *layers of pure phase tar (A033son)*

Figure 2.6: *Examples of soil cores from the source zone at Amersfoort showing the presence of mobile pure product and layering of NAPL lenses (van Leeuwen & Gerritse, 2016)*

2.7 Previous and On-going Research at Amersfoort

2.7.1 Stimulation Batch Experiments

A series of batches were created to compare the bioremediation potential of different redox conditions by stimulating anaerobic batches with different electron acceptors and substrates (Table 2.1). Batch bottles were prepared in a an inflatable nitrogen gas bag in order to maintain anaerobic conditions. Batch experiments were carried out in triplicate in 200 ml serum bottles with butyl/teflon lined septa. Batches contained 40 g of source-zone sediment from borehole A005 (depth: 10-10.5 m)

Figure 2.7: *Examples of soil cores from the immobile residual zone. (Gkekas, 2014)*

and groundwater from well A003A. Anaerobic, 1M stock solutions were prepared for each electron acceptor (nitrate, sulfate and chlorate) and substrate (acetate and succinate) and added to each treatment bottle respectively (Table 2.1). Control batches were prepared to account for abiotic transformations in bottles and sterilized with 100 mg/L NaN_3, 100 mg/L $HgCl_2$ and autoclaved at 121°C for 20 minutes. To compare the performance of the stimulated batches against the natural field conditions, a 'no addition' set of batches was prepared with no additional electron acceptors or substrates added. Batches were then inverted (septa down) on a shaker at 100 rpm in a climate chamber at 20°C.

Table 2.1: *Summary of batch experiment treatments. Batches were prepared anaerobically in triplicate.*

Batch No.	Treatment	Details
8	Sterile	100 mg/L NaN_3 + 100 mg/L HgCl2 + autoclaved
9	No Addition	
10	Nitrate	10 mM $NaNO_3$
11	Nitrate & Succinate	10 mM $NaNO_3$ & 2mM Succinate
12	Nitrate & Acetate	10 mM $NaNO_3$ & 3mM Acetate
13	Sulfate	10 mM $NaSO_3$
14	Chlorate	10 mM $NaClO_3$

Some batches were dosed as second and a third time with additional electron acceptors and/or substrate (Table B.2) and monitored for anion concentrations over the course of the first year of the experiment. At the time of this research the batch experiments had been in operation for three years, shaking inverted in a climate chamber at 20°C. Significant changes in tar composition were apparent from visual inspection of the high series batches. Stimulated batches containing electron acceptors and substrate had distinctly less tar stuck to the glass and there appeared to be less tar remaining overall (Figure 1.4).

2.7.2 Partitioning Batch Experiments

Batch experiments were performed in 2015 to test the differential dissolution behavior of components from pure phase tar (van Leeuwen, 2018). These experiments were necessary to calculate the source zone depletion, mass flux and dissolution behavior of tar from different locations on site (van Leeuwen, 2018). Two experiments were conducted, the first compared the equilibrium concentration of mobile components in the aqueous phase from tar samples from six different locations within the source zone on site. The second compared the effect of the tar/water ratio (v/v) to determine how dilution affects the partitioning of mobile tar components. At the time of this research the batch experiments has been completed and the GC-MS results were available for

interpretation.

(a) *Tar samples from different areas on site* (b) *Tar A010F with increasing water volumes*

Figure 2.8: *Partitioning batch experiments performed in 2015 (van Leeuwen, 2018).*

Batch experiments were carried out in 20 ml glass vials with silicone/PTFE caps and crimp sealed. In total, six tar samples were tested in vials which contained 13 ml of groundwater (well 323, 9-10 m), 2 ml of tar, and 5 ml of headspace (Figure 2.8a). Vials were rotated for five weeks on a test tube rotator (Labinco BV, The Netherlands). For the analysis of mobile tar components, 200 μL of sample was extracted from the vials and diluted in 11.8 ml of MilliQ water and analyzed by GC-MS (TNO, Utrecht). The location of the wells where the tar was sampled can be found in Figure 2.5.

A second set of batch experiments were performed with the most 'original' tar sample from site, located directly below the former tar lagoons, from well A010F. Six batch bottles were prepared with tar-water dilution ratios ranging from 1:10 to 1:3660 (Figure 2.8b). Bottles were sterilized with 25 mg/L of $HgCl_2$ to prevent degradation during the experiment. Mobile tar components were analyzed by GC-MS (TNO) by extracting 100 μL from vials and diluting in 12 ml MilliQ water in 20 ml glass vials.

Tar from different locations in the source zone partitioned substantially different benzene concentrations to the aqueous phase in experiment vials after 5 weeks (Figure 2.9). Tar from well A010F had the highest aqueous concentration of benzene, 44 mg/L, while tar from well A012A, located 45m upstream of well A010F, had only 0.2 mg/L of benzene. Similarly, the highest toluene concentrations were also measured in the A010F vial and the lowest in vial A012A, though the concentration difference was much less, 12 mg/L, between the highest to the lowest compared to the benzene concentration difference of 43.8 mg/L. All other components differed negligibly between the different tar vials.

Tar from well A010F was diluted with increasing volumes of water. The concentration of benzene that partitioned to the aqueous phase differed substantially between the lowest and highest dilutions (Figure 2.10). The aqueous benzene concentration decreased from 24.2 mg/L in the 1:10 dilution batch to only 1.2 mg/L in the 1:3613 batch. Similarly, toluene decreased from 20.1 mg/L to 3.8 mg/L for the same batch bottles. Styrene and m/p-xylene differed by 2.6 and 1.3 mg/L, respectively, between the lowest and highest dilution bottles. All other components differed negligibly between the dilution vials.

These results suggested that benzene followed by toluene are the first components to be depleted in the source zone. With increasing distance from the center of the source zone, the equilibrium aqueous concentration of benzene in the tar samples decreased sharply (Figure 2.9).

Furthermore, Brock (2016) performed liquid chromatography mass spectroscopy (LC-QTOF-

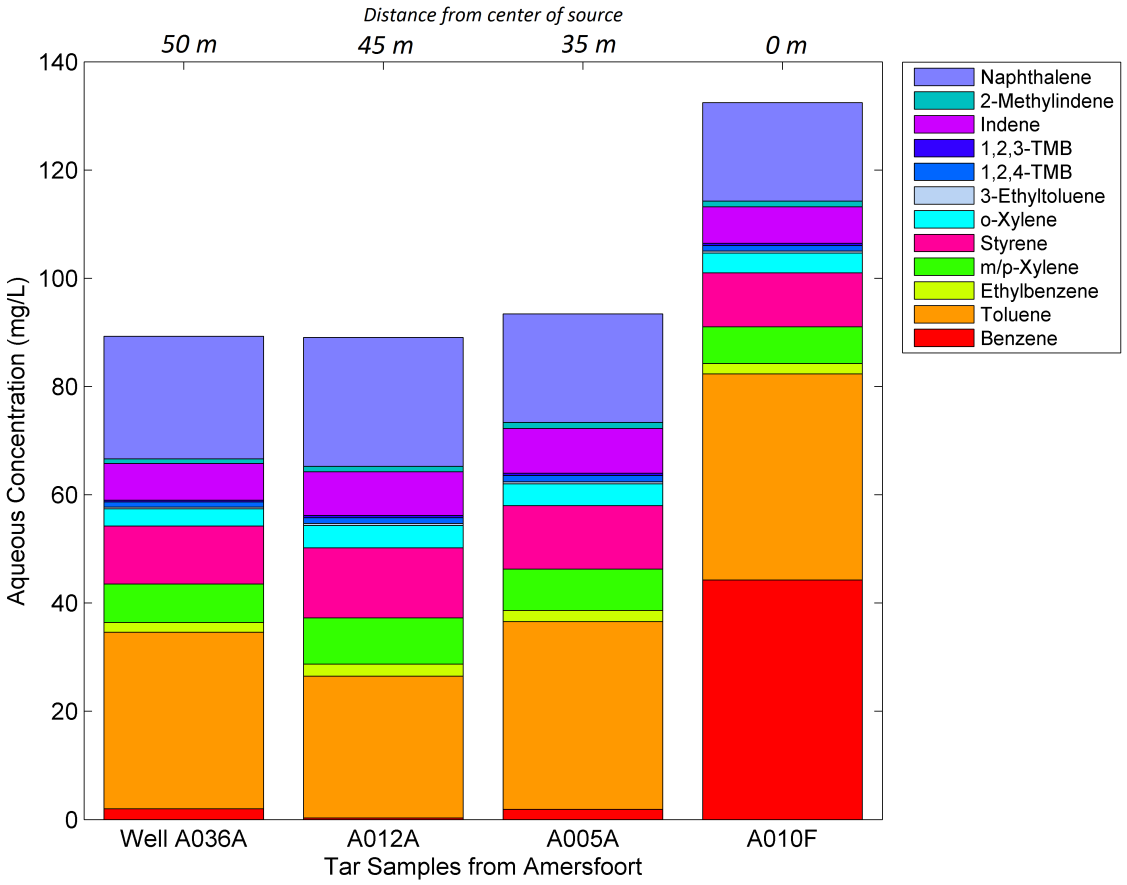

Figure 2.9: *Partitioned concentrations measured in the aqueous phase from batch vials from tars from different locations within the same source zone. Left to right: decreasing distance from the center of source: A036A 50 m, A012A 45 m, A005A 35 m and A010F 0 m from center of source zone.*

MS) to identify and quantify signature metabolites of mobile tar components within the tar-water samples from different sites. High metabolite concentrations were found in the tar-water samples, which was supported by further analysis of samples by Raptis *et al.* (2015). This suggested that degradation was taking place within the source zone, a conclusion supported by research from Meckenstock *et al.* (2014).

The results from the dilution batch experiments were used to calculate the initial concentration of mobile tar components within the tar sample in this research following the method of Rixey *et al.* (1999). Furthermore, the partitioning coefficients for the same mobile tar components were calculated and used to estimate the concentration of components of the tar from the different locations on site (first experiment).

2.7.3 Field Work

Wagner (2015) investigated the occurrence of signature metabolites of BTEX and PAH components to determine if anaerobic degradation was taking place in-situ. Signature metabolites of toluene and naphthalene were found in both the source and plume zones (Wagner, 2015). Moreover, metabolites for benzene, xylene, trimethylbenzene and phenanthrene were also found. Wagner (2015) also correlated redox geochemical conditions with degradation on site and found toluene and naphthalene degradation took place in the first aquifer under nitrate reducing conditions, while in the second aquifer degradation occurred in iron reducing conditions. Furthermore, the presence

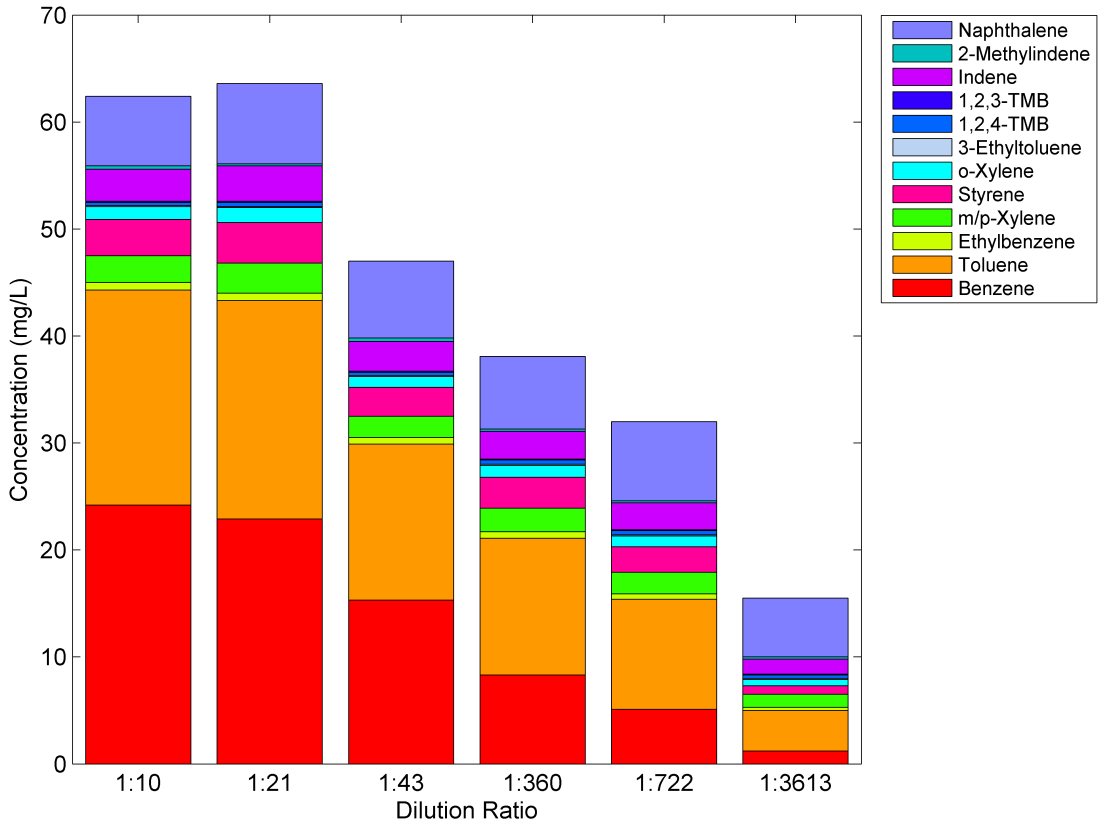

Figure 2.10: *Aqueous concentration of batch experiments with increasing tar/water (v/v) ratios. Concentration measurements after 5 weeks at equilibrium, tar from well A010F.*

of nitrate was correlated with low metabolite concentrations, whereas the absence of nitrate was correlated with high metabolite concentrations. This counter intuitive result was postulated to be due to the more complete degradation of metabolite components in the presence of nitrate, and the accumulation of metabolites as a result of degradation slowing down when nitrate was limited.

Raptis *et al.* (2015) performed microbial analysis to detect the functional genes of microorganisms present through qPCR to determine if aromatic degradation was taking place in the first and second aquifers. His results indicated that anaerobic degradation of toluene, and possibly benzene, was taking place in both aquifers. His results supported the conclusions of Wagner (2015) that toluene degradation occurred under nitrate reducing conditions within the first aquifer. Furthermore, the results indicated the potential for degradation in the first aquifer under sulfate reducing conditions as well. Finally, bacterial populations (gene count per ml groundwater) in the source zone were substantially higher than in the plume zone, indicating that bacteria on site were able to survive in this very toxic environment. This supported the results of Wagner (2015) who found metabolite concentrations in pure phase tar samples used in batch experiments.

Brock (2016) performed LC-QTOF-MS to identify and quantify signature metabolites in field samples and found evidence of indene degradation through the presence of carboxyl methyl indene and indanoic acid. The presence of benzene acetic acid in field samples suggested styrene degradation was occurring in some monitoring wells on site (van Leeuwen, 2018). Brock (2016) also performed DNA analysis and found methanogenic archea in field samples from wells with nitrate and sulfate reducing conditions, indicating the occurrence of micro-niches or overlapping redox zones. Finally, the highest total bacteria were found at or near the source zone, further supporting the idea that source zone degradation is currently taking place in Amersfoort.

van Logtestijn (2017) continued the metabolite and DNA analysis of field samples in addition to isotope fractionation to determine in-situ degradation rates. van Logtestijn (2017) found iron and manganese reducing conditions in the majority of the plume zone and sulfate and nitrate reducing conditions found only at the fringes. His results support the work of Bauer *et al.* (2008) and Meckenstock *et al.* (2015) who propose a plume-fringe conceptual model of contaminated site, rather than the traditional redox-zonation model. Finally, the isotope, metabolite and qPCR data indicated the majority of degradation was taking place at or near the source zone, agreeing with the results of Brock (2016); Raptis *et al.* (2015) and Wagner (2015).

Based on the results from the batch and field samples, which demonstrated the potential for biostimulation under nitrate reducing conditions, a field scale trial was conducted at Amersfoort between April 2016-January 2017. The objective of the field trial was to stimulate degradation of mobile tar components with the addition of nitrate as a terminal electron acceptor. The trial consisted of two transects, one of which was stimulated with nitrate while the second was a control. For detailed results from the first trial see van Logtestijn (2017) or Appendix A (Field Work).

Briefly, the first field trail found that metabolite concentrations initially increased in both the stimulated and control transect, indicating that recirculation of groundwater alone influenced degradation rates. Increased degradation through mixing has previously been observed by MacQuarrie & Sudicky (1990) andSong & Seagren (2008). However, in the stimulation transect, metabolite concentrations decreased after the initial peak, indicating continued degradation in the presence of nitrate. DNA results agreed with the metabolite data; gene assays increased in both the control and stimulated transects. The highest gene copies were found in the stimulated transect, coinciding with the peak concentration of the nitrate plume. This suggested a temporary increase in microbial activity, which decreased after the nitrate plume had passed.

The overall conclusions from the first field trial were that stimulation by nitrate injection increased microbial degradation but only temporarily. It was proposed that the bacterial exposure to nitrate was too short to establish a substantial degrader population and that longer or continuous exposure to nitrate could more effectively stimulate degradation. See Appendix A (Field Work) for more information about the first field trial and details of the second field trail conducted.

Chapter 3

Methods and Materials

3.1 Stimulation Batch Experiments

To quantify the concentration of mobile tar components in the stimulation batch experiments, a novel method for headspace GC-FID measurements was developed. This method was designed to be fast, non-destructive and give accurate results for sample with pure phase NAPL in the bottle. Headspace samples were ideal as they required only 25 minute runs and no prior preparation for the batch bottle. The alternative to headspace samples, aqueous samples, would have required the repeated removal of the liquid from the batch experiments, in addition to the time consuming sample preparation necessary. The headspace method allowed the quantification of methane gas and 12 mobile aromatic compounds previously identified as of significant interest in partitioning experiments. Methane was of interest as it indicated methanogenesis in batch bottles. From Henry's law (Eq. 2.4), both the aqueous and gas phase concentrations were calculated for each of the 12 components. This method assumed the concentration of PAHs larger than (methyl)naphthalene in the aqueous phase to be negligible due to their low solubility.

Quantifying the concentration of mobile aromatics in the gas and aqueous phase was the first step in the mass balance of mobile tar components to evaluate the bioremediation potential of different electron acceptors/substrates. Furthermore, the initial GC-FID measurements of the batches revealed higher concentrations of benzene in the stimulated batches than the sterile and no addition batches. However, only benzene, toluene and methane gas were measured in the initial analyses. The concentration of the remaining nine aromatics of interest were quantified to test the theory of the tar acting as a hydrophobic matrix, sorbing aromatic hydrocarbons from the aqueous phase and lowering concentrations in the no addition and sterile batches. If the concentration of mobile aromatics increased as a result of stimulated biodegradation this would identify a clear risk of source zone remediation.

3.1.1 Hydrocarbon Stock Solutions

A 0.2 g/L hydrocarbon stock solution was prepared with eleven aromatic hydrocarbons of interest (Table 2.1). The proportion of the eleven chemicals in the stock mixture reflected the maximum solubility proportions of the same chemicals in the field, scaled down to a 0.2 g/L solution. The stock solution was used to create calibration curves and dose batch experiments.

A serum bottle (500 ml) with 500 ml of MilliQ water was flushed with 100% N_2 gas for 30 minutes. The gas was run over a glass column of hot (350°C) copper flakes to remove any trace oxygen from the gas. Naphthalene was added as a solid and the headspace was flushed for an additional 5 minutes. The bottle was then crimp sealed with a viton stopper and aluminium cap. The bottle was placed on a stirrer at 100 rpm for four days, and then the stirrer was increased

Table 3.1: *Chemicals used to create the hydrocarbon stock solution used for calibration of GC-FID measurements. Concentrations given for final concentration in the bottle, based on the maximum dissolution ratio of chemicals in the field scaled to a 0.2 g/L solution.*

Chemical	Volume	Unit	Purity (≥%)	Concentration (mg/L)	Brand
Benzene	30	μL	99	53	Janssen Chimica
Toluene	26	μL	99.5	44	Lab Scan
Ethylbenzene	3	μL	99	6	Janssen Chimica
p-xylene	4	μL	99	8	Janssen Chimica
m-xylene	4	μL	99	8	Janssen Chimica
o-xylene	17	μL	99	30	Janssen Chimica
Styrene	5	μL	99.5	10	Fluka
1,2,4-trimethylbenzene	1	μL	98	2	Aldrich
1,2,3-trimethylbenzene	1	μL	Analytical Grade	1	Fluka
Indene	8	μL	99	16	Sigma-Aldrich
Naphthalene	16	mg	99	32	Sigma-Aldrich
Sodium Bromide	2.5	ml	-	250	

to 300 rpm for two days to fully dissolve the naphthalene. Sodium bromide was then added as a tracer (2.5 ml of a 50 g/L stock solution). Finally, the remaining chemicals were added using 10-50 μL glass syringes. To increase the dissolution of the chemicals the bottle was placed in a shaking incubator at 30 °C and 100 rpm for one week. Table 3.1 summarizes the volumes of chemicals added, their respective purities and calculated final concentrations in the serum bottle.

3.1.2 Analytical Methods

All 21 batch bottles (7 treatments, 3 replicates) were analyzed for volatile aromatic hydrocarbon using an Agilent 6850 GC-FID system equipped an Agilent HP-1 column (0.32 mm x 30 m). The FID detector was set at 250°C and the injector at 200°C with a split ratio of 5:1. The final oven temperature program was 3 minutes at 40°C, followed by an increase of 10°C/min to 90°C and held constant for 4 minutes then increased by 10°C/min to 220°C. The program was run with constant pressure of 5 psi with helium carrier gas. Headspace samples (0.5 ml) were withdrawn from batch bottles with a 1 ml glass, Pressure-Lock syringe. Sterile disposable needles were first flushed with N_2/CO_2 gas (80%/20%).

Hydrocarbons were also measured by GC-MS. The 'A' replicate from each treatment was analyzed. In the case of the nitrate batches (batch 10) the 'B' replicate was analyzed as the 'A' series had previously leaked and the bottle no longer contained an aqueous phase. Samples were extracted in a UV flow cabinet (Telstar EF/S). Batch bottles caps were sterilized prior to sample withdrawal by flaming with ethanol. Batch bottles were shaken to ensure well mixed sample withdrawal. Samples were analyzed in 20 ml glass vials with 11.3 ml MilliQ water and and sterilized with 0.6 ml of 0.5 g/L $HgCl_2$ (25 mg/L final concentration). Vials were crimp sealed with silicone/PTFE magnetic caps. Batch samples of 0.1 ml were withdrawn using 1 ml sterile, disposable plastic syringes. Syringes were first flushed with N_2/CO_2 gas (80%/20%) and needle tips were disposed of between sampling and injection to 20 ml vials to ensure no oil was transferred on the needle tip. Samples were analyzed within 24 hours.

GC-MS analysis was performed by TNO (Utrecht, Netherlands) on a Shimadzu GC-2019 with a Shimadzu QP-2010Plus mass spectrometer and Varian VF-624ms column (0.25 mm x 30 m). Samples were heated to 75°C for 20 minutes and extracted with a syringe also at 75°C. Headspace samples (250 μL) were taken with a PAL autosampler. The injector temperature was 200°C with

a split ratio of 5:1. The oven temperature program was 1 minute at 40°C , followed by an increase of 10°C/min to 200°C then increased by 20°C/min to 300°C and held for 1 minute. The program was run with constant flow of 1 ml/min with helium carrier gas and ion source temperature of 200°C. Five internal standards were used (benzene-d6, toluene-d8, ethylbenzene-d10, 1,3,5-trimethylbenzene-d12 and naphthalene-d8). Calibration was done with external standards (10-100 μL) with the following concentrations in methanol; 2, 20, 50, 100 and 200 mg/L.

3.1.3 Peak Identification and Calibration Curves

The retention time for the hydrocarbons of interest and methane gas were identified on the GC-FID by injecting headspace samples from 20 ml serum bottles with each target analyte dissolved in the aqueous phase. The GC-FID analysis was then fine-tuned to allow acceptable separation between components of interest and calibration vials were prepared to quantify each analyte of interest.

A nine-point standard calibration curve was created by spiking distilled water with a known concentration from the stock hydrocarbon mixture. Standards were prepared in 100 ml serum bottles and ranged from 10-320 times diluted from the hydrocarbon mixture. Standards were prepared with the same headspace/water ratio (v/v) as the original batch experiments. Serum bottles were filled with MilliQ water and 5 ml $HgCl_2$ (0.5 g/L stock solution for final concentration of 25 mg/L in bottles), and closed with viton stoppers and crimp sealed with aluminium caps. Next, the hydrocarbon stock solution was injected into the bottles using glass, gas tight syringes. Bottles were created in duplicate. Headspace GC-FID measurements were taken and the aqueous concentration to peak area were plotted. A second degree polynomial provided the best fit to the data for each of the eleven hydrocarbons (Figures B.1 and B.2). The calibration curves were then used to calculate the concentration in batch bottles from the peak areas measured on the GC-FID.

Methane, 1- and 2-methylnaphthalene were calibrated separately by spiking distilled water in 50 ml serum bottles. Standard bottles were prepared with the same headspace to water ratio as the original batch experiments. Standard concentrations ranged from 1-10 mg/L for methane and 0.5-10 mg/L for 1- and 2-methylnaphthalene. Linear calibration curves were calculated by plotting the standard concentrations against their respective peak areas from GC-FID measurements (Figure B.2).

3.2 Tar as a Hydrophobic Matrix: Batch Experiments

3.2.1 Initial Tar Concentration and K_{nw} Calculation

Results from the partitioning batch experiments performed by van Leeuwen (2018) were used to calculate the initial concentration and partitioning coefficient of mobile tar components following the method outlined in Rixey *et al.* (1999). The method assumed linear partitioning, where the equilibrium concentration of component i in the NAPL (C_n^i) and aqueous (C_{aq}^i) phases can be related by their partitioning coefficient (K_{nw}^i);

$$K_{nw}^i = \frac{C_n^i}{C_{aq}^i} \tag{3.1}$$

and a mass balance of component i in the batch bottle gives;

$$M_n(C_n^{i,\circ} - C_n^i) = V_{aq}C_{aq}^i \tag{3.2}$$

where M_n is the mass of NAPL, $C_n^{i,\circ}$ is the initial concentration in the NAPL, C_n^i is the concentration in the NAPL following dissolution to the aqueous phase, V_{aq} is the aqueous volume in the

batch and C^i_{aq} is the aqueous concentration after dissolution of components i from the NAPL to the water.
Combining equations 3.1 and 3.2 gives;

$$\frac{1}{C^i_{aq}} = \frac{1}{C^{i,\circ}_n}(\frac{V_{aq}}{M_n}) + \frac{K^i_{nw}}{C^{i,\circ}_n} \tag{3.3}$$

From the batch experiments with different tar-water volume ratios we know C^i_{aq} and the $\frac{V_{aq}}{M_n}$. Plotting $\frac{1}{C^i_{aq}}$ vs. $\frac{V_{aq}}{M_n}$ gives a graph with a linear slope of $\frac{1}{C^{i,\circ}_n}$ and a y-intercept of $\frac{K^i_{nw}}{C^{i,\circ}_n}$, from which K^i_{nw} and $C^{i,\circ}_n$ were determined.

A significant limitation of this method, however, is that very low solubility and/or low concentration tar components will not partition from the tar to the aqueous phase in detectable concentrations in the relatively small water volumes used (max: 11.5 L). Highly insoluble components, for example PAHs, will be underestimated, or not be able to be calculated at all. PAHs are expected to be a significant proportion of the tar based on previous coal tar characterizations (Fraser *et al.*, 2008; King & Barker, 1999; Peters & Luthy, 1993; van Leeuwen, 2018), though the concentration in the water is expected to be low due to the low solubility.

3.2.2 Current Partitioning Batch Experiment Preparation

Batch experiments were created to test the hypothesis of the tar acting as a hydrophobic matrix and retaining components in the tar and out of the aqueous phase. Several reference NAPLs were considered (liquid silicone, petroleum jelly, silicone rubber, activated charcoal) and a bituminous material was chosen. The bituminous material (Shell Tixophalte) was chosen as it was a DNAPL, sticks to glass during shaking and easily obtained from local hardware stores (Figure 3.1). Pure tar from site (well A005A-2, depth: 9-10 m, collected: June 17, 2015) was used in a second series of batch experiments (Figure 3.1). Tar from this location was chosen as the original stimulation batch experiments contained contaminated sediment from the same well (A005). Using tar from the same location on site allowed the best comparison between the new and old batch experiments. Batches were also prepared anaerobically to be consistent with the original batch experiments.

Eight sets of batches were prepared. Table 3.2 summarizes the batch treatments and replicates. The experiments were performed in 200 ml glass bottles closed with viton stoppers (Rubber BV, Hilversum, The Netherlands) and crimp sealed with aluminium caps. Sterile control batches were prepared to account for abiotic transformations during the experiments.

The first series of batches (batches 1-4) were prepared with 95 ml of Milli-Q water flushed with N_2/CO_2 (95%/5%) for 10 minutes in the water and 2 minutes in the headspace to render the batches anaerobic. The N_2/CO_2 gas was run over a glass column of hot (350°C) copper flakes to remove any trace oxygen from the gas. To sterilize the bottles, 5 ml of 0.5 g/L $HgCl_2$ stock solution was added for a final concentration of 25 mg/L.

The second series of batches (batches 5-8) were prepared with 95 ml of clean groundwater from well 323 (depth: 8-9 m, collected: July 27, 2017) located upstream of the contamination. The groundwater and tar collected from site were stored in a climate chamber at 4 °C. Batch bottles were flushed for 2 minutes in the headspace with N_2/CO_2. Flushing in the water was not necessary as the groundwater collected from site was kept under anaerobic conditions and after use the bottle headspace was flushed with N_2/CO_2 to remain anaerobic during subsequent storage. All batches were sterilized with 2 ml of 5 g/L $HgCl_2$ stock solution for a final concentration of 100 mg/L. One batch was sterilized with and additional 2 ml of 5 g/L NaN_3 stock solution for a final concentration of 100 mg/L and was autoclaved for 20 minutes at 121 °C (Astell). This additional sterilization replicated the technique used for the original Amersfoort tar batch experiments and was necessary to compare the effect of autoclaving and NaN_3 on the partitioning behaviour of tar.

Figure 3.1: *Top: Batch 1 with bitumen and Bottom: Batch 8 with tar from site (well A005A).*

The bitumen was added to the bottles before flushing while the tar from site was added through the septa after flushing the water to prevent loss of aromatics. The bitumen was too viscous and difficult to work with to add to bottles after flushing the water.

Previous batch experiments contained sediment with tar. However, for the current batch experiments only pure phase tar was added to keep the initial experiment simple and examine only the effect of tar on the partitioning of target analytes. The volume of the tar (V_{tar}) was calculated based on the mass of sediment added to the original batch experiments ($M_{sed} = 40$ g), the reported porosity ($\eta = 0.32$) and bulk density of the sediment from site ($\rho_{soil} = 1.7$ g/cm^3) and estimated NAPL saturation of the soil ($\theta_{sat}^{Tar} = 0.2$) (Palm *et al.* 2010);

$$V_{tar} = \frac{M_{sed} \times \eta \times \theta_{sat}^{Tar}}{\rho_{soil}} \approx \quad 1.65 cm^3 \tag{3.4}$$

An error in the initial calculation resulted in 3.6 cm^3 of tar being added to the batches, and not the 1.6 cm^3 calculated. This error did not affect the overall results, however, as the purpose of the experiment was to observe whether components partitioned into the tar from the aqueous phase ans this was still valid with the extra tar volume.

Table 3.2: *Details of batch experiments performed. Batches were amended with one or more stock solutions; 0.6 ml benzene (B), 4 ml hydrocarbon mix (HC) or 5 ml of an organic stock mix (Org).*

Batch	Non-Aqueous Phase	Stock Solution	No. Bottles	Sterilization		
				$HgCl_2$ *(mg/L)*	NaN_3 *(mg/L)*	Autoclave
1	Bitumen	B, Org	3	25		
2	Bitumen	HC	2	25		
3	*	B, Org	3	25		
4	*	HC	2	25		
5	Tar*	-	3	100		
6	Tar*	-	3	100	100	x
7	*	B	3	100		
8	Tar	B	3	100		

*Indicates control batch used to monitor abiotic transformations

Table 3.3: *Summary of chemicals and their properties used to create the benzene and organic stock solutions*

Chemical	Volume	Unit	Purity	Concentration	Brand
Benzene Stock			(%)	(mg/L)	
Benzene	400	μL	99	1,800	Janssen Chimica
Organic Stock					
Benzene	23	μL	99	100	Janssen Chimica
Toluene	23	μL	99.5	100	Lab Scan
Chlorobenzene	18	μL	99.5	100	Fluka
1,2-Dichlorobenzene	15	μL	99	100	Fluka
1,3-Dichlorobenzene	15	μL	99	100	Fluka

3.2.3 Stock Solutions

Batches were amended with one or more stock solutions; (1) a benzene solution, (2) a 0.2 g/L hydrocarbon solution or (3) a 0.5 g/L organic solution. Injection of pure benzene to batch bottles would have required a prohibitively small volume and therefore a 20 mM stock solution was prepared. The benzene solution was used to observe the partitioning behavior of a single chemical added to the aqueous phase. Benzene was chosen as it was observed to be elevated in the stimulation batch experiments with added electron acceptors during initial measurements. The hydrocarbon mix contained 11 of the most abundant contaminants found in plume zone on site, with relative concentrations reflecting their maximum solubility scaled down to a 0.2 g/L solution (Table 3.1).

However, a key disadvantage of the hydrocarbon mix was that the initial concentration of chemicals varied over orders of magnitude. Therefore, a second solution was created with 5 organic chemicals, all with an initial concentration of 100 mg/L (Table 3.3). This solution also contained 3 chemicals not found in the hydrocarbon mix to have an even distribution of $\log K_{ow}$ values between 2.1 and 3.6. This even distribution of $\log K_{ow}$ values was necessary to observe how chemicals, with the same initial concentration, partitioned to the NAPL based soley on their $\log K_{ow}$ values and to confirm this phenomena was not limited to chemicals only found in tar from site but general to hydrophobic components.

The benzene and organic stocks were prepared in 200 ml serum bottle by flushing 200 ml Milli-Q water with 100% N_2 gas for 10 minutes, followed by 2 minutes in the headspace. Bottles were

then crimp sealed with viton stoppers and aluminum caps. Viton was chosen, over for example butyl stoppers, to prevent diffusion of chemicals through the stopper.

For the benzene solution, 400 μL was added through the septa using a 500 μL glass, gas-tight syringe. For the organic solution benzene, toluene, chlorobenzene, 1,2-dichlorobenzene and 1,3-dichlorobenzene were injected through the septum to achieve a final concentration in the bottle for each chemical of 100 mg/L. The bottles were then placed in an incubating platform shaker at 100 rpm and 30°C for 48 hours to fully dissolve the mixtures. See section 3.1.1 and Table 3.1 for the preparation of the hydrocarbon stock solution.

Batches were injected with the same stock solutions three times. After each injection the batches were shaken by hand for 1 minute, then inverted on a platform shaker (100 rpm) in a climate chamber (21°C). Headspace GC-FID measurements were taken at regular intervals (ex. 1, 3, 5, 24, 96, 168 hours and up to 600 hours after injection) using the method described in Section 3.1.2. The batches were amended with the same volume and concentration of stock each time.

3.2.4 Concentration Calibration Curves

Six additional calibration bottles were prepared with known concentrations of each of the five chemicals in the organic stock bottle by spiking Milli-Q water with the organic stock solution. Calibration bottles were prepared in 50 ml serum bottles and crimp sealed with viton stoppers. The headspace to aqueous volume ratio was kept consistent with the original batch experiments with 60% headspace 40% aqueous volume. Concentrations ranged from 0.5 mg/L to 30 mg/L. Headspace GC-FID measurements were taken and the aqueous concentration was plotted against peak area. A second degree polynomial provided the best fit to the data (Figure B.4). This calibration curve was then used to calculate the concentration in batch bottles from the peak areas measured on the GC-FID.

3.2.5 Mass Balance and K_{nw} Calculations

Control batches (Batch No. 3, 4 and 7) were injected with stock solutions (benzene, hydrocarbon mix, organic mix) simultaneously with treatment batches. In this way, the concentration of spiked components in the control batch could be measured and averaged from the control batch concentrations to determine the actual injected concentration to treatment batches. This check was necessary because each time the stock solutions were sampled the aqueous phase decreased in volume. According to Henry's Law, the aqueous phase then reaches an equilibrium with the gas phase, resulting in a decrease in the aqueous phase concentration in the stock bottle. This effect was most notable in the hydrocarbon stock solution, which was also used for other experiments, and large volumes (>50 ml) were extracted at a time. During the course of the experiments 200 ml of the 500 ml hydrocarbon stock bottle were consumed, or 40% of the total volume. Control batches could also be monitored for abiotic loss of chemicals in this way as well.

The partitioning coefficients for each chemical and NAPL were calculated based on the equilibrium concentration after each addition of stock solution. Equilibrium was defined as when the concentration was stable, usually within 24 hours after injection for the tar and 168 hours after injection for the bitumen batches. The difference between the concentration added to the batches and the concentration measured on the GC-FID was used to calculate the mass transfer into the NAPL. From Henry's law the gas phase concentration (C_g^i) of each component i was calculated given the known aqueous phase concentration (C_{aq}^i) injected (Eq. 2.3). The dimensionless Henry's constant can be calculated from the Henry's constant for each components as:

$$K_h^i = \frac{H_C^i}{R \times T} \tag{3.5}$$

Table 3.4: *Relevant parameters for mass balance calculations for the consitituents of stock solutions and NAPL used in batch experiments.*

	Henry's Constant[a] (*atm-ml/mol*)	K_h^{i} [a] (-)	$LogK_{ow}$ [b] (-)
Tar Constituents			
Methane	6.6E+05	27.2	0.6
Benzene	5480	0.23	2.1
Toluene	6740	0.28	2.7
Ethylbenzene	7880	0.33	3.2
p-Xylene	6300	0.26	3.2
m-Xylene	6300	0.26	3.2
Styrene	2610	0.11	3.1
o-Xylene	5350	0.22	3.0
1,2,4-Trimethylbenzene	5700	0.24	3.8
1,2,3-Trimethylbenzene	3180	0.13	3.7
Indene	1590	0.07	2.9
Naphthalene	460	0.02	3.3
2-Methylnapthalene	515	0.02	3.6
1-Methylnapthalene	514	0.02	3.3
Reference			
Chlorobenzene	3700	0.15	2.8
1,2-Dichlorobenzene	1900	0.08	3.5
1,3-Dichlorobenzene	3100	0.13	3.4

[a] (Sander, 2015), [b] (National Center for Biotechnology Information, n.d.)

where H_C^i is the Henry's constant, R is the universal gas constant (8.314 N m mole^{-1} K^{-1}) and T is temperature in Kelvin (22°C or 295.15 K). Table 3.4 summarizes the Henry's constants and dimensionless Henry's constants for relevant chemicals (Mayer & Hassanizadeh, 2005).

The equilibrium measured concentration for the control batches with tar (batch 5 and 6) were compared against the calculated aqueous concentration given the calculated partitioning coefficients from the original partitioning experiments (Table 3.4). The expected aqueous concentration was determined by performing a mass balance calculation for the concentrations in each phase, given the known volume of each phase in the bottle.

$$M_T^i = M_n^i + M_{aq}^i + M_g^i \tag{3.6}$$

$$M_T^i = C_n^i V_n + C_{aq}^i V_{aq} + C_g^i V_g \tag{3.7}$$

$$M_T^i = K_{nw}^i C_{aq}^i V_n + C_{aq}^i V_{aq} + K_h^i C_{aq}^i V_g \tag{3.8}$$

Where M^i is the mass of component i, V the volume and C^i the concentration of component i and subscripts T indicate the total, n the non-aqueous, aq the aqueous and g the gas phase, respectively. K_h^i is the dimensionless Henry's coefficient and K_{nw}^i is the NAPL-water partitioning coefficient of component i.

Rearranging and solving for C_{aq}^i gives:

$$C_{aq}^i = \frac{M_T^i}{K_{nw}^i V_n + V_{aq} + K_h^i V_g} \tag{3.9}$$

Without a known partitioning coefficient, the initial mass of component i in the NAPL was not known prior to addition to the batch. The mass was determined by measuring the concentration of component i which partitioned from the NAPL into the aqueous phase prior to stock addition and the equilibrium concentration after stock addition. This method gave preliminary results for the partitioning coefficient for components with previously unknown NAPL-water partitioning coefficients.

The total mass of component i in the bottle after each stock addition (M_T^i) was equal to the initial total mass in the bottle, in this case the mass in the NAPL ($M_n^{i,1}$), plus the mass added from the stock (M_{stock}^i):

$$M_T^i = M_n^{i,1} + M_{stock}^i \tag{3.10}$$

Combining this with equation 3.6 and rearranging gives the equation for calculating the partitioning coefficient:

$$K_{nw}^i = \frac{M_g^{i,2} - M_g^{i,1} + M_{aq}^{i,2} - M_{aq}^{i,1} - M_{added}^i}{V_n(C_{aq}^{i,1} - C_{aq}^{i,2})} \tag{3.11}$$

3.3 Total Extraction of Stimulation Batch Experiments

3.3.1 Proposed Total Extraction Protocol

For the total extraction of the stimulation batch experiment, the conceptual model of the bottles was simplified to consider only 3 phases and 2 categories of tar components. The phases included (1) the headspace (gas), (2) aqueous and (3) solids/tar (sediment/tar). The two categories of tar components were the volatile aromatic hydrocarbons and the non-volatiles consisting of the aliphatic and non-volatile aromatic fraction.

Studies have shown that anaerobic degradation results in a well established sequence of removal: first straight-chained alkanes, followed by branched and unsaturated aliphatics, then monocyclic and finally polycyclic hydrocarbons (Jones *et al.*, 2008; Williams *et al.*, 1986; Volkman *et al.*, 1984). Therefore, for the batch experiments it was proposed that the visual loss of tar may have been the result of the loss of straight chain alkanes as a first step of degradation. Furthermore, GC-MS analysis (TNO, Utrecht) of stimulation batches had a characteristic 'hump' at the end of chromatograms which increased from the sterile to no addition to sulfate batches (Figure B.16). It was suggested that this hump was composed of alkanes broken down from the tar matrix to the aqueous phase. Therefore a method to determine the alkane composition of the sterile (batch no. 8), no addition (batch no. 9) and sulfate (batch no. 13) batches was developed.

Figure 3.2 summarizes the phase and corresponding analytical method for each the volatile and non-volatile components. To extract the tar/solids fraction acetone was be added to batches to fully dissolve the remaining tar. Acetone was chosen as the solvent for this method as it had already been confirmed to be compatible with the GC-MS method from TNO. Other solvents, such as methanol, were discussed but were not compatible fir the GC-MS or GC-FID methods. The volume of acetone necessary to dissolve the tar was determine by creating practice batches (see sub-section Practice Batch Bottles below). Due to the time constraints of this thesis, only the first two steps (gas and aqueous phase quantification) were performed for the stimulation batches 8,9 and 13 while the method was proved to work for all steps using the practice batches.

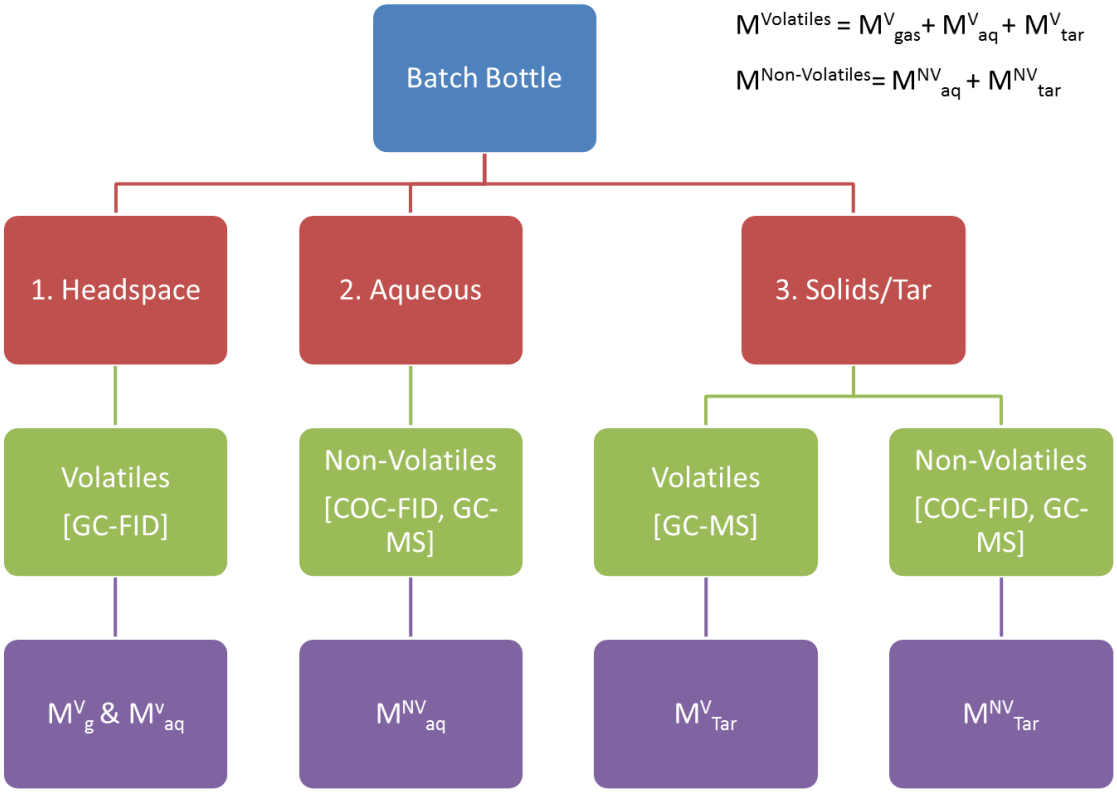

Figure 3.2: *Flowchart of proposed total extraction protocol. Three phases in the batch considered, (1) the headspace (gas), (2) aqueous and (3) solid/tar (NAPL). Tar components were split into two categories for quantification, volatile and non-volatile, reflecting the different analyses required. Volatile components quantified with previously developed method for headspace GC-FID measurements. Aqueous concentrations determined and headspace concentrations calculated with Henry's constant. Non-volatile components in the aqueous phase analyzed with COC-GC-FID measurements, developed in this chapter. The final stage of the total extraction is the addition of acetone to fully extract the tar/solid phase and quantification done by GC-MS (TNO, Utrecht) and COC-GC-FID. In addition to COC-GC-FID, identification of unknown tar components done with GC-MS.*

3.3.2 Stock Solutions

A saturated alkane standard (Sigma-Aldrich, Germany) was used which contained all alkanes from C_7-C_{30} dissolved in hexane, each with a concentration of 1000 μg/L. The stock was diluted 1/10 (v/v), run on the GC-FID and GC-MS and compared with sample runs to give a preliminary estimate of what alkanes, if any were present. Sqaulane ($\geq$ 99% purity, Fluka) was co-injected as a quantification standard on FID measurements. A stock solution,C_0 = 1,508 μg/ml, was diluted to three concentrations (301.6, 262.2, 150.8 μg/ml) and run on the GC-FID to determine the optimal concentration for calibration based on peak appearance. The lowest concentration, 150.8 μg/ml, gave the best peaks (symmetric, no tailing or peak saturation) and was used as the quantification standard co-injected with batch samples. Finally during small column chromatography hexane/dichloromethane (DCM) mixtures of 3/2 (v/v) and 9/1 (v/v) were created. In 100 ml volumetric flask 30 ml of hexane and 20 ml DCM was added for the 3/2 mix, and in second 100 ml volumetric flask 90 ml of hexane with 10 ml of DCM was added for the 9/1 mix. Flasks were closed with glass stoppers and mixes were made fresh weekly.

3.3.3 Practice Batch Bottles

Five additional batch bottles were prepared to determine the necessary volume of acetone to dissolve the tar in experimental batches, to practice the extraction techniques using small column chromatography and finally to develop the GC-FID and GC-MS methodologies.

Practice batches contained sediment with residual tar from borehole A005 (depth: 9-10 m collected: June 17, 2015) and groundwater from well A036 (depth: 8-9 m, collected: July 27, 2017) to be consistent with the original stimulation batch experiments. Table 3.5 summarizes the sediment, groundwater and acetone (purity ≥99.5%, Sigma-Aldrich) volume ratios in the practice bottles. Different sediment to water to acetone ratios were created to determine the necessary volume of acetone to fully dissolve tar in batch sediment.

Table 3.5: *Practice Batch Preparation. Batch 1* was created by adding additional acetone to batch 1 through the septa when clearly the tar had not dissolved after 1 month of mixing.*

Batch	1	1*	2	3	4	5
Tar/Sediment (g)	40	40	40	15	1	40
Groundwater (ml)	100	100	100	100	0	100
Acetone (ml)	10	100	50	50	10	0

Practice batches were prepared in 200 ml serum bottles and cleaned by flushing twice with methanol (purity ≥99.8%, Sigma-Aldrich) and then five times with MilliQ water and allowed to dry in a fume hood for 48 hours. Bottles were placed on scale, tared and sediment added directly to bottle using a glass funnel and metal spatula first flushed with acetone to clean. Groundwater, followed by acetone were added using sterile, disposable 50 ml plastic pipettes. Bottles were capped and crimp sealed with butyl/PTFE lined septa. If necessary, additional acetone was added to batches through the septa using disposable, 10 ml plastic syringes.

Bottles were mixed first on a rotary mixer (Rabinco Rotator), however were found to be too heavy for the small mixer and moved to a platform shaker (Innova 2100, New Brunswick Scientific) at 100 rpm. Bottles were stored on the shaker in a climate chamber at 20°C .

3.3.4 Preliminary Mass and Volume Measurements

Prior to extraction, preliminary measurements (mass and volume) of each batch from the stimulation batch experiment were recorded. An empty, 200 ml batch bottle was filled with increments of 10 ml of MilliQ water and the height of water marked on the outside of the bottle. This measurement bottle was used to record the approximate volume of the aqueous phase left in each of the batch bottles. The gas phase volume was calculated by subtracting the aqueous phase volume from the known total bottle volume. This volume check was necessary as the batch bottles had been sampled several times over the 3 year experimental period and aqueous phase volumes varied between 60 ml and 100 ml.

3.3.5 Small Column Chromatography

Small column chromatography was used to prepare batch samples for analysis on GC-FID and GC-MS systems. Several stationary media and solvents were tested to determine the best media-solvent combination for preparation of batch samples. Media included anhydrous magnesium sulfate ($MgSO_4$, ≥98% purity, Merck, Germany) and sodium sulfate (Na_2SO_4, ≥99% purity, Merck, Germany) to remove water from samples, aluminum oxide (alumina MP Biomedicals, Germany) to separate samples into polar and non-polar fractions and silver impregnated silica gel (AgSi) to

separate hydrocarbons into saturated and unsaturated fractions. Solvents included pure n-hexane (≥95% purity, VWR Chemicals), DCM (≥99.8% purity, VWR Chemicals), ethyl acetate (≥99.8% purity, Merck), as well as the hexane/DCM mixes outlined above.

Separation of saturated and unsaturated hydrocarbons

Attempts were made to separate samples into saturated and unsaturated hydrocarbon fractions. Separating these components would have resulted in simpler chromatograms for analysis. Separation was attempted on practice batch 1*, with 50% groundwate, 50% acetone. This batch was meant to simulate the last step in the total extraction protocol, the analysis of the tar by dissolving it into an aqueous phase with a solvent (acetone). Aqueous phase samples of 1 ml was withdrawn from the bottle using a disposable 1ml plastic syringes and transferred to 4 ml glass sample vials with Teflon-lined screw caps (*sample vial*). Several glass, 4 ml collection vials were washed with acetone, labeled and weighed prior to use on a scale accurate to 1 mg.

The sample was dried under a gentle stream of N_2 gas at 30°C for several hours. Remaining water was removed by small column chromatography over a dry packed $MgSO_4$ column. A Pasteur pipette was plugged with pre-extracted cotton and 4 cm of $MgSO_4$ added to the column. The column was tapped gently to tightly pack the $MgSO_4$, eliminating large air pockets. The column was flushed with two column volumes of 9:1 (v/v) hexane/DCM and the liquid discarded. All of the sample was then transferred to the column by pipette and collected in the same sample vial. The water fraction was removed with a pipette and discarded from the sample vial.

Saturated and unsaturated hydrocarbons were separated over an AgSi column (Silica gel, 70-230 mesh size, Merck). Alkanes and mono-unsaturated alkenes were eluted with hexane, followed by 9:1 hexane/DCM and unsaturated hydrocarbons were eluted with ethyl acetate. The AgSi column was prepared by plugging a second Pasteur pipette with pre-extracted cotton and pre-made AgSi added and the column gently tapped to pack.

The column was flushed first with two column volumes of hexane and the liquid discarded. The sample from the $MgSO_4$ column was then transferred by pipette to the AgSi column and collected in a new vial (*collection vial*). The sample vial was flushed twice with hexane and also transferred to the AgSi column. The column was eluted with additional hexane until the collection vial was filled to the neck of the bottle.

The sample vial was then flushed with 9:1 (v/v) hexane/DCM and added to the AgSi column. The column was eluted with additional 9:1 hexane/DCM and collected in a second collection vial until the vial was full. Finally, the sample vial was flushed with ethyl acetate and eluted over the AgSi column, collected in a third vial and the column eluted with enough ethyl acetate to fill the collection vial. All collection vials were then dried under a gentle stream of N_2 gas at 30°C (approx. 10-15 minutes). Vials were weighed and enough hexane added to concentrate samples to 1 mg/ml and analyzed by GC-FID.

Final Extraction Method

Stimulation batches 8C (Sterile), 9C (No addition) and 13C (Sulfate) were chosen to test the total extraction method. These batches were chosen based on their GC-MS results (Figure B.3). The sterile batches (8) had the lowest overall concentration of hydrocarbons, the no addition (9) batch had a moderate concentration of hydrocarbons and the sulfate batch (13) had the highest concentration. The 'C' replicate was chosen from each treatment as was sampled the least, meaning the aqueous volume was the closest to the original 100 ml added.

From batch bottles two, 1 ml samples were transferred to glass 4 ml sample vials with Teflon-lined screw caps using disposable 1 ml plastic syringes. Collection vials were flushed with acetone to clean, labeled and weighed prior to sample collection. Sterile disposable needles were first flushed with N_2/CO_2 (80%/20%) to prevent oxygen introduction to the anaerobic bottles. Sample vials

were dried overnight under a gentle stream of N_2 gas at 30°C and then weighed again.

One of the two sample vials was set aside for later use and the other sample separated into non-polar and polar fractions. Samples were separated with small column chromatography over basic alumina by eluting first with 9:1 (v/v) hexane/DCM followed by ethyl acetate. Polar fractions were collected and stored for later analysis. The alumina was activated by heating overnight at 150°C then dry packed in 150 mm long Pasteur pipette columns and tapped to tightly pack. The column was flushed 9:1 (v/v) hexane/DCM and collected in a clean, weighed 4 ml collection vials and kept as a column blank.

Dried samples were first dissolved in 9:1 hexane/DCM and a pipette used to mix sample vials thoroughly. Samples were transferred using the same pipette to the alumina column. This process of flushing the sample vial with solvent and the transferring to the column was repeated until the collection vial was filled to the screw-top neck. Sample vials were then flushed with ethyl acetate and the process repeated and collected in a second collection vial.

Collection vials were then dried under a gentle stream of N_2 gas at 30°C, weighed and enough hexane added to make a 1 mg/ml sample. Vials were then mixed briefly on a Genie Vortex touch mixer and analyzed on GC-FID using the methods described above. The second 1 ml sample which was set aside after sample collection was also dissolved in hexane, mixed and analyzed directly on GC-FID, without small column treatment for comparison.

Recovery Test

A recovery test was performed using two concentrations of squalane to determine the loss of sample through the alumina chromtatographic columns. Two concentrations of squalane were analyzed (C_1 = 1.51 mg/ml, C_2 =0.151 mg/ml). Samples of 1 ml were taken in glass, 4 ml screw cap vials. Samples were first run on the GC-FID (1 μL) then the same procedure for the final extraction was followed.

The percent recovered (PR) was calculated as;

$$PR = \frac{PeakArea_{t2}}{PeakArea_{t1}} \tag{3.12}$$

Where $PeakArea_{t1}$ is the measured peak area of squalane injected prior to column chromatography over alumina and $PeakArea_{t2}$ the measured peak area after treatment on the alumina column.

3.3.6 Sulfur Removal

Elemental sulfur interferes with the analysis of hydrocarbons on GC-MS systems and can damage columns and therefore must be removed prior to analysis. Elemental sulfur is relatively easily removed from samples by reacting with copper and is precipitated out as copper sulfate (EPA, 1996).

Sulfur removal was tested using three forms of copper; (1) activated granular copper, (2) activated copper powder and (3) copper powder with no pre-treatment. Activation of the copper in this case refers to rinsing with dilute hydrochloric acid (HCl). The best option of these three copper treatments was chosen based on maximizing the removal of copper, minimizing he number of copper treatments and minimizing the overall loss of sample. In all cases copper treatment was performed after quantification of samples on GC-FID but before identification on GC-MS.

Method 1: Activated Granular Copper

Granular copper (0.2-0.6 mm, Sigma-Aldrich, Germany) was activated by rinsing with a small amount of 2 M HCl (HCL Fuming 37%, Merck). The HCl was then carefully pipetted off and the copper granules were flushed with MilliQ water several times until the pH = 7. The pH was tested

using color-fixed pH indicator strips (Fisher Scientific). The water was then pipetted off and the granules washed twice with methanol and twice with dichloromethane. Several copper granules were added to samples after chromatography on alumina and dissolved in 2 ml of DCM with a small Teflon coated magnetic stir bar. Samples were stirred overnight at 300 rpm.

After mixing, copper sulfate was filtered from samples by small column chromatography on sodium sulfate (Na_2SO_4). A Pasteur pipette (150 mm) was plugged with pre-extracted cotton and 4 cm of Na_2SO_4 was added. The column was rinsed with DCM and the liquid discarded. Samples were transferred from the vials with the copper granules to the column and eluted to weighed 4 ml sample vials. The copper granules were flushed with additional DCM and the liquid added the the column until collection vials were full, approximately 4 ml.

Method 2: Activated Powdered Copper
The copper powder method was modified from EPA method 3660B for sulfur removal with copper (EPA, 1996). Copper powder (< 63 μm, 99.7% purity, Merck, Germany) was activated by flushing with a small amount of 2 M HCl to form a thick slurry. The slurry was then washed with several times with MilliQ water until the pH = 7, as measured by color-fixed pH indicator sticks. The copper powder was then rinsed twice with acetone ($\geq$ 99% purity, Merck) and dried under a gentle stream of N_2 gas at 30°C. Copper powder was made fresh for each day's use as it quickly oxidized and became inactivated when stored at room temperature (Blumer, 1957).

A small amount of copper powder was added to a 12 ml test tube, approximately filling the tube to the 1 ml mark. Dried sample vials were flushed with 2.5 ml of DCM and added to the tube with the copper powder. The tube was covered with aluminum foil and mixed on a Vortex Genie mixer for 3 minutes at 20*100rpm. The copper powder was then allowed to settle in the tube and the sample carefully removed by drawing off the liquid with a disposable pipette and transferring to a clean, weighed 4 ml glass vial. In some samples the eluent was drawn off the copper powder and run through a small column containing Na_2SO_4 and flushed with DCM to compare the effect of filtering the sample versus allowing the copper to settle naturally.

Method 3: Common Copper Powder
Riis & Babel (1999) found no substantial difference between activated copper and copper with no pre-treatment for sulfur removal when the mixing time was doubled. As pre-treatment of the copper was time consuming, the effect of common copper powder with no pre-treatment was tested on our samples. Following the method of Riis & Babel (1999), samples in 2 ml of hexane were treated with a small amount of common copper powder ($\sim$ 120 mg) and sonicated for 20 minutes in an ultrasonic water bath (Branson 200). The supernatant liquid was then drawn off using a disposable pipette to a clean, weighed collection vial.

For all treatments, collection vials were dried under a gentle stream of N_2 gas at 30°C, weighed and the sample dissolved in hexane to 1 mg/L. Samples were then analyzed on a GC-FID equipped with an elemental sulfur detector (see next section). This process was repeated until the sulfur signal was at or below $\sim$100 pico-amperes (pA).
The total reduction of sulfur, R_S, in the samples was calculated as;

$$R_S = 1 - \frac{Peak_{t2}}{Peak_{t1}} \tag{3.13}$$

Where $PeakArea_{t1}$ was the measured maximum peak height of sulfur injected prior to copper treatment and $Peak_{t2}$ the maximum peak height after all copper treatments.

3.3.7 Analytical Methods

Volatile aromatic hydrocarbons were measured using an Agilent 6850 GC-FID using the methods described in Section 3.1.2. Non-volatile hydrocarbons were measured using liquid, cool on-column injection with a HP 6890 series GC system and Agilent CP-Sil 5 CB column (0.32 mm x 30 m), equipped with both an FID and a flame photometric detector (FPD) for sulfur analysis (COC-GC-FID). The FID was set at 330°C and FPD at 200°C . The oven temperature program was 50°C, followed by an increase of 18°C/min to 130°C and then increased by 4°C/min to 300°C and held for 20 minutes. The program was run with constant pressure of 100 kPa with helium carrier gas. Liquid samples of 1 μL were injected using a 10 μL syringe, flushed 10 times with each ethylacetate and hexane before and after use. Samples were co-injected with 1 μL squalane ($C_{30}H_{62}$, C_{sq} = 0.1508 mg/ml)

Hydrocarbon samples were then analyzed using an Agilent 7890B GC with an Agilent 5977 MSD and a CP-Sil 5 CB column (0.32 mm x 25 m). The oven temperature program was 50°C, followed by an increase of 18°C/min to 130°C and then increased by 4°C/min to 320°C and held for 5 minutes, then a decrease of 100°C to 50°C and held for 10 minute. Samples were injected by autosampler and a solvent delay of 4 minutes was used. The program was run with constant flow of 1.6 ml/min and helium carrier gas. An internal calibrant, perfluorotributylamine (PFTBA) was used to improve mass spectral accuracy. Best results are achieved with PFTBA when it is injected at the end of each sample run at an oven temperature of 50°C (Wang & Prest, 2006). PFTBA was injected to the MSD between 64-66 minutes at the end of each sample run. The acquisition type was profile mode, the tune type EI and gain factor set to 1.

Two practice batches were analyzed on GC-MS (TNO, Utrecht) using the method described in Section 3.1.2. Batches tested were batch 2 (40 g sediment/tar, 100 ml groundwater and 50 ml acetone) and batch 3 (15 g tar, 100 ml groundwater and 50 ml acetone). Samples were analyzed in 20 ml glass vials with 11.3 ml MilliQ water and and 0.6 ml of 0.5 g/L $HgCl_2$ (25 mg/L final concentration). Vials were crimp sealed with silicone/PTFE magnetic caps. Batch samples of 0.1 ml were withdrawn using 1 ml sterile, disposable plastic syringes. Syringes needle tips were disposed of between sampling and injection to 20 ml vials to ensure no oil was transferred on the needle tip. Samples were analyzed within 24 hours.

3.3.8 Hydrocarbon Identification and Mass Balance

Volatile aromatic hydrocarbons were identified based on their established retention time on the GC-FID (see Section 3.1.3) for the gas and aqueous phase in each batch. Headspace and aqueous volumes recorded prior to batch measurements were used to calculate the mass in each of batch 8C, 9C and 13C.

Non volatile hydrocarbons were quantified by co-injection with squalane on the GC-FID (Jones *et al.*, 2008). Peak areas of analytes were compared with the peak area of squalane at a known concentration by;

$$C^i_{vial} = \frac{Area^i_{vial} \times C_{sq}}{Area_{sq}} \tag{3.14}$$

$$C^i_{batch} = \frac{C^i_{vial} \times V^{hexane}_{vial}}{V_{sample}} \tag{3.15}$$

Where C^i_{vial} was the concentration of component i in the collection vial (μg/L), $Area^i_{vial}$ the peak area of component i as measured on the GC-FID, $Area_{sq}$ the peak area of the concentration of

squalane, C_{sq} (μg/μL), injected, V_{vial}^{hexane} the volume of hexane added to the collection vial, and V_{sample} the volume of sample analyzed, (0.001 L^{-1} for all samples).

Hydrocarbons were identified on the GC-MS using the on-board standard perfluorotributylamine (PFTBA) as an internal calibration, run with each sample (Prest & Wang, 2009). Cerno MassWorks^{TM} software version 4.0 was used to create a calibration file which was then automatically applied to each sample run with PFTBA. The 16 largest peaks from the GC-FID analysis were identified on the GC-MS using CLIPS^{TM}, available in MassWorks. CLIPS (Calibrated Line-shape Isotope Profile Search), used isotope profiles to determine the elemental composition of unknown peaks. The possible elements were narrowed down to search for only elements appearing in a previous qualitative analysis of the Amersfoort tar (van Leeuwen, 2018). This greatly narrowed the search criteria for chemical formula, reducing the uncertainty in chemical identification.

From the list of possible chemical formula, the theoretical mass spectra for each formula were compared with the calibrated mass spectrum of the peak in question and the highest spectral accuracy formula were considered. These formula were then compared with the list from previous analysis to determine the most likely chemical formula for the unknown elements. Finally, the accurate mass centroid data were exported from MassWorks and input to the NIST MS Search Library to determine the most likely chemical structure(s). In some cases, multiple peaks corresponded with the same molecular formula during the mass spectra search, and when input to the NIST search library isomers of the same components were given. In these cases, and for simplicity, the isomers were grouped and quantified together as one.

The calibration method was tested on a standard mixture with known elements to confirm the identification accuracy. Known elements in the mixture were heptadecane, 2-nonadecanone, octacosane and triacontane.

Chapter 4

Results

4.1 Stimulation Batch Experiments

4.1.1 GC-FID Method Development

The oven temperature program was adjusted until good peak separation for 12 of the 13 volatile aromatic components was achieved. A hold at 90°C for 4 minutes allowed better separation of ethylbenzene, styrene and o-xylene. However, m-xylene and p-xylene could not be separated as they co-eluted at $\sim$ 8.8 minutes (Figure 4.1). Retention times of components were very consistent and varied less than $\pm$ 0.05 minutes from their recorded values for the majority of measurements. The coefficient of variation for peak areas from the same calibration bottles were calculated. The coefficient varied between a minimum 4.1%, for benzene, and a maximum of 10.1%, for 1-methylnaphthalene (Table 4.1).

Table 4.1: *Coefficient of variation for GC-FID calibration runs. Calculated as the average coefficient of variation for each of the nine dilutions, which were each measured on the GC-FID at least twice.*

Tar Component	Coefficient of Variation (%)
Benzene	4.1
Toluene	5.9
Ethylbenzene	4.8
m/p-xylene	4.9
styrene	9.7
o-xylene	8.7
1,2,4-trimethylbenzene	6.8
1,2,3-trimethylbenzene	5.4
indene	6.9
Naphthalene	9.8
2-Methylnaphthalene	7.8
1-Methylnaphthalene	10.1

4.1.2 Aqueous Phase Concentrations

The stimulation batches generally had good correlation between replicates of the same treatment (Table 4.2). Benzene, however, varied the most in the sulfate and chlorate batches. In the sulfate

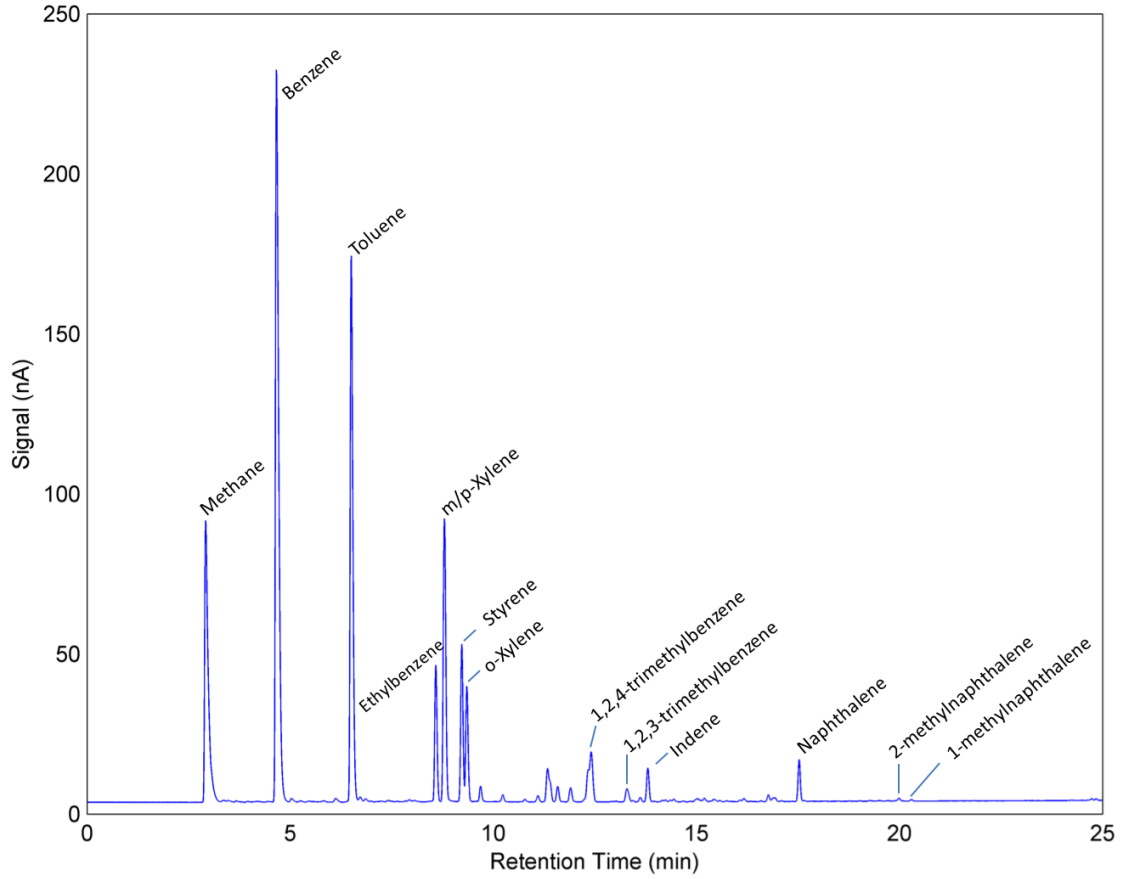

Figure 4.1: *Example chromatogram of 13 target analytes identified and calibrated for GC-FID measurements. m-Xylene and p-xylene co-eluted at ∼ 8.8 minutes and could not be separated.*

and chlorate batches, only the 'C' replicates received an additional 2mM of sulfate and chlorate, respectively, after 11 months (Table B.2). In all other batch treatments the replicates were dosed uniformly. Batches were prepared with contaminated sediment from site. It is possible that the concentration and distribution of tar within the sediment was not uniform, and that batches began with different initial conditions accounting the differences between the replicates. As the batches were not analyzed for tar components initially, however, this hypothesis cannot be proven.

The lowest benzene concentrations were measured in the no addition batch (0.3 ± 0.1 mg/L). The highest concentrations of benzene were measured in the nitrate batches (10 nitrate, 11 nitrate & succinate and 12 nitrate & acetate) with average concentrations of 8.4 ± 0.3 mg/L, 8.5 ± 0.5 mg/L, 8.6 ± 0.1 mg/L respectively. Batch 10A has previously leaked and contained no aqueous phase at the time of measurements. Methane was detected in all batches except the sterile batch. Methane concentrations ranged from 2-3 mg/L in treatment batches, with the highest concentration in the sulfate batches (Figure 4.2).

The lowest toluene concentrations were measured in the sterile batches (2.3 ± 0.2 mg/L) and the highest in the nitrate & acetate batches (6.4 ± 0.1 mg/L). Low ethylbenzene was measured in the sterile (0.7 ± 0.01 mg/L), no addition (0.56 ± 0.1 mg/L), sulfate (0.8 ± 0.2 mg/L) and chlorate (0.55 ± 0.2 mg/L) batches. Sterile batches had the lowest concentration for m/p-xylene, styrene, o-xylene, 1,2,3- and 1,2,4-trimethylbenzene and indene. The highest concentrations for m/p-xylene, styrene and o-xylene were measured in the nitrate & acetate batches, and the highest concentration for 1,2,3- and 1,2,4-trimethylbenzene, indene, naphthalene, 1- and 2-methylnaphthalene were measured in the chlorate batches.

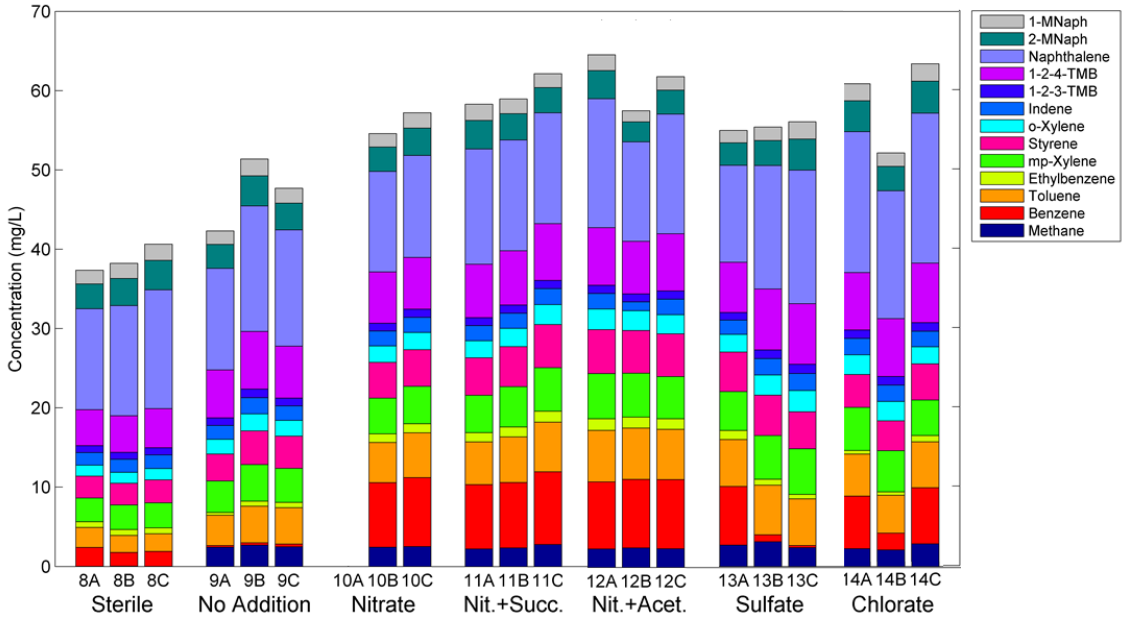

Figure 4.2: *Concentration in the aqueous phase from headspace GC-FID measurements for stimulation batches for 13 mobile aromatic components. Note: Batch 10A was dry at the time of measurement, therefore it was not measured. MNaph = methylnaphthalene, TMB = trimethylbenzene*

To understand the different behavior of components in the tar the concentration of components in the in the aqueous phase were compared with their relative solubilities for the sterile batch. The most soluble component measured was benzene and the least soluble was indene (Table B.3). Relatively high solubility compounds, benzene and toluene, were on average 3.4 and 2.5 times higher than the concentration in the sterile batches. Moderately soluble compounds, styrene, m/p/o-xylenes and ethylbenzene, between 1.4-1.7 times higher than sterile. Low solubility components, naphthalenes and methylbenzenes, were only 1-1.2 times the concentration of sterile components. Only indene deviated from this pattern, being 1.5 times higher in treatment batches. However, this may be due to the comparatively lower partitioning coefficient of indene ($\log K_{ow} = 2.9$) compared to it's low solubility.

Tar was added to the bottles within the sediment and therefore the total mass of the tar and the concentration of individual components within the tar was not exactly known. The mole fractions of components within the tar were not known.

GC-MS concentrations (TNO, Utrecht) were generally higher for all mobile tar components measured compared to the GC-FID measurements for the same batches (Figure 4.4). Naphthalene, for example, was on average 10 times higher in the GC-MS measurements than the GC-FID measurement, while 1- and 2-methylnaphthalene were 36 and 28 times higher respectively. The sterile batch showed the smallest differences between GC-FID and GC-MS measurements. Naphthalene had the highest concentration in all batches, followed by 2- and 1-methylnaphthalene respectively. Together, naphthalene and methylnaphthalene accounted for 67-83% of the hydrocarbons measured by GC-MS. The same three components measured by GC-FID in comparison accounted for only between 33-50%.

Differences observed between GC-FID and GC-MS measurements could have resulted from the different sampling method used. GC-MS measurements were performed on samples which contained 100 μL of liquid extracted from batch bottles dissolved in an additional 11.9 ml of water. During sample extraction, small amounts of tar were visibly withdrawn into the syringe,

Table 4.2: *Coefficient of variation between batch treatments, calculated for the three batch replicates.*

	Coefficient of Variation (%)						
	Sterile	No Addition	Nitrate	Nitrate & Succinate	Nitrate & Acetate	Sulfate	Chlorate
Methane	33.7	4.5	1.7	9.7	2.5	11.3	14.4
Benzene	13.7	21.6	3.3	5.5	1.3	113.6	42.6
Toluene	6.8	8.6	5.5	6.2	1.1	3.1	7.8
Ethylbenzene	1.3	24.9	2.5	7.1	3.8	29.1	30.0
m/p-xylene	1.7	6.0	2.3	6.0	2.7	6.4	7.8
styrene	2.5	9.3	1.0	6.0	1.5	3.7	7.6
o-xylene	2.1	6.5	2.4	6.0	2.6	7.4	6.7
1,2,4-trimethylbenzene	2.7	6.3	1.2	2.6	24.0	7.8	1.9
1,2,3-trimethylbenzene	2.4	6.1	1.3	1.8	1.3	8.0	0.8
indene	3.6	7.6	0.5	2.6	4.0	8.6	1.7
Naphthalene	6.7	8.6	0.7	1.8	10.6	13.1	6.5
2-Methylnaphthalene	7.0	9.1	5.3	5.4	13.8	14.0	11.2
1-Methylnaphthalene	6.8	9.9	6.6	6.4	13.9	13.9	10.9

as tar was suspended within the aqueous phase (Figure 4.3). Therefore despite switching the needle tip between sample withdrawal and injection to the final measurement vial, small droplets of suspended tar were added to the measurement vials. These droplets fully dissolved in the measurement vials, as no suspended tar was visible in the larger water volume. It is hypothesized that these droplets tar could account for the difference in concentration measurements between the GC-FID and the GC-MS.

The concentration of benzene and toluene were less in all batches than the concentration of groundwater from well A003A used to create the batches (Figure 4.5). The concentrations of 1,2,3- and 1,2,4-trimethylbenzene, indene, naphthalene, 1- and 2-methylnaphthalnene were higher in all batches than the groundwater added. In the sterile batch the concentration of ethylbenzene, m/p-xylene, styrene and o-xylene were all lower than the groundwater added, while the concentrations of these hydrocarbons varied between the batch treatments (Figure 4.5).

4.2 Tar as a Hydrophobic Matrix: Batch Experiments

4.2.1 Initial Tar Concentrations and K_{ow} Calculations

Of the 25 mobile tar components measured by GC-MS for the tar from well A010F, 14 were above the detection limit. Following the methods of Rixey *et al.* (1999), $\frac{1}{C_{aq}^{i}}$ vs. $\frac{V_{aq}}{M_n}$ were plotted for the batch dilutions (Figure B.5). Table 4.3 summarizes the calculated $\log K_{nw}$. Two components, 1-and 2-methylnaphthalene, resulted in negative slopes and the the $\log K_{ow}$ could not be calculated. The initial concentration of aromatic tar components for tar from well A010F was then calculated as $\frac{1}{slope}$ from each of the plots. The initial concentration of aromatic tar components for tar from wells A005A, A036A and A012A were calculated assuming the partitioning coefficients of tar A010F were applicable to these tars as well (Figure 4.6).

Naphthalene was the single largest component in the tar for each of the different wells, accounting for between 59-67% of the total concentration of aromatics measured (Figure 4.6). Toluene and m/p-xylene were the next largest components in each of the tars. Benzene had the lowest concentration in all of the tars except for well A010F, where benzene comprised 2.6% of the total

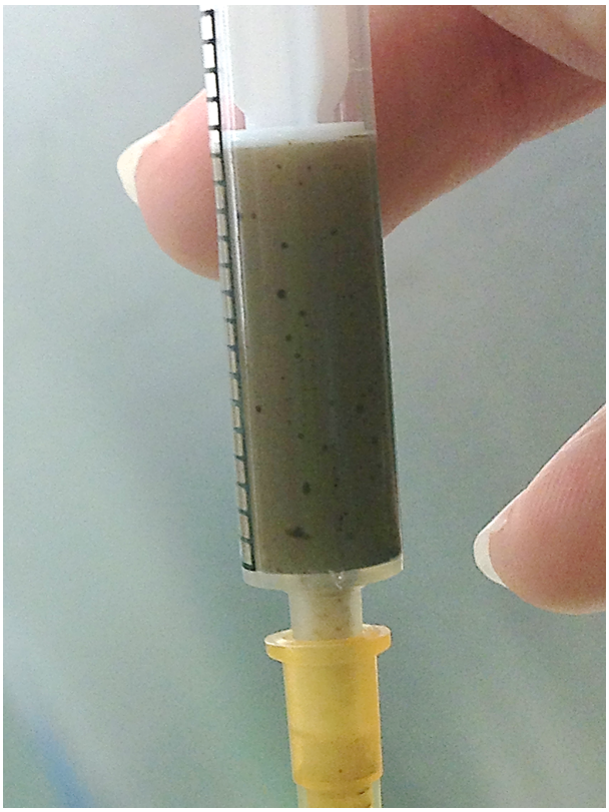

Figure 4.3: *Tar micro-droplets visible (black dots) in sample from batch bottles citepVan-Leeuwen2018.*

concentration of hydrocarbons (Figure 4.6). Decreased benzene concentration was correlated with increased naphthalene concentrations, with the lowest naphthalene and highest benzene concentration in tar A010F and the highest naphthalene and lowest benzene concentrations in well A012A (Figure 4.6).

The concentration of volatile aromatics measured in the partitioning experiments was found to account for only approximately 40% of the total mass of the tar. The other 60% is likely to consist of aliphatics, PAHs and heterocyclic compounds based on a previous tar characterization by ALcontrol Laboratories (2011)

4.2.2 Partitioning Behavior in Current Batch Experiments

Stock solution chemicals partitioned from the aqueous phase to the NAPL inversely proportional to their $\log K_{ow}$ values. Therefore, chemicals with the highest $\log K_{ow}$ had the lowest equilibrium aqueous concentrations when compared to their spiked concentration (Table 4.4). In all batches, benzene, with the lowest partitioning coefficient, had the highest aqueous concentration at equilibrium. In batch 1 and 2 the chemicals with the highest partitioning coefficients (dichlorobenzenes and naphthalene/trimethylbenzenes for the organic and hydrocarbon solution additions respectively) had concentrations below the minimum calibrated concentration.

Visual observations of batches 5 and 6 showed differences in tar adhesion to the glass bottle due to the sterilization techniques used ($HgCl_2$ alone vs. $HgCl_2$, NaN_3 and autoclaving). Batch 5 tar appeared more diffuse in the bottle, while batch 6 showed greater adhesion to the glass, with distinct patches of tar (Figure 4.7). However, no difference in equilibrium concentrations were observed between the two batches (Figure 4.9). Batches 5 and 6 were measured weekly over a period of 2 months. Concentrations for each of the 11 hydrocarbons of interest changed

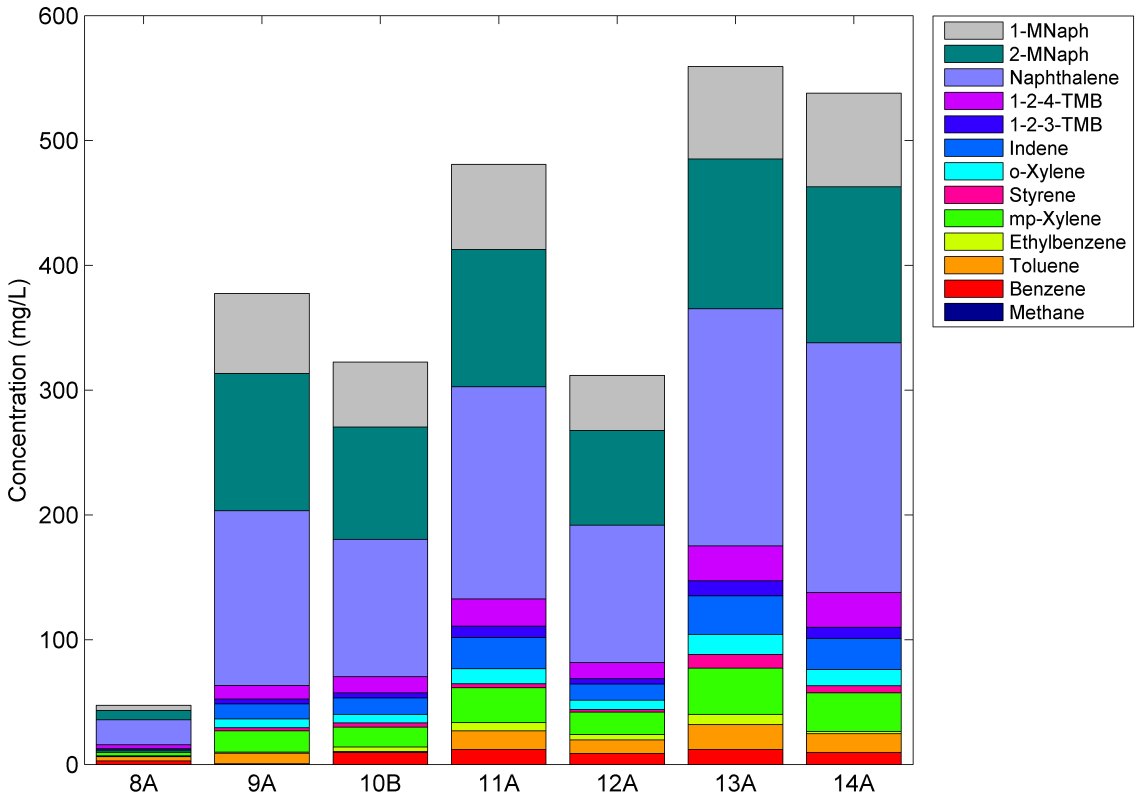

Figure 4.4: *Concentration in the aqueous phase from aqueous samples, analysis on GC-MS (TNO, Utrecht). MNaph = methylnaphthalene, TMB = trimethylbenzene*

little during this period. Concentrations measured after eight weeks were within a few percent of the concentrations measured after 24 hours. In batch 5, the greatest changes were observed for naphthalene, which decreased by 13% and benzene, which increased by 8% over the 8 week period. The other volatiles in batch 5 were within ± 5% of the 24 hour concentrations (Figure B.8). In batch 6 benzene also increased by 8% over 8 weeks, with all other components within ± 3% (Figure B.8). Therefore, as no difference between the sterilization methods was observed the results from the current partitioning batches may be compared with the original stimulation batch experiments, though different sterilization techniques were used.

The equilibrium concentration for batches 5 and 6 (sterile) corresponded well with the calculated aqueous concentrations for most chemicals. Only toluene, styrene and naphthalene had higher than expected concentrations (Figure 4.9). When compared with the original batch experiments, with sediment and residual tar from well A005A and groundwater from well A003A and different electron acceptors/substrates, the sterile batch (batch no. 8) had substantially lower concentrations of all tar components, except benzene and naphthalene (Figure 4.9).

The rate of partitioning differed between the tar and bitumen batches. When spiked to the tar (batch 8), benzene diffused rapidly from the aqueous phase to the NAPL. Concentration measurements as little as 5 minutes after injection showed no difference to subsequent measurements up to 168 hours later (Figure 4.8). In contrast, benzene spiked to bitumen batches, either alone or in the hydrocarbon mix, took over 24 hours to diffuse into the bitumen (Figure 4.8).

Benzene, in all three spiked solutions, partitioned from the aqueous phase to the gas phase and NAPL in roughly the same proportions in the majority of batches (Table 4.4). For bitumen batches (batch 1 and 2) the aqueous phase accounted for on average 34 ± 4% of the total mass of

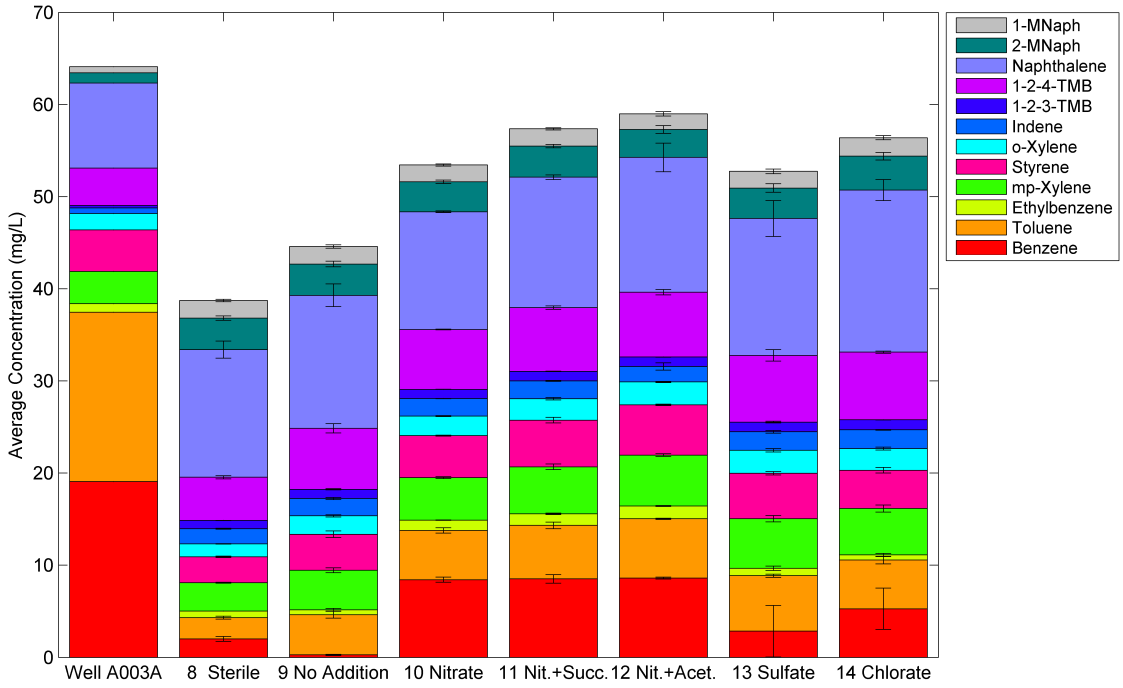

Figure 4.5: *Average concentration of high series batch experiments compared with the concentration of groundwater added to the batches, GC-FID analysis. Error bars show one standard deviation. MNaph = methylnaphthalene, TMB = trimethylbenzene*

benzene, the gas phase 11 ± 1% and the bitumen 55 ± 5% (Table B.4). In the tar batch 8, less benzene remained in the aqueous phase, only 17± 2% on average with the gas phase accounting for 6 ± 1% and the tar 77 ± 3%.

4.2.3 Mass Balance and K_{nw} Calculations

For batch 8, a mass balance of the theoretical benzene concentration initially and at equilibrium after each injection was calculated and compared with the measured concentrations. The measured concentrations were 25-40% larger in each case (Table 4.5). This suggests a lower $\log K_{nw}$ would more accurately predict the equilibrium concentration partitioned to the aqeuous phase. A $\log K_{nw}$ of 2.2 (K_{nw} = 158) results in the lowest error (2-10%) between theoretical and measured concentrations. All calculated $\log K_{nw}$ for chemicals in the bitumen batches were lower than the $\log K_{ow}$ from literature (Table B.4).

Plots of the concentration of batch mixtures (organic, hydrocarbon solutions) versus the $\log K_{ow}$ for the respective compound show a clear trend. Above a $\log K_{ow}$ value of 3.5 solution components appear to partition completely into the NAPL.

1- and 2-methylnaphthalene were the largest PAH components able to be measured using headspace GC-FID and GC-MS methods. The $\log K_{nw}$ could not be calculated for either using the methods from Rixey *et al.* (1999), however, and therefore the initial concentration could not be calculated for any of the tars. It is likely that 1- and 2-methylnaphthalene also compose a substantial portion of the tar, based on their relatively large $\log K_{ow}$ from literature and their moderate concentrations in the tar-water partitioning batches.

See Appendix Figures B.12 to B.15 for graphics of the concentration of spiked solutions in each batch over time.

Table 4.3: *Calculated $logK_{nw}$ values, values with (-) could not be calculated from the batch experiments. $LogK_{ow}$ values from literature for reference.*

	$LogK_{ow}$ [a]	$LogK_{nw}$
Benzene	2.1	2.3
Toluene	2.7	3.0
Ethylbenzene	3.2	3.5
p-Xylene	3.2	3.5
m-Xylene	3.2	3.5
Styrene	3.1	3.0
o-Xylene	3.0	3.5
1,2,4-Trimethylbenzene	3.8	4.2
1,2,3-Trimethylbenzene	3.7	4.2
Indene	2.9	3.5
Naphthalene	3.3	4.1
2-Methylnapthalene	3.6	-
1-Methylnapthalene	3.3	-
3-Ethyltoluene	3.6	4.1
2-methylindene	2.6	3.9

[a] (National Center for Biotechnology Information, n.d.)

4.3 Total Extraction of Stimulation Batch Experiments

4.3.1 Practice Batch Bottles

Visually, only batch 4 (1 g of tar/sediment and 10 ml of pure acetone) appeared to fully dissolve the tar within the bottle (Figure 4.10). All other batches had tar either still adhered to the glass (batch 1, batch 1*, batch 2), or a slick of oil on the top of the aqueous phase (batch 1*, batch 3, Figure 4.10). Moreover, aqueous samples from batch 2 and 3 were analyzed on GC-MS (TNO, Utrecht). Batch 3, which contained only 15 g of tar/sediment compared to the 40 g in batch 2, was expected to have only a 38% (15g/40g) of the concentration of batch 2. The batches had similar concentrations of most components, differing substantially only for the larger naphthalene components (naphthalene, methylnaphthalenes, 2-ethylnaphthalene and dimethylnaphthalenes, Figure 4.11). The total concentration of tar components in batch 2 was 393 mg/L and batch 3 was 254 mg/L, therefore batch 3 contained approximately 64% of the concentration of batch 2, not the 38% expected. This clearly demonstrates that the tar was not fully extracted in either of these batches.

4.3.2 Small Column Chromatography

Separation of saturated and unsaturated hydrocarbons proved difficult to achieve. The unsaturated fraction, eluted from practice batch 1* (50/50 groundwater/acetone) over silver impregnated silica gel with hexane, showed little difference from the saturated fraction, eluted with ethyl acetate. Only the beginning of the chromatogram, between 2-6 minutes was substantially different between the two fractions. Clearly the method did not work as intended, as there should have been no overlap between the chromatograms with the unsaturated fraction containing the aromatics and the saturated fraction containing the n-alkanes. Based on these results this method was not pursued further. Furthermore, removing water from samples over the $MgSO_4$ column was eliminated as it was time consuming and instead samples were dried overnight under N_2 gas at 30°.

Samples prepared with small column chromatography over alumina resulted in the loss of

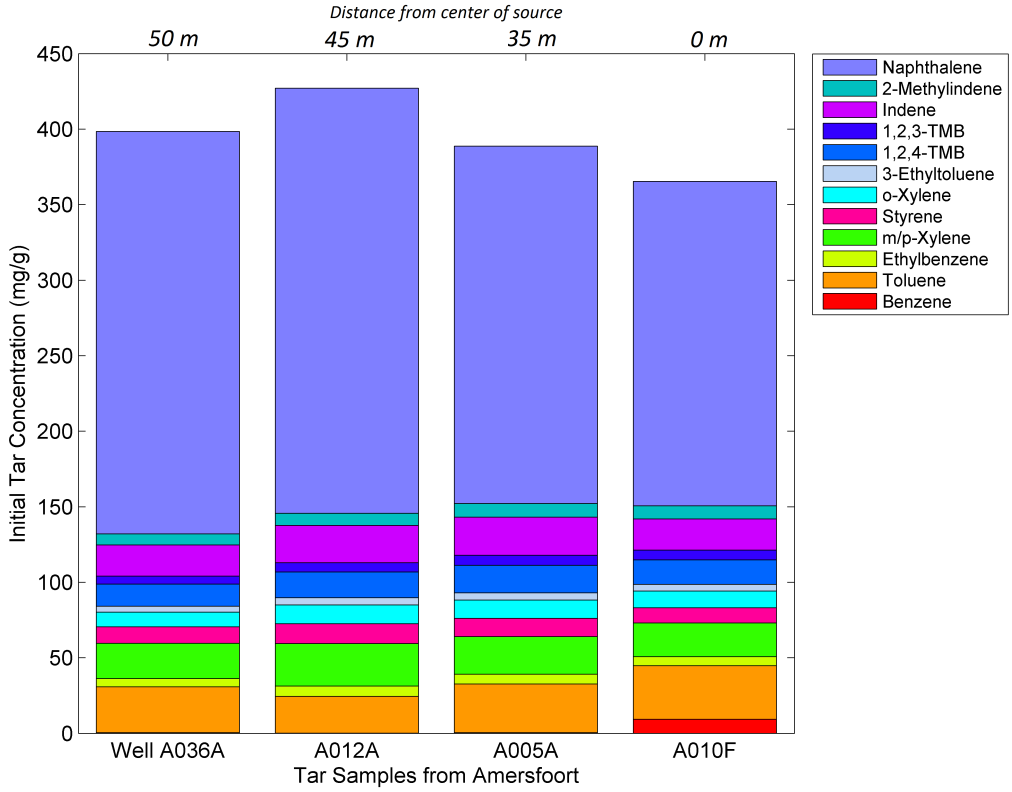

Figure 4.6: *Calculated initial concentration of aromatic tar components for tar sampled from different locations within the same source zone. Calculations based on the method of Rixey* et al. *(1999). Left to right: decreasing distance from the center of the source zone: A036A 50 m, A012A 45 m, A005A 35 m and A010F 0 m (center of source).*

components with a retention time above 15 minutes compared to samples with no pre-treatment (Figure B.19). Squalane recovery, however, was 90-93% for the two concentrations tested over the alumina columns (Table 4.6). This demonstrates that a more representative recovery standard be used in the future.

4.3.3 Sulfur Removal

Elemental sulfur can damage GC-MS columns and therefore needed to be removed prior to analysis. Both activated copper granules and activated copper powder were successful in reducing the elemental sulfur in samples. Common copper powder, with no pre-treatment, did not have any effect on sulfur concentrations (Table 4.7). Activated copper granules required the most number of treatments and were the most time consuming, requiring samples be mixed overnight. Activated copper powder was also time consuming in that fresh powder had to be made everyday, as powder from 1 day before removed substantially less sulfur than new powder. However, activated powder required only 4 minutes of mixing on a vortex mixer, compared with stirring copper granules overnight. In total, copper granules required more than a week to reduce sulfur peaks to acceptable levels, while the copper powder required several treatments which were completed in a single day.

No difference was observed for samples extracted with copper powder when the supernatant liquid was filtered through the Na_2SO_4 column to remove suspended copper powder compared with directly sampling the supernatant without filtering. Furthermore, hexane with suspended copper powder was run on the GC-FID and no interference was observed in the signal. For both the copper granules and the copper powder treatments, substantial sample was lost, as observed by

Table 4.4: *Percent of spiked concentration measured at equilibrium for each batch and stock solution pair. Chemicals listed in order of increasing logK_{ow}. Equilibrium was the last measured concentration, though equilibrium may have been reached earlier. Times since batch injection varied between 72 - 600 hours. Concentrations below the minimum calibrated concentration indicated by (-).*

			Spiked Concentration at Equilibrium (%)		
	Chemical	$LogK_{ow}$	Injection 1	Injection 2	Injection 3
Batch 1	*Benzene Solution*				
	Benzene	2.1	33.6	30.4	38.5
Batch 1	*Organic Solution*				
	Benzene	2.1	36.8	30.5	17.5
	Toluene	2.7	10.4	12.4	12.6
	Chlorobenzene	2.8	7.0	8.1	9.9
	1,2-Dichlorobenzene	3.4	-	-	-
	1,3-Dichlorobenzene	3.5	-	-	-
Batch 2	*Hydrocarbon Solution*				
	Benzene	2.1	36.8	35.2	36.0
	Toluene	2.7	19.5	19.0	19.3
	Indene	2.9	11.7	12.3	12.0
	Styrene	3.0	12.2	13.4	12.8
	o-Xylene	3.1	7.1	7.1	7.1
	Ethylbenzene	3.2	5.2	5.4	5.3
	m/p-Xylene	3.2	5.0	5.1	5.1
	Naphthalene	3.3	-	-	-
	1,2,3-Trimethylbenzene	3.7	-	-	-
	1,2,4-Trimethylbenzene	3.8	-	-	-
Batch 8	*Benzene Solution*				
	Benzene	2.1	15.1	20.9	15.0

the reduction in signal on the GC-FID/FPD system. As a result of fewer treatments, less sample was lost with copper powder though, resulting in better GC-MS analysis.

4.3.4 Hydrocarbon Identification and Mass Balance

Of the volatile aromatic hydrocarbons in the batch bottles, naphthalene was the most abundant, accounting for 30-36% of components measured in the aqueous phase (Figure 4.13). The sterile batch had the highest benzene concentration (1.51 mg/L) in the aqueous phase, while sulfate had the least (0.25 mg/L). This was in agreement with the initial measurements of benzene as the 'C' replicate for sulfate had low benzene, while the 'A' replicate has high benzene concentration, increasing the average. Generally, the sulfate batch had the highest concentration of each component in the batches when compared to the no addition, with the exception of benzene and ethylbenzene and the sterile batch had substantially lower concentration of all components. For higher $logK_{ow}$ components, such as the methylnaphthalenes, the difference between sterile and treatment batches was less pronounced.

The sterile batch had no methane gas while the no addition had the highest concentration, 2.37

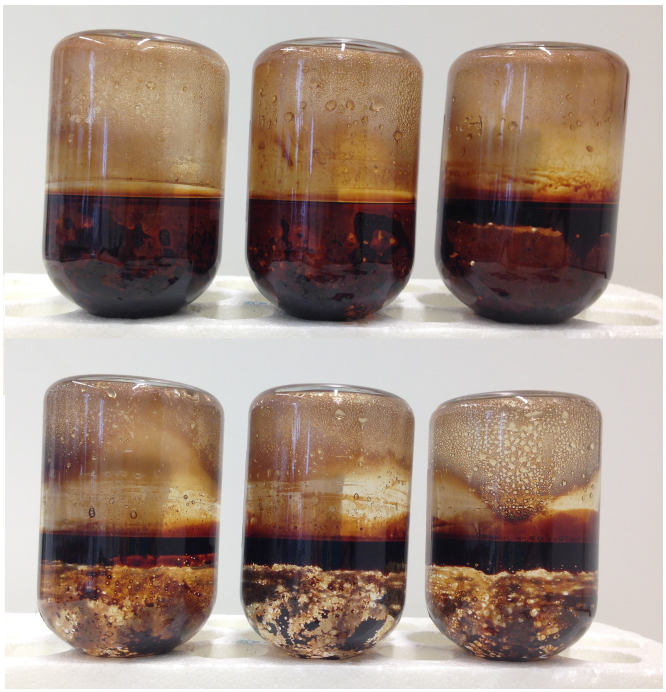

Figure 4.7: *Comparison of sterile batches. Top: Batch 5 sterilized with only 100 mg/L $HgCl_2$, Bottom: Batch 6 sterilized with 100 mg/L $HgCl_2$, 100 mg/L NaN_3 and autoclaved for 20 minutes at 121 °C. Batch 6 shows distinctly different tar dispersion in the bottle than batch 5, however no effect was observed on equilibrium concentrations of target analytes.*

Table 4.5: *Theoretical benzene concentration in batch 8 compared with the averaged actual concentration ± one standard deviation.*

		Benzene Concentrations (mg/L)		
	Initial	Injection 1	Injection 2	Injection 3
Actual	2.1 ± 0.1	3.6 ± 0.1	5.4 ± 0.3	6.7 ± 0.1
Theoretical ($\log K_{ow}$=2.3)	1.6	2.8	3.9	5.0
Theoretical ($\log K_{ow}$=2.2)	2.1	3.5	4.9	6.6

mg/L followed by the sulfate, 1.99 mg/L. Overall, the sulfate had the highest total concentration of aromatic hydrocarbons in the aqueous phase, 44.5 mg/L gŁ, followed by the no addition batch, 40.4 mg/L and the sterile batch had the least, 31.6 mg/L.

The accuracy of the PFTBA internal calibration method was tested on a standard with known elements. For each element 3-4 chemical formula were given with high mass spectral accuracy. In each case the formula with the highest accuracy was the known element. The spectral accuracies ranged from 94.6-98.9%. In comparison, the NIST search resulted in more than 30 possible chemical components, with relatively low probabilities (6.3-54.6%), where the highest probability did not always correspond with the known element. Spectral accuracy and the NIST probability for each of the four known elements is given in Table B.6.

All of the 16 peaks identified in the stimulation batch extraction for batches 8, 9 and 13 were PAHs. Alkanes, identified by comparing the retention times of alkanes from the C_7-C_{30} standard, were either absent or too small to quantify on either the GC-FID or GC-MS. Table B.7 summarizes the formulas derived from MassWorks, their spectral accuracy, the NIST chemical structures and NIST probabilities of components identified. In some cases multiple components were found in

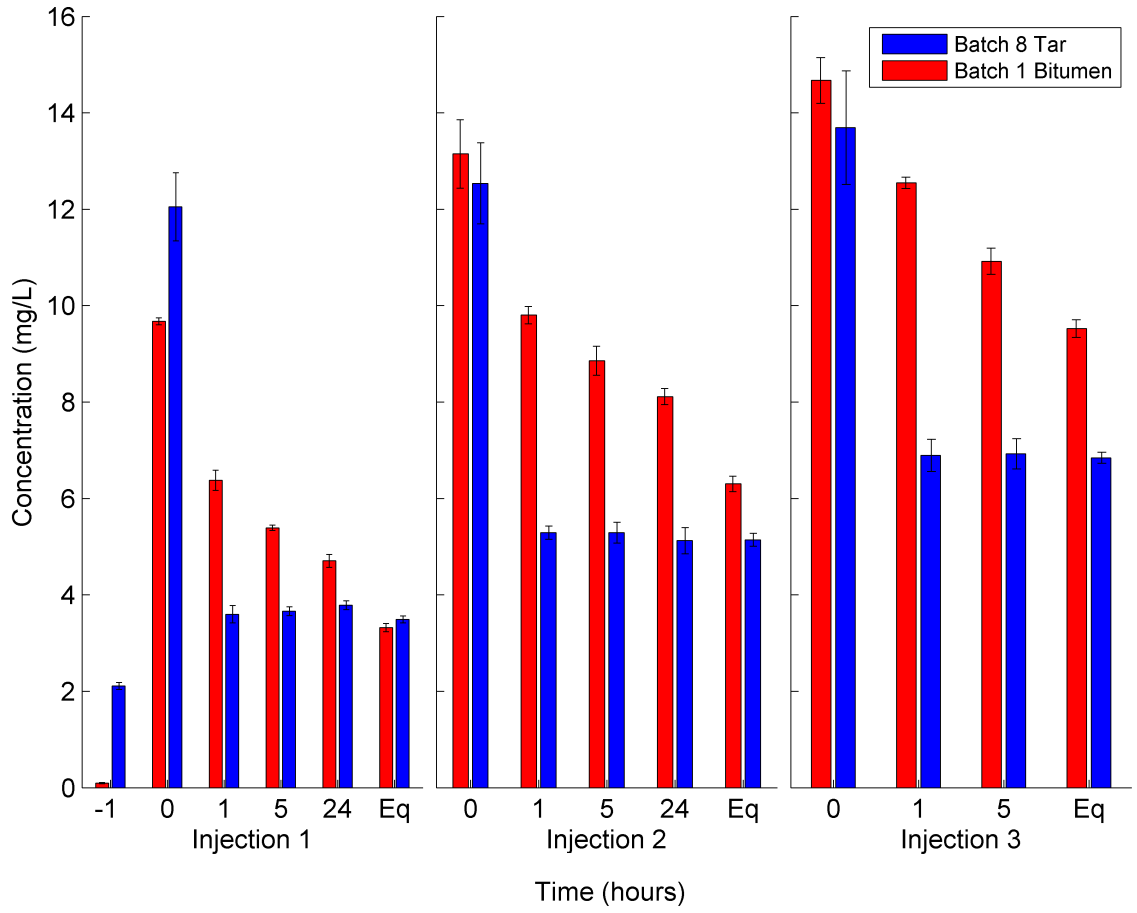

Figure 4.8: *Comparison of aqueous concentration of benzene in batch 1 (bitument) and batch 8 (tar) as a function of time after spiking. Error bars show one standard deviation. The last concentration is the equilibrium concentration for each batch.*

Table 4.6: *Squalane recovery test on alumina column at two different concentrations.*

	Peak Area		
Concentration (mg/ml)	Before Column	After Column	% Recovered
0.1508	196.5	182.9	93.1
1.508	2681	2415.5	90.1

NIST with similar probabilities and have been reported here. These same components were all found previously from the qualitative tar analysis (van Leeuwen, 2018). Figure B.22 gives the chemical structure for components for reference. The spectral accuracy was very high for all compounds, 92-99.5% while the NIST chemical structures probabilities were lower, 11-77.5%.

The smallest PAH identified was fluorene, a two-ring PAH, while the largest was benzo[ghi]perylene, a 6-ring PAH (Figure B.22). The no addition batch (9C) had the highest total concentration of PAHs in the aqueous phase, with 586 mg/L, followed by sulfate (13C) with 507 mg/L and the sterile batch had the least with 278 mg/L, less than half the no addition batch. In the no addition batch phenanthrene was the most abundant, with 91.5 mg/L, followed by methyl phenanthrene (75.4 mg/L) and fluoranthrene (72 mg/L), methylpyrene (67.7 mg/L) and 9,10-dimethylanthracene (56.9 mg/L). In all batches these five PAHs accounted for more than 60% of the total concentration (Figure 4.15).

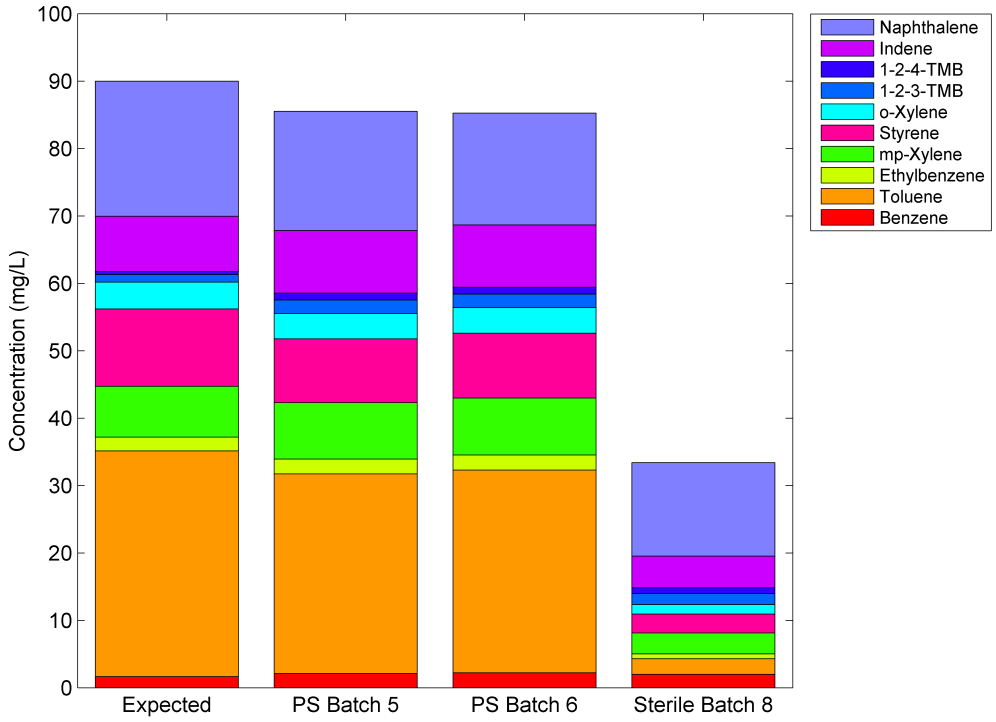

Figure 4.9: *Comparison of the expected partitioned concentration of the new partitioning batch experiments with pure phase tar from well A005A (PS Batch 5, PS Batch 6) and the original stimulation batch experiment (Sterile Batch 8) with residual tar from well A005A.*

Table 4.7: *Percent sulfur reduction of different copper treatment methods. Total treatment time given as number of days required to complete all treatments.*

Method	No. Treatments	Reduction	Total Time Required
Copper Granules	> 5	98.3%	>5 days
Activated Copper Powder	1-3	97.5%	1 day
Common Copper Powder	-	0%	-

The sterile batch had the lowest concentration for all PAH compounds (Figure B.24). The no addition batch had the highest concentration for all components except benz[a]anthracene, benzofluoranthene, benzo[ghi]perylene and dibenzo[a,e]fluoranthene, of which the sulfate batch had slightly higher concentrations (Figure B.24).

The PAHs with the largest concentration difference between the no addition and sulfate batches were 2-methyl-9H-fluorene, dibenzothiophene, phenanthrene, methyldibenzothiophene, methyl phenanthrene, 9,10-Dimethylanthracene and fluoranthene (Figure B.24). These components accounted for 95% of the concentration difference between the sulfate and no addition batches. Overall the no addition batch has slightly higher concentrations of 3- and 4-ring PAHs, and the sulfate batch slightly higher concentrations of the remaining 5- and 6-ring PAHs.

In total, PAHs comprised the vast majority, 88-89%, of the total mass measured in the aqueous phase of stimulated batch experiments. Heterocyclic, suflur containing PAHs accounted for between 6-8% and volatile aromatics 4-5% (Figure 4.14). Table B.8 summarizes the aqueous phase concentration of the aromatic and PAH concentrations measured for each of the three batches.

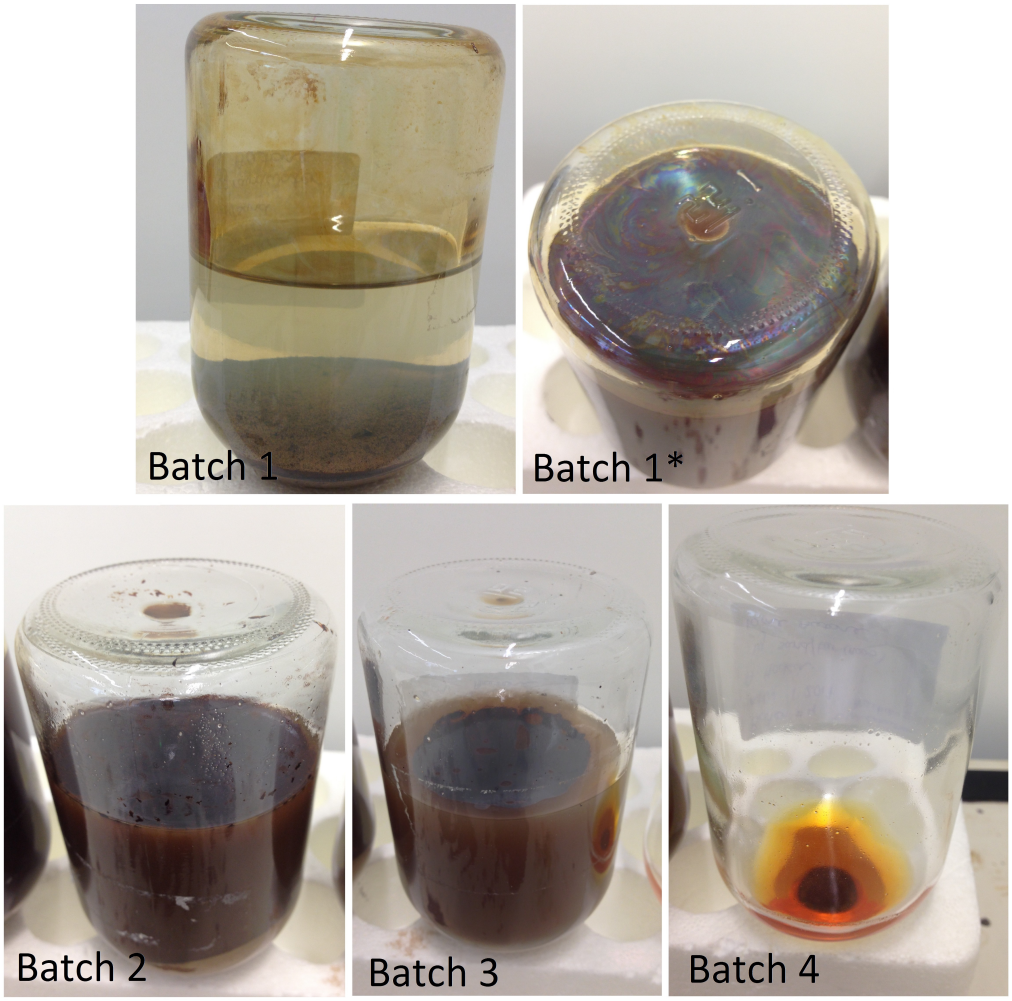

Figure 4.10: *Practice batch photo after 1 month of mixing. All but batch 4 have some amount of undissolved tar left in the batch bottle after mixing. Batch 4, with only 1 g of tar and 10 ml of acetone fully dissolved.*

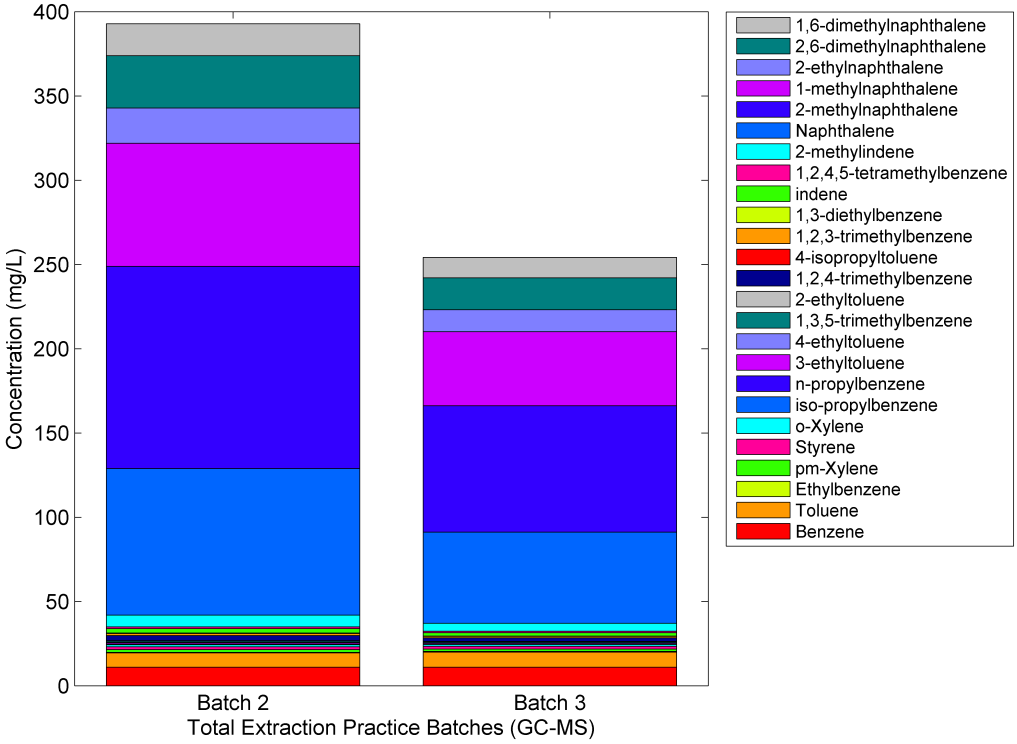

Figure 4.11: *GC-MS analysis of 25 mobile tar components for total extraction practice batches 2 and 3.*

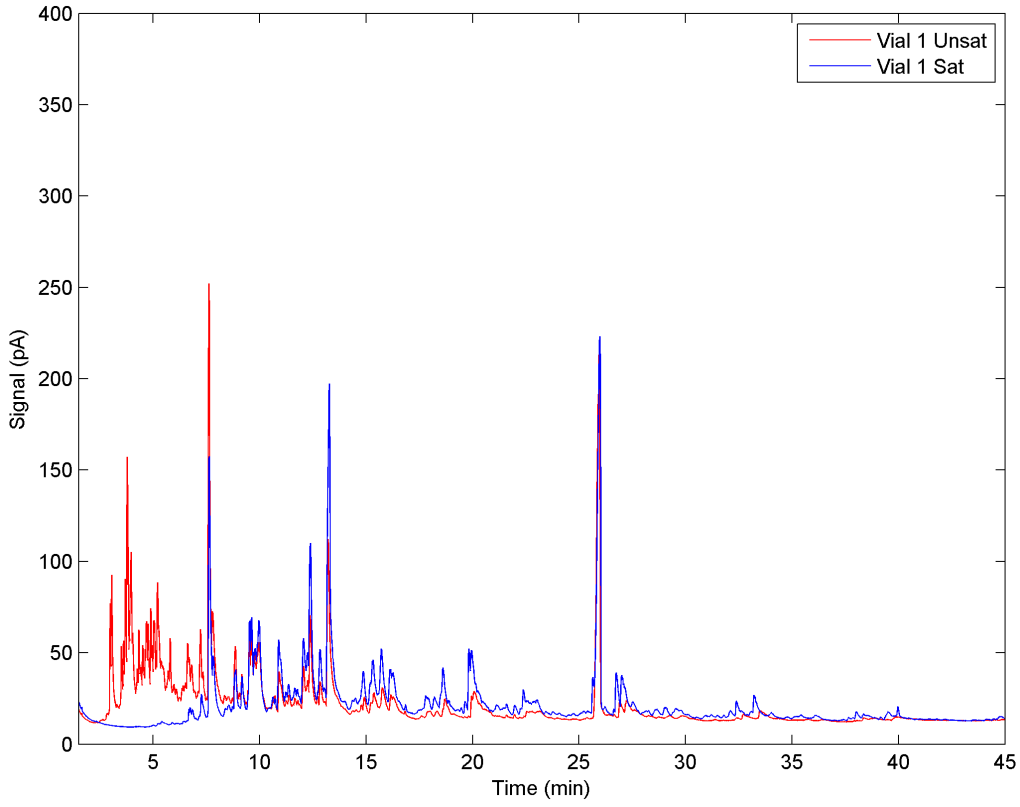

Figure 4.12: *Chromatogram of unsaturated and saturated fraction obtained from small column chromatography on silver impregnated silica gel.*

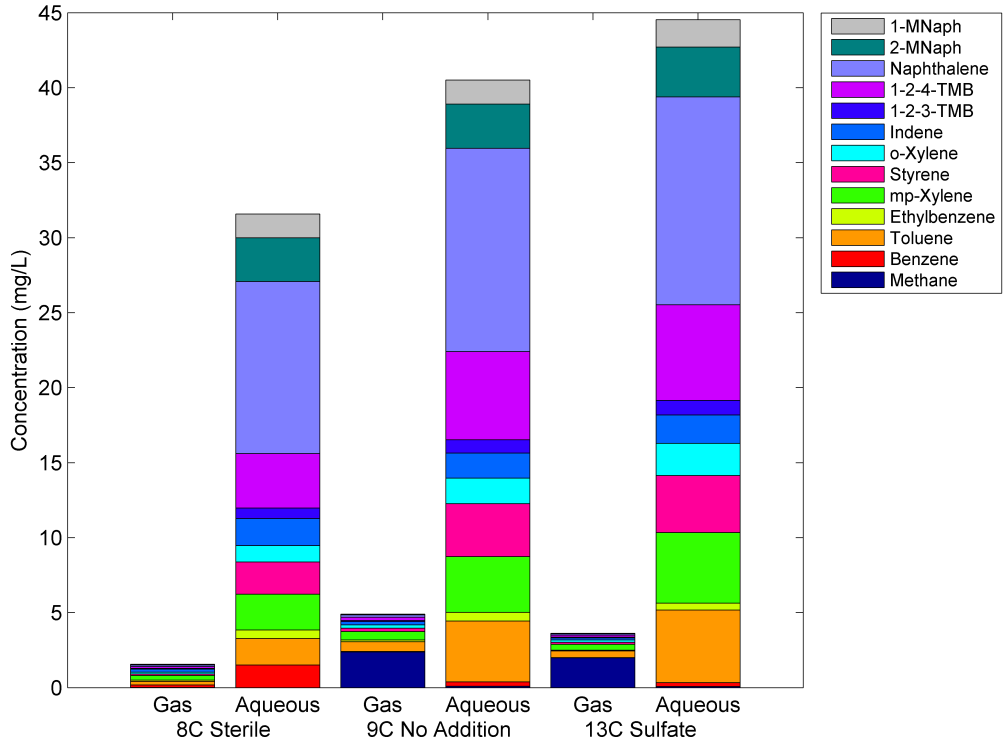

Figure 4.13: *Concentration of volatile aromatic hydrocarbons and methane in the gas and aqueous phase of batches 8C, 9C and 13C. Note: TMB = trimethylbenzene and MNaph = methylnaphthalene*

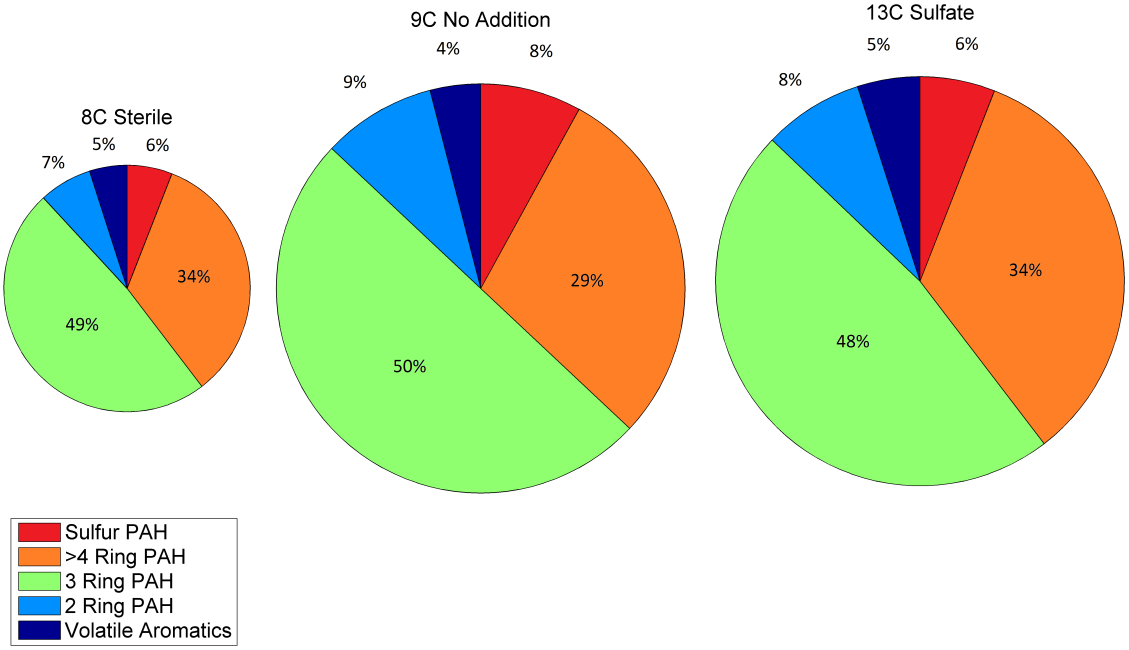

Figure 4.14: *Total concentration of hydrocarbons in the gas and aqueous phase, measured using GC-FID headspace analysis and COC-GC-FID/GC-MS aqueous phase samples for batches 8C (sterile), 9C (no addition) and 13C (sulfate). Hydrocarbons grouped into five categories for comparison to previous analysis by AlControl B.26. Pie Charts scaled to relative total concentration in each batch. The total mass of hydrocarbons measured for each batch: 8C Sterile 310 mg/L, 9C No addition 630 mg/L, 13C Sulfate 550 mg/L.*

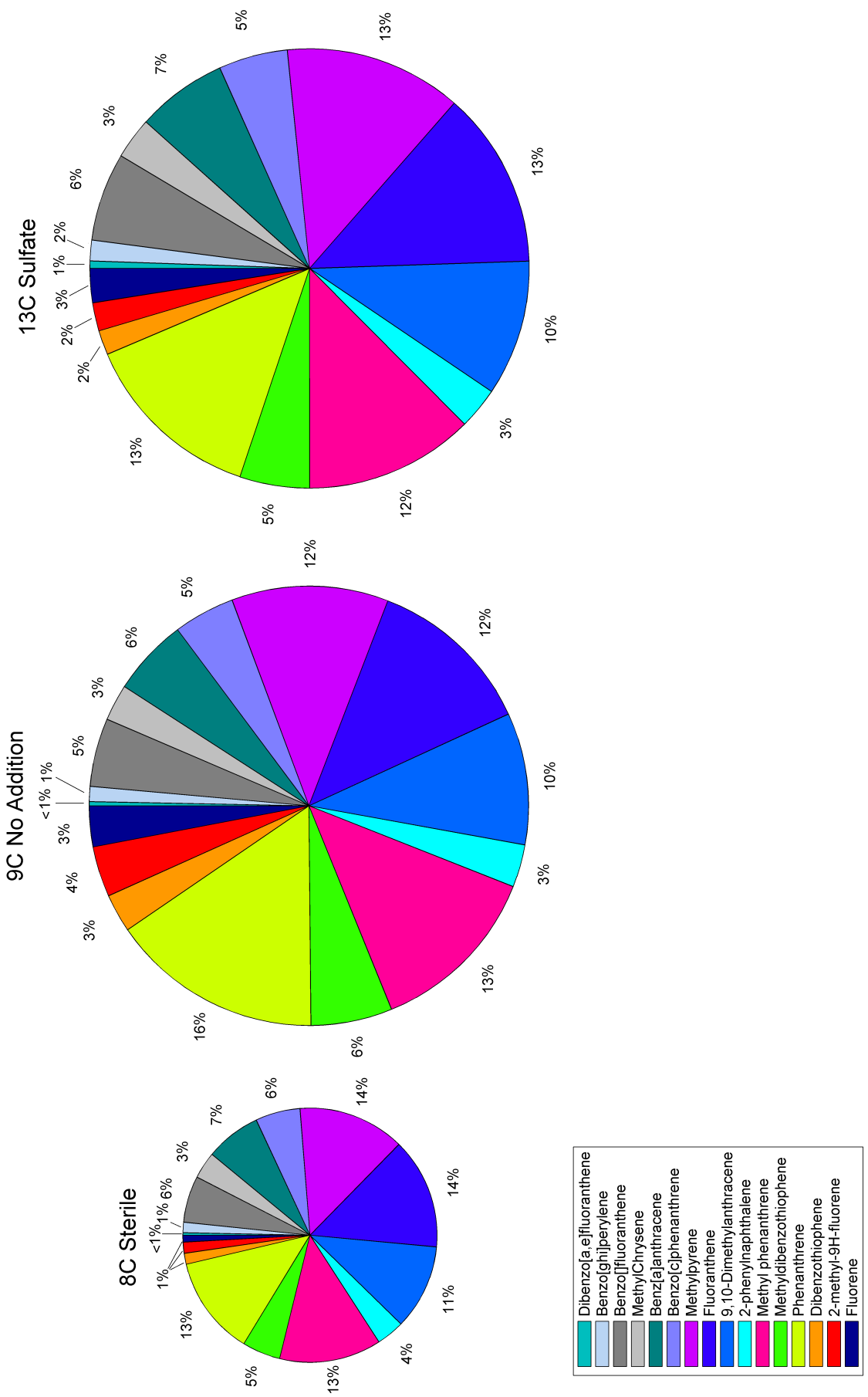

Figure 4.15: *Composition of PAHs identified from stimulation batches from total extraction protocol (Sterile, No Addition and Sulfate), as measured by COC-GC-FID/GC-MS. Pie Charts scaled to relative total concentration of PAHs in each batch. The total mass of PAHs for each batch: 8C Sterile 280 mg/L, 9C No addition 590 mg/L, 13C Sulfate 510 mg/L.*

Chapter 5

Discussion

5.1 GC-FID Method Development

The first research objective was to develop a GC-FID method to quantify the concentration of volatile aromatic hydrocarbons in the stimulation batch treatments. The method was accurate, reliable and in addition to quantifying volatile aromatics was also able to detect methane, an important indicator of bacterial degradation. Furthermore, the because the method used headspace samples instead of aqueous phase samples, it was less disruptive to the on-going batch experiments and required less preparation time. Finally, aqueous samples were found to overestimate the concentration of mobile tar components due to the presence micro-droplets of suspended tar in the aqueous phase. This overestimation is likely limited to measurements in the presence of pure phase tar and measurements in plume zones (ex. field measurements) are most likely not affected.

Measurements in the sterile batches differed the least from the GC-FID measurements as the tar in these bottles was the least visibly degraded, adhered the most to the glass sides of the bottle and therefore the least tar was suspended in the water samples taken. Furthermore, creosote and coal tars are abundant in naphthalenes and other PAHs (Birak & Miller, 2009; Gallacher *et al.*, 2017; Peters & Luthy, 1993). Dissolved tar, suspended in aqueous samples would then release primarily PAHs to the measurement vials, accounting for why naphthalene and methylnaphthalene component concentrations differed the most between the GC-MS and GC-FID measurements. From the partitioning coefficients calculated for mobile tar components, as little at 10 μL in droplets could have accounted for the difference observed between GC-FID and GC-MS measurements.

It is worth noting that micro-droplets not readily visible to the naked eye could also have been withdrawn within aqueous samples as well. To determine size and abundance of tar micro-droplets suspended in the aqueous phase, additional analyses would be required (eg. microscopy, high resolution imagery). The GC-FID measurements may have be affected by tar stuck to the glass in the headspace. The effect of the equilibrium between the tar and gas on headspace concentration measurements was not considered in this research but would be interesting to consider in future work. Good correlation between the results for GC-MS and GC-FID measurements for samples which lacked a NAPL though agreed well and therefore the effect of NAPL-gas partitioning on measurements may be low. This research highlights the importance of the choice of method as it can greatly influence the final results.

5.2 Stimulation Batch Experiments

The first research question was - *do the aqueous concentrations of volatile aromatic hydrocarbons vary between batch treatment?* GC-FID measurements of the stimulation batches resulted in sub-

stantial differences between the sterile, no addition and stimulated batches. However, an initial assumption of the research question was that biodegradation would lower the aqueous phase concentration of hydrocarbons and therefore the batch with the lowest aqueous concentration would indicate the best electron acceptor/substrate pair for in-situ biostimulation.

However, observations from the batch experiments show that concentrations of the most soluble components increased in stimulated batches compared to sterile. Furthermore, when the sterile batch concentrations were compared with the groundwater concentrations initially added to the batches, the sterile batch concentrations were lower for the six most soluble components; benzene, toluene, styrene, xylenes and ethylbenzene (Table B.3). The 6 least soluble components, indene, 2-Methylnaphthalene, 1-Methylnaphthalene, Naphthalene, 1,2,4-trimethylbenzene, 1,2,3-trimethylbenzene, all increased in concentration in the sterile batches.

The aqueous phase samples analyzed by TNO on the GC-MS found similar patterns for benzene concentrations. Therefore the decrease in benzene concentration cannot be explained by the NAPL sorbing concentrations from the gas phase resulting in lower concentration calculations in the sterile batches. The aqueous phase itself must have lower concentrations of benzene in the sterile batches.

This phenomena could be explained when the location of the groundwater and tar in the batches is considered. Tar in the batches was sampled from well A005A, located in the source zone, while the water in the batches was sourced from well A003A, located 70 m farther downstream (Figure 1.2). Dissolution from the NAPL pool to passing groundwater is governed by the solubility and mole fraction of tar components. Groundwater downstream from the source zone therefore has high concentrations of components with relatively high solubilities (benzene for example) and/or high mole fractions (naphthalenes for example, Fraser *et al.* 2008).

Recall the example of the parcel of water flowing through the subsurface from Section 2.2, Figure 5.1. Upstream of the source zone, the groundwater concentration of tar components is zero. The parcel then encounters the NAPL pool and there is equilibrium between the NAPL pool/groundwater interface, causing dissolution of tar components to the aqueous phase (zone (1) in Figure 5.1, Mayer & Hassanizadeh 2005). This equilibrium leads to an increase in concentration of tar components in the aqueous phase and a decrease in the NAPL at that location. Over time this creates a concentration gradient of tar components in the source zone, with the highest concentrations in the NAPL the furthest downgradient (Johnson *et al.*, 2006).

This gradient in concentrations was found for benzene in the partitioning experiments performed by van Leeuwen (2018). With increasing distance from the center of the source zone, the concentration of benzene in the tar samples decreased sharply (Figure 4.6). This decrease suggests that benzene is the first component to be depleted in the source zone. This is consistent with other studies, which have found that benzene and other soluble mono-aromatic components are the first to deplete in source zones (Eberhardt & Grathwohl, 2002; Fraser *et al.*, 2008; Peters *et al.*, 1999).

The gradient in tar concentration with distance along the source zone influenced the equilibrium within the stimulation batch experiments. The groundwater added to the batches from well A003A was located 70 m downgradient of the source zone well A005A. The equilibrium aqueous concentration of benzene from well A005A (1.9 mg/L) was lower than from well A010F (44 mg/L) located 35 m downgradient (van Leeuwen, 2018). Therefore, when groundwater from well A003A, with 20 mg/L of benzene, was added to the batch experiments the aqueous and NAPL were not in equilibrium. To equilibrate, benzene partitioned from the aqueous phase to the tar phase. This explains the lower concentrations of benzene and other relatively soluble components in the sterile batches compared to the groundwater concentrations used to make the batches.

Previous research on site has shown that the majority of degradation takes place at or near the source zone (Brock, 2016; Raptis *et al.*, 2015; van Logtestijn, 2017; Wagner, 2015). Furthermore, dispersion and mixing within the plume zone decrease the concentration of mobile tar components (Mayer & Hassanizadeh, 2005). Therefore degradation and dilution effects explain why the concen-

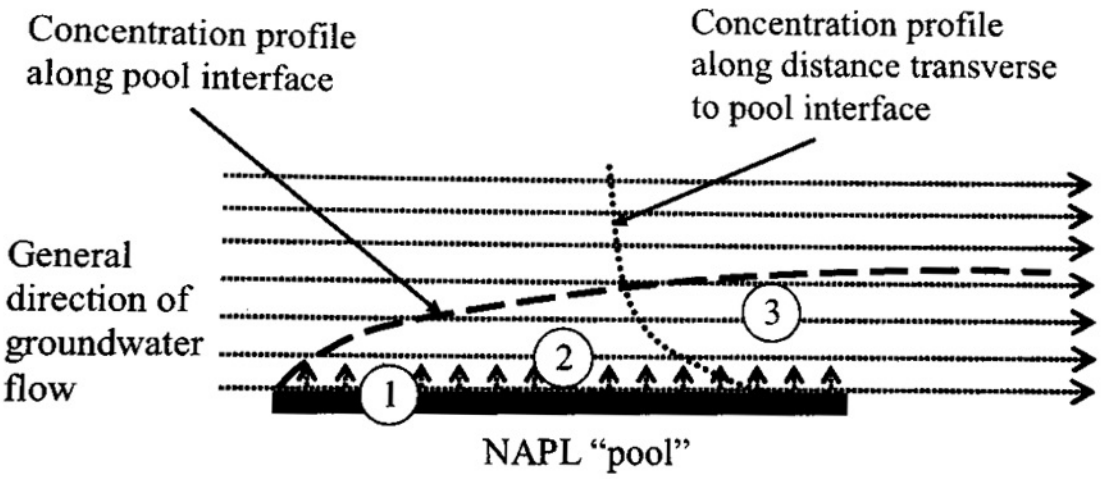

Figure 5.1: *Model of NAPL pool dissolution from Mayer & Hassanizadeh (2005). (1) Equilibrium at the interface between NAPL pool and passing groundwater, (2) Dispersion of NAPL in aqueous phase away from the surface of the pool, (3) Advection of dissolved NAPL components with groundwater flow.*

tration in well A003A was lower than the predicted maximum solubility concentrations observed in the partitioning experiment for well A010F (Figure 2.9).

The second research question was - *does biodegradation cause the tar to release less degradable, high solubility components, resulting in higher aqueous concentrations of tar components?* The results indicate that in the batches with additional electron acceptors and substrate, the bacteria were able to degrade the tar below to a critical mass. At this point the storage capacity of the tar was substantially reduced and could not retain all hydrocarbons and some were released back to the aqueous phase. This phenomena was found to be limited to only the most soluble tar components (eg. BTEX). Lower solubility components such as naphthalene were unaffected by the change in tar mass, as observed by their stable concentration between the batch treatments (Figure 4.5).

These conclusions were supported by the metabolite and qPCR data from previous research. The sum of signature metabolites were lowest in the stimulated batches (10-14), which suggested continued degradation of metabolites due to the additional electron acceptors causing the critical loss of tar (Brock, 2016). In contrast, the no addition batch (9) had higher metabolite concentrations than the sterile batch (8) (Brock, 2016). This suggested that degradation took place initially, but may have slowed as a result of the depletion of electron acceptors. The presence of methane in batches suggests that degradation by methanogenesis may be occurring. The lack of electron acceptors limited the degree of degradation, resulting in the lower concentration of benzene observed without the critical loss of tar.

Rival explanations for the visible loss of tar with the measured increase in volatiles in the aqueous phase include bacterial release of biosurfactants during degradation. Some species of bacteria release biosurfactants which can increase the solubility of hydrocarbons in the aqueous phase. Increasing the solubility increases the availability of NAPL components to bacteria for degradation (Das & Chandran, 2011; Leahy & Colwell, 1990; Muñoz *et al.*, 2007). Previous research on the stimulation batch experiments investigated whether rhamnolipids, a biosurfactant released by *Pseudomonas aeruginosa* bacteria were present in the batches (van Logtestijn, 2017). No evidence of rhamnolipids were found in batch samples analyzed (van Logtestijn, 2017).

5.3 Tar as a Hydrophobic Matrix: Batch Experiments

The current partitioning batch experiments showed that when benzene was added to batch bottles it almost immediately partitioned into the NAPL, resulting in only a slight increase in the aqueous phase concentration. Measurements as little as 5 minutes after addition were in equilibrium (Figure B.15). This confirmed the hypothesis that when groundwater with a higher benzene concentration was added to the stimulation batches, much of the benzene partitioned from the aqueous phase to the tar phase (Figure 4.5). Therefore the answer to the third research question - *does the tar act as a hydrophobic matrix, adsorbing aqueous phase concentrations of aromatic hydrocarbons?* - is yes, and the effect was most pronounced for high $\log K_{ow}$ components and components in which the tar was previously depleted.

It is worth noting that the partitioning batch experiments performed for this research were created with pure phase tar from well A005A. However, the original stimulation batch experiments used tar in sediment from well A005A. The partitioning coefficients calculated from the dissolution batch experiments performed by van Leeuwen (2018) predicted the equilibrium aqueous phase concentration of mobile tar components well (Figure 4.9). However, the sterile batch from the stimulation batch experiments had lower than calculated concentrations for all components but benzene and naphthalene (Figure 4.9). Toluene was especially low compared with the pure phase tar partitioning. The tar mixed in the sediment was likely more depleted in the soluble components than the pure phase tar as a result of increased weathering (Johnson *et al.*, 2006).

The equilibrium naphthalene concentration was unaffected by the location of the tar from the source zone (Figure 2.9), the tar:water (v:v) dilution ratio for tar from the same location (Figure 2.10), whether pure phase or residual tar was used (Figure 4.9) or the degree of degradation of tar (Figure 4.5). This suggests that naphthalene is strongly sorbed within the NAPL, is not subject to appreciable depletion over time due to dilution and therefore source zone biostimulation may have little effect on increasing the dissolution rate of naphthalene and other low solubility components.

Of the components measured, naphthalene accounted for the largest percent of the total concentration (Figure 4.6). Moreover, a reference bituminous NAPL showed that when batch bottles were spiked with mixtures of hydrocarbons or organic solutions, the most hydrophobic components partitioned into the NAPL faster and at higher concentrations than the less hydrophobic components (Figures B.13 and B.14). The data suggest that components with a $\log K_{ow}$ above 3.5 partitioned completely to the NAPL (Figures B.10 and B.11). This supports the idea that low solubility, high partitioning coefficient components likely account for a majority of the tar. This is supported by previous analysis of the Amersfoort oil, which found that monocyclic aromatic hydrocarbons account for as little at 15% of the total tar, while PAHs accounted for more than 63% (ALcontrol Laboratories, 2011). To quantify the proportion of non-volatile aromatics in the tar, the total extraction protocol was developed.

5.4 Total Extraction of Stimulation Batch Experiments

Research from Peters & Luthy (1993) on solvent extraction of coal tar suggest total dissolution of NAPL in a system with 10% coal tar, 80% acetone and 10% water. This corresponds well with the results of practice batch 4, which contained 1 g of sediment/tar and 10 ml of acetone and was the only batch which fully dissolved the tar. In our system with 100 ml of groundwater and 1-3 ml of tar in the sediment, approximately 400 ml of acetone would be required. The bottles themselves have a total volume of 245 ml so this is clearly not feasible without opening the bottles or performing sequential extractions. However, of the seven stimulation batch treatments, the sterile batches have the most tar visually remaining, while in all other treatments bioremediation has reduced the total volume of tar. Therefore it is likely that only the sterile batches will require

the full volume of acetone. Furthermore, when the batches are extracted with acetone, the volatile aromatic hydrocarbons will have already been quantified for the aqueous and gas phases, meaning batches which require more acetone can be opened without the loss of volatiles affecting the mass balance.

Small column chromatography provided no appreciable benefit for sample preparation as it was not possible to separate saturated and unsaturated hydrocarbons. Furthermore, the column filtered out PAHs with a retention time above 15 minutes, corresponding to the majority of the 4- and all 5-, 6-ring PAHs (Figures B.19 and B.21). Based on results from other studies, it is possible that not enough solvent was used during column chromatography to elute the larger PAH compounds from the column (Fedorak & Westlake, 1984; Le Dreau *et al.*, 1997; Ministry of Water Land and Air Protection, 2003; Xu *et al.*, 2015). Approximately 4 ml of solvent was used to extract the non-polar fraction for each sample, while other studies have used 20-30 ml, though the size of columns varied. However, as the samples with no pre-treatment performed well it is recommended that the column chromatography step be eliminated in the total extraction protocol.

Removal of elemental sulfur was necessary to avoid damage to the columns on the GC-MS and obtain the most accurate results. Sulfur removal was best achieved with activated copper powder, prepared fresh for each day's use. If more samples require treatment however, it is recommended that the copper powder be frozen as per the methods of Blumer (1957) so that new powder does not have to be prepared every day. Alternatively, the use of activated copper granules is recommended because the granules can achieve the same sulfur reduction, though they require more treatments and some additional sample loss.

The PFTBA internal calibration method worked very well and greatly improved the identification accuracy of unknown peaks in batch samples. Alone the NIST search library provided too many possible chemical names and structures for unknown peaks with relatively low probabilities for accurate chemical identification. The addition of PFTBA as an internal calibrant at the end of each GC-MS run improved mass measurement accuracy, narrowed the list of possible chemical formulas and provided calibrated accurate mass centroid data which was input to the NIST library search.

The third objective of this research was to develop a method to perform a mass balance of hydrocarbons in stimulation batch bottles. COC-GC-FID was used to quantify non-volatile aromatic hydrocarbons and GC-MS calibrated with internal standard PFTBA was used to identify the 16 most abundant compounds. Aliphatics in the aqueous phase were expected, however, all components identified were PAHs. The pattern in PAH concentrations differed from that of the volatile aromatics, as the highest total concentrations were found in the no addition batch, not the sulfate batch. The no addition batch had substantially higher concentrations of low molecular weight PAHs, fluorene through fluoranthene (Figure B.24). However, the higher molecular weight PAHs, benz[a]anthracene through dibenzo[a,e]fluoranthene, were slightly higher in the sulfate batch (Figure B.24).

The stimulated batches (batch no 10-14) had undergone substantially more degradation than the no addition batches, as evidenced by the visual loss of tar, low metabolite concentrations and high bacterial gene counts (Brock, 2016; van Logtestijn, 2017; Wagner, 2015). The PAHs identified in the stimulation batches have $\log K_{ow}$ values between 4.4-6.7 (Table B.7). Applying the theory of the tar acting as a hydrophobic matrix, retaining only low solubility/high $\log K_{ow}$ components within the NAPL when the tar is degraded below a critical mass, in order for the concentrations of the relatively lower $\log K_{ow}$ components (fluorene-fluoranthene) to be *higher* in the no addition batch than the sulfate batch there must have been more degradation of these components in the sulfate batch than the no addition. Otherwise results similar to the higher $\log K_{ow}$ components (benz[a]anthracene through dibenzo[a,e]fluoranthene) would be expected, where the sulfate batch concentrations are similar or slightly higher.

Metabolite data from field and batch experiments suggest PAHs degradation occurs both in-situ and in batch experiments. Brock (2016) found phenanthroic acid, a possible metabolite of phenanthrene, in all high series batches and some field samples. Significantly, phenanthroic acid was absent in metabolite screening of pure tar samples, suggesting degradation occurs only outside the source zone. Fluorenoic acid, a metabolite of fluorene, was also found in some batch and field samples, indicating the degradation of fluorene. Finally, indications of other PAH degradation occurring in batches include the presence of 4-hydroxy benzoic acid (a possible metabolite of phenol), acenaphthenoic acid (acenaphthene), biphenyl-carboxylic acid (biphenyl) and acenaphthylenoic acid (acenaphthylene) were also present in some batches (Brock, 2016). Finally, 2-naphthoic acid, a signature metabolite of naphthalene, was found in all batch treatments, including the sterile batch.

Therefore, degradation of PAHs in batch experiments may be occurring and the data from the current analysis of PAH concentrations suggest the sulfate batches may have been stimulated to degrade PAHs more than is naturally occurring on site. These results are significant, as PAHs were found to comprise 90% of the tar and PAH degradation rates are generally low when compared with other hydrocarbons (Birak & Miller, 2009). The concentrations of PAHs in other treatment batches should be quantified to compare the relative success of different electron acceptors to stimulate degradation. Finally, batch bottles should be extracted with acetone in order to quantify the concentration of volatile aromatic hydrocarbons and PAHs in the remaining tar phase. Only then can conclusive results comparing the batch treatments be obtained.

5.5 Liquid Phase Stability of NAPL Components

The liquid phase stability of NAPL components has not yet been considered in the batch experiments. The liquid phase stability refers to components in NAPL which are solid at ambient temperature, such as many PAHs (Birak & Miller, 2009). As discussed already, as NAPLs weather in the subsurface, the more soluble components will deplete first due to dissolution to passing groundwater (Birak & Miller, 2009). This causes a shift in the composition of the remaining NAPL, increasing the mole fractions of less soluble components (Birak & Miller, 2009; Fraser *et al.*, 2008; King & Barker, 1999). The shift in NAPL composition can result in some PAHs exceeding the NAPL solubility limit and causing them to precipitate out (Peters *et al.*, 1997, 2000).

Two important factors to consider for the liquid phase stability of PAHs are; (1) components NAPL solubility limits, and (2) non-deal behavior observed for multicomponents NAPLs. Peters *et al.* (2000) observed non-ideal behavior in NAPL containing synthetic PAHs mixture, where methylnaphthalene co-precipitated with phenanthrene, despite not having reached it's solubility limit in the NAPL. The implications here is that for very complex mixtures, such as the Amersfoort tar, where 980 components have been identified, the liquid phase solubility relationships between components will be highly complex. Moreover, the NAPL solubility limit of components is not known and therefore determining how different PAHs interact in the batch bottles and precipiate or co-precipitate will be extremely difficult.

This phenomena has not been considered within the scope of this research. However, the phase of contaminants is an important consideration as the dissolution and partitioning behavior are dependent on whether a component is present as a pure phase or within a NAPL (Peters *et al.*, 1997). If present as a pure phase, the maximum aqueous concentration is determined solely by the component solubility. However, if a component is present within a multicomponent NAPL, dissolution depends on both the mole fraction and solubility limit. Therefore, understanding the phase stability of NAPL components and coupling this with knowledge of biodegradation will ensure that the most effective remediation technologies are prioritized which maximize degradation while limiting risk to human health.

Chapter 6

Conclusions

Batch experiments were created to compare the biostimulation potential of different redox conditions by stimulating anaerobic batches with contaminated tar and groundwater with different electron acceptors and substrates. To quantify the concentration of mobile aromtic tar components in each batch, a novel method for headspace GC-FID measurements was developed. The designed method was fast, non-destructive and gave more accurate results for batches with pure phase NAPL in the bottle than aqueous phase methods. The method was able to reliably quantify 12 mobile aromatic compound as well as methane gas in batch bottles.

The concentration of volatile aromatic hydrocarbons differed substantially between the batch treatments. The sterile batches had the lowest overall concentration of hydrocarbons of any of the batch treatments. In contrast, the stimulated batches had the highest concentrations of hydrocarbons while visibly the least tar. This result was initially counter-intuitive, as degradation was hypothesized to result in lower concentrations in the aqueous phase. However, the data suggested that the tar was not only a source of hydrocarbons but also a sink, where hydrocarbons are kept out of the aqueous phase as a result of equilibrium partitioning between the NAPL and water phases. The treatment batches were found to have been degraded below a critical mass of tar, resulting in the tar releasing the more soluble components to the aqueous phase.

Partitioning batch experiment data were analyzed from previously conducted experiments to quantify the partitioning coefficient and concentration of tars from different locations within one source zone. These data were used in conjunction with new batch experiments to determine if the tar present in batch experiment was functioning as a hydrophobic matrix, causing components to partition from the aqueous phase to the tar phase within batches.

The experiments showed that the tar was indeed sorbing the spiked concentrations of hydrocarbons, resulting in lower aqueous phase concentrations. These effects were most pronounced for low solubility, high partitioning coefficient components, with $\log k_{ow}$ values above 3.5. Furthermore, rapid partitioning of benzene was observed for batches tested with pure phase tar from site, with equilibrium concentrations after as a little as 5 minutes.

No effect of sample location, dilution or degradation resulted in substantial concentration changes of naphthalene in any batch experiment. This was likely the result of naphthalene's relatively low solubility, high partitioning coefficient and high mole fraction in the tar. However, experimental limitation did not allow the quantification of the partitioning coefficient or initial concentration in the tar of components larger than naphthalene. Therefore a total extraction method was developed to quantify the concentration of tar components in each of the gas, aqueous and tar phases within the batches.

An optimal ratio of 10/10/80 (v/v/v) for tar/water/acetone was found to fully extract tar present in stimulation batches, which agreed well with published data (Peters & Luthy, 1993).

Small column chromatography failed to separate unsaturated and saturated hydrocarbon fractions for COC-GC-FID analysis and in fact filtered out large PAHs components. Elemental sulfur removal was best achieved with activated copper powder prior to analysis on GC-MS and was necessary to prevent damage to the GC column.

In the aqueous phase, PAHs ranging from 2 to 6 aromatic rings were found in the sterile, no addition and sulfate batch treatments. The highest concentration was found in the no addition batch, followed by the sulfate batch and the sterile batch had the lowest over all concentration. The no addition batch was found to have slightly higher concentrations of 3- and 4- ring PAHs and the sulfate batch higher concentrations of 5- and 6- ring PAHs, suggesting possible increased degradation of lower ring PAHs in the sulfate batch. This was supported by previous research which found metabolites in batch and field samples, indicating the natural and stimulated degradation of PAHs.

Analysis of the stimulation batch experiments has resulted in a fundamental shift in how the efficacy of degradation is evaluated in the batch bottles. Aqueous concentrations are no longer sufficient to evaluate the remediation potential of added electron acceptor-substrate pairs in the batches with pure phase NAPL and the mass of tar components in each phase of the batches is necessary to draw accurate conclusions.

In summary, batches stimulated with additional electron acceptors resulted in tar being degraded below a critical mass. The critical loss of tar resulted in substantially higher aqueous concentrations of benzene. This was alarming as benzene is one of the most toxic and mobile tar components and a known carcinogen (EPA, 2009). The data suggest that source zone remediation through biostimulation could result in net loss of NAPL, at the risk of releasing large concentrations of NAPL bound benzene to the groundwater, potentially increasing plume zone concentrations and extent. This research has highlighted an important risk of source zone remediation and further work in this area will be critical to the successful and safe implementation of source zone remediation in the future.

6.1 Recommendations and Future Work

Below are general recommendations and ideas for future work.

Experiments with tar from sediment samples from the same well as pure phase tar samples (well A010F) showed decreased aqueous concentrations of components, likely the result of increased weathering. Future work could include quantifying the extent of depletion of tar components in residual zones, in addition to the variation in pure phase areas.

Activated powder was more efficient for sulfur removal in this preliminary study as only 3 samples were treated. It was feasible to perform multiple copper treatments and check the sulfur content on the GC-FID after each treatment within a single day. If more samples will be treated in the future (ex. $\geq$5) and time allows, the granules may be the more efficient option. The copper granules require more treatments and therefore take longer to complete the sulfur reduction but require less hands-on time in the laboratory. Furthermore, with many samples the iterative, treat-check method employed with the powder, where each sample was treated with copper and immediately run on the GC-FID to check the sulfur reduction, would not be possible due to the run-time (30 minutes) constraints of the GC-FID.

It is recommended that aqueous samples extracted be dried solely under N_2 gas at 30° degrees, small column chromatography be eliminated and samples injected directly to the GC-FID with no pre-treatments. A suitable PAH internal standard not present in the tar should be tested and used for quantification by co-injection. For identification of PAHs byGC-MS, the internal calibrant PFTBA was invaluable in providing high spectral mass accuracy and narrowing possible chemical

formula.

A protocol to obtain aqueous phase sampled from batches without the interference of tar droplets should be explored. In some cases, for example the quantification of non-volatile components can only be done with aqueous samples and not with headspace samples. Filtering sampled may be one method of removing droplet, centrifuging samples another. However these methods must be quantitatively explored.

The total extraction on the 3 batches (sterile, no addition and sulfate) should be completed by extraction with acetone to prove the disappearance of tar components and the overall mass loss of tar in the batches. Moreover, the remaining four batches (nitrate, nitrate and succinate, nitrate and acetate and chlorate) not sampled should also be extracted and quantified to compare the relative effectiveness of the different electron acceptor/substrate pairs.

An additional set of batches should be prepared to examine tar which is subject to aerobic degradation to prove that degradation results in the release of soluble tar components, as the sorbtion of tar components has already been proven in the current research.

Finally, a computer model should be developed to explore how source zone remediation may impact the Amersfoort site. The model could couple the dose of electron acceptors added to the different batches and the associated release and loss of tar components observed from the total extraction of the batches. Extrapolation to site conditions would give valuable insight into how, for example, the concentration and extent of the plume zone may increase as a result of the release of soluble tar components or how source zone longevity will be affected as a result of mass losses.

Furthermore, a model could explore how combining source zone stimulation with plume zone stimulation and/or augmentation could prevent the spread of plume zone contamination. Degradation rates could be obtained from the current stimulation and augmentation field trial ongoing at Amersfoort (see Appendix A).

References

Abu Laban, Nidal, Selesi, Draženka, Jobelius, Carsten, & Meckenstock, Rainer U. 2009. Anaerobic benzene degradation by Gram-positive sulfate-reducing bacteria. *FEMS Microbiology Ecology*, **68**(3), 300–311.

Albrechtsen, Hans-jorgen, & Winding, Anne. 1992. Microbial biomass and activity in subsurface sediments from Vejen, Denmarl. *Microbial Ecology*, **23**, 303–317.

ALcontrol Laboratories. 2011. *Teerkarakterisatietest.* Tech. rept. ALcontrol Laboratories Hawarden.

Alvarez, Pedro J. J., & Illman, Walter A. (Walter Arthur). 2006. *Bioremediation and natural attenuation : process fundamentals and mathematical models.* Hoboken, New Jersey: Wiley-Interscience. John Wiley & Sons, Inc. Publication.

Alvarez, Pedro J.J., Anid, Paul J., & Vogel, Timothy M. 1991. Kinetics of aerobic biodegradation of benzene and toluene in sandy aquifer material. *Biodegradation*, **2**(1), 43–51.

Ball, Harold A., Johnson, Hope A., Reinhard, Martin, & Spormann, Alfred M. 1996. Initial reactions in anaerobic ethylbenzene oxidation by a denitrifying bacterium, strain EB1. *Journal of Bacteriology*, **178**(19), 5755–5761.

Bauer, Robert D., Maloszewski, Piotr, Zhang, Yanchun, Meckenstock, Rainer U., & Griebler, Christian. 2008. Mixing-controlled biodegradation in a toluene plume - Results from two-dimensional laboratory experiments. *Journal of Contaminant Hydrology*, **96**(1-4), 150–168.

Bekins, Barbara, Rittmann, Bruce E., & MacDonald, Jacqueline A. 2001. Natural attenuation strategy for groundwater cleanup focuses on demonstrating cause and effect. *Eos, Transactions, American Geophysical Union*, **82**(5), 57–58.

Beller, H.R. R, & Reinhard, M. 1995. The role of iron in enhancing anaerobic toluene degradation in sulfate-reducing enrichment culutres. *Microbial Ecology*, **30**(1), 105–114.

Berdugo-Clavijo, Carolina, Dong, Xiaoli, Soh, Jung, Sensen, Christoph W., & Gieg, Lisa M. 2012. Methanogenic biodegradation of two-ringed polycyclic aromatic hydrocarbons. *FEMS Microbiology Ecology*, **81**(1), 124–133.

Birak, P. S., & Miller, C. T. 2009. Dense non-aqueous phase liquids at former manufactured gas plants: Challenges to modeling and remediation. *Journal of Contaminant Hydrology*, **105**(3-4), 81–98.

Blumer, Max. 1957. Removal of Elemental Sulfur from Hydrocarbon Fractions. *Analytical Chemistry*, **29**(7), 1039–1041.

Brock, Olaf. 2016. *Detection of metabolite biomarkers indicating anaerobic biodegradation of oil-gas tar in soil column and batch experiments and in-situ Internship report.* Tech. rept. January. Deltares.

Caldwell, Matthew E., & Suflita, Joseph M. 2000. Detection of phenol and benzoate as intermediates of anaerobic benzene biodegradation under different terminal electron-accepting conditions. *Environmental Science and Technology*, **34**(7), 1216–1220.

Callaghan, Amy V. 2013. Metabolomic investigations of anaerobic hydrocarbon-impacted environments. *Current Opinion in Biotechnology*, **24**(3), 506–515.

Carr, Cynthia S., Garg, Sanjay, & Hughes, Joseph B. 2000. Effect of dechlorinating bacteria on the longevity and composition of PCE-containing nonaqueous phase liquids under equilibrium dissolution conditions. *Environmental Science and Technology*, **34**(6), 1088–1094.

Chang, B.V, Shiung, L.C, & Yuan, S.Y. 2002. Anaerobic biodegradation of polycyclic aromatic hydrocarbon in soil. *Chemosphere*, **48**(7), 717–724.

Coates, J D, Anderson, R T, & Lovley, D R. 1996. Oxidation of Polycyclic Aromatic Hydrocarbons under Sulfate-Reducing Conditions. *Applied and Environmental Microbiology*, **62**(3), 1099–1101.

Conrad, Stephen H., Wilson, John L., Mason, William R., & Peplinski, William J. 1992. Visualization of residual organic liquid trapped in aquifers. *Water Resources Research*, **28**(2), 467–478.

Cunningham, Jeffrey A., Rahme, Halla, Hopkins, Gary D., Lebron, Carmen, & Reinhard, Martin. 2001. Enhanced in situ bioremediation of BTEX-contaminated groundwater by combined injection of nitrate and sulfate. *Environmental Science and Technology*, **35**(8), 1663–1670.

Da Silva, M L B, Daprato, R C, Gomez, D E, Hughes, J B, Ward, C H, & Alvarez, P J J. 2006. Comparison of bioaugmentation and biostimulation for the enhancement of dense nonaqueous phase liquid source zone bioremediation. *Water Environment Research*, **78**(13), 2456–2465.

da Silva, Marcio L B, & Alvarez, Pedro J J. 2004. Enhanced Anaerobic Biodegradation of Benzene-Toluene-Ethylbenzene-Xylene-Ethanol Mixtures in Bioaugmented Aquifer Columns. *Applied and Environmental Microbiology*, **70**(8), 4720–4726.

Das, Nilanjana, & Chandran, Preethy. 2011. Microbial degradation of petroleum hydrocarbon contaminants: an overview. *Biotechnology Research International*, **2011**, 13.

Daugulis, Andrew J. 2001. Two-phase partitioning bioreactors: A new technology platform for destroying xenobiotics. *Trends in Biotechnology*, **19**(11), 457–462.

Dou, Junfeng, Liu, Xiang, Hu, Zhifeng, & Deng, Dong. 2008. Anaerobic BTEX biodegradation linked to nitrate and sulfate reduction. *Journal of Hazardous Materials*, **151**(2-3), 720–729.

Eberhardt, Christina, & Grathwohl, Peter. 2002. Time scales of organic contaminant dissolution from complex source zones: Coal tar pools vs. blobs. *Journal of Contaminant Hydrology*, **59**(1-2), 45–66.

Edwards, E. A., & Grbic-Galic, D. 1992. Complete mineralization of benzene by aquifer microorganisms under strictly anaerobic conditions. *Applied and Environmental Microbiology*, **58**(8), 2663–2666.

Edwards, E. A., Wills, L. E., Reinhard, M., & Grbic-Galic, D. 1992. Anaerobic degradation of toluene and xylene by aquifer microorganisms under sulfate-reducing conditions. *Applied and Environmental Microbiology*, **58**(3), 794–800.

Elshahed, M. S., Gieg, L. M., McInerney, M. J., & Suflita, J. M. 2001. Signature metabolites attesting to the in situ attenuation of alkylbenzenes in anaerobic environments. *Environmental Science and Technology*, **35**(4), 682–689.

EPA. 1996. *Method 3660B Sulfur Cleanup*. Tech. rept. December 1996. U.S. Environmental Protection Agency.

EPA. 2009. *National Drinking Water Regulations MCL Booklet May 2009*. Tech. rept. U.S. Environmental Protection Agency.

EPA. 2013. *Introduction to In Situ Bioremediation of Groundwater*. Tech. rept. U.S. Environmental Protection Agency.

Eriksson, Mikael, Sodersten, Erik, Yu, Zhongtang, Dalhammar, Gunnel, & Mohn, William W. 2003. Degradation of Polycyclic Aromatic Hydrocarbons at Low Temperature under Aerobic and Nitrate-Reducing Conditions in Enrichment Cultures from Northern Soils. *Applied and Environmental Microbiology*, **69**(1), 275–284.

Fedorak, P. M., & Westlake, D. W S. 1984. Microbial degradation of alkyl carbazoles in Norman Wells crude oils. *Applied and Environmental Microbiology*, **47**(4), 858–862.

Foght, Julia. 2008. Anaerobic biodegradation of aromatic hydrocarbons: Pathways and prospects. *Journal of Molecular Microbiology and Biotechnology*, **15**(2-3), 93–120.

Fraser, M., Barker, J. F., Butler, B., Blaine, F., Joseph, S., & Cooke, C. 2008. Natural attenuation of a plume from an emplaced coal tar creosote source over 14 years. *Journal of Contaminant Hydrology*, **100**(3-4), 101–115.

Gallacher, Christopher, Thomas, Russell, Lord, Richard, Kalin, Robert M., & Taylor, Chris. 2017. Comprehensive database of Manufactured Gas Plant tars. Part A. Database. *Rapid Communications in Mass Spectrometry*, **31**(15), 1231–1238.

Garcia-Junco, Marta, Gomez-Lahoz, Cesar, Niqui-Arroyo, Jose-Luis, & Ortega-Calvo, Jose-Julio. 2003. Biosurfactant- and Biodegradation-Enhanced Partitioning of Polycyclic Aromatic Hydrocarbons from Nonaqueous-Phase Liquids. *Environmental Science & Technology*, **37**(13), 2988–2996.

Geller, J.T., & Hunt, J.R. 1993. Mass transfer from nonaqueous phase organic liquids in water-saturated porous media. *Water Resource Research*, **29**(4), 833–845.

Gerritse, Jan, Marsman, Annemieke, Brock, Olaf, van Logtestijn, Merijn, Hockin, Alex, van der Waals, Marcelle, & van Leeuwen, Johan A. 2017. *Onderzoek naar de anaerobe afbraak van benzeen op de locatie van een voormalige vetgasfabriek*. Tech. rept.

Gkekas, Stefanos. 2014. *Effect of limited warming on residual oil-gas tar (Masters Thesis)*.

Goossen, R. M. J, & Booms, A, Th. H. 2013. *Aanvullend bodemonderzoek probleemstelling Vetgasfabriek te Amersfoort*. Tech. rept. Aveco de Bondt.

Haritash, A. K., & Kaushik, C. P. 2009. Biodegradation aspects of Polycyclic Aromatic Hydrocarbons (PAHs): A review. *Journal of Hazardous Materials*, **169**(1-3), 1–15.

Herzyk, Agnieszka, Maloszewski, Piotr, Qiu, Shiran, Elsner, Martin, & Griebler, Christian. 2014. Intrinsic potential for immediate biodegradation of toluene in a pristine, energy-limited aquifer. *Biodegradation*, **25**(3), 325–336.

Hu, Zhi-feng, Dou, Jun-feng, Liu, Xiang, Zheng, Xi-lai, & Deng, Dong. 2007. Anaerobic biodegradation of benzene series compounds by mixed cultures based on optional electronic acceptors. *Journal of Environmental Sciences*, **19**(9), 1049–1054.

Jobelius, Carsten, Anneser, Bettina, Griebler, Christian, Meckenstock, Rainer U, Reineke, Anne, Frimmel, Fritz H, & Zwiener, Christian. 2011. Metabolites indicate hot spots of biodegradation and biogeochemical gradients in a high-resolution monitoring well. *Environmental Science & Technology*, **45**(2), 1–12.

Johnson, Paul, Lundegard, Paul, & Liu, Zhuang. 2006. Source Zone Natural Attenuation at Petroleum Hydrocarbon Spill Sites—I: Site-Specific Assessment Approach. *Ground Water Monitoring & Remediation*, **26**(4), 82–92.

Jones, D. M., Head, I. M., Gray, N. D., Adams, J. J., Rowan, A. K., Aitken, C. M., Bennett, B., Huang, H., Brown, A., Bowler, B. F. J., Oldenburg, T., Erdmann, M., & Larter, S. R. 2008. Crude-oil biodegradation via methanogenesis in subsurface petroleum reservoirs. *Nature*, **451**(7175), 176–180.

King, Mark W G, & Barker, James F. 1999. Migration and natural fate of a coal tar creosote plume 1 . Overview and plume development. *Journal of Contaminant Hydrology*, **39**, 249–279.

Kleemann, Rita, & Meckenstock, Rainer U. 2011. Anaerobic naphthalene degradation by Gram-positive, iron-reducing bacteria. *FEMS Microbiology Ecology*, **78**(3), 488–496.

Kunapuli, Umakanth, Lueders, Tillmann, & Meckenstock, Rainer U. 2007. The use of stable isotope probing to identify key iron-reducing microorganisms involved in anaerobic benzene degradation. *ISME Journal*, **1**(7), 643–653.

Langenhoff, Alette, Richnow, Hans, & Gerritse, Jan. 2009. Benzene Degradation at a Site Amended with Nitrate or Chlorate. *Bioremediation Journal*, **13**(4), 180–187.

Langenhoff, Alette A. M., Zehnder, Alexander J. B., & Schraa, Gosse. 1996. Behaviour of toluene, benzene and naphthalene under anaerobic conditions in sediment columns. *Biodegradation*, **7**(3), 267–274.

Le Dreau, Y., Jacquot, F., Doumenq, P., Guiliano, M., Bertrand, J. C., & Mille, G. 1997. Hydrocarbon balance of a site which had been highly and chronically contaminated by petroleum wastes of a refinery (from 1956 to 1992). *Marine Pollution Bulletin*, **34**(6), 456–468.

Leahy, Joseph G, & Colwell, Rita R. 1990. Microbial Degradation of Hydrocarbons in the Environment. *Microbiological Reviews*, **54**(3), 305–315.

Mackay, Donald, Shiu, Wan Ying, Maijanen, Aila, & Feenstra, Stan. 1991. Dissolution of non-aqueous phase liquids in groundwater. *Journal of Contaminant Hydrology*, **8**(1), 23–42.

MacQuarrie, K. T.B., & Sudicky, E. A. 1990. Simulation of biodegradable organic contaminants in groundwater: 2. Plume behavior in uniform and random flow fields. *Water Resources Research*, **26**(2), 223–239.

Majora, David W., Mayfielda, Colin I., & Barkerb, James F. 1988. Biotransformation of Benzene by Denitrification in Aquifer Sand. *Ground Water*, **26**(1), 8–14.

Mayer, Alex S., & Hassanizadeh, S. Majid. 2005. *Soil and Groundwater Contamination: Non-aqueous Phase Liquids—Principles and Observations*. Water Resources Monograph, vol. 17. Washington, D. C.: American Geophysical Union.

McCray, John E., Tick, Geoffrey R., Jawitz, James W., Gierke, John S., Brusseau, Mark L., Falta, Ronald W., Knox, Robert C., Sabatini, David A., Annable, Michael D., Harwell, Jeffrey H., & Wood, A. Lynn. 2011. *Remediation of NAPL Source Zones : Lessons Learned from Field Studies at Hill and Dover AFB*. Tech. rept. U.S. Environmental Protection Agency.

Meckenstock, R. U., von Netzer, F., Stumpp, C., Lueders, T., Himmelberg, A. M., Hertkorn, N., Schmitt-Kopplin, P., Harir, M., Hosein, R., Haque, S., & Schulze-Makuch, D. 2014. Water droplets in oil are microhabitats for microbial life. *Science*, **345**(6197), 673–676.

Meckenstock, Rainer U., Safinowski, Michael, & Griebler, Christian. 2004. Anaerobic degradation of polycyclic aromatic hydrocarbons. *FEMS Microbiology Ecology*, **49**(1), 27–36.

Meckenstock, Rainer U., Elsner, Martin, Griebler, Christian, Lueders, Tillmann, Stumpp, Christine, Aamand, Jens, Agathos, Spiros N., Albrechtsen, Hans Jørgen, Bastiaens, Leen, Bjerg, Poul L., Boon, Nico, Dejonghe, Winnie, Huang, Wei E., Schmidt, Susanne I., Smolders, Erik, Sørensen, Sebastian R., Springael, Dirk, & Van Breukelen, Boris M. 2015. Biodegradation: Updating the Concepts of Control for Microbial Cleanup in Contaminated Aquifers. *Environmental Science and Technology*, **49**(12), 7073–7081.

Meckenstock, Rainer U., Boll, Matthias, Mouttaki, Housna, Koelschbach, Janina S., Cunha Tarouco, Paola, Weyrauch, Philip, Dong, Xiyang, & Himmelberg, Anne M. 2016. Anaerobic degradation of benzene and polycyclic aromatic hydrocarbons. *Journal of Molecular Microbiology and Biotechnology*, **26**(1-3), 92–118.

Mellage, Adrian, Eckert, Dominik, Grösbacher, Michael, Inan, Ayse Z., Cirpka, Olaf A., & Griebler, Christian. 2015. Dynamics of Suspended and Attached Aerobic Toluene Degraders in Small-Scale Flow-through Sediment Systems under Growth and Starvation Conditions. *Environmental Science and Technology*, **49**(12), 7161–7169.

Mendoza-Sanchez, Itza, Autenrieth, Robin L., McDonald, Thomas J., & Cunningham, Jeffrey A. 2010. Effect of pore velocity on biodegradation of cis-dichloroethene (DCE) in column experiments. *Biodegradation*, **21**(3), 365–377.

Ministry of Water Land and Air Protection. 2003. *Aliphatic / Aromatic Separation of Extractable Petroleum Hydrocarbons in Solids or Water by Silica gel Fractionation*. Tech. rept. British Columbia Ministry of Water, Land and Air Protecttion, BC2003.

Müller, Juliana B, Ramos, Débora T, Larose, Catherine, Fernandes, Marilda, Lazzarin, Helen S C, Vogel, Timothy M, & Corseuil, Henry X. 2017. Combined iron and sulfate reduction biostimulation as a novel approach to enhance BTEX and PAH source-zone biodegradation in biodiesel blend-contaminated groundwater. *Journal of Hazardous Materials*, **326**, 229–236.

Muñoz, Raul, Villaverde, Santiago, Guieysse, Benoit, & Revah, Sergio. 2007. Two-phase partitioning bioreactors for treatment of volatile organic compounds. *Biotechnology Advances*, **25**(4), 410–422.

National Center for Biotechnology Information. *PubChem Search*.

Palm, Henk, van der Veer, Marcel, Broode, Jan, van der Ham, Carle, & Bakker, Laurent. 2010. *Geohydologische onderzoek vetgasfabriek te Amersdoort*. Tech. rept. Tauw, Deventer.

Peters, Catherine A., & Luthy, Richard G. 1993. Coal-tar dissolution in water-miscible solvents - experimental evaluation. *Environmental Science & Technology*, **27**(13), 2831–2843.

Peters, Catherine A., Mukherji, Suparna, Knightes, Christopher D., & Weber, Walter J. 1997. Phase stability of multicomponent NAPLs containing PAHs. *Environmental Science and Technology*, **31**(9), 2540–2546.

Peters, Catherine A., Knightes, Christopher D., & Brown, Derick G. 1999. Long-term composition dynamics of PAH-containing NAPLs and implications for risk assessment. *Environmental Science and Technology*, **33**(24), 4499–4507.

Peters, Catherine A., Wammer, Kristine H., & Knightes, Christopher D. 2000. Multicomponent NAPL solidification thermodynamics. *Transport in Porous Media*, **38**, 57–77.

Pfeiffer, Patricia, Bielefeldt, Angela R., Illangasekare, Tissa, & Henry, Bruce. 2005. Partitioning of dissolved chlorinated ethenes into vegetable oil. *Water Research*, **39**(18), 4521–4527.

Ponsin, Violaine, Coulomb, Bruno, Guelorget, Yves, Maier, Joachim, & Höhener, Patrick. 2014. In situ biostimulation of petroleum hydrocarbon degradation by nitrate and phosphate injection using a dipole well configuration. *Journal of Contaminant Hydrology*, **171**, 22–31.

Prest, Harry, & Wang, Yongdong. 2009. *Cerno Bioscience MassWorks : Acquiring Calibration Data on Agilent GC / MSDs*. Tech. rept. Agilent Technologies.

Ramsburg, C. Andrew, Thornton, Christine E., & Christ, John A. 2010. Source Zones Containing Chlorinated Ethene Dense. *Environmental Science & Technology*, **44**(23), 9105–9111.

Ramsburg, C. Andrew, Christ, John A., Douglas, Scott R., & Boroumand, Ali. 2011. Analytical modeling of degradation product partitioning kinetics in source zones containing entrapped DNAPL. *Water Resources Research*, **47**(3), 1–14.

Raptis, Panagiotis, Gerritse, Jan, Van Leeuwen, Johan A., & Sutton, Nora. 2015. *A microbial analysis to assess the anaerobic degradation of oil/tar contamination in the subsurface Internship Report*. Tech. rept. October. Deltares.

Reinhard, M., Shang, S., Kitanidis, P. K., Orwin, E., Hopkins, G. D., & Lebron, C. A. 1997. In situ BTEX biotransformation under enhanced nitrate- and sulfate- reducing conditions. *Environmental Science and Technology*, **31**(1), 28–36.

Riis, V, & Babel, W. 1999. Removal of sulfur interfering in the analysis of organochlorines by GC-ECD. *The Analyst, The Royal Society of Chemistry*, **124**(12), 1771–1773.

Rixey, W. G., Garg, Sanjay, & Nie, Yan. 1999. Comparison of the fixed-bed and batch leaching characteristics of aromatic compounds in residually trapped crude oils and oily wastes. *Journal of Hazardous Materials*, **64**(2), 137–156.

Rockne, Karl J, Chee-sanford, Joanne C, Sanford, Robert A, Hedlund, Brian P, Staley, James T, & Strand, Stuart E. 2000. Anaerobic Naphthalene Degradation by Microbial Pure Cultures under Nitrate-Reducing Conditions. *Applied and Environmental Microbiology*, **66**(4), 1595–1601.

Sander, R. 2015. Compilation of Henry's law constants (version 4.0) for water as solvent. *Atmospheric Chemistry and Physics*, **15**(8), 4399–4981.

Song, Xin, & Seagren, Eric A. 2008. In Situ Bioremediation in Heterogeneous Porous Media : Dispersion-limited scenario. *Environmental Science & Technology*, **42**(16), 6131–6140.

van der Waals, Marcelle J., Atashgahi, Siavash, da Rocha, Ulisses Nunes, van der Zaan, Bas M., Smidt, Hauke, & Gerritse, Jan. 2017. Benzene degradation in a denitrifying biofilm reactor: activity and microbial community composition. *Applied Microbiology and Biotechnology*, **101**(12), 5175–5188.

van der Zaan, Bas M., Saia, Flávia Talarico, Stams, Alfons J. M., Plugge, Caroline M., de Vos, Willem M., Smidt, Hauke, Langenhoff, Alette A. M., & Gerritse, Jan. 2012. Anaerobic benzene degradation under denitrifying conditions: Peptococcaceae as dominant benzene degraders and evidence for a syntrophic process. *Environmental Microbiology*, **14**(5), 1171–1181.

van Leeuwen, Johan A. 2017. *Push-Pull test Vetgasfabriek Uitgangspunten geleerd in het project.*

van Leeuwen, Johan A. 2018. *PhD Manuscript - In Progress.* Ph.D. thesis, Utrecht University, Utrecht.

van Leeuwen, Johan A., & Gerritse, Jan. 2016. *Microbial degradation of mobile tar components.* Tech. rept. Deltares, Utrecht.

van Logtestijn, Merijn. 2017. *Natural vs . stimulated anaerobic biodegradation at the tar contaminated site in Amersfoort Internship report.* Tech. rept. April. Deltares.

Volkman, John K., Alexander, Robert, Kagi, Robert I., Rowland, Steven J., & Sheppard, Peter N. 1984. Biodegradation of aromatic hydrocarbons in crude oils from the Barrow Sub-basin of Western Australia. *Organic Geochemistry*, **6**(C), 619–632.

Wagner, Thomas. 2015. *A metabolomics study to asses the anearobic biodegradation of BTEX-and PAH contamination in situ.* Tech. rept. Deltares, Utrecht.

Wang, Yongdong, & Prest, Harry. 2006. Accurate mass measurement on real chromatographic time scale with a single quadrupole mass spectrometer. *Chromatography*, **27**(3), 2–7.

Williams, J. A., Bjorøy, M., Dolcater, D. L., & Winters, J. C. 1986. Biodegradation in South Texas Eocene oils - Effects on aromatics and biomarkers. *Organic Geochemistry*, **10**(1-3), 451–461.

Wilson, Barbara H., Smith, Garmon B., & Rees, John F. 1986. Biotransformations of selected alkylbenzenes and halogenated aliphatic hydrocarbons in methanogenic aquifer material: a microcosm study. *Environmental Science & Technology*, **20**(10), 997–1002.

Xu, Meiying, He, Zhili, Zhang, Qin, Liu, Jin, Guo, Jun, Sun, Guoping, & Zhou, Jizhong. 2015. Responses of Aromatic-Degrading Microbial Communities to Elevated Nitrate in Sediments. *Environmental Science and Technology*, **49**(20), 12422–12431.

Yang, Su-Cai, Song, Yun, Wang, Dong, Wei, Wen-Xia, Yang, Yan, Men, Bin, & Li, Jia-Bin. 2016. Application of nitrate to enhance biodegradation of gasoline components in soil by indigenous microorganisms under anoxic condition. *Environmental Technology*, **37**(9), 1045–1053.

Appendix A

Field Work

A.1 Introduction

A field trial was conducted between April 2016 and January 2017 at Amersfoort to stimulate degradation of mobile tar components with the addition of nitrate as a terminal electron acceptor. Mobile tar components were previously proven to degrade under anaerobic, nitrate reducing conditions in laboratory batch and column experiments (van Leeuwen & Gerritse, 2016). The trial consisted of two transects, each with two injection wells, one extraction well and 3 monitoring wells (Figure A.2). Additional reference wells up and down gradient of the transects were also monitored.

One transect was stimulated with nitrate while the second served as a control, where groundwater was recirculated with no addition of nitrate. Mixing groundwater has been shown to increase microbial activity without further stimulation (Meckenstock *et al.*, 2015). Table A.1 summarizes the pumping and sampling schedule from the first field trial. During the trial, wells were sampled five times for groundwater geochemical parameters, the concentration of mobile tar components and metabolites and the microbial conditions. For detailed results from the first trial see (van Logtestijn, 2017).

Table A.1: *Schedule of activities and sampling rounds for the second recirculation field trial.*

Date	Sampling Code	Activity
April 5 2016	T0	Sampling (Initial Condition)
May 20 2016		Start Recirculation Pumping
June 13 2016	T1	Sampling
June 30 2016		Stop Recirculation Pumping
July 14 2017		Start Nitrate Injection
Aug 24 2016		Stop Nitrate Injection
Aug 31 2016	T2	Sampling
Nov 15 2016	T3	Sampling
Jan 11 2017	T4	Sampling

Briefly, the first field trail found that metabolite concentrations initially increased in both the stimulated and placebo transect, indicating that recirculation of groundwater alone influenced degradation rates. This has been observed by MacQuarrie & Sudicky (1990) and Song & Seagren (2008). However, only in the stimulation transect did metabolite concentrations decrease after the initial increase, indicating nitrate was required for continued degradation.

DNA results agreed with the metabolite data. Gene assays increased in both the placebo and stimulated transects. The highest gene copies were found in M72 in the stimulated transect, coinciding with the peak of the nitrate plume. Wells M71 and IN71/72 located 5 m and 10 m upstream, however, were lower. This suggested a temporary increase in microbial activity, which decreased after the nitrate plume had passed. The overall conclusions from the first field trial were that stimulation by nitrate injection increased microbial degradation but only temporarily. It was proposed that the bacteria exposure to nitrate was too short to establish a substantial degrader population.

A second field trial was implemented with multiple injections to provide a semi-continuous supply of nitrate to expose native bacteria to nitrate long enough to substantially increase hydrocarbon degradation rates. Furthermore, bacteria specifically cultured to degrade benzene in nitrate reducing conditions were injected with nitrate in the former placebo transect (*augmented transect*). Similar to the first trial, degradation was monitored during the current trial by measuring groundwater geochemistry, mobile tar component concentrations and microbial conditions. Preliminary results from the first three injections are presented here.

A.2 Methods

A.2.1 Field Trail Set Up

For the current recirculation field trial, the former placebo transect (wells IN61-M63) was augmented with a bacterial culture grown in the lab (van der Waals *et al.*, 2017). The bacteria were grown anaerobically in nitrate reducing conditions and benzene was the sole electron donor. For a full description of the medium and batch operation see van der Waals *et al.* (2017) and van der Zaan *et al.* (2012). The stimulation transect (wells IN71-M73) was stimulated again in the current trial. Having been exposed to nitrate in the first trial, native bacteria in the soil of the stimulated transect may have adapted to degrade mobile tar components under nitrate reducing conditions. Therefore, to determine the effects of bioaugmentation it was necessary to augment the placebo transect, where nitrate was not injected in the first field trial.

The same pumping set-up as the first trial was used (Figure A.1). Groundwater from extraction wells O6 and O7 was pumped anaerobically to mixing tanks where 125 kg of sodium nitrate ($NaNO_3$) was added to a total groundwater volume of 500 L. Tracers were added to monitor the transport and dilution of the injected nitrate in each transect; 100 g lithium chloride to the augmented tank and 250 g of sodium bromide (NaBr) to the stimulated tank. The tanks were mixed using submerged pond pumps until the $NaNO_3$ was dissolved. Once the nitrate was dissolved, the mixture was injected at a rate of 3 L/hr to the two injection wells of each transect. In the augmented transect bacteria and medium (46 L) were injected after a minimum 1 day delay. The delay was to allow a nitrate plume to form around the injection well so that the bacteria were injected into the plume to increase access to the electron acceptor (Figure A.1). Bacteria and medium were pumped directly to the outflow pipe of the nitrate tanks to mix prior to injection. Nitrate pumping continued for atleast one day after the bacteria vessel was empty.

A.2.2 Sample Collection

Fifteen groundwater wells were sampled six times between May 2017 and January 2018 at Amersfoort (Figure A.2). The electrical conductivity (EC), pH, redox, O_2 and temperature were measured in the field using a flow through cell and TWT Multi 340i and pH/cond 3320 meters. The groundwater level was measured as meter below ground surface (mbgs) using a dip meter.

Samples for the analysis of volatile aromatic hydrocarbons were collected during each sampling

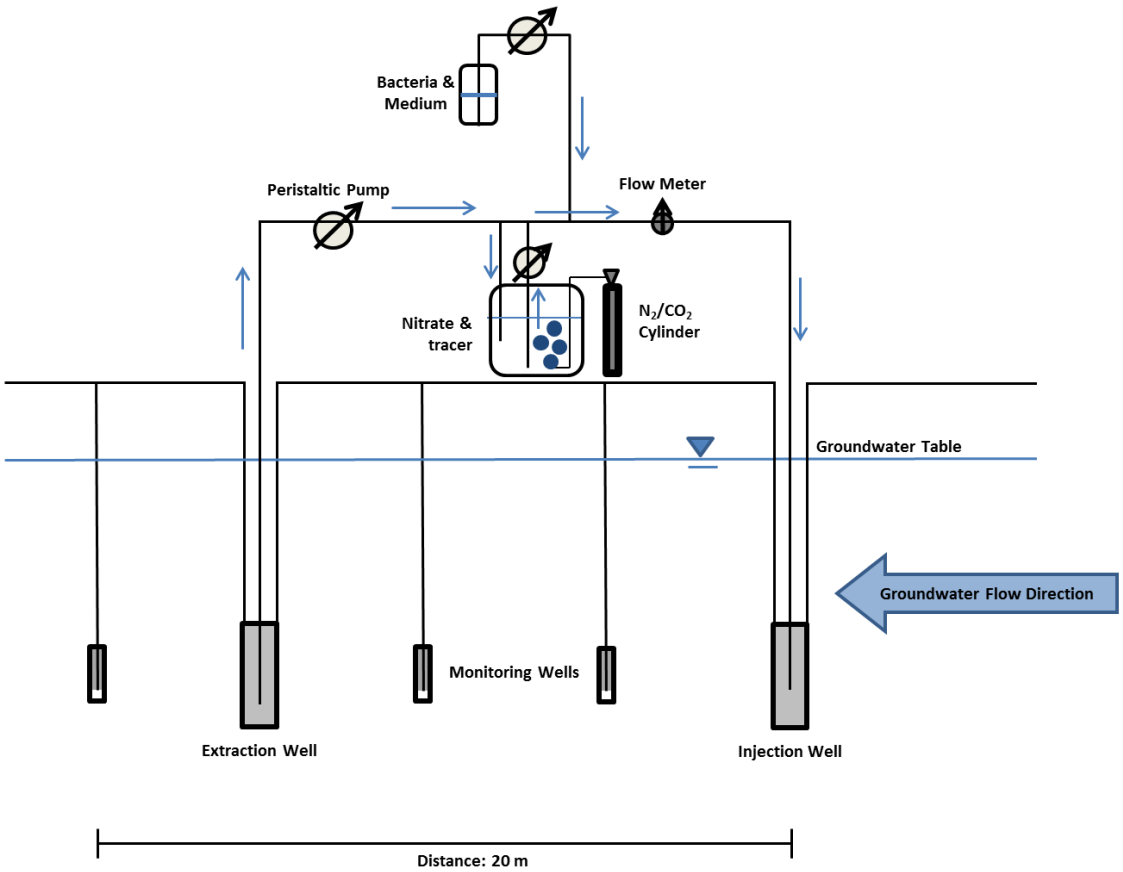

Figure A.1: *Biostimulation & bioaugmentation pump set up. Groundwater from extraction wells was pumped to mixing tanks where nitrate and tracer solutions were added. The tanks were kept anaerboic using N_2/CO_2 gas cylinders. The groundwater with nitrate and tracer was then pumped back into the injection wells. In the case of the augmented transect, specialized bacteria and medium were also added to the injection line and pumped into the groundwater (van Leeuwen, 2017)*

event and additional samples were collected during three sampling events (T5, T8, T10) for DNA, cation, anion, dissolved organic carbon (DOC) and GC-MS analysis. Samples for stable isotope and LC-qTOF were also taken and stored for later use.

Groundwater samples for GC-FID, GC-MS and anion analysis were collected in three 20 ml glass vials. Samples were sterilized in the field with 1 ml of 0.5 g/L $HgCl_2$ prior to sample collection. Groundwater was extracted anaerobically and sample vials were filled completely and crimp sealed with silicon/PTFE aluminum caps. Samples were stored at 4°C until analysis. In the lab, samples for GC-FID and GC-MS were reduced to 12 ml using disposable plastic syringes. Samples were allowed to equilibrate to room temperature for several hours prior to headspace analysis on GC-FID or GC-MS. Volatile aromatic hydrocarbons were measured using an Agilent 6850 GC-FID and GC-MS analysis was performed by TNO (Utrecht, Netherlands) using the methods described in the Methods chapter, Subsection 3.3.7.

Groundwater was collected anaerobically in 1L green, glass bottles and filled completely in the field. Bottles were stored in portable coolboxes immediately after collection and during transportation. Samples were vacuum filtered (Millipore, Merck) withing 24 hours of collection using Microfil filtration funnels (250 ml) and S-pak Membrane Filters (0.45 μm x 47 mm). Sample volumes varied between 250 and 300 ml per filter (three filters per sample), with the exception of one highly turbid sample (Well IN72 T8) where only 100 ml was filtered for each channel. Filters were then

Table A.2: *Schedule of activities and sampling rounds for the second recirculation field trial. Bold activities indicate injection of nitrate and bacteria. Partial sampling: field parameters and GC-FID sample collection, full sampling: partial sampling activities plus DNA, anion, cation, DOC, LC-qTOF, GC-MS and stable isotope sample collection.*

Date	Sampling Code	Activity
July 18 2017	T5	Full Sampling (Initial Condition)
Sept 19-Oct 4 2017		**1st Nitrate Injection (500 L)**
Sept 21-26 2017		**1st Bacteria Injection (46 L)**
Oct 10 2017	T6	Partial Sampling
Oct 31 2017	T7	Partial Sampling
Nov 6-10 2017		**2nd Nitrate Injection (500 L)**
Nov 7-9 2017		**2nd Bacteria Injection (46 L)**
Nov 21 2017	T8	Full Sampling
Jan 4 2018	T9	Partial Sampling
Jan 15-22 2018		**3rd Nitrate Injection (500 L)**
Jan 16-19 2018		**3rd Bacteria Injection (46 L)**
Jan 30 2018	T10	Full Sampling

cut in half using flamed scissors and stored in sterilized plastic sample vials at -81°C. qPCR analysis was performed by Deltares (Utrecht, Netherlands) for total bacteria, *Peptococcaceae*, benzene carboxylase and naphthylmethylsuccinate synthase (nmsA) concentrations (gene copies per ml).

Anion samples were collected in 2 ml glass vials, sterilized with 100 μL of 0.5 g/L $HgCl_2$. Samples were filtered over 0.45 μm nylon syringe filters and filled completely in the field. Cation samples were collected in 60 ml plastic screw cap bottles, acidified with 600 μL of nitric acid. Anion and fatty acid contents were measured on a Dionex and cations by ICPMS by Deltares (Utrecht, Netherlands).

A.3 Results

A.3.1 Groundwater Geochemistry

Anion and cation samples were analyzed to determine the initial conditions (T5), conditions after the second nitrate injection (T8) and conditions after the third nitrate injection (T10). The concentration of anions and cations in the well can be found in Figures A.19 through A.24. Nitrate, nitrite, lithium and bromide initial concentrations (T5) were low or below detection for all wells. Chloride concentrations varied between 3-35 mg/L in wells with no apparent pattern (Figure A.21). Initial sodium concentrations were higher in the stimulated transect wells M71-M73, 50-58 mg/L, while the reference wells and augmented transect were lower, around 10 mg/L (Figure A.19).

The nitrate concentrations closely matched the EC concentrations observed for T8 and T10 (Figure A.23). The nitrite concentrations were higher than the background concentration in the same wells for T8 (IN61/71-M61/72) and T10 (IN61/71-M62/72, Figure A.24). Nitrite concentrations were higher in the stimulated transect than the augmented transect. Conservative tracers, LiBr and NaCl were injected in the stimulated and augmented transects respectively. Bromide was elevated in the same wells as the EC for the stimulated transect (Figure A.20). No clear trend in chloride concentrations was observed due to the spatially and temporarily variable background concentrations (Figure A.21). Lithium concentrations were low at T8 and T10, could only be detected in the injection wells and were not indicative of the extent or the location of the nitrate

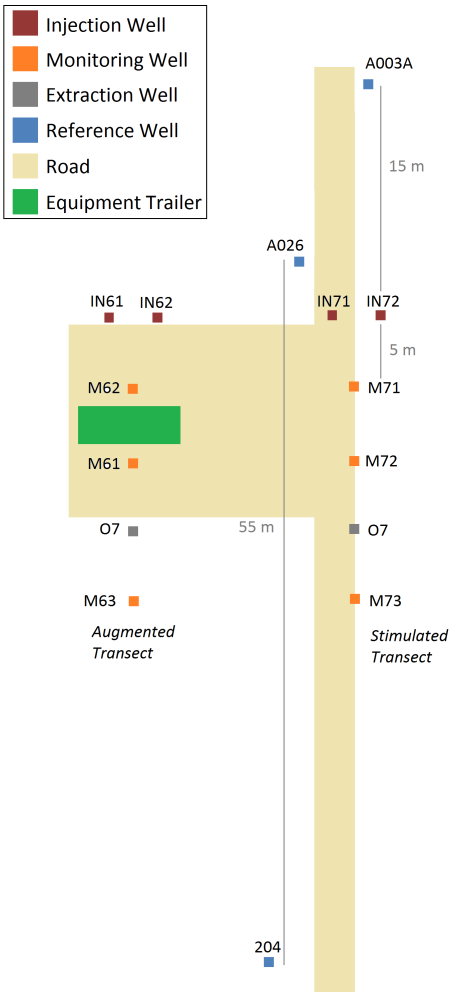

Figure A.2: *Conceptual model of site layout, distances are approximately to scale.*

plume (Figure A.22).

Monitoring the EC showed the progress of the nitrate plume clearly (Figures A.5 and A.6). The EC was low in both the augmented and stimulated transects prior to addition of the nitrate (T5). The EC increased in both injection wells in the stimulated and augmented transects after the first injection period (T6). The nitrate plume broke through to the first monitoring wells M61 and M71 at T7, located 5 m from the injection wells. The second addition of nitrate substantially increased the EC measured in the injection wells in both transects. In the augmented transect, the EC also increased in the first monitoring well M61, while in the stimulated transect the EC in M71 remained constant. A small increased in the EC was observed in M72 in the stimulated transect, indicating breakthrough of the nitrate plume in the stimulated transect 10 m downstream from the injection wells. At T9, the plumes in both transects had peaks in the first monitoring well (M61, M71) and the front of the plume was detected in the second monitoring well (M62, M72). The EC decreased in the injection wells, dropping to 1000 μS/cm or less in the augmented transect and to 3000 μS/cm in IN71 and near zero in IN72 at T9. After the third addition of nitrate (T10), the EC increased again in the injection and first monitoring wells of both transects. The highest EC was measured in the second monitoring well (M62, M72) of both transects, indicating the transport distance of the second nitrate injections and the front of the plume (first nitrate injection) had broken through to the extraction wells (O6 and O7) in both transects.

Transport of the nitrate plume, as observed by the progress of the EC measured in each transect,

indicated a higher than expected groundwater velocity. Based on observations from the first field trial, the groundwater velocity was estimated at 24 m/year, as the nitrate plume traveled approximately 5 m in 77 days between sampling events T2 and T3 (Figure A.25). Observations from the current trial suggest a higher velocity of 42 m/yr. The EC peak broke through to the extraction wells in each transect, located 15 m from the injection wells, in 133 days between the start of the first injection (Sept. 19, 2017) and the last sampling event (T10, Jan. 30, 2018).

The redox measurements followed the general trend of the EC measurements in each transect. Initially (T5) all wells measured had negative redox measurements (reducing conditions) with the exception of M63 and O7, which had the only positive redox measurements (Figures A.7 and A.8). In the stimulation transect, the redox potential became positive coincident with the EC increasing in each well as the nitrate plume traveled through the transect. By T10 the redox potential was positive in all but the last monitoring well (M63). In the augmented transect the redox potential less closely followed the EC measurements, though positive measurements were consistently taken in the injection and first monitoring well for all sampling events after T5.

The redox conditions of upstream wells A003A, A026A and downstream well 204 fluctuated for each sampling event. In particular, measurements for sampling T9 and T10 were positive in some wells. This was coincident with changes observed in the groundwater level measured on site. The groundwater levels were on average 0.5 and 0.7 m higher on T9 and T10 receptively. The groundwater temperature in all wells was on average 13.1°C, decreasing to 12.0°C (T9) and 11.4°C (T10), coincident with the change in groundwater level observed.

Little change in the pH of upstream well A003A was observed for all measurements, where the pH was on average 5.8. The pH increased moving downstream, increasing to an average of 6.1 in A026A (15 m downstream) and 6.2 in well 204 (70 m downstream). The pH in the transects varied between 5.5 and 7.0, with the average for the stimulated transect being slightly higher, pH between 6.1-6.7 (Figure A.10), than the augmented transect, pH between 5.8-6.2 (Figure A.9).

The oxygen concentration was consistently low for the majority of wells, between 0.05-0.08 mg/L on average. In the augmented transect a suspected leak in the injection lines caused near saturation oxygen concentration during the T10 sampling (IN61 8.33 mg/L and IN62 7.2 mg/L, not shown in the scale of Figure A.11). O_2 concentrations were also slightly elevated for IN61 at T7 (0.23 mg/L) and in IN62 at T9 (0.2 mg/L) in the augmented transect. In the stimulation transect O_2 levels increased in M71 for T9 and T10 (0.64 mg/L and 0.34 mg/L) and in O7 for T10 (0.14 mg/L, Figure A.12).

A.3.2 Concentration of Mobile Tar Components

The concentration for 12 mobile tar components and methane as summarized in Figures A.17 and A.18 for the augmented and stimulated transects respectively. Concentrations of all mobile tar components decreased sharply from the upstream wells A003A and A026A to the injection wells IN61/62 and IN71/72 for most components. However, naphthalene, 1- and 2-methylnaphthalene and 1,2,3- and 1,2,4-trimethylbenzene concentrations changed little from upstream wells A003A to downstream well 204. Concentrations of benzene, toluene and styrene decreased the most from upstream well A003A to well 204, consistent with measurements during first field trial (Figures A.17, A.18, A.26 and A.27).

Concentrations changed little for the majority of mobile tar components measured in both transects from T5 to T10 with the exception of toluene and benzene in the stimulation transect. The concentration of benzene and toluene were plotted with the EC in the same graph to visualize the location and transport of the nitrate plume (Figures A.3 and A.28). The concentration of each toluene and benzene were compared between the augmented and stimulated transects.

In the stimulated transect, the initial concentration (T5) of toluene varied along the transect

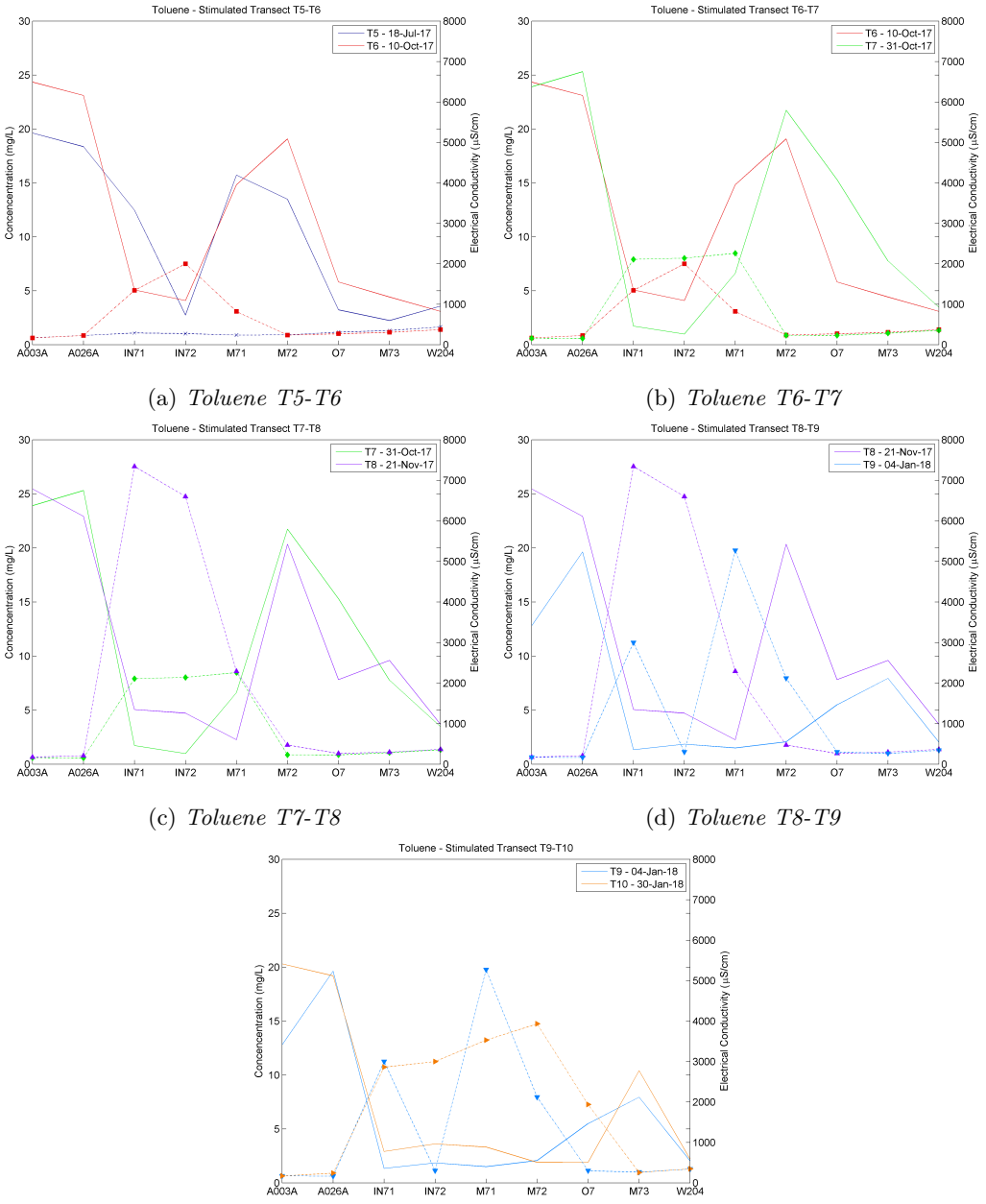

(a) *Toluene T5-T6*

(b) *Toluene T6-T7*

(c) *Toluene T7-T8*

(d) *Toluene T8-T9*

(e) *Toluene T9-T10*

Figure A.3: *Aqueous toluene concentration (solid line) in the stimulation transect plotted against the electrical conductivity (dashed line) at the same sampling time for T5-T10*

with the highest concentration in M71 and the lowest in M73 (Figure A.3a). The first addition of nitrate (T6) resulted in a decrease in IN71 and a slight increase in IN72, such that they both had concentration of approximately 4-5 mg/L (Figure A.3a). Groundwater flowed naturally (no pumping) between T6 and T7 and concentrations of toluene decreased in well IN71, IN72 and M73, the three wells where the EC was elevated (nitrate plume location, Figure A.3b). Nitrate was injected a second time between T7 and T8 and the concentration of toluene increased in IN71 and IN72 but decreased further in M71 (Figure A.3c). Groundwater flowed under natural flow conditions again between T8 and T9 and again the concentration of toluene decreased in IN71, IN72 and M71 and now M72. The EC (nitrate) plume extended from IN71 through to well M72 at T9 (Figure A.3d). The third nitrate injection occurred between T9 and T10. The concentration

of toluene increased in the injection wells again but remained low in M72 and decreased in O7, located at the front of the existing nitrate (EC) plume. The high peak of toluene, located at T5 in well M71 was pushed out ahead of the EC plume in each sampling event, such that at T10 the concentration of toluene was low in all wells but M73 (Figure A.3e).

The benzene concentration in the stimulated plume followed a similar pattern as the toluene but to a lesser degree. In contrast to the toluene concentration, between T6 and T7 no change in benzene was measured in injection well IN71 and IN72 after the first nitrate injection (Figure A.28). However, after the second nitrate injection, between T8-T9 the concentration of benzene decreased in IN71, IN72, M71, M72 and remained low in O7. Benzene concentrations increased only slightly between T9-T10 after the third nitrate injection, similar to the toluene concentrations. Similar to the the toluene concentration, a peak of higher concentration benzene appeared to be pushed out ahead of the nitrate plume, leaving lower concentrations behind.

Comparing the behavior of benzene and toluene in the augmented transect with the stimulated transect, a similar 'push' of higher concentration benzene and toluene ahead of the nitrate plume was observed between T5 and T10 (Figures A.29 and A.30). However, in contrast with the stimulated transect, no decrease in toluene or benzene concentrations were observed during the natural flow period between injections (T6-T7 and T8-T9).

A.3.3 Microbial Conditions

The total bacteria, given as gene copies per ml of sample, varied little between sampling events (T5, T8, T10, Figures A.4a and A.4b). No clear difference was observed between the augmented or stimulated transect. In general the T10 samples had lower than the T5 or T8 sampling events.

In the stimulation transect *Peptococcaceae* were detected in all wells but IN71 (Figure A.4d). In the augmentation transect *Peptococcaceae* were only present in the injection wells IN61, IN62 and extraction well O6 (Figure A.4d). At T8, after the second nitrate injection, *Peptococcaceae* were present in all sampling wells but M63 in the augmentation transect. At T10, after the third nitrate injection *Peptococcaceae* were again present in all wells but wells O6 and M63. The presence of *Peptococcaceae* appears to correlate with the locations of the nitrate plumes, if lagging a little behind. *Peptococcaceae* increased at T10 in M71, while the nitrate plume peaked in M72. Reference wells varied, with *Peptococcaceae* present at T5 in A026 only, at T8 in A003 only and at T10 in A0026. No gene copies were detected at any time in downstream well 204.

The benzene carboxylase (abcA) gene was detected initially only in the stimulation transect, in all wells but IN71 (Figure A.4f). No gene copies were detected in the augmentation transect at T5. After the second nitrate injection (T8), abcA was measured in all wells in the stimulation transect but only the injection wells of the augmented transect (Figure A.4f). After the third nitrate injection (T10), the gene was detected in all but one well (M72) in the stimulation transect. In the augmentation transect only IN61 had the gene present. Gene copy concentrations were lower at T10 than at T8 in all wells where the gene was detected.

abcA was initially absent in all reference wells (A003, A026 and 204, T5) but detected in A003A at T8 and A026 at T10 similar to the *Peptococcaceae* assay. Naphthylmethylsuccinate synthase (nmsA) was detected in the stimulation transect (except M71) and downstream well 204 initially at T5 (Figure A.4g). At T8, after the second nitrate injection, nmsA was present in all stimulation wells, but absent in the augmentation and reference wells. Data for T10 was not yet available. The nmsA assay appeared to correlate with the nitrate plume location, with the highest gene copies in the injection wells IN71 and IN72 (Figure A.4h).

A.4 Discussion

Preliminary results from the first three injections of the field trail suggest that toluene degradation was stimulated by the addition of nitrate. When pumping stopped after the first and second nitrate injections, the concentration of toluene decreased in the wells where the nitrate plume was located (T7, T9). Results after pumping stopped for the third injection were not yet available at this time.

Possible benzene degradation was also observed after the second nitrate injection, suggesting benzene may have had a longer lag time for degradation than toluene. The degradation of toluene before benzene is supported by other studies (Cunningham *et al.*, 2001; Dou *et al.*, 2008; Hu *et al.*, 2007; da Silva & Alvarez, 2004; Yang *et al.*, 2016).

No degradation of mobile tar components was evident in the bioaugmentation transect at any sampling time. However, as Albrechtsen & Winding (1992) and Meckenstock *et al.* (2015) have presented, in anaerobic environments it may take several months to years to establish a critical bacterial population size for detectable degradation. Therefore a lack of quick response in the form hydrocarbon degradation should not be immediately interpreted as a failure to establish an augmented bacterial population. Therefore continued monitoring is necessary in both the stimulated and augmented transects.

If the addition of nitrate was responsible for the degradation of toluene in the stimulation transect, similar results would be expected in the augmentation transect, which received nitrate in addition to bacteria. However, the stimulation transect had previously been exposed to nitrate in the first recirculation field test, where a pulse of high concentration nitrate was injected.

Studies have shown that 'preconditioning' aquifer systems can result in degrader biomass growth which persist for months or years (Herzyk *et al.*, 2014; Mellage *et al.*, 2015; Meckenstock *et al.*, 2015). The stimulation transect received a pulse of nitrate in the first field trial, which likely resulted in the proliferation of nitrate reducing bacteria capable of degrading toluene. The supply of nitrate was finite however, and once the pulse of nitrate was gone degradation halted. When the supply of nitrate was reestablished in the current trial, the biomass already present in the soil degraded the toluene with no lag time. Therefore it is possible that with a continued supply of nitrate to the augmentation transect, degrader biomass could also be established through stimulation alone.

Increased precipitation in December 2017 and January 2018 resulted in a higher groundwater table for measurements on T9 and T10 in comparison to previous measurements. Dilution would have decreased the concentration of all measured tar components, therefore the decrease in only toluene observed at T9 is not due to dilution.

Results from metabolite and qPCR data from the first recirculation test indicate that stimulation did result in a temporary increase in degradation rates (van Logtestijn, 2017). An initial increase of metabolite concentrations was observed in both transects, likely as a result of the increased groundwater circulation from pumping. However, in the stimulated transect the concentration of total metabolites decreased after nitrate addition, as a result of continued degradation of metabolites due to the abundance of nitrate as an electron acceptor. In the placebo wells no decrease in metabolite concentrations was observed after the initial increase, suggesting degradation halted or slowed substantially.

No clear trend was observed in the total bacteria, which was similar to the results of the first recirculation trial (van Logtestijn, 2017). *Peptococcaceae* were initially absent in the placebo (augmentation) transect but present in the stimulation transect in the first trial, indicating the heterogeneous nature of field site microbiology. *Peptococcaceae* gene counts increased in injection well IN62 and extraction well O6 at T4 (van Logtestijn, 2017). This increase was determined to be a result of the increased circulation of groundwater, as no nitrate was added to the placebo transect. In contrast, the stimulated transect *Peptococcaceae* gene counts increased in all wells at

T4 as a result of the nitrate addition.

The data from the current trial suggest nitrate stimulates *Peptococcaceae* growth, as gene counts increased in augmentation wells IN61 through O6 for T8 and IN61 through M72 for T10. Benzene carboxylase, on the other hand, does not appear to be influenced solely by the addition of nitrate. In the first trial, benzene carboxylase was initially absent in all but extraction well O6 and reference well A003A. Th addition of nitrate to the stimulation well increased gene countes in wells IN71, IN72 M71 M72 and extraction well O7. No change in the placebo well was observed. If benzene carboxylase was correlated to the addition of nitrate, gene counts in both the augmentation and stimulation transects would be expected in the current trial as nitrate was added to both transects. However, only the stimulation transect, where the gene was initially detected increased in concentration. The gene for benzene carboxylase was detected in the injection wells in the augmented transect at T8, but gene counts decreased in IN61 at T10 and were absent in IN62.

The groundwater velocity was found to be twice as high as calculated from the first field trial. Previous site characterization found highly variable hydraulic conductivity on site (Palm *et al.*, 2010). The hydraulic conductivity ranged from a low of 1.73 m/day to 5.14 m/day, with an average of 2.82 m/day (Palm *et al.*, 2010). Breakthrough of the EC from well M71 to M72 (5 m) between T2 and T3 (77 days) gave a groundwater velocity of 24 m/year. Given a hydraulic gradient on site of approximately 0.004 m/m and porosity of 0.32, the calculated velocity from the EC break through corresponded with the highest measured hydraulic conductivity on site.

However, breakthrough of EC from the current trial suggests groundwater velocity almost twice as high (41 m/year) as the plume broke through to the extraction well (15 m) at T10 (133 days since start of injection). This suggests either an error in the field parameters (hydraulic gradient, conductivity or porosity), increased overall groundwater velocity due to pumping or the development of preferential flow paths due to pumping.

Increased flow velocities can have positive or negative effects on contaminated groundwater systems (Meckenstock *et al.*, 2015). In column experiments, low and medium velocities resulted in only incomplete dechlorination of cis-DCE while high velocity columns resulted in complete dechlorination (Mendoza-Sanchez *et al.*, 2010). The authors suggested that high velocities spread bacteria throughout the column and resulted in higher microbial diversity within columns. Furthermore, increased velocities can result in higher longitudinal and transverse dispersion, increasing mixing between contaminants and electron acceptors, resulting in higher degradation rates (Song & Seagren, 2008). Modeling suggested that increased advection increased the surface area of the plume-fringe by spreading the contaminated plume into less electron-acceptor depleted zones (MacQuarrie & Sudicky, 1990; Song & Seagren, 2008). Increased groundwater velocity could explain the initial increase in metabolites as reported in the placebo transect in the first field trial, without the addition of nitrate.

However, increased advection can also result in preferential flow paths where low conductivity zones are bypassed and degradation is restricted (Meckenstock *et al.*, 2015). Furthermore, increased advection can disturb the delicate balance at the 'plume-fringe' between ideal geochemical conditions for the microbes and nutrient and contaminant availability. High spatial resolution sampling is required to identify flow paths and the distribution of contaminants and electron acceptors at the fringe (Jobelius *et al.*, 2011; Meckenstock *et al.*, 2015).

A.5 Conclusions

A second recirculation field trail was performed at Amersfoort, a site with significant hydrocarbon contamination. To compare the effects of stimulation versus combined stimulation/augmentation, two parallel transects were treated on site. One transect was stimulated with nitrate alone while a

second transect was treated with nitrate and an anaerobic bacterial culture. The bacterial culture was grown anaerobically in the lab over a period of 14 years with benzene as the sole electron donor under nitrate reducing conditions (van der Waals *et al.*, 2017). Preliminary results from the first three injection periods on site were presented. Possible toluene degradation was observed in the stimulation transect, while no degradation was observed in the augmentation transect. The stimulated transect may have been preconditioned with a previous injection of nitrate, establishing a bacterial culture in the subsurface ready to degrade toluene with little or no lag time once nitrate was reintroduced. The lack of degradation observed in the augmented transect could be due to a delay in establishing the degrader biomass or simply the failure of the injected bacteria to thrive in the environment on site. Continue monitoring on site is necessary to confirm toluene and possible benzene degradation in the stimulated transect and to verify if there is a lag period for the injected bacteria to establish a viable degrader population in the augmented transect.

A.6 Future Work

Considerations for the field trail going forward are summarized here. Conservative tracers were injected in each transect to monitor the progress of the injected plume. Bromide in the stimulated transect performed well and was measured in wells where the EC was high, indicating the transport of the plume. Lithium however was only measured in the injection wells. Higher concentrations or an alternative tracer is suggested in order to better track the progress of the plume. Background chloride concentrations in the range of 5-35 mg/L masked chloride transport in the augmented transect.

Alternating tracers with each injection is also suggested. Previous modeling of conditions on site found no cross-over between the injected plumes. Therefore the same tracers could be used in both transects, and by alternating the tracer in each injection the transport of each subsequent injection could be tracked. Tracking each injected plume would simplify the determination of whether dilution or mineralization was taking place in each well. Currently, only the bulk transport of the injections can be monitored and it is not possible to distinguish the interface between injections and therefore calculating the dilution or mineralization rate is difficult as it varies along the transect.

A.7 Appendix

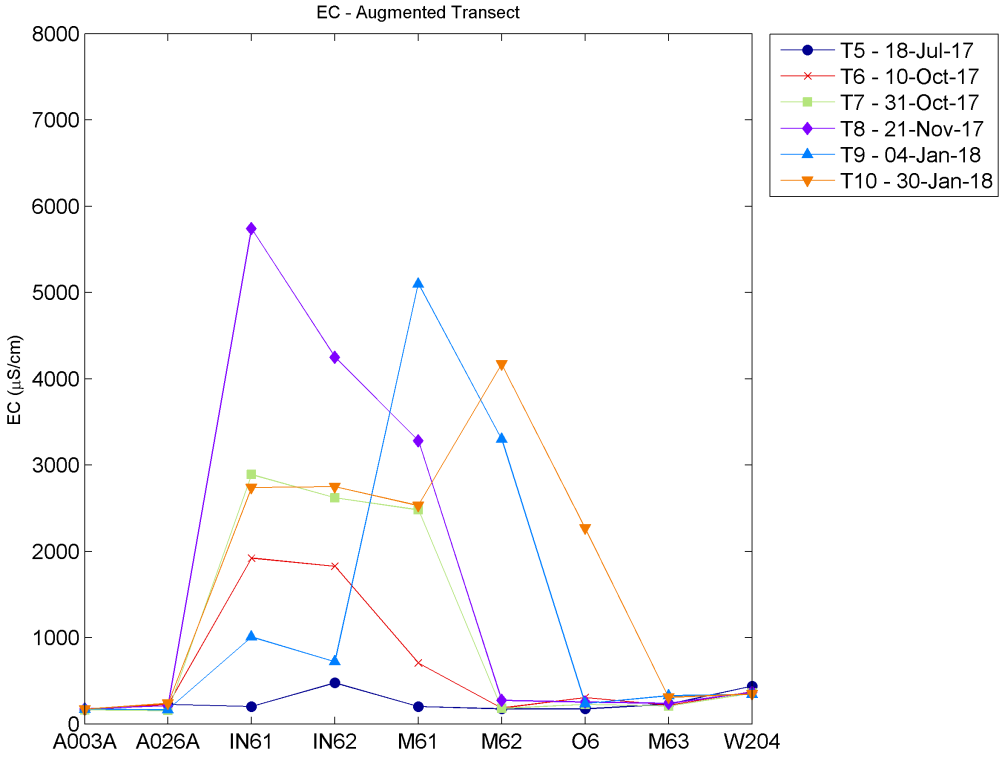

Figure A.5: *Electrical conductivity measured in the field for the augmented transect*

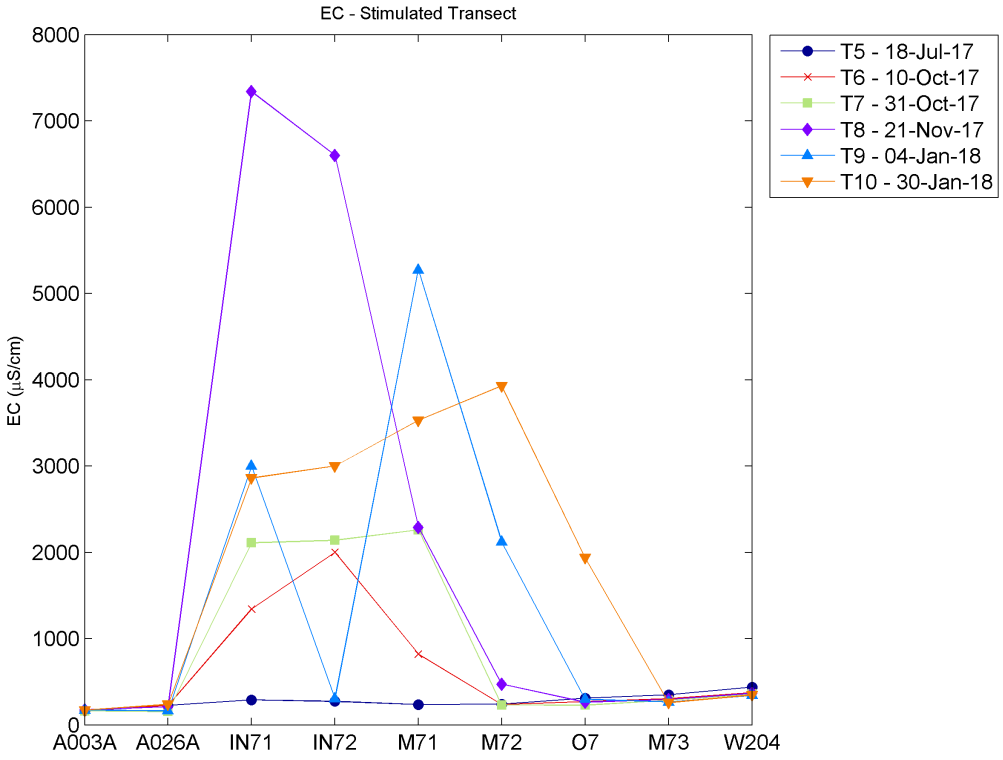

Figure A.6: *Electrical conductivity measured in the field for the stimulated transect*

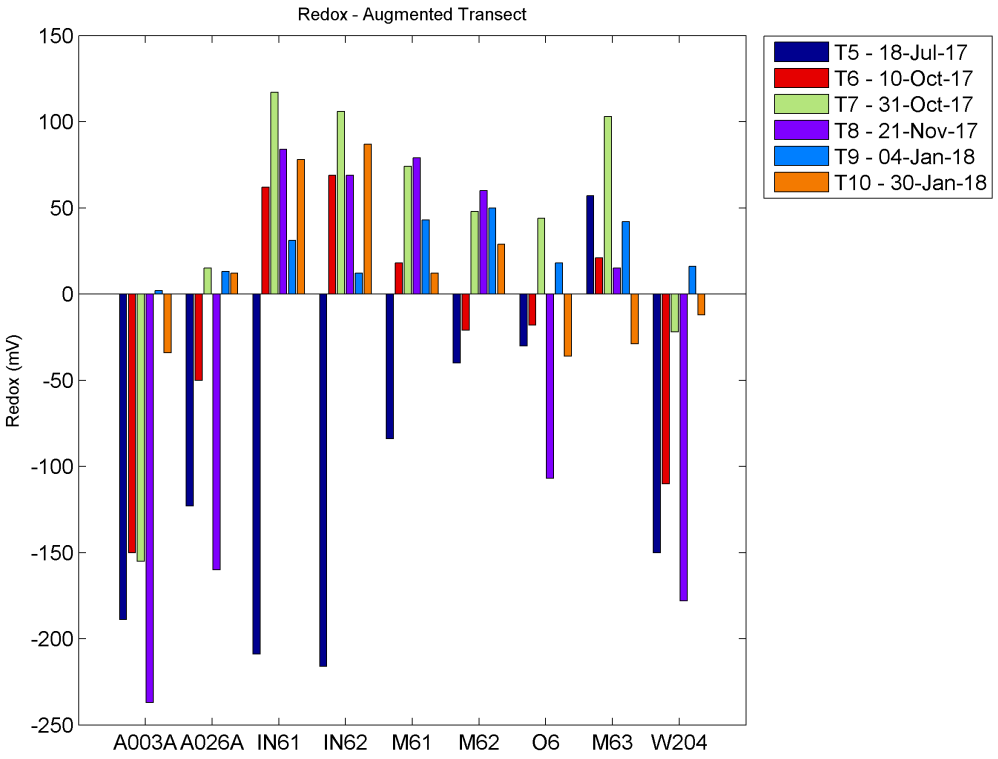

Figure A.7: *Redox potential measured in the field for the augmented transect*

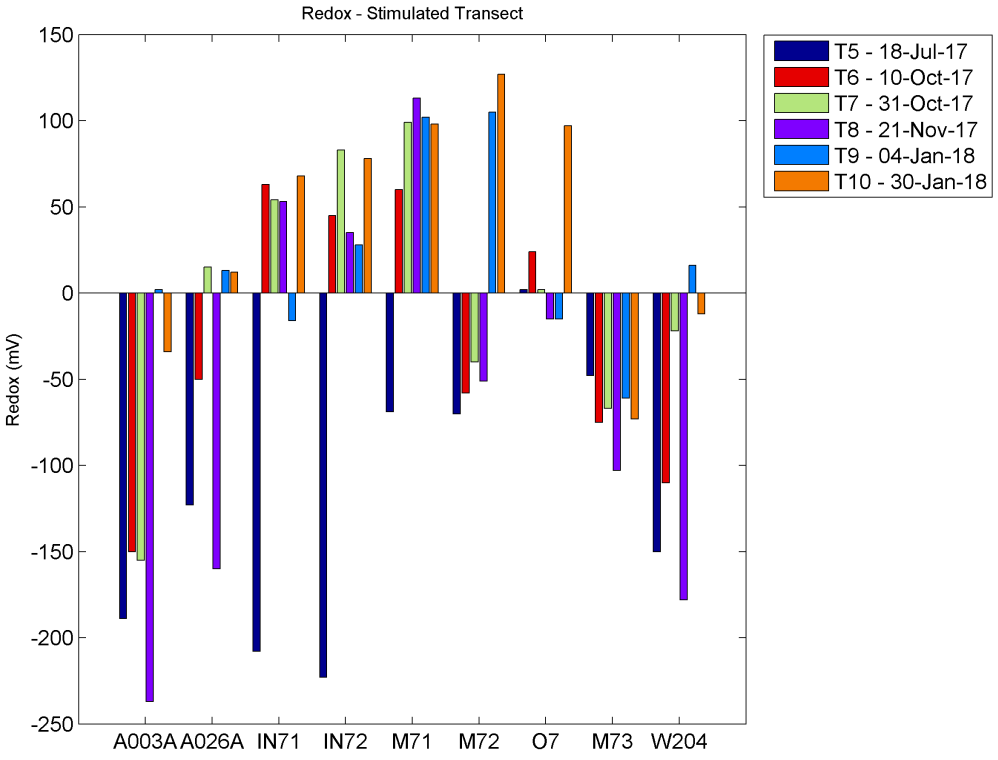

Figure A.8: *Redox potential measured in the field for the stimulated transect*

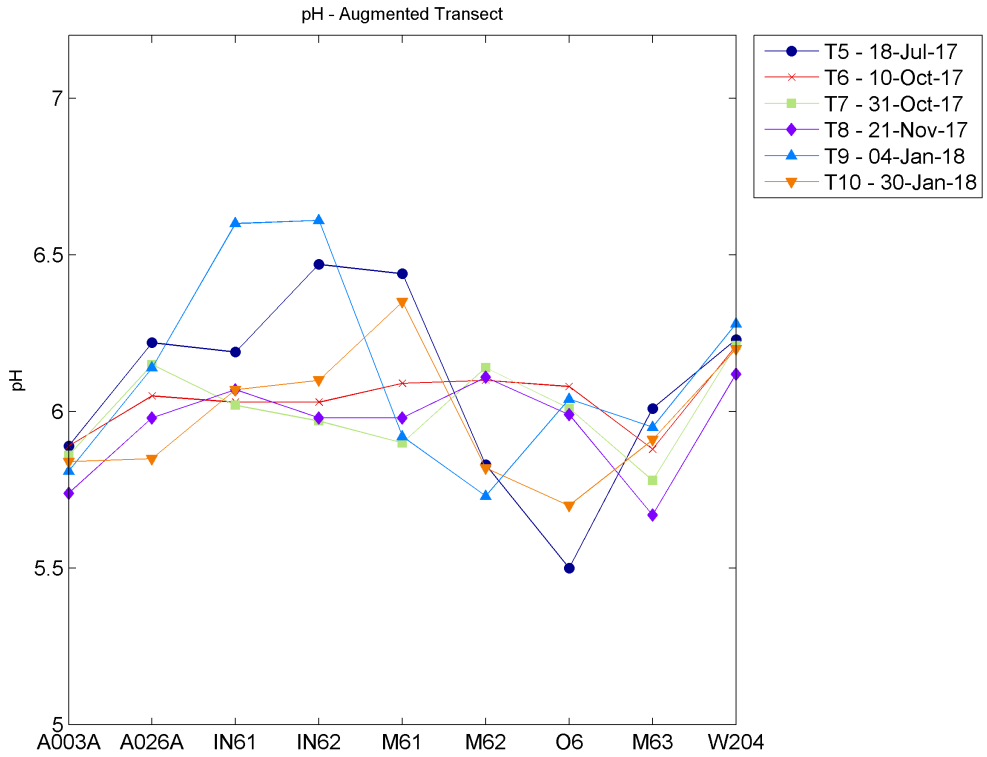

Figure A.9: *pH measured in the field for the augmented transect*

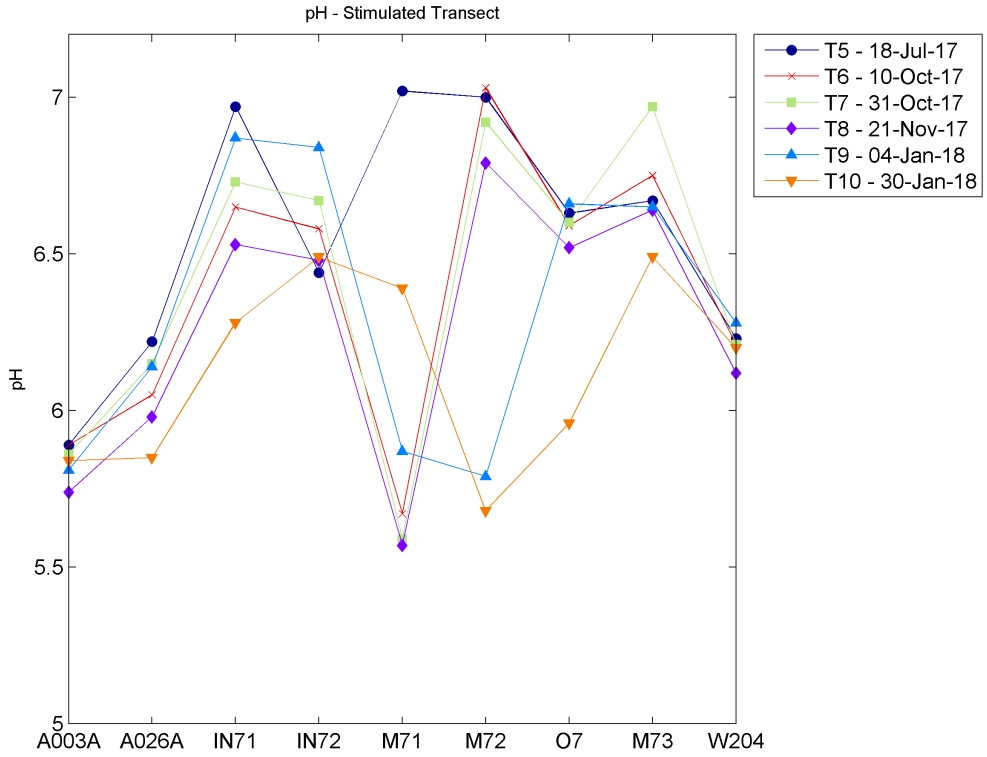

Figure A.10: *pH measured in the field for the stimulated transect*

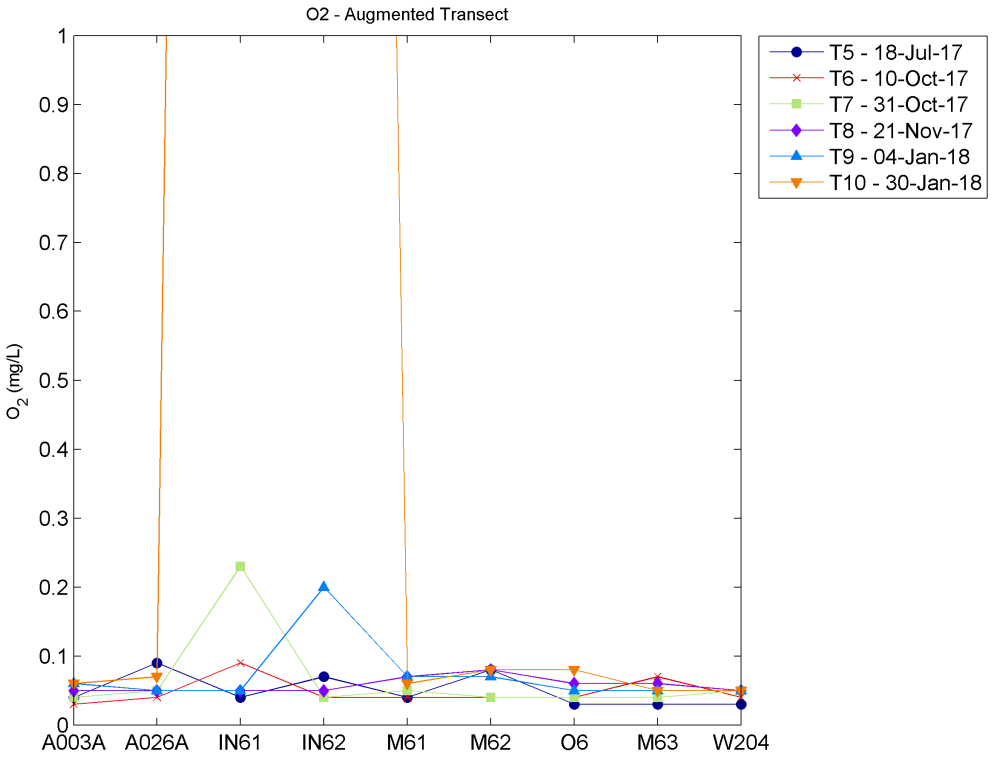

Figure A.11: *Oxygen concentration measured in the field for the augmented transect. Not shown: Oxygen concentrations peaked in well IN61 and IN62 at 8.33 and 7.2 mg/L due to a leak in the pumping set-up.*

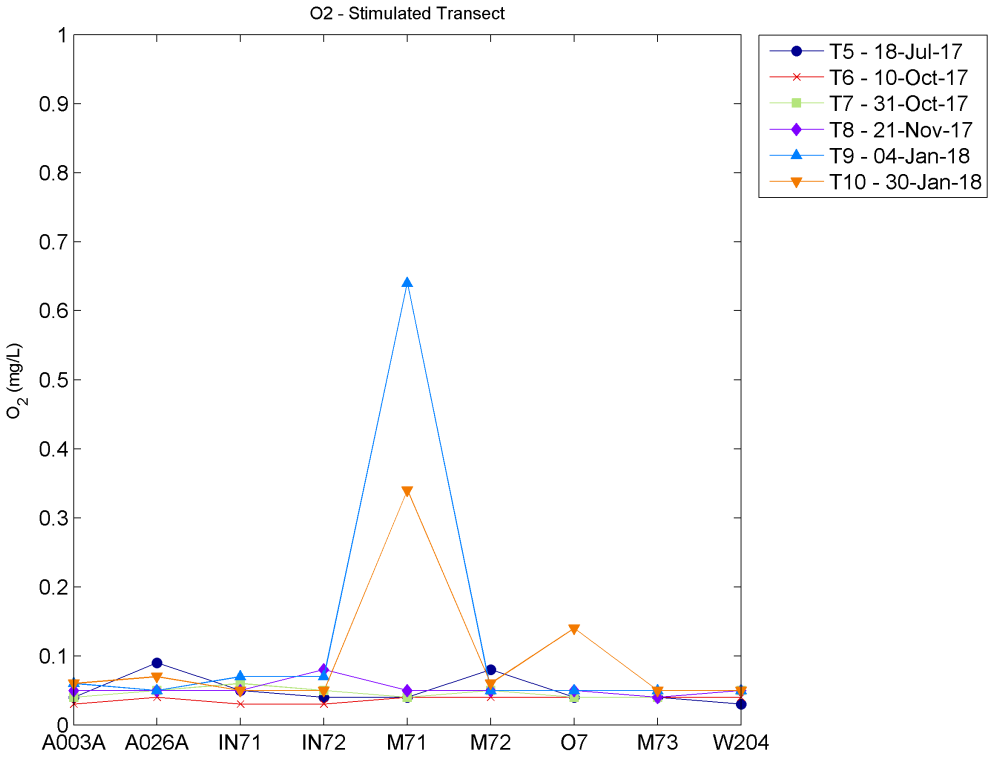

Figure A.12: *Oxygen concentration measured in the field for the stimulated transect.*

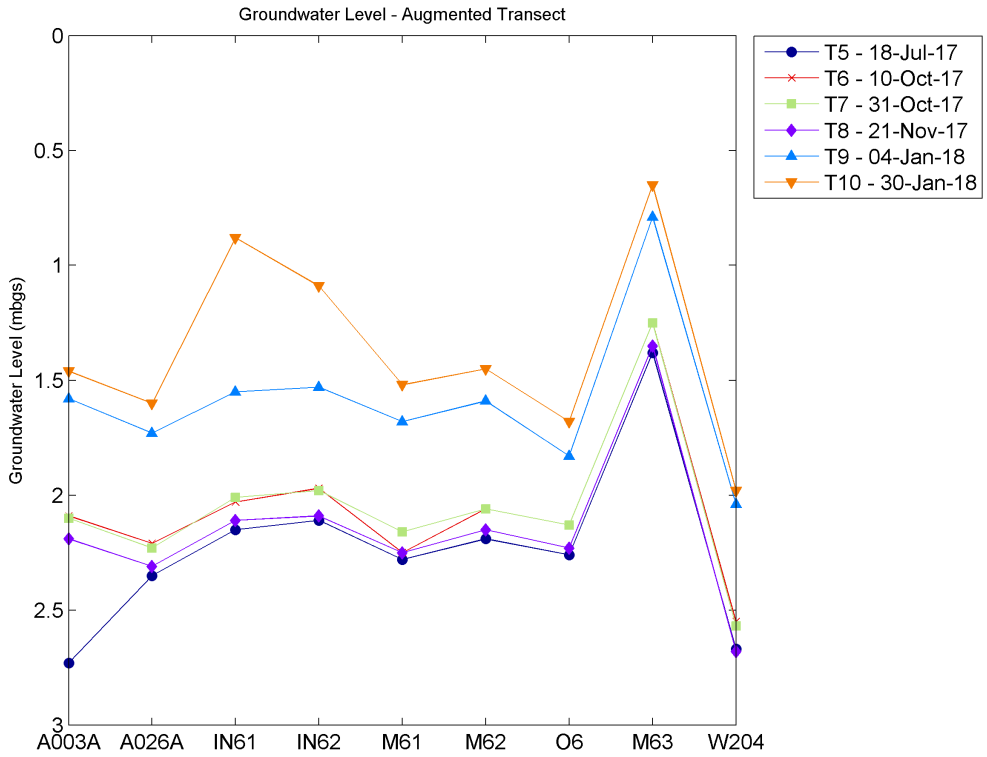

Figure A.13: *Groundwater level measured in the field, as meters below ground surface (mbgs) for the augmented transect.*

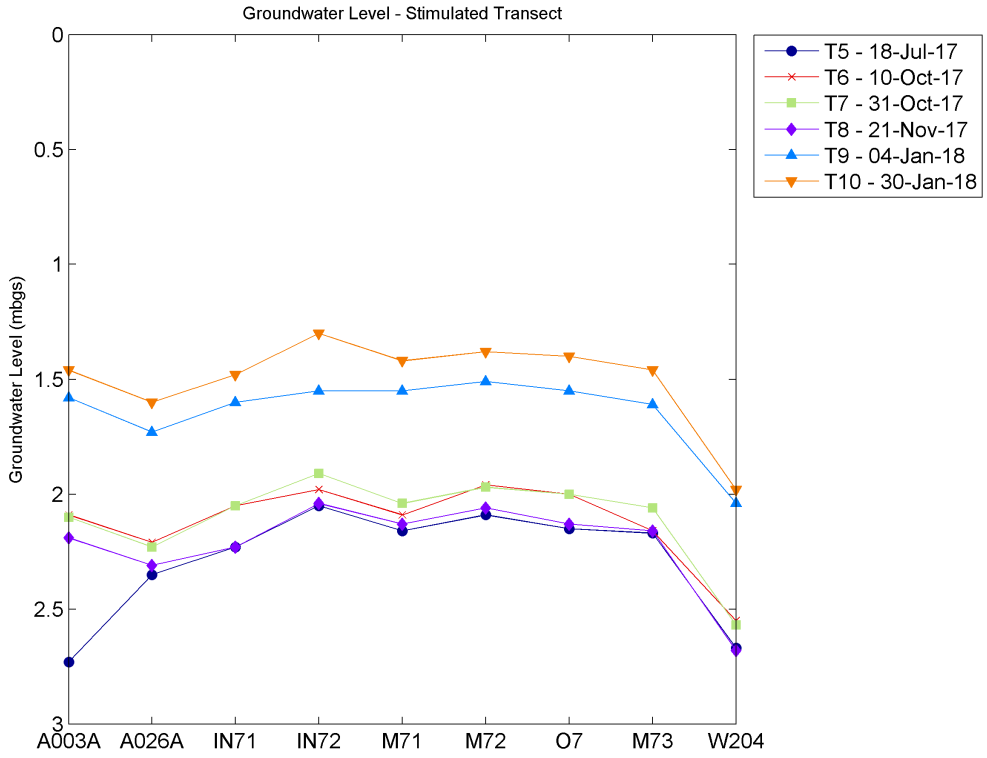

Figure A.14: *Groundwater level measured in the field, as meters below ground surface (mbgs) for the stimulated transect.*

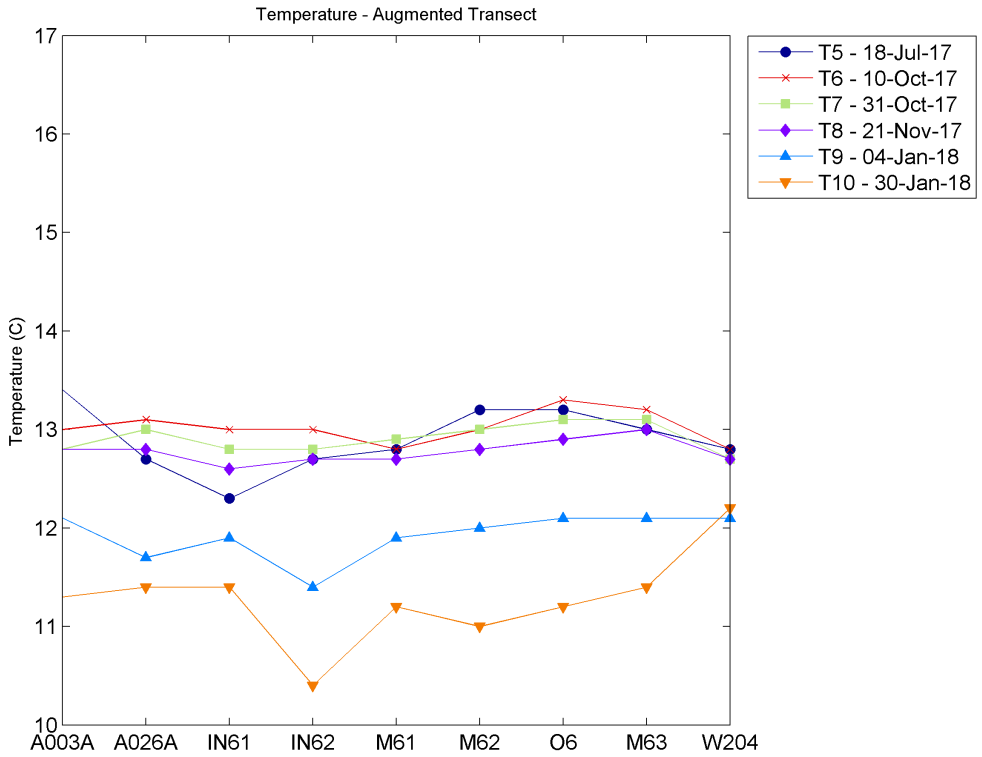

Figure A.15: *Groundwater temperature measured in the field for the augmented transect*

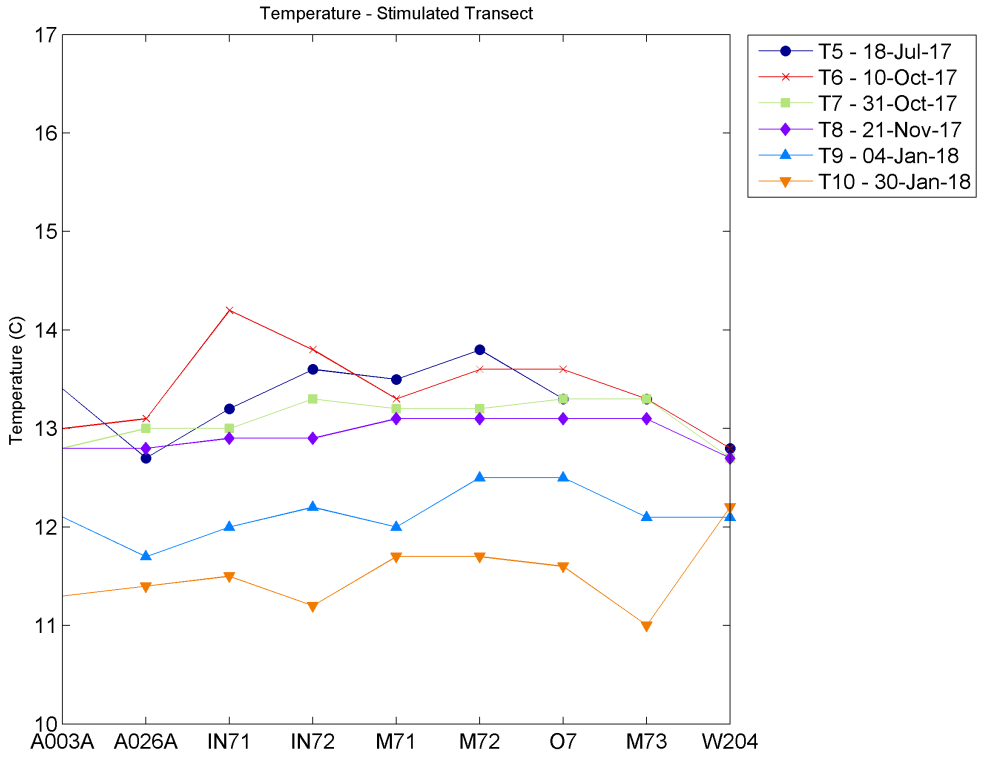

Figure A.16: *Groundwater temperature measured in the field for the stimulated transect*

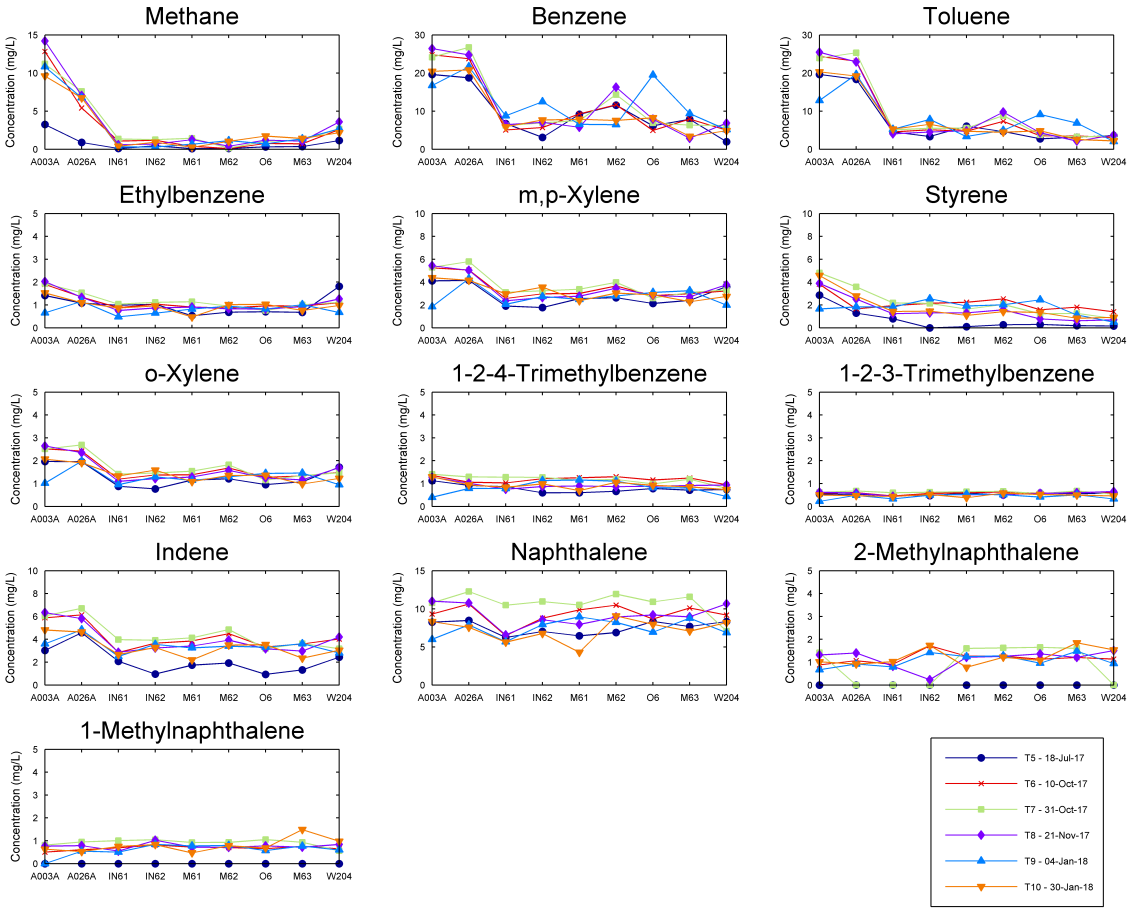

Figure A.17: *Summary of mobile aromatic hydrocarbons and methane for sampling events T5-T10 for the augmented transect.*

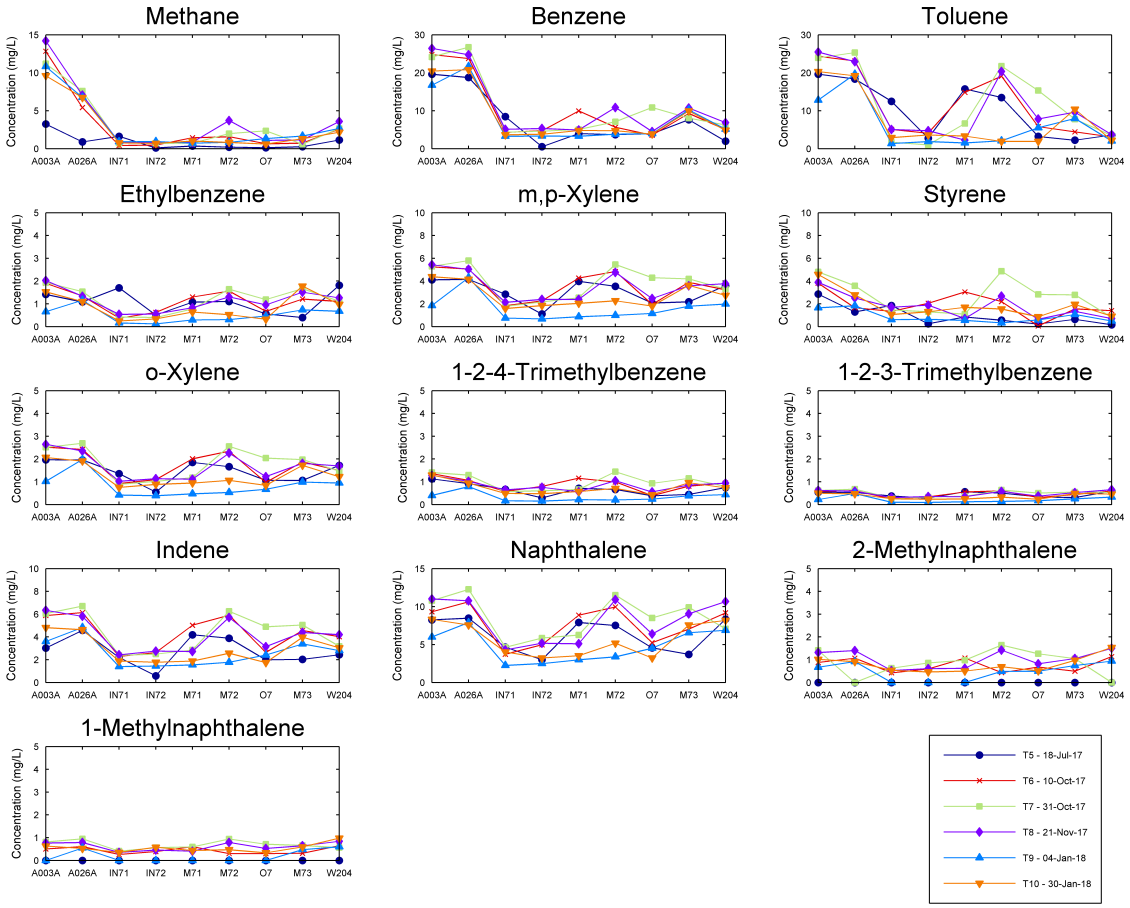

Figure A.18: *Summary of mobile aromatic hydrocarbons and methane for sampling events T5-T10 for the stimulated transect.*

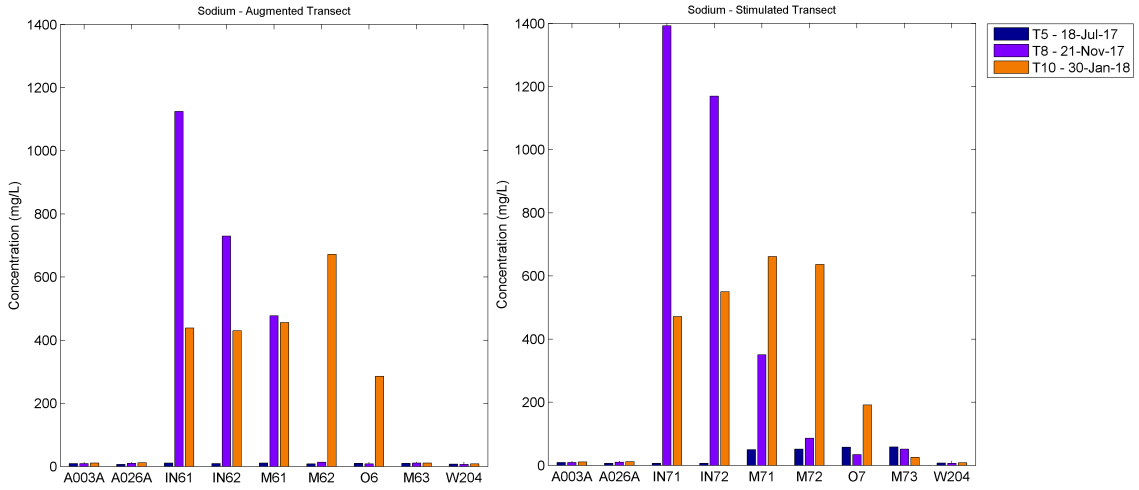

Figure A.19: *Sodium concentration for the augmented transect (left) and the stimulated transect (right)*

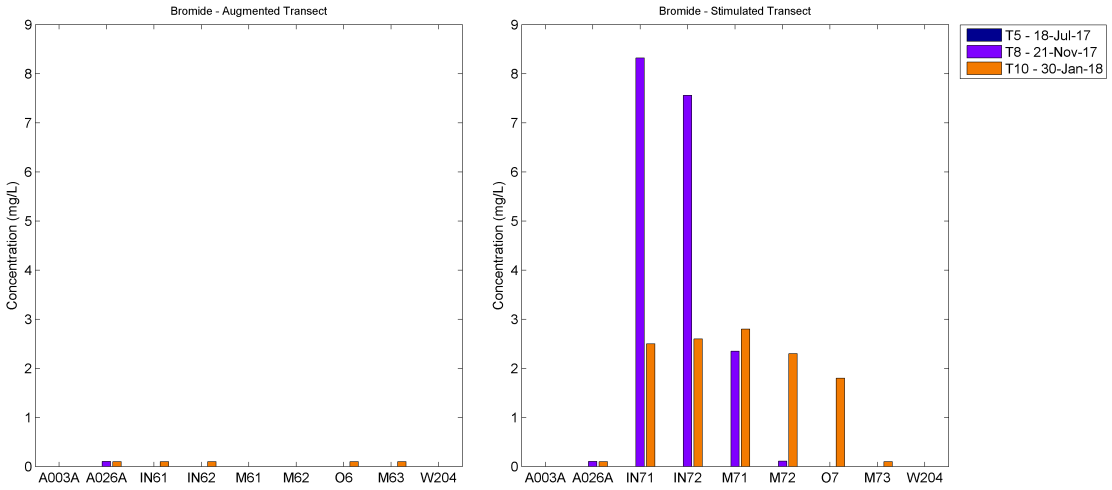

Figure A.20: *Bromide concentration for the augmented transect (left) and the stimulated transect (right)*

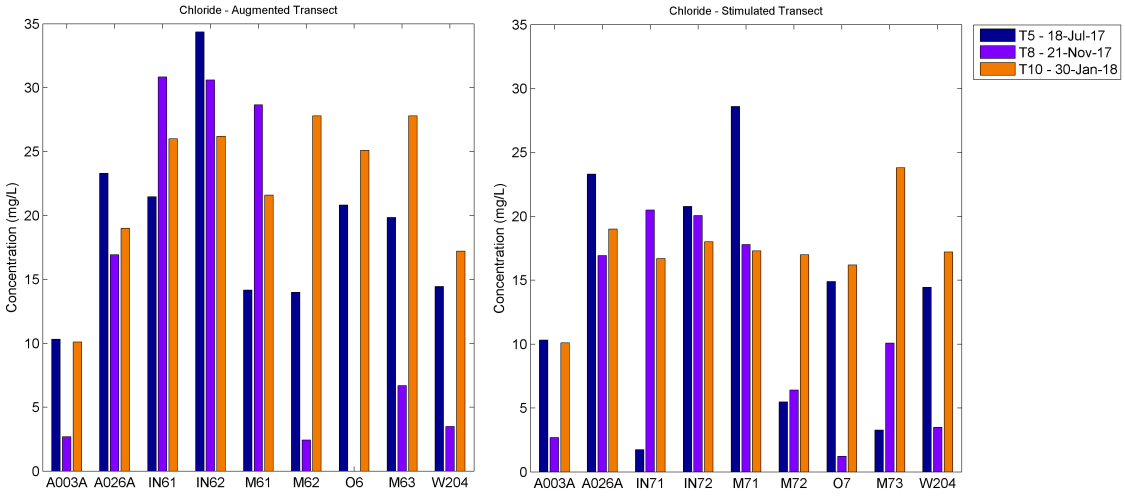

Figure A.21: *Chloride concentration for the augmented transect (left) and the stimulated transect (right)*

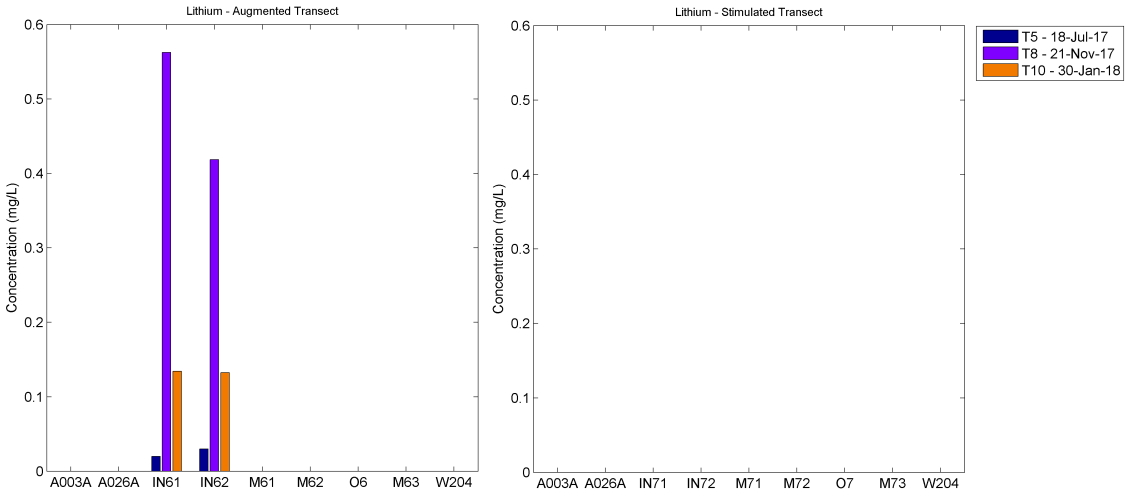

Figure A.22: *Lithium concentration for the augmented transect (left) and the stimulated transect (right)*

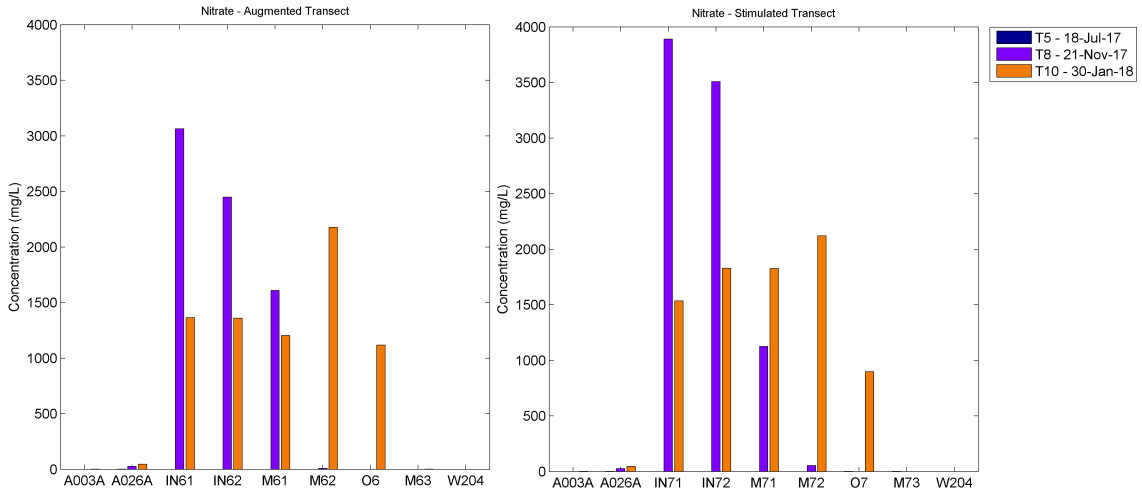

Figure A.23: *Nitrate concentration for the augmented transect (left) and the stimulated transect (right)*

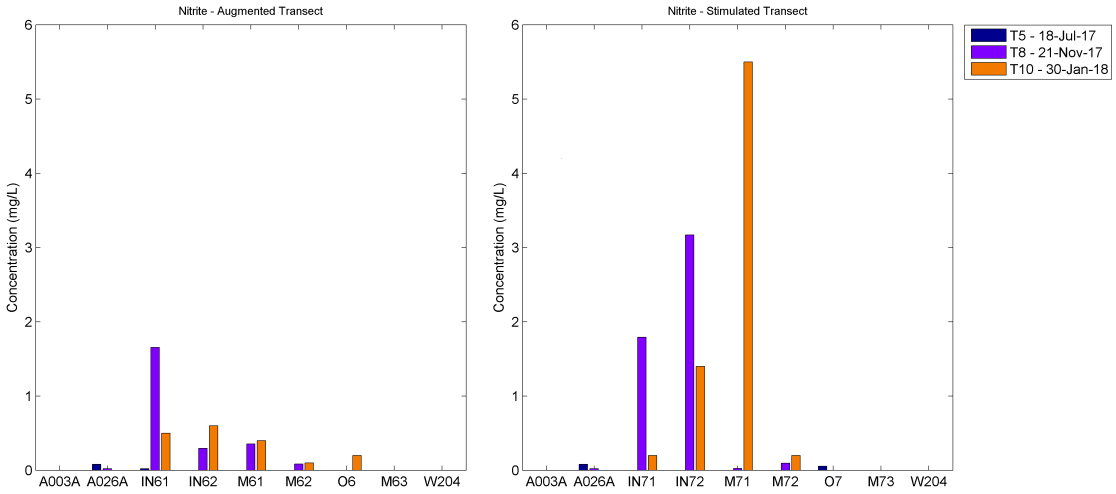

Figure A.24: *Nitrite concentration for the augmented transect (left) and the stimulated transect (right)*

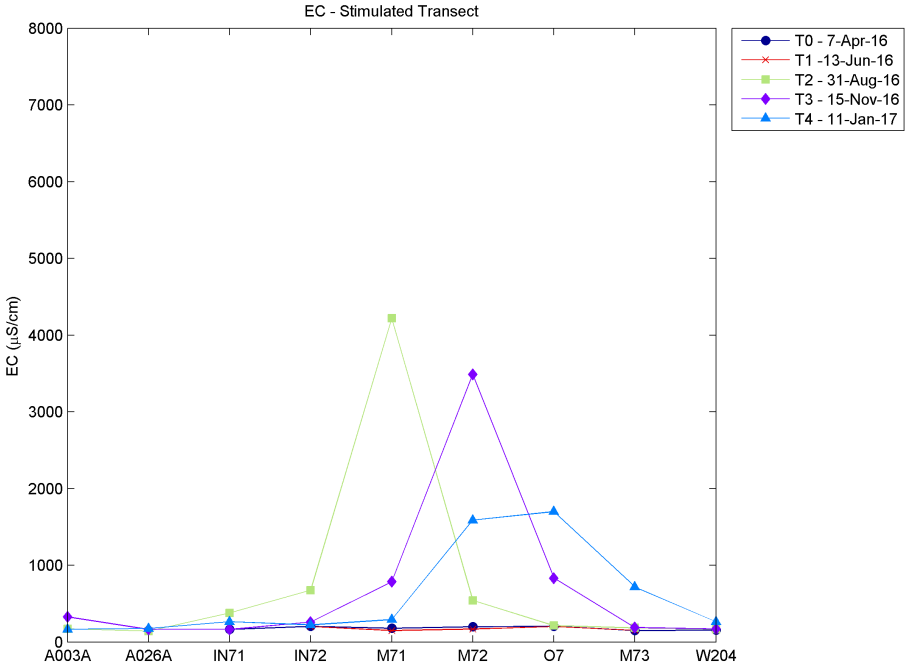

Figure A.25: *Electrical conductivity measured in the field for the augmented transect for the first recirculation field trial.*

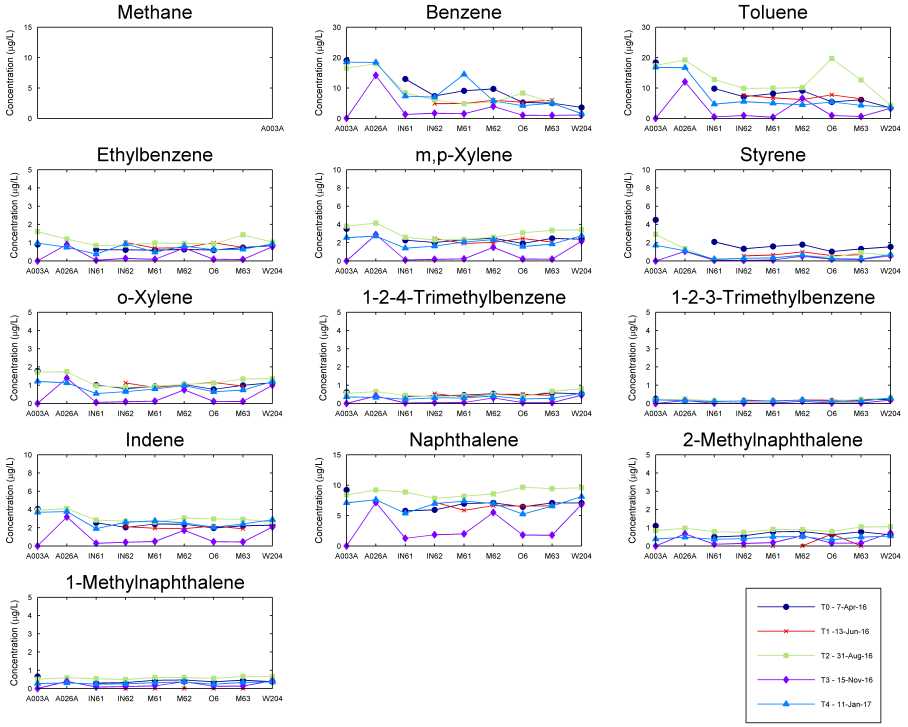

Figure A.26: *Summary of mobile aromatic hydrocarbons and methane for sampling events T0-T4 (first field trial) for the placebo transect.*

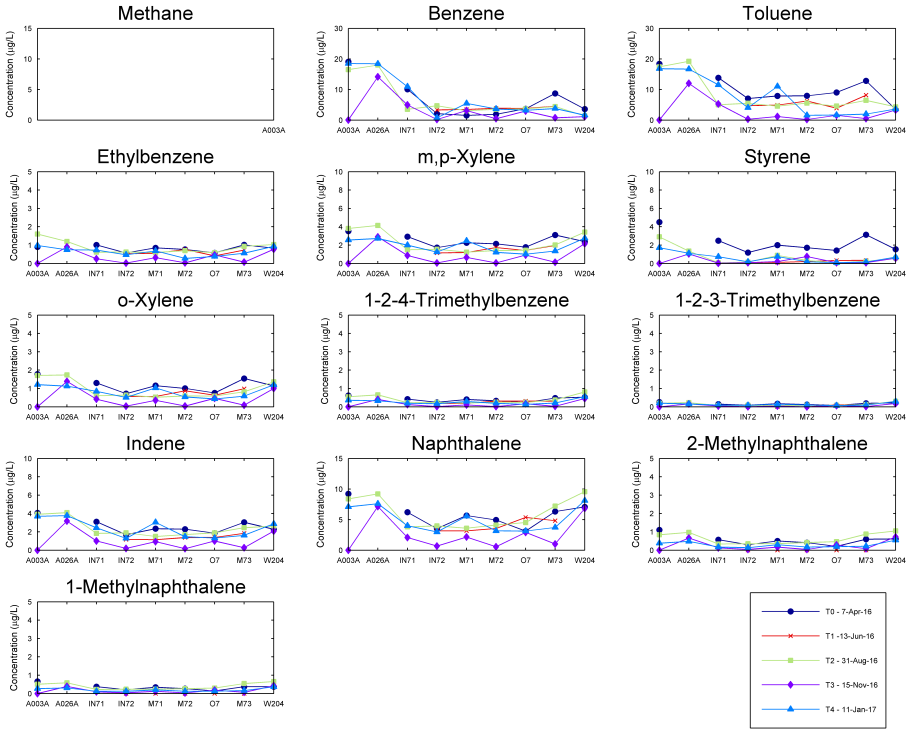

Figure A.27: *Summary of mobile aromatic hydrocarbons and methane for sampling events T1-T4 (first field trial) for the stimulated transect.*

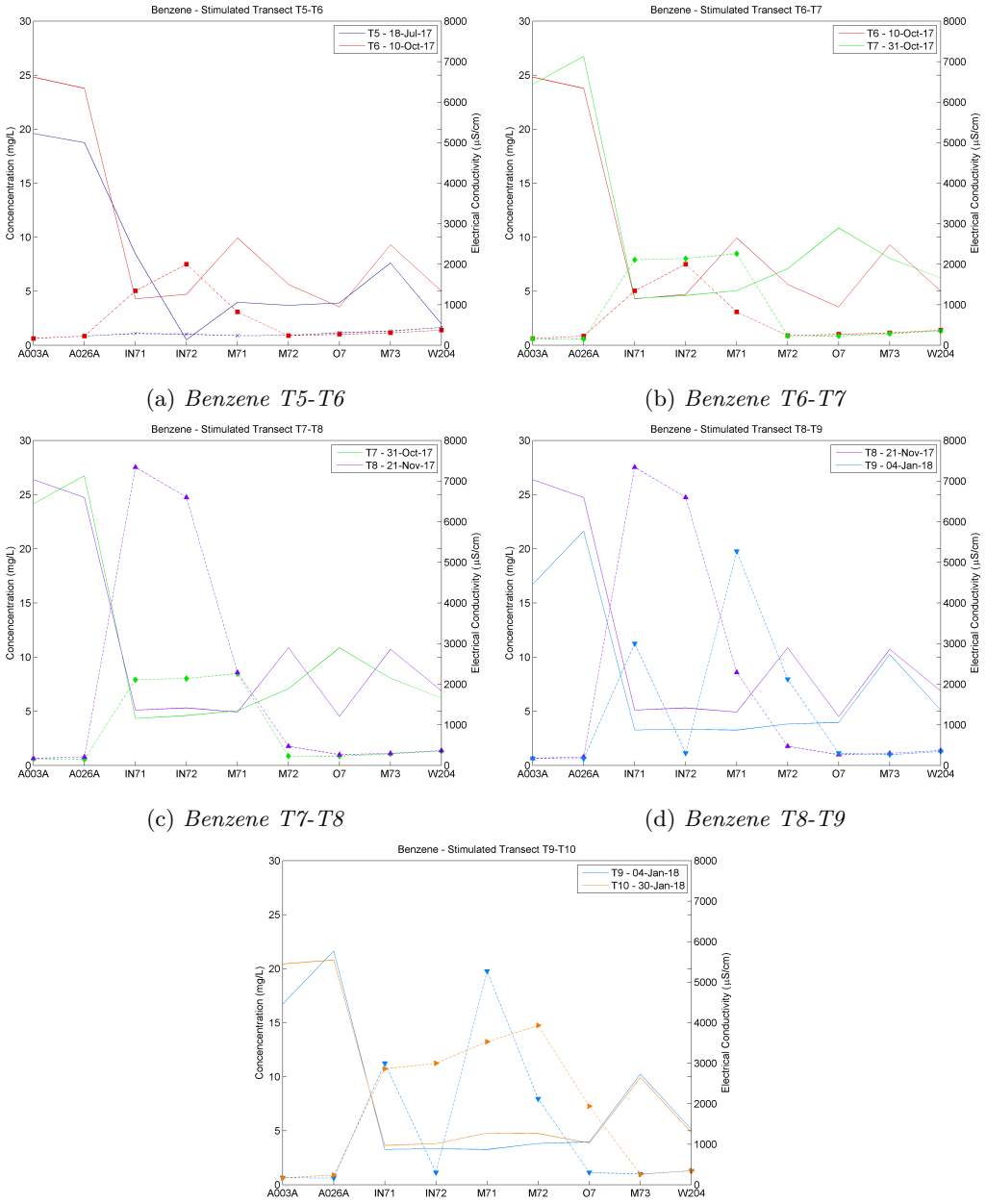

(a) *Benzene T5-T6*

(b) *Benzene T6-T7*

(c) *Benzene T7-T8*

(d) *Benzene T8-T9*

(e) *Benzene T9-T10*

Figure A.28: *Aqueous benzene concentration (solid line) in the stimulated transect plotted against the electrical conductivity (dashed line) at the same sampling time for T5-T10*

(a) *Benzene T5-T6*

(b) *Benzene T6-T7*

(c) *Benzene T7-T8*

(d) *Benzene T8-T9*

(e) *Benzene T9-T10*

Figure A.29: *Aqueous benzene concentration (solid line) in the augmented transect plotted against the electrical conductivity (dashed line) at the same sampling time for T5-T10*

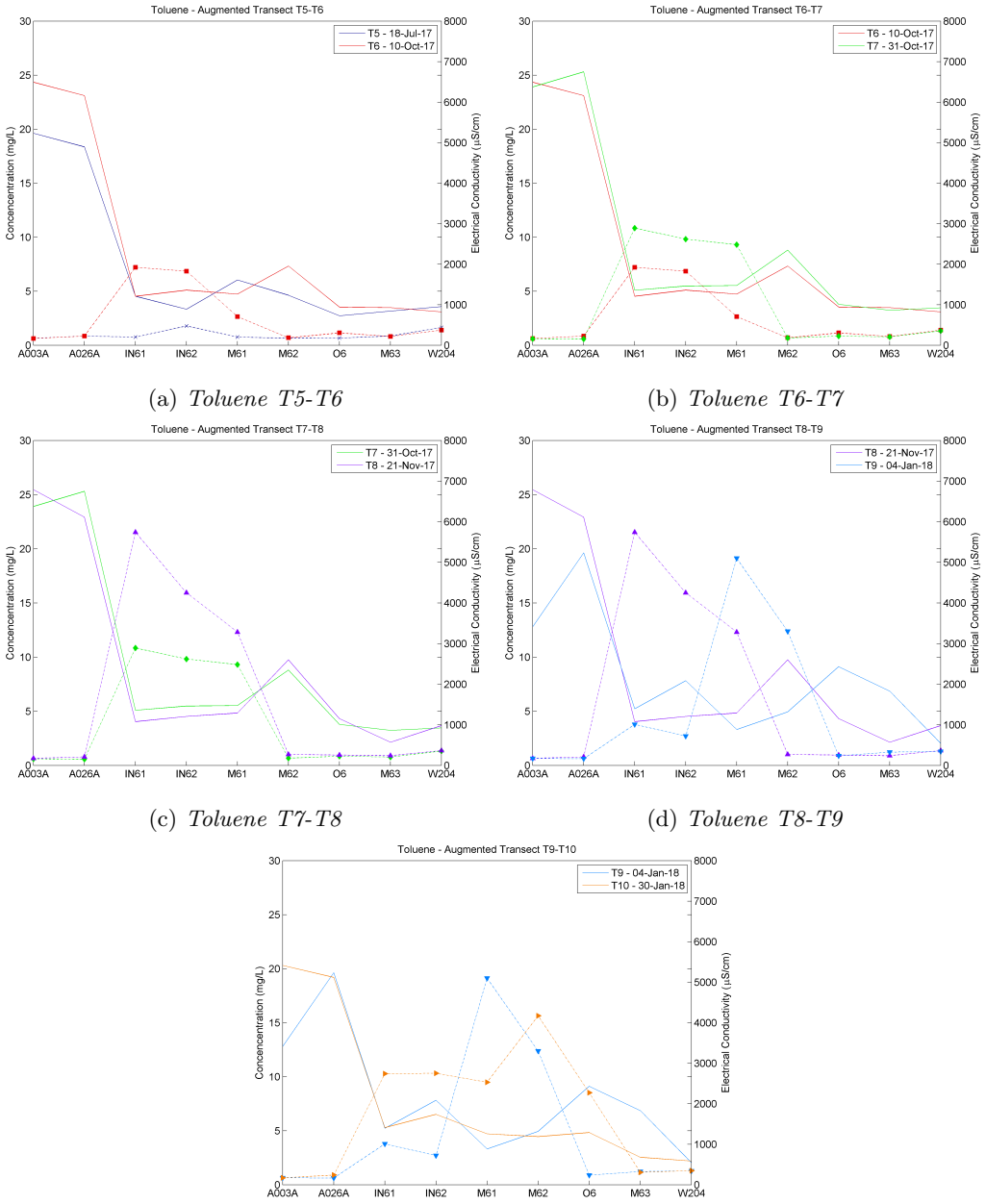

(a) *Toluene T5-T6*

(b) *Toluene T6-T7*

(c) *Toluene T7-T8*

(d) *Toluene T8-T9*

(e) *Toluene T9-T10*

Figure A.30: *Aqueous toluene concentration (solid line) in the augmented transect plotted against the electrical conductivity (dashed line) at the same sampling time for T5-T10*

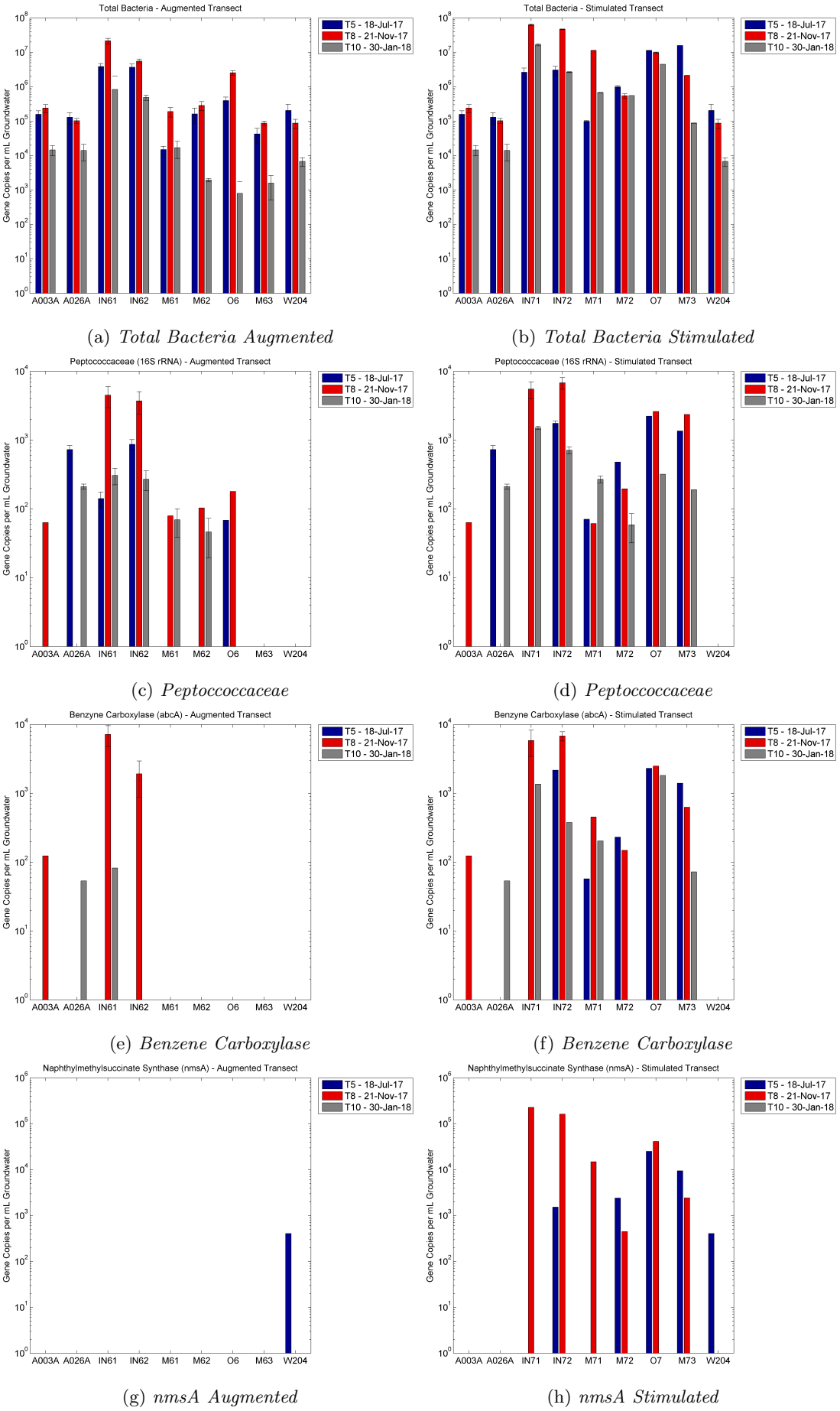

(a) *Total Bacteria Augmented*

(b) *Total Bacteria Stimulated*

(c) *Peptococcaceae*

(d) *Peptococcaceae*

(e) *Benzene Carboxylase*

(f) *Benzene Carboxylase*

(g) *nmsA Augmented*

(h) *nmsA Stimulated*

Figure A.4: *DNA Results for the stimualted and augmented trasnect for; (a,b) total bacteria, (c,d) Peptococcaceae, (e,f) benzene carboxylase and (g,h) nmsA genes. Data analysed by Deltares (Utrecht, Netherlands)*

Appendix B

Supporting Information

Table B.1: *Summary of relevant pathways and enzymes responsible for degradation of select aromatic hydrocarbons and their respectice metabolites (Callaghan, 2013), abcA = benzene carboylase, bssA = benzene succinate synthase, nmsA = naphthyl-2-methylsuccinate synthase*

Parent Compound	Metabolite	Pathway	Enzyme
Benzene	Phenol	Hydroxylation	
	Toluene	Methylation	
	Benzoate	Carboxylation	abcA
Toluene	Benzylsuccinate	Fumerate	bssA
	Cinnamic Acid		
o-Xylene	2-methylbenzylsuccinate	Fumerate	bssA
m-Xylene	3-methylbenzylsuccinate	Fumerate	bssA
p-Xylene	4-methylbenzylsuccinate	Fumerate	bssA
Ethylbenzene	1-phenylethylsuccinate	Fumerate	bssA
	1-phenylethnol	Hydroxylation	
Styrene	Benzeneacetic acid		
Naphthalene	2-methylnaphthalene	Methylation	
	2-naphtoic acid	Carboxylation	
2-methylnaphthalene	Naphthyl-2-methylsuccinate	Fumerate	nmsA
Phenanathrene	Phenanthrene-2-carboxylic acid	Carboxylation	
Biphenyl	Biphenyl-4-carboxylic acid	Carboxylation	
Indane	Indanoic acid	Cometabolic	
Indene	Indenoic acid	Cometabolic	
Acenaphthene	Acenaphthenoic acid	Cometabolic	
	Acenaphthyl methylsuccinate	Methylation	
Acenaphthylene	Acenaphthylenoic acid	Cometabolic	
1-methylnaphthalene	1-methyl-2-naphthoic acid	Carboxylation	
	1,2-dimethylnaphthalene	Cometabolic / Methylation	

Table B.2: *Dosing schedule for stimulation batch experiments.*

Batches		Treatment	May 13, 2014	September 8, 2014	March 26, 2015
8	A	Sterile	100 mg/L $HgCL_2$+ 100mg/L NaN_3		
8	B	Sterile	100 mg/L $HgCL_2$+ 100mg/L NaN_3		
8	C	Sterile	100 mg/L $HgCL_2$+ 100mg/L NaN_3		
9	A	No Addition			
9	B	No Addition			
9	C	No Addition			
10	A	Nitrate	10 mM $NaNO_3$		
10	B	Nitrate	10 mM $NaNO_3$		
10	C	Nitrate	10 mM $NaNO_3$		
11	A	Nitrate + Succinate	10 mM $NaNO_3$+ 2mM $C_4H_6O_4$	2mM $C_4H_6O_4$	10 mM NaNO3+ 2mM $C_4H_6O_4$
11	B	Nitrate + Succinate	10 mM $NaNO_3$+ 2mM $C_4H_6O_4$	2mM $C_4H_6O_4$	10 mM NaNO3+ 2mM $C_4H_6O_4$
11	C	Nitrate + Succinate	10 mM $NaNO_3$+ 2mM $C_4H_6O_4$	2mM $C_4H_6O_4$	10 mM NaNO3+ 2mM $C_4H_6O_4$
12	A	Nitrate + Acetate	10 MM $NaNO_3$+ 4mM CH_3COO^-	4mM CH_3COO^-	10 mM $NaNO_3$
12	B	Nitrate + Acetate	10 MM $NaNO_3$+ 4mM CH_3COO^-	4mM CH_3COO^-	10 mM $NaNO_3$
12	C	Nitrate + Acetate	10 MM $NaNO_3$+ 4mM CH_3COO^-	4mM CH_3COO^-	10 mM $NaNO_3$
13	A	Sulfate	10mM Na_2SO_4		
13	B	Sulfate	10mM Na_2SO_4		
13	C	Sulfate	10mM Na_2SO_4		2mM Na_2SO_4
14	A	Chlorate	10mM $NaClO_3$		
14	B	Chlorate	10mM $NaClO_3$		
14	C	Chlorate	10mM $NaClO_3$		2mM $NaCLO_3$

B.1 Stimulation Batch Experiments

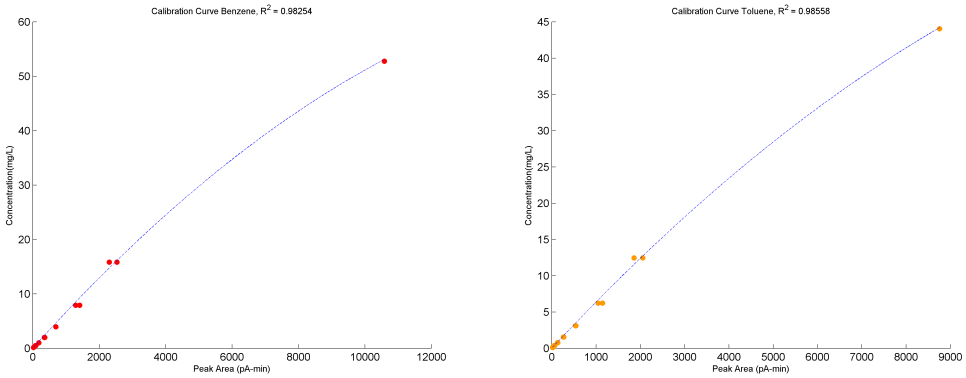

(a) *Benzene*

(b) *Toluene*

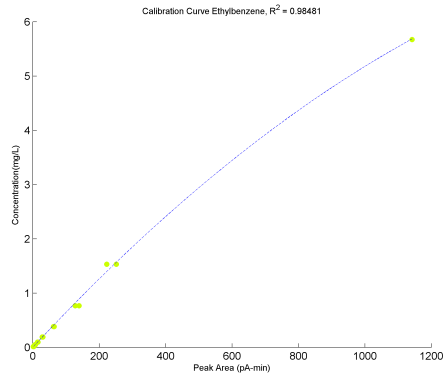

(c) *Ethylbenzene*

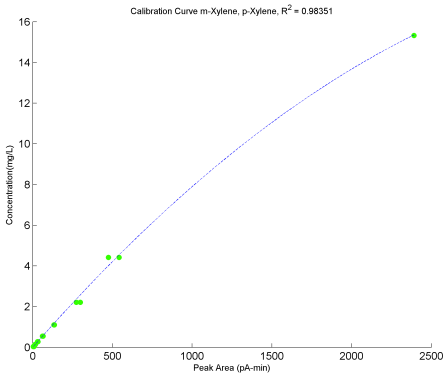

(d) *m/p-Xylene*

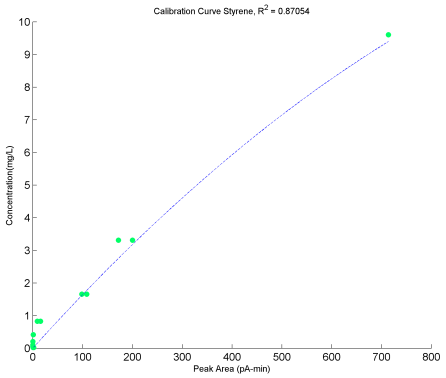

(e) *Styrene*

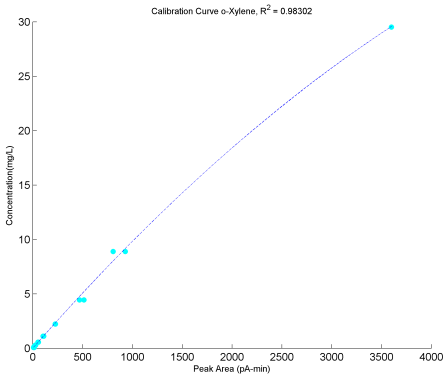

(f) *o-Xylene*

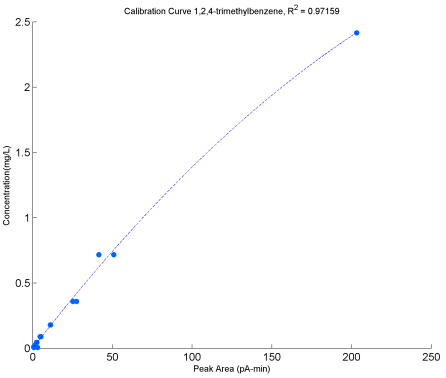

(g) *1,2,4-trimethylbenzene*

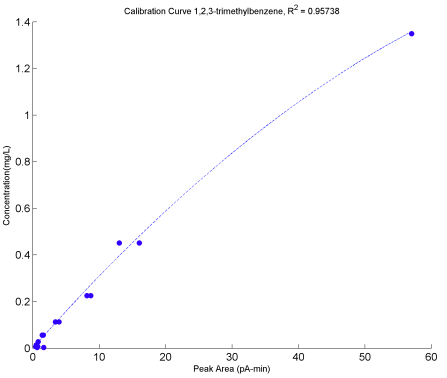

(h) *1,2,3-trimethylbenzene*

Figure B.1: *Calibration for aromatic hydrocarbons*

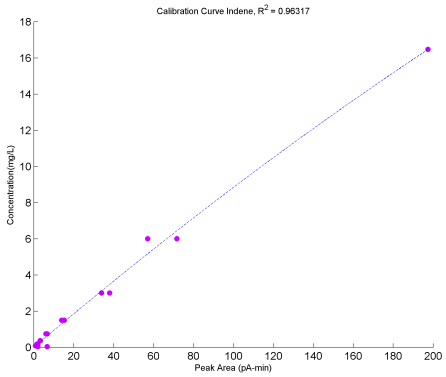

(a) *Indene*

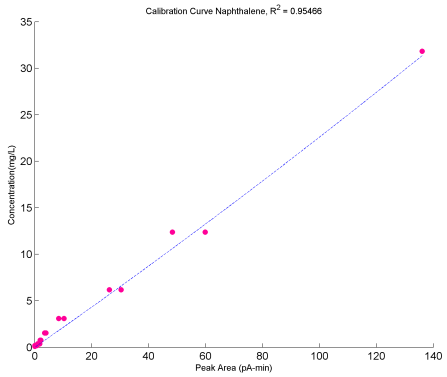

(b) *Naphthalene*

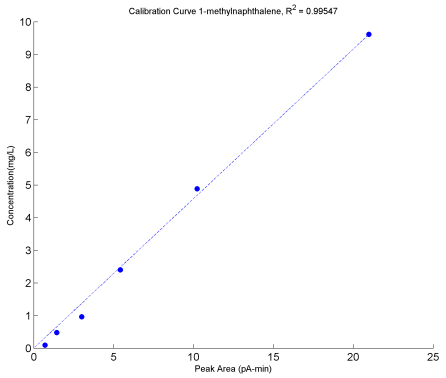

(c) *1-Methylnaphthalene*

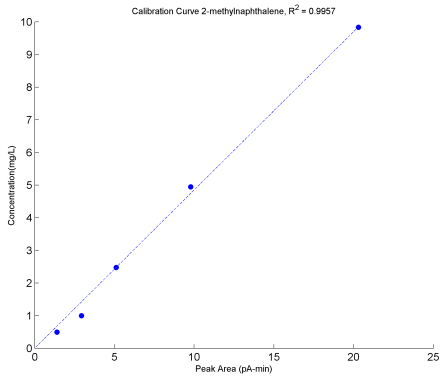

(d) *2-Methylnaphthalene*

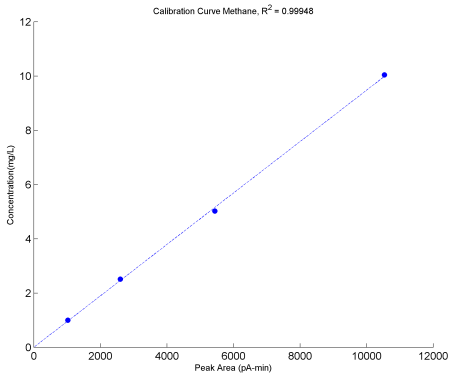

(e) *Methane*

Figure B.2: *Calibration for aromatic hydrocarbons continued.*

Table B.3: *Density, solubility and molar mass for principal components measured.*

	Density (g/L)	Solubility (g/L)	Molar Mass (g/mol)
Benzene	876.5	1.79	78.11
Toluene	866.0	0.52	92.14
Ethylbenzene	866.5	0.15	106.17
p-xylene	861.0	0.17	106.17
m-xylene	860.0	0.16	106.17
o-xylene	880.0	0.18	106.17
styrene	909.0	0.30	104.15
1,2,4-trimethylbenzene	876.1	0.06	120.19
1,2,3-trimethylbenzene	890.0	0.06	120.20
indene	997.0	0.02	116.16
Naphthalene	1150.0	0.03	128.17
2-Methylnaphthalene	1005.8	0.02	142.20
1-Methylnaphthalene	1020.2	0.03	142.20

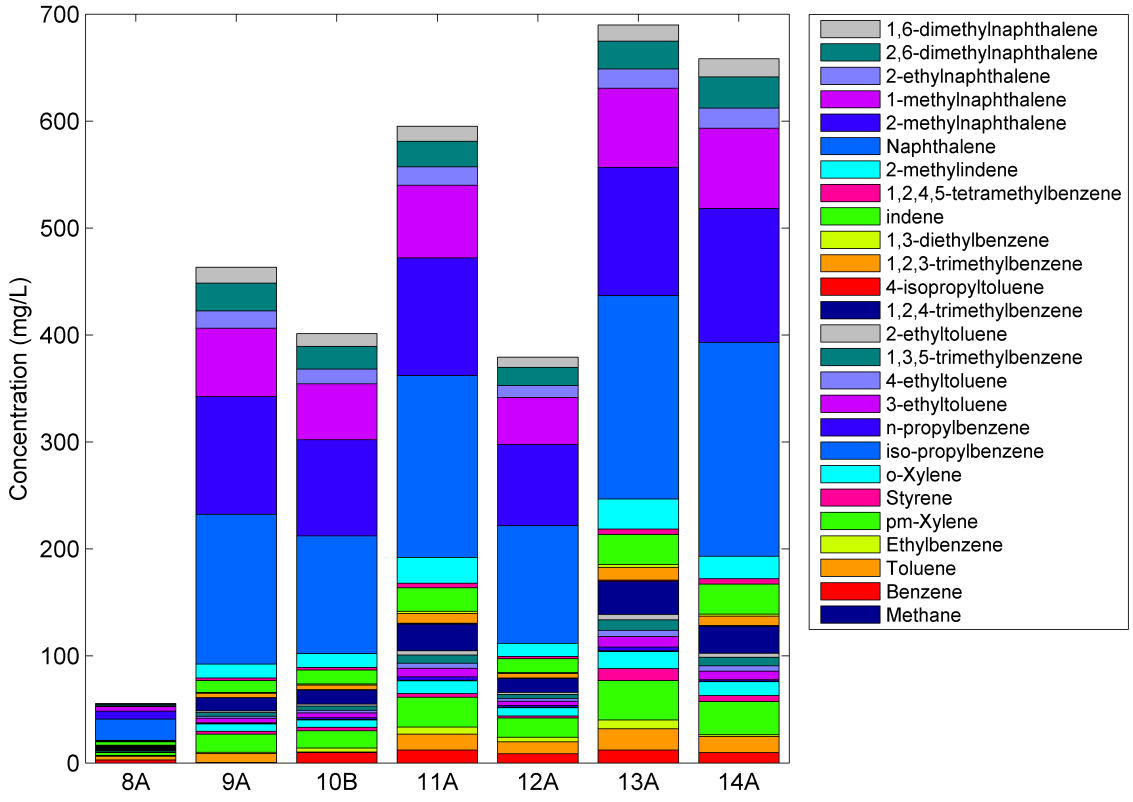

Figure B.3: *Concentration in the aqueous phase from aqueous samples, analysis performed by TNO (Utrecht) on GC-MS. Concentration of 25 hydrocarbons (full analysis).*

B.2 Tar as a Hydrophobic Matrix: Batch Experiments

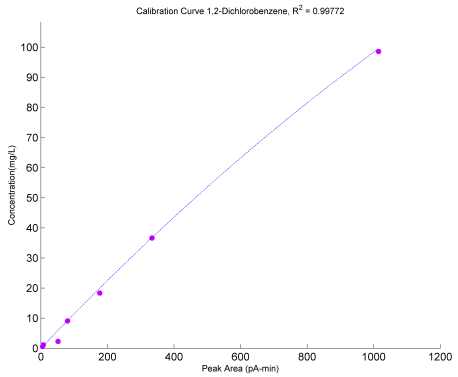

(a) *1,2-Dichlorobenzene*

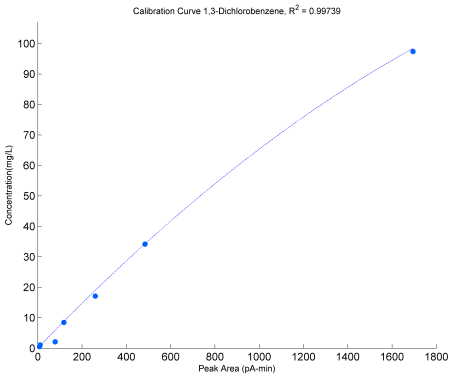

(b) *1,3-Dichlorobenzene*

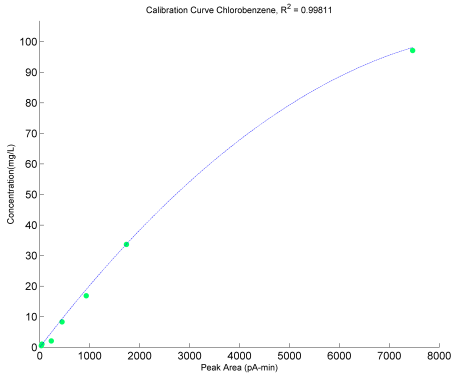

(c) *Chlorobenzene*

Figure B.4: *Calibration curves for organic stock mix chemicals*

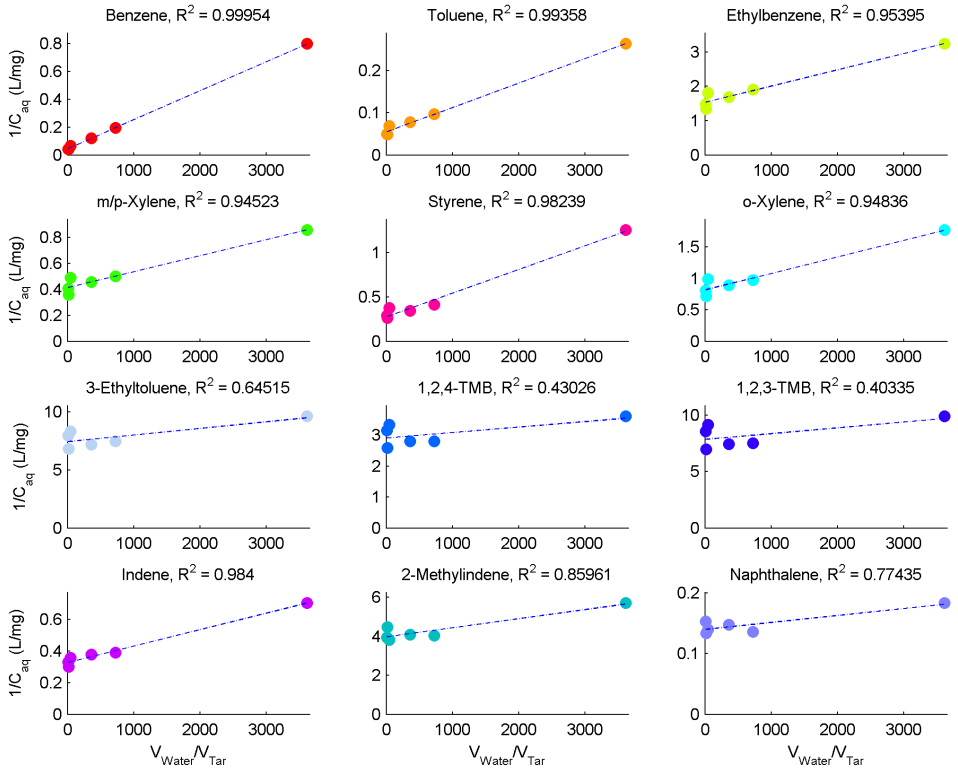

Figure B.5: *Plots of* $\frac{1}{C_{aq}^{i}}$ *vs.* $\frac{V_{aq}}{M_n}$ *gives graph with a linear slope of* $\frac{1}{C_n^{i,\circ}}$ *and a y-intercept of* $\frac{K_{nw}^{i}}{C_n^{i,\circ}}$, *from which* K_{nw}^{i} *and* $C_n^{i,\circ}$ *were be determined Rixey* et al. *(1999)*

Figure B.6: *Batch 2 Bitumen and MilliQ water and control and Batch 4*

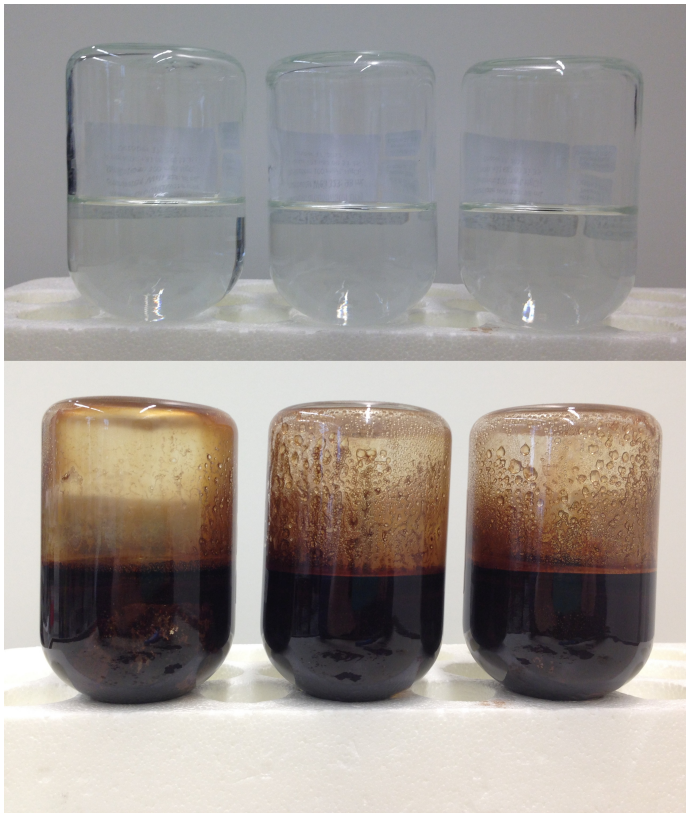

Figure B.7: *Control Batch 7 and Batch 8 with tar from A005*

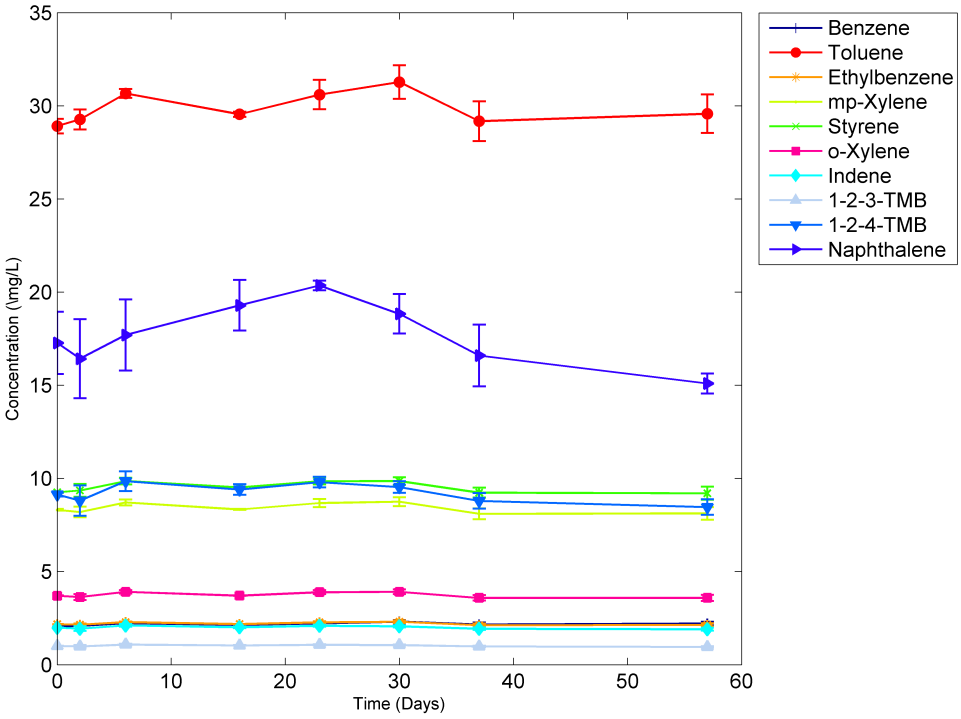

Figure B.8: *Batch 5: Average concentration of aromatic hydrocarbons in the aqueous phase over time. Error bars show one standard deviation of three batches measured.*

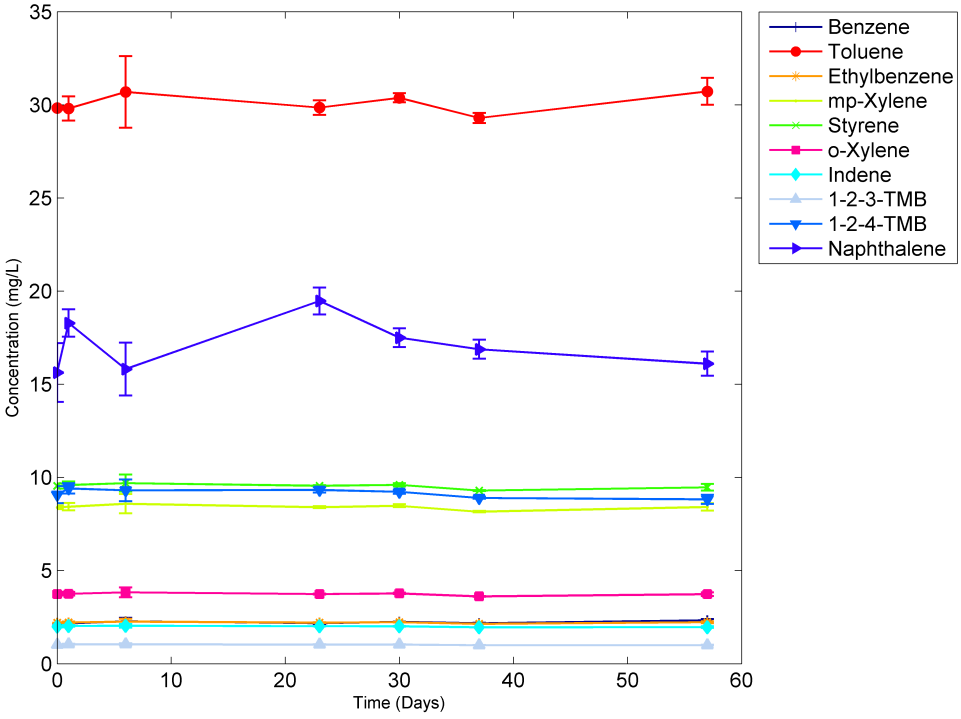

Figure B.9: *Batch 6: Average concentration of aromatic hydrocarbons in the aqueous phase over time. Error bars show one standard deviation of three batches measured.*

Table B.4: *Percent of total mass of each chemical in the aqueous, gas and NAPL in each bottle. Values given are the mean of the three replicates in each batch series and three injections of chemical solution ± the standard deviation. The calculated logK_{nw} is listed for each chemical-NAPL pair and could only be calculated for chemicals with which did not completely partition to the NAPL. Chemicals are listed in order of increasing logK_{ow}.*

				Percent of Total Mass in Each Phase		
	Chemical	Log K_{ow}	LogK_{nw}	Aqueous	Gas	NAPL
Batch 1	*Benzene Solution*					
	Benzene	2.1	1.8	35.2 ± 4.8	11.3 ± 1.6	53.5 ± 6.4
Batch 1	*Organic Solution*					
	Benzene	2.1	1.7	38.0 ± 2.8	12.2 ± 0.9	49.8 ± 3.6
	Toluene	2.7	2.4	12.5 ± 0.2	4.9 ± 0.1	82.6 ± 0.3
	Chlorobenzene	2.8	2.6	8.4 ± 1.2	1.8 ± 0.3	89.8 ± 1.4
	1,2-Dichlorobenzene	3.4	-	-	-	100.0
	1,3-Dichlorobenzene	3.5	-	-	-	100.0
Batch 2	*Hydrocarbon Solution*					
	Benzene	2.1	1.8	34.4 ± 3.6	11.1 ± 1.2	54.5 ± 4.8
	Toluene	2.7	2.3	14.7 ± 4.1	5.8 ± 1.6	79.4 ± 5.7
	Indene	2.9	2.8	6.7 ± 2.5	0.6 ± 0.2	92.6 ± 2.7
	Styrene	3.0	2.8	7.0 ± 3.0	1.1 ± 0.1	92.0 ± 4.0
	o-Xylene	3.1	3.0	5.2 ± 2.4	1.6 ± 0.8	93.1 ± 3.2
	Ethylbenzene	3.2	2.9	4.8 ± 2.1	2.2 ± 1.0	92.9 ± 3.0
	m/p-Xylene	3.2	3.0	4.6 ± 2.0	1.7 ± 0.7	93.6 ± 2.7
	Naphthalene	3.3	-	-	-	100.0
	1,2,3-Trimethylbenzene	3.7	-	-	-	100.0
	1,2,4-Trimethylbenzene	3.8	-	-	-	100.0
Batch 8	*Benzene Solution*					
	Benzene	2.1	2.2	17.6 ± 2.4	5.7 ± 0.8	76.8 ± 3.2

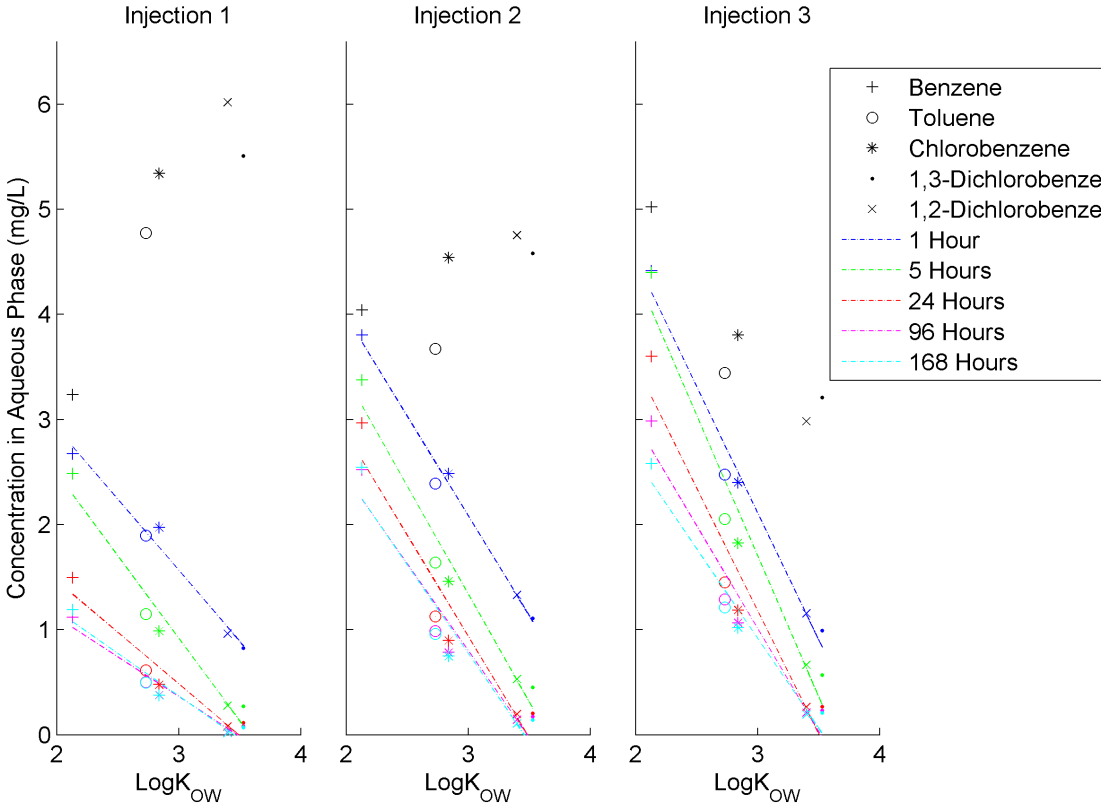

Figure B.10: *Batch 1: Organic solution concentration versus $logK_{ow}$ values from literature after 1, 5, 24, 96 and 168 hours after each injection. Dashed lines are linear trendlines for component at each measurement interval.*

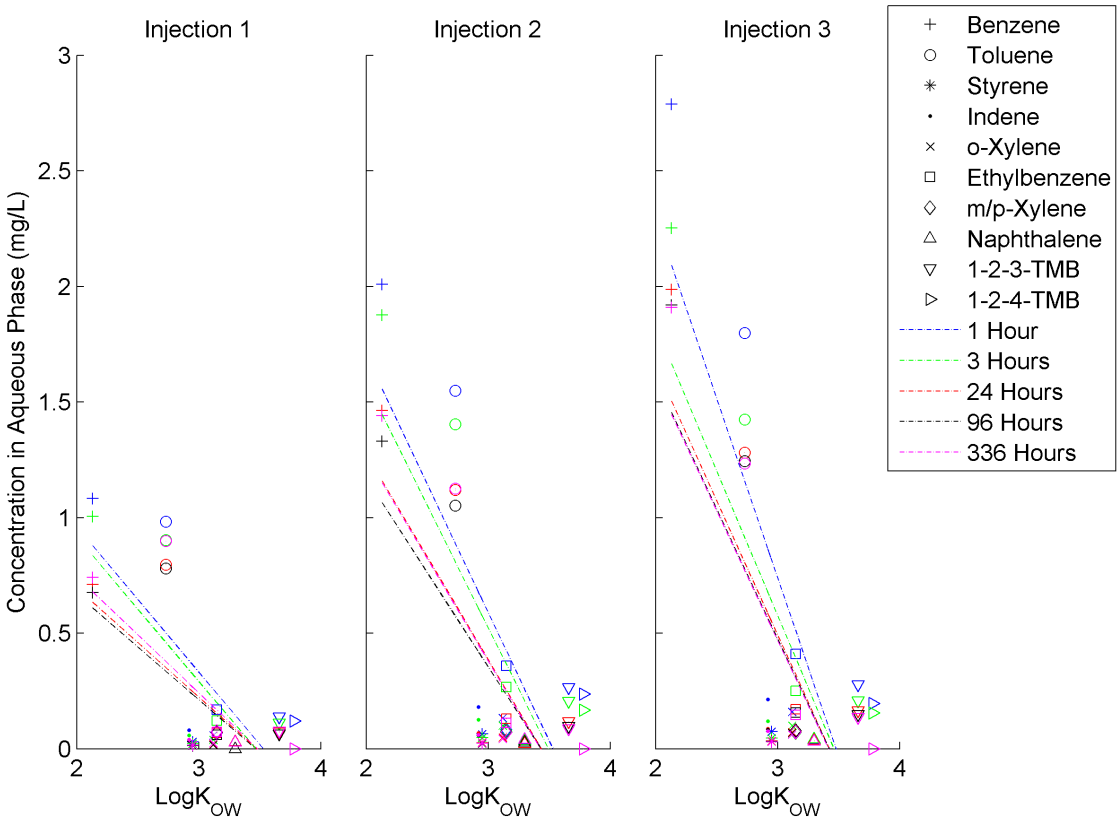

Figure B.11: *Batch 2: Hydrocarbon solution concentration versus $logK_{ow}$ values from literature after 1, 3, 24, 96 and 336 hours after each injection. Dashed lines are linear trendlines for component at each measurement interval.*

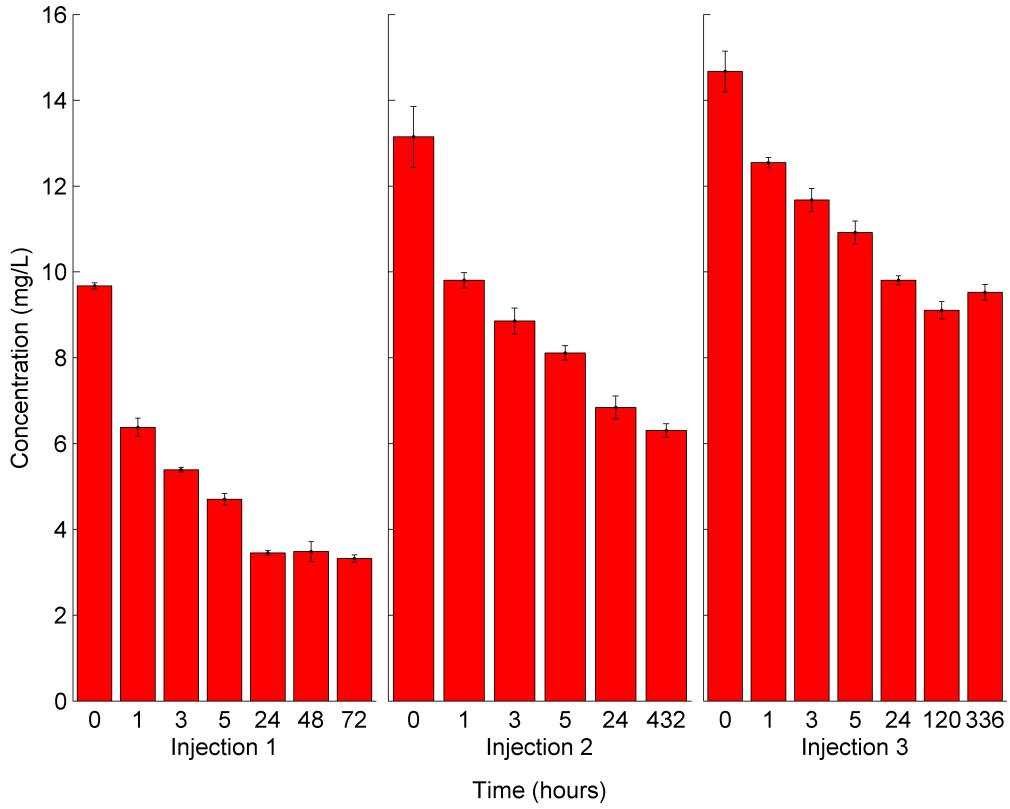

Figure B.12: *Batch 1 Benzene solution. Average concentration with standard deviation error bars for 3 injections monitored over time.*

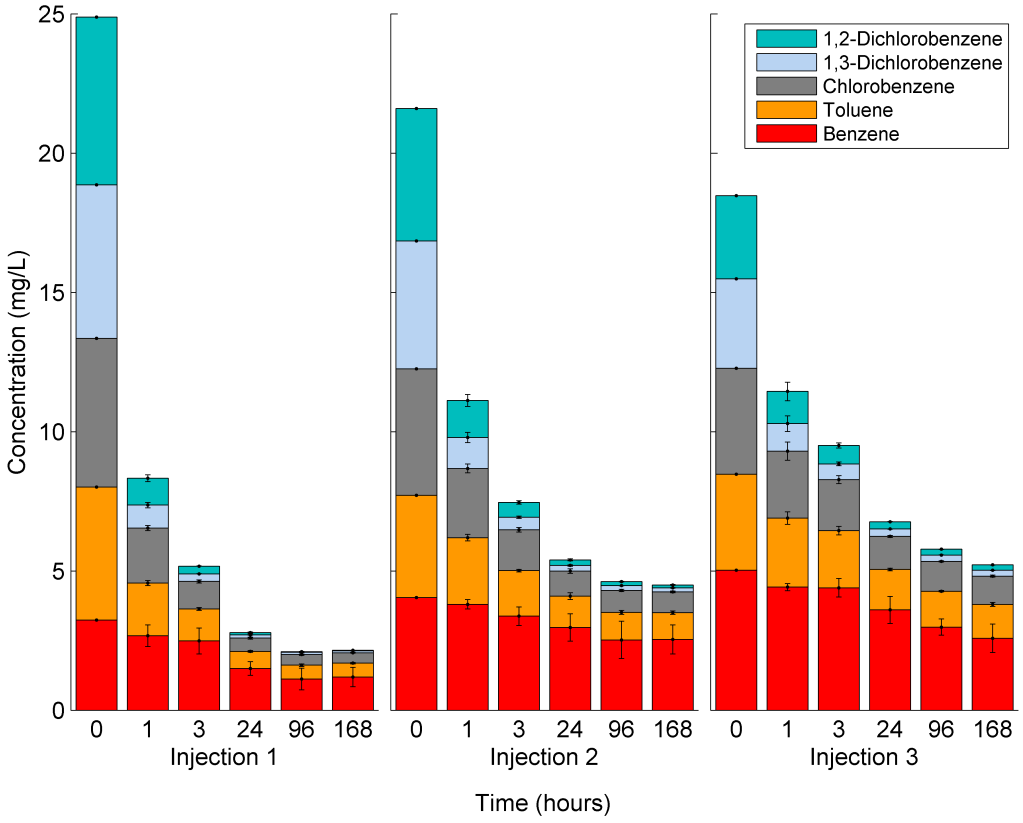

Figure B.13: *Batch 1 Organic Solution. Average concentration with standard deviation error bars for 3 injections over time.*

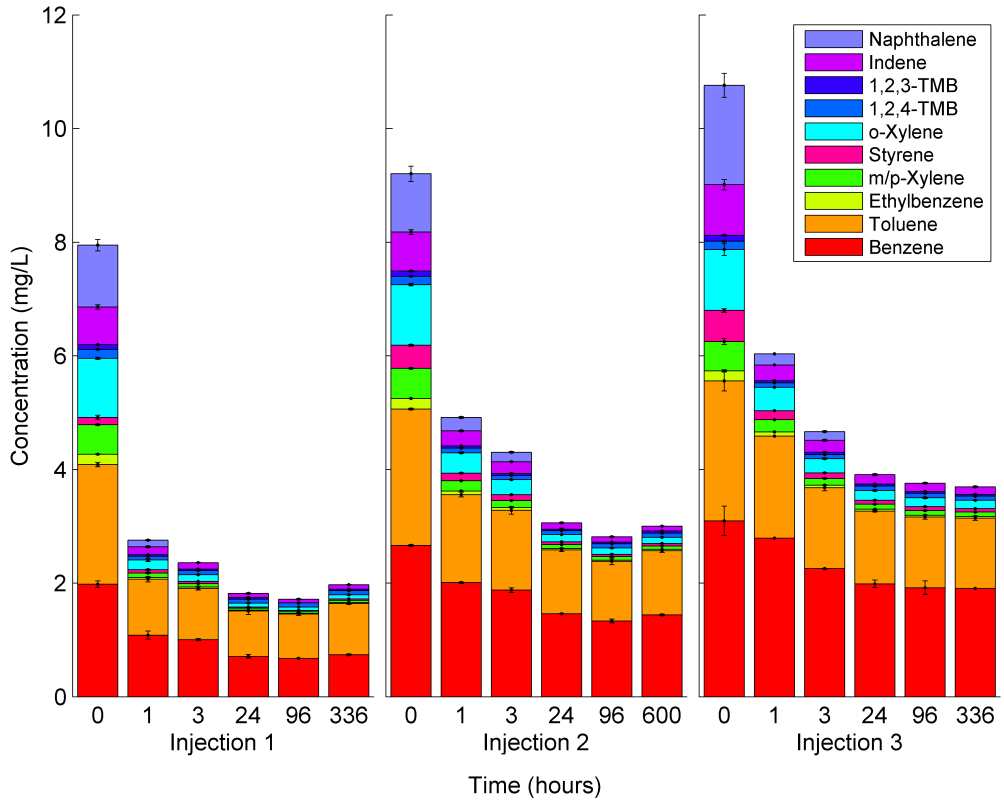

Figure B.14: *Batch 2 Hydrocarbon Mix. Average concentration with standard deviation error bars for 3 injections monitored over time.*

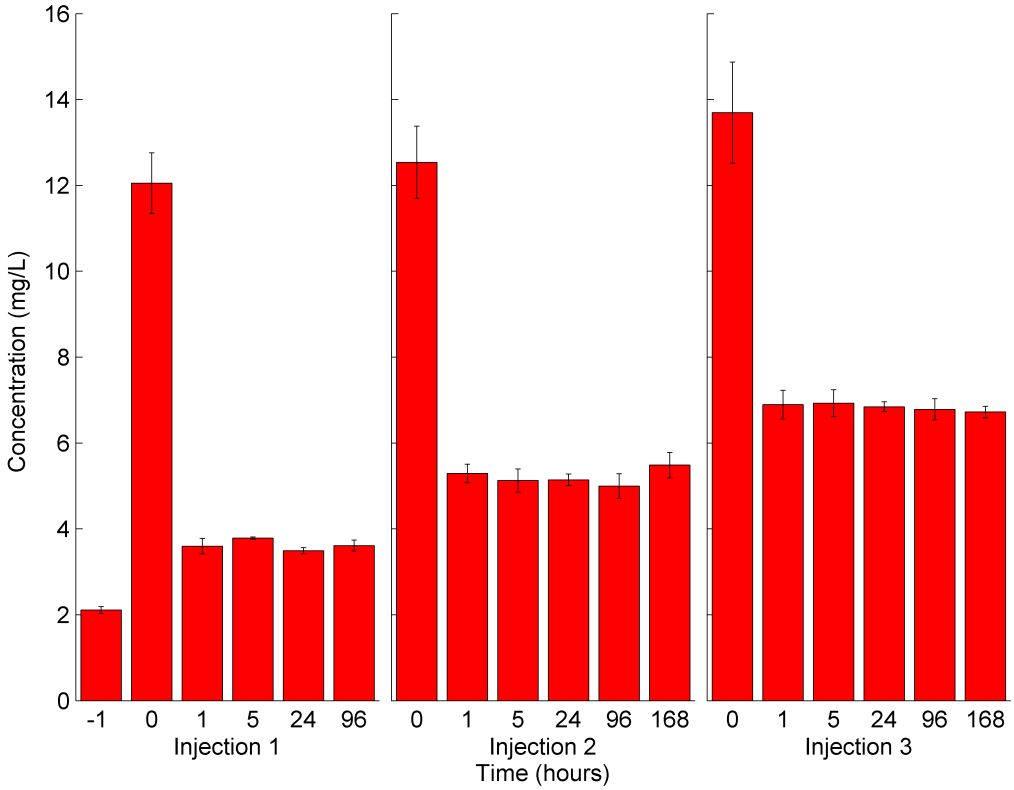

Figure B.15: *Batch 8 Benzene. Average concentration with standard deviation error bars for 3 injections monitored over time.*

B.3 Total Extraction of Stimulation Batch Experiments

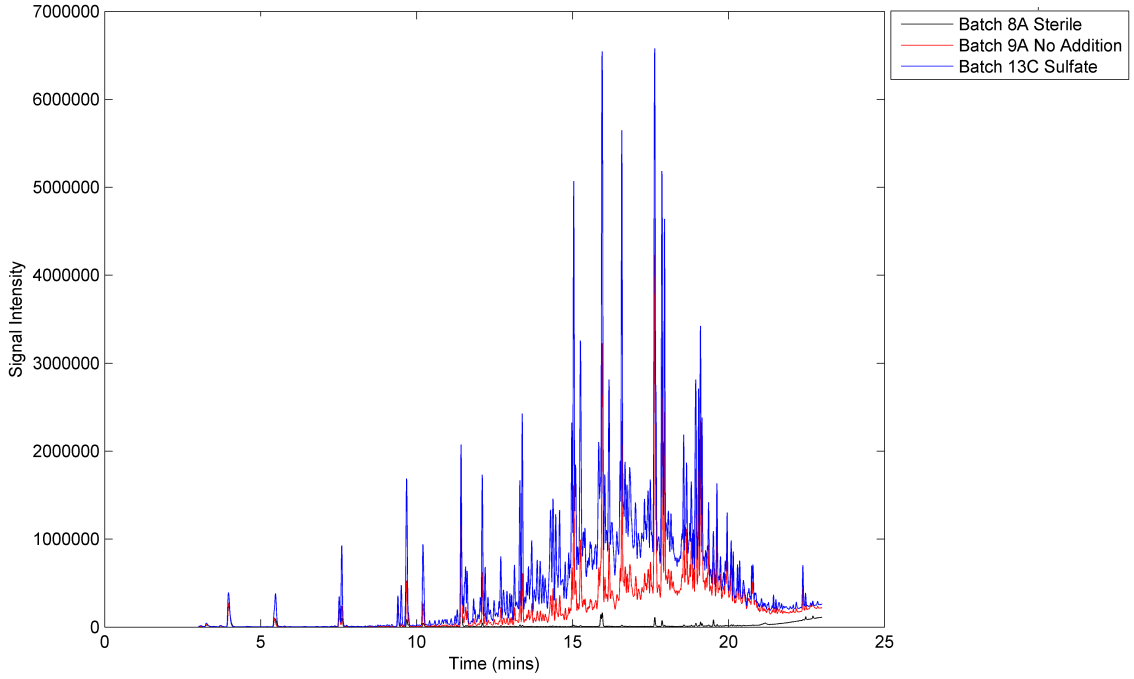

Figure B.16: *GC-MS measurements (TNO, Utrecht) of the sterile (black line), no addition (red line) and sulfate (blue line) batches showing an undefined hump in the chromatogram near the end of the run, possibly indicating the presence of alkanes. The size of the hump correlated well with the degree of degradation observed in batches, with almost no bump in the sterile batch, a sizable hump in the no addition and the largest in the sulfate batch.*

Table B.5: *Preliminary mass and volume measurements of stimulation batch bottles*

Batch	Weight (g)	Sediment Volume (ml)	Aqueous Vol (ml)	Headspace Vol (ml)
8A	234.52	15	70	175
8B	253.44	15	90	155
8C	242.35	10	80	165
9A	237.93	15	80	165
9B	245.94	15	80	165
9C	255.01	15	90	155
10A	179.45	dry	dry	dry
10B	258.18	15	95	150
10C	258.63	15	90	155
11A	264.38	15	100	145
11B	243.66	15	80	165
11C	255.04	15	90	155
12A	230.15	15	70	175
12B	226.39	15	60	185
12C	250.26	15	90	155
13A	264.7	15	110	135
13B	261.52	15	100	145
13C	221.24	15	60	185
14A	233.83	15	70	175
14B	213.59	15	50	195
14C	261.2	15	100	145

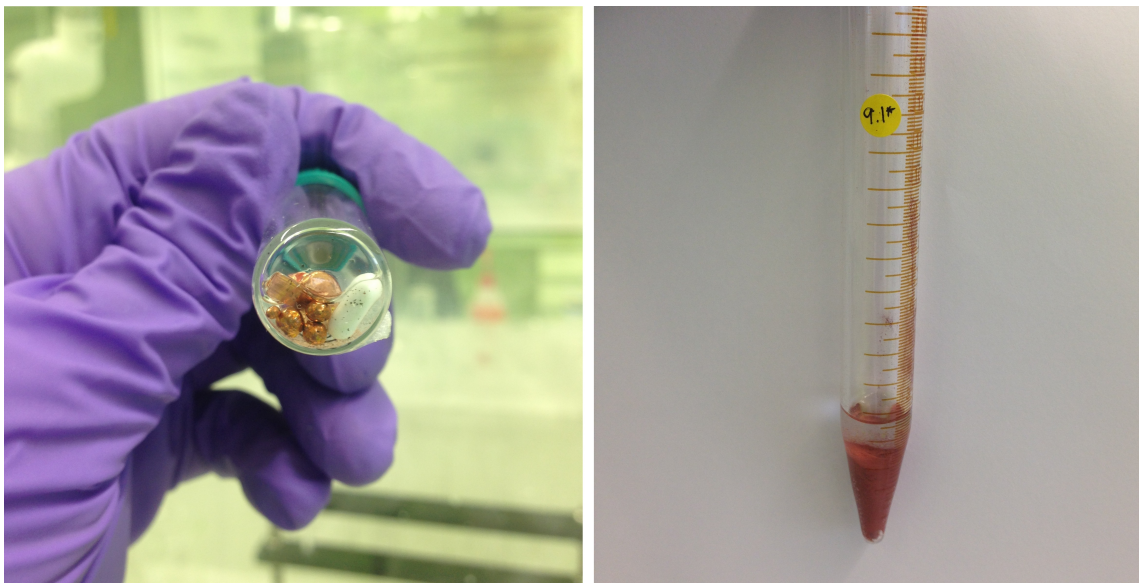

Figure B.17: *Left: Copper Granules, black spots are sulfate in samples reacted with copper and precipitated out. Right: Copper powder with sample in a test tube prior to mixing*

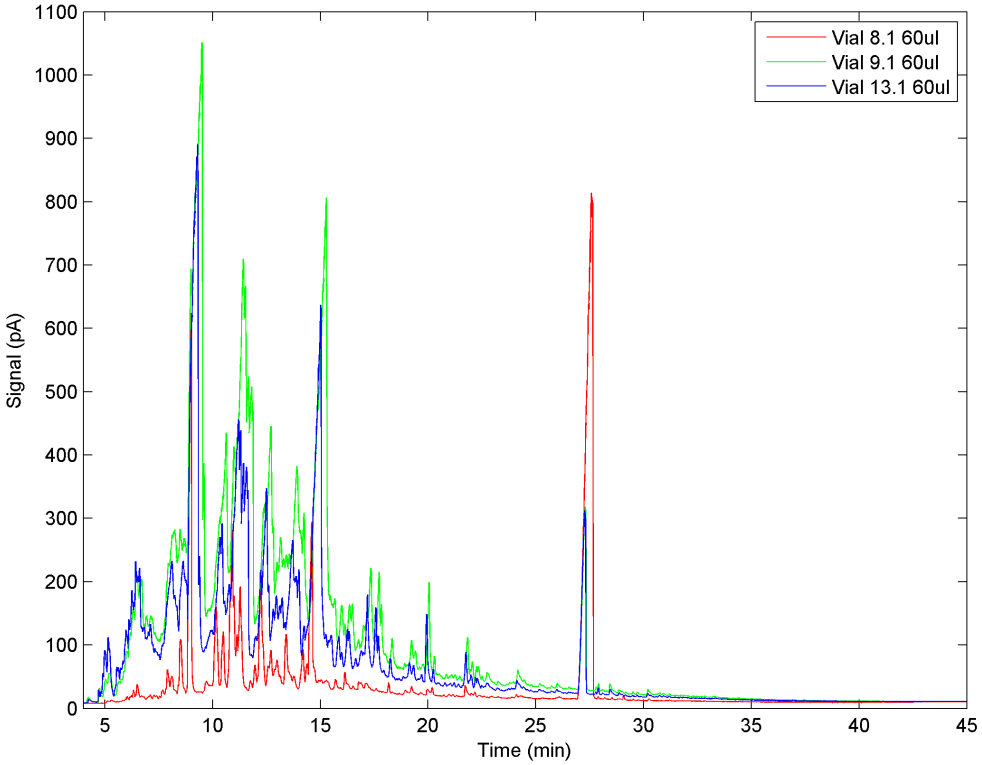

Figure B.18: *Chromatograms of each batch 8C (Sterile), 9C (No addition) and 13C (Sulfate) in the same volume of hexane (60 μL) to show difference in aqueous concentration between batches. Note: Batch 8C injected initially with higher concentration of squalance, hence the larger peak*

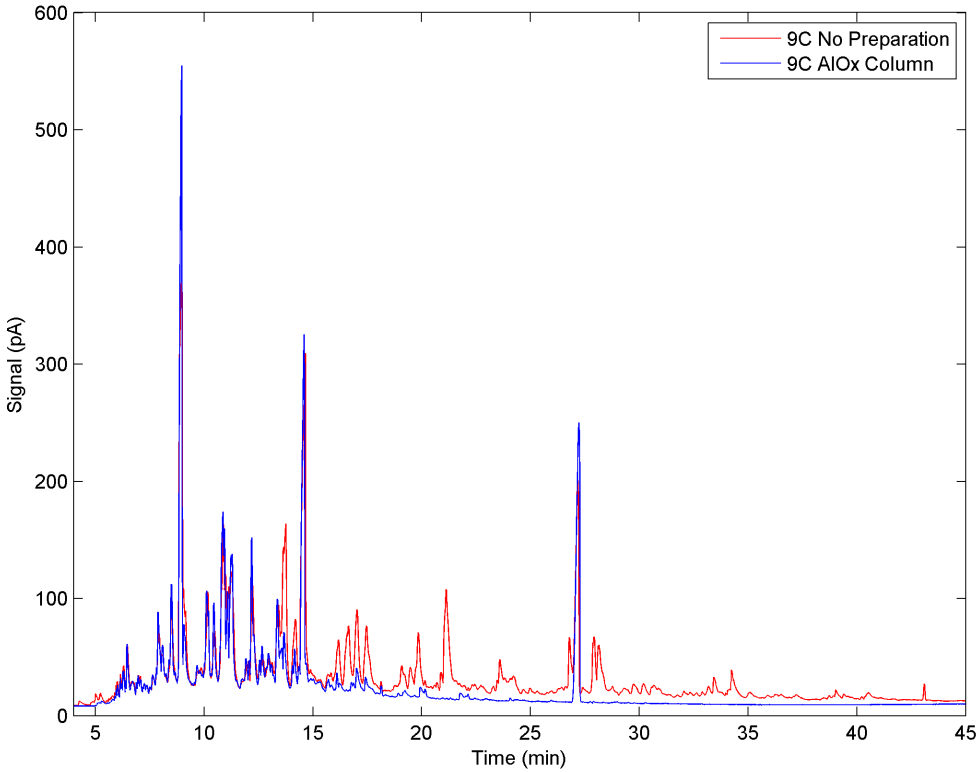

Figure B.19: *Chromatograms of batch 9C (No addition) samples. Blue line shows sample run through alumina column, red line no prior sample preparation. Column chromatography to prepare samples appears to filter out components above a retention time of 15 minutes.*

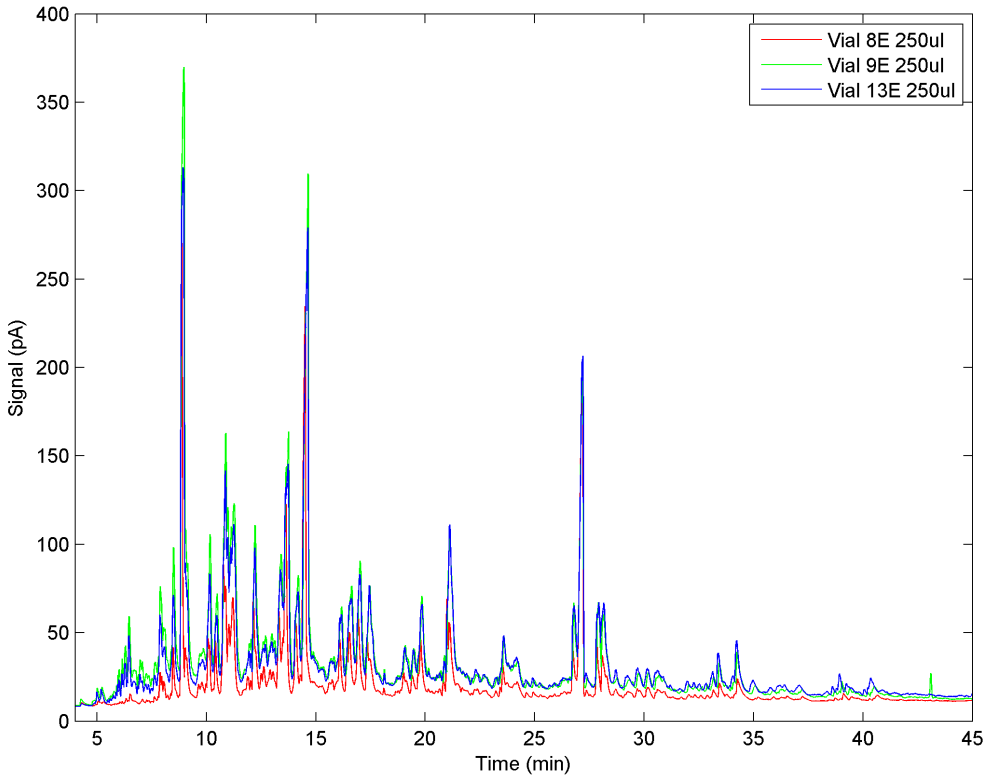

Figure B.20: *Chromatograms of each batch 8C (Sterile), 9C (No addition) and 13C (Sulfate)in the same volume of hexane (250 µL) to show difference in aqueous concentration between batches for samples run without any preparation (no column chromatography).*

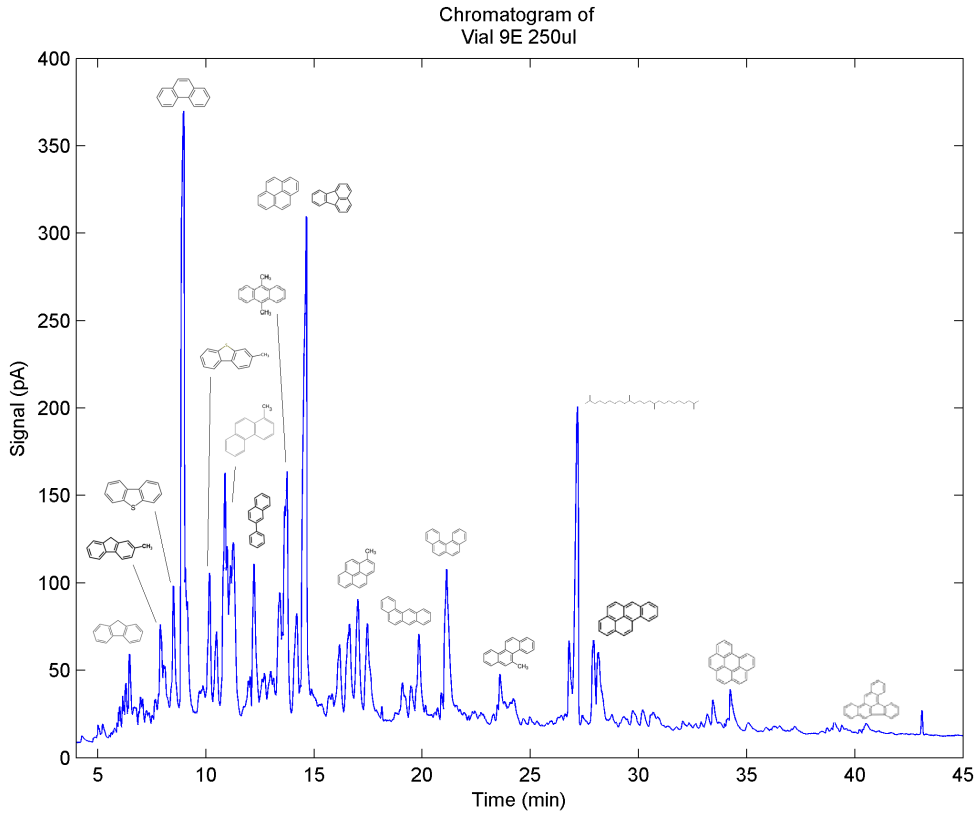

Figure B.21: *Chromatograms of batch 9E showing the peak and corresponding PAH identified using GC-MS.*

Table B.6: *Standard measured by GC-MS using PFTBA internal calibration. Spectral accuracy (%) and NIST probability (%) given for four known elements.*

Chemical	Formula	Spectral Accuracy (%)	NIST Probability (%)
Heptadecane	C17H36	96.77	30.40
2-nonadecanone	C19H38O	98.86	54.60
Octacosane	C28H58	96.74	9.81
Triacontane	C30H62	94.60	6.27

Table B.7: *Identification of analytes from GC-MS analysis based on spectral accuracy and NIST library search.*

Retention Time (mins)	Formula	Spectral Accuracy (%)	NIST	NIST Probability (%)	Molar Mass (g/mol)	$LogK_{ow}$
6.5	C13H10	97.87	Fluorene	61.3	166.22	4.2
7.9	C14H12	94.13	2-methyl-9H-fluorene	26.0	180.25	4.5
8.5	C12H8S	99.04	Dibenzothiophene	36.7	184.26	4.4
8.9	C14H10	98.87	Phenanthrene	35.0	178.23	4.5
10.2	C13H10S	99.51	Methyldibenzothiophene	32.9	198.28	4.7
10.9	C15H12	99.48	Methyl phenanthrene	17.1	192.26	5.1
12.2	C16H12	98.76	2-phenylnaphthalene	21.3	204.27	5.1
13.7	C16H14	98.92	9,10-Dimethylanthracene	12.6	206.23	5.7
14.6	C16H10	99.40	Fluoranthene	31.9	202.26	5.2
			Pyrene	22.5		4.9
17.0	C17H12	97.29	Methylpyrene	26.3	216.28	5.4
19.9	C18H12	97.70	Benzo[c]phenanthrene	43.1	228.29	5.7
21.1	C18H12	98.70	Benz[a]anthracene	34.9	228.29	5.8
23.6	C19H14	94.56	5-methylChrysene	11.7	242.32	6
26.8	C20H12	95.87	Benzo[]fluoranthene	22.0	252.32	6.4
			Benzo[]pyrene	17.0		6
			Perylene	16.0		5.8
34.2	C22H12	95.69	Benzo[ghi]perylene	39.1	276.34	6.6
			Indeno[1,2,3-cd]pyrene	37.6		7
40.3	C24H14	92.60	Dibenzo[a,e]fluoranthene	44.9	302.38	6.7

A. Hockin

Table B.8: *Summary of concentration of all components in the sterile (8C), no addition (9C) and sulfate (13C) treatment batches. Concentrations given for the aqueous phase except for methane, given as the gas phase concentration.*

		Concentration (mg/L)		
Component	Chemical Formula	Sterile (8C)	No Addition (9C)	Sulfate (13C)
Methane (gas)	CH4	0.0	2.4	2.0
Benzene	C6H6	1.5	0.3	0.3
Toluene	C7H8	1.8	4.1	4.8
Ethylbenzene	C8H10	0.6	0.6	0.5
m/p-xylene	C8H10	2.4	3.7	4.7
styrene	C8H8	2.1	3.5	3.8
o-xylene	C8H10	1.1	1.7	2.2
1,2,4-trimethylbenzene	C9H12	1.8	1.7	1.9
1,2,3-trimethylbenzene	C9H12	0.7	0.9	1.0
indene	C9H8	3.6	5.9	6.4
Naphthalene	C10H8	11.5	13.6	13.9
2-Methylnaphthalene	C11H10	2.9	3.0	3.3
1-Methylnaphthalene	C11H10	1.6	1.6	1.8
Fluorene	C13H10	2.4	17.6	12.8
2-methyl-9H-fluorene	C14H12	3.9	21.8	10.5
Dibenzothiophene	C12H8S	3.9	16.5	9.1
Phenanthrene	C14H10	35.1	91.5	68.3
methyldibenzothiophene	C13H10S	13.5	35.2	26.0
(1 or 2)-methyl phenanthrene	C15H12	36.0	75.4	63.2
2-phenylnaphthalene	C16H12	9.9	18.5	15.5
9,10-Dimethylanthracene	C16H14	30.1	56.9	50.6
Fluoranthene/Pyrene	C16H10	39.2	72.1	66.0
1-methylpyrene	C17H12	37.7	67.7	66.3
benzo[c]phenanthrene	C18H12	15.8	26.4	25.7
benz[a]anthracene	C18H12	19.7	33.2	33.8
5-methylChrysene	C19H14	9.5	15.7	15.5
Benzo[]fluoranthene, Benzo[]pyrene, perylene	C20H12	16.4	29.5	32.9
Benzo[ghi]perylene, indeno[1,2,3-cd]pyrene	C22H12	3.7	6.6	7.7
Dibenzo[a,e]fluoranthene	C24H14	0.9	1.8	2.7
Total		309.2	629.1	553.1

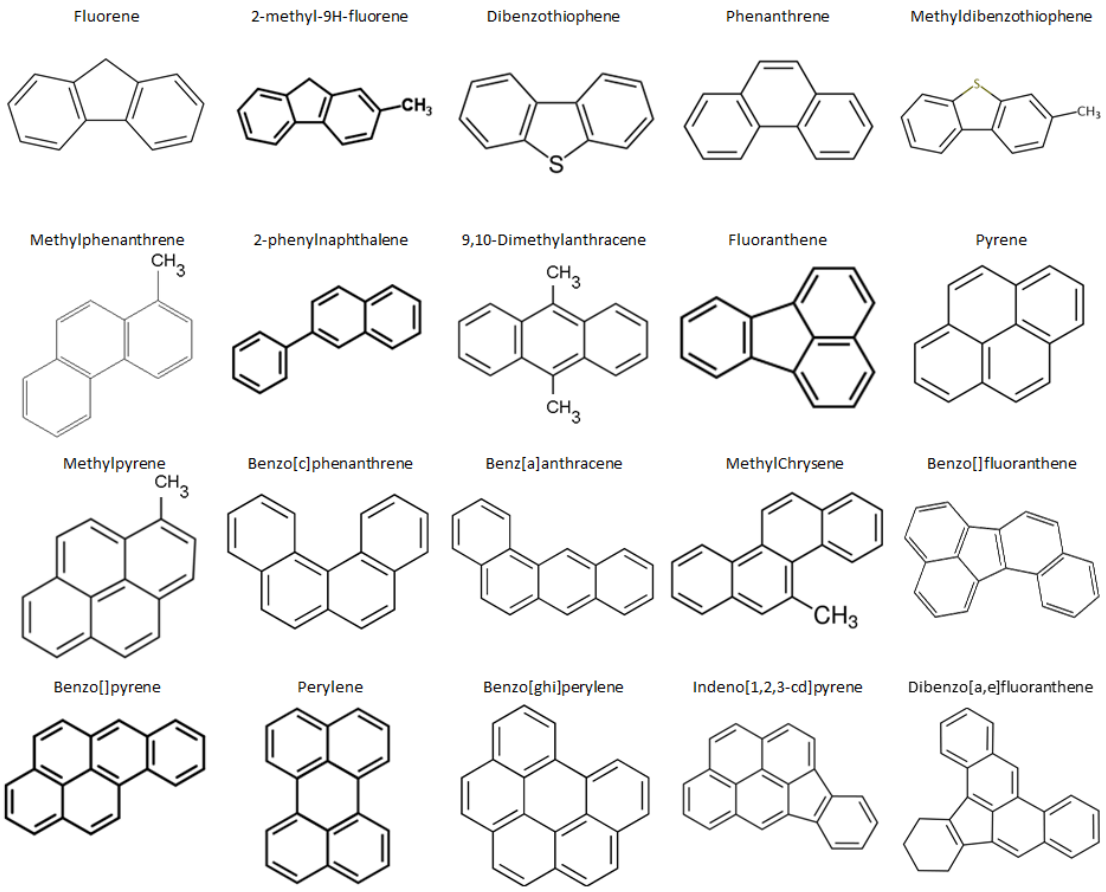

Figure B.22: *Summary of PAH structures for components found in the total extraction of the stimulation batch experiments*

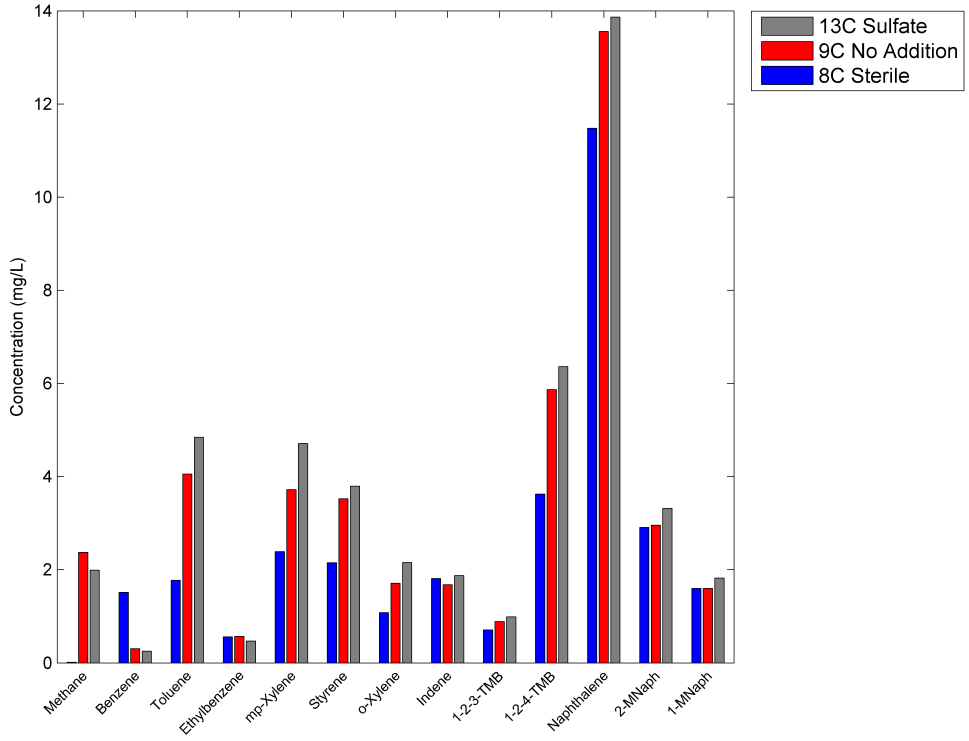

Figure B.23: *Concentration of volatile aromatic hdyrocarbons in the aqueous phase, comparison of component concentrations between batch treatments.*

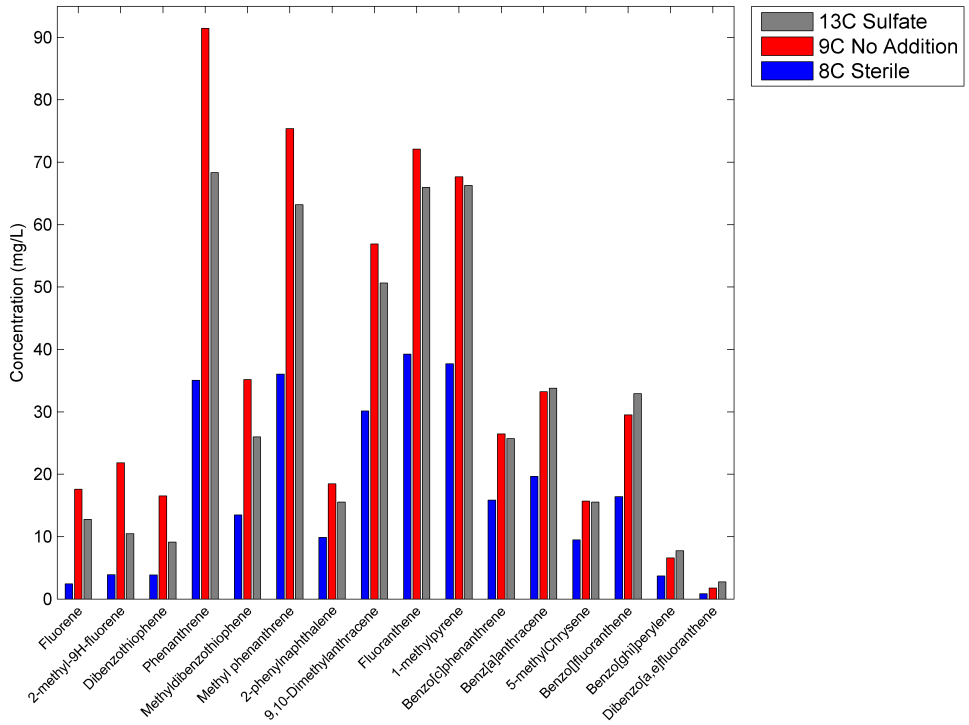

Figure B.24: *Concentration of PAHs in the aqueous phase, comparison of component concentrations between batch treatments.*

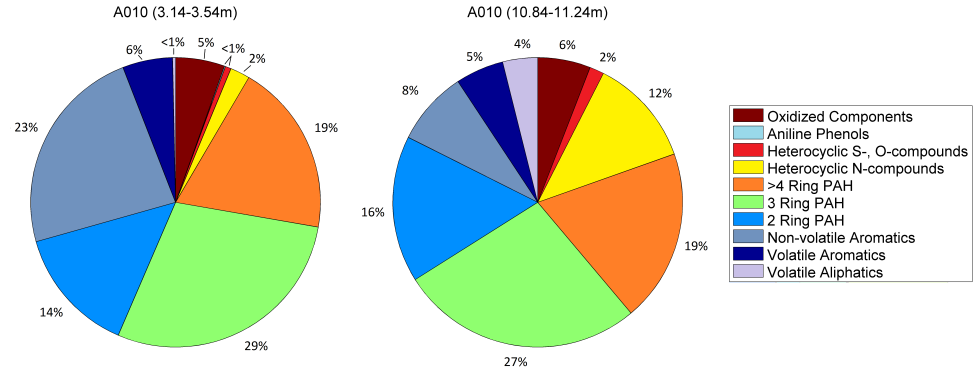

Figure B.25: *Concentration fraction for 10 categories of components measured in tar characterization (ALcontrol Laboratories, 2011)*

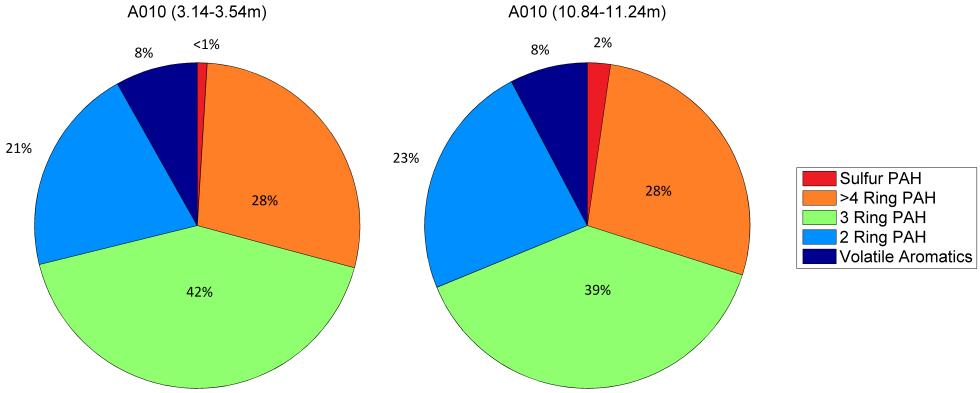

Figure B.26: *Concentration fraction for 5 categories of components measured for comparison to concentration fractions measured in this research (ALcontrol Laboratories, 2011)*